Groupe de renormalisation fonctionnel et événements rares

Farkaš, Lucija Nora

SORBONNE UNIVERSITÉ

Doctoral thesis
of Sorbonne University and University of Zagreb

Specialty : Physics

École Doctorale n°564: Physique en Île-de-France and
Doctoral studies in physics by the University of Zagreb, Faculty of Science (PMF)

realised

in "Laboratoire de Physique Théorique de la Matière Condensée"
and Scientific Center of Excellence for Quantum and Complex Systems

under thesis directors
dr. sc. Ivan Balog and DR CNRS Gilles Tarjus

presented by

Lucija Nora FARKAŠ

Thesis subject:

Functional renormalization group and rare events

Defended on 13 December 2023 in Paris, France

In front of the jury composed of

M.	Pawel Marek JAKUBCZYK	Reporter
M.	Bertrand BERCHE	Reporter
M	Dominique MOUHANNA	President of the jury
M.	Denis Karl SUNKO	Examiner
M.	Danko RADIĆ	Examiner
M.	Gilles TARJUS	Thesis co-director
M.	Ivan BALOG	Thesis co-director

THÈSE DE DOCTORAT
DE SORBONNE UNIVERSITÉ ET UNIVERSITÉ DE ZAGREB

Spécialité : Physique

École Doctorale n°564: Physique en Île-de-France et
"Doctoral studies in physics by the University of Zagreb, Faculty of Science (PMF)"

réalisée

au Laboratoire de Physique Théorique de la Matière Condensée et "Scientific Center of Excellence for Quantum and Complex Systems"

sous la direction de
dr. sc. Ivan Balog and DR CNRS Gilles Tarjus

présentée par

Lucija Nora FARKAŠ

Sujet de la thèse:

Groupe de renormalisation fonctionnel et événements rares

Soutenue le 13 décembre 2023

Devant le jury composé de

M.	Pawel Marek JAKUBCZYK	Rapporteur
M.	Bertrand BERCHE	Rapporteur
M	Dominique MOUHANNA	Président de jury
M.	Denis Karl SUNKO	Examinateur
M.	Danko RADIĆ	Examinateur
M.	Gilles TARJUS	Directeur de Thèse
M.	Ivan BALOG	Directeur de Thèse

SORBONNE UNIVERSITÉ

Doktorska teza
Sveučilišta Sorbonne i Sveučilišta u Zagrebu

Specijalizacija : Fizika

École Doctorale n°564: Physique en Île-de-France i
Doktorski studij fizike Sveučilišta u Zagrebu, Prirodoslovno-matematičkog fakulteta (PMF)

realizirana

u "Laboratoire de Physique Théorique de la Matière Condensée"
i Znanstvenom centru izvrsnosti za kvantne i kompleksne sustave

pod mentorstvom
dr. sc. Ivana Baloga i DR CNRS Gillesa Tarjusa

prezentira

Lucija Nora FARKAŠ

Naslov teme:

Funkcionalna renormalizacijska grupa i rijetki događaji

Obranjeno 13. prosinca 2023. u Parizu, Francuska

Pred komisijom sačinjenom od

M.	Pawel Marek JAKUBCZYK	Ocjenjivač
M.	Bertrand BERCHE	Ocjenjivač
M	Dominique MOUHANNA	Predsjednik komisije
M.	Denis Karl SUNKO	Ispitivač
M.	Danko RADIĆ	Ispitivač
M.	Gilles TARJUS	Mentor
M.	Ivan BALOG	Mentor

Acknowledgments

Lucija Nora Farkaš acknowledges the support of the QuantiXLie Centre of Excellence, a project cofinanced by the Croatian Government and European Union through the European Regional Development Fund - the Competitiveness and Cohesion Operational Programme (Grant KK.01.1.1.01.0004).

Résumé long en Français

Depuis son introduction, le Groupe de Renormalisation est devenu l'outil théorique de prédilection pour comprendre et décrire les comportements collectifs caractérisés par une invariance d'échelle émergente à proximité d'une transition de phase continue. Il offre un cadre conceptuel puissant, mais les résultats exacts étant rares, la recherche de schémas d'approximation génériques et efficaces a été très active dès le départ. Une ligne de recherche récente part d'une formulation exacte du Groupe de Renormalisation, sous la forme d'un Groupe de Renormalisation Fonctionnel (GRF) pour les fonctionnelles génératrices dépendant d'une échelle de coupure infra-rouge et introduit des approximations potentiellement non-perturbatives via des ansatzes pour la fonctionnelle génératrice étudiée. La question que nous abordons est de savoir dans quelle mesure de tels schémas d'approximation génériques sont capables de décrire des problèmes spécifiques où le comportement à longue distance implique des configurations fortement non-uniformes avec, par exemple, des excitations localisées.

Un exemple d'un tel schéma d'approximation au sein du GRF est le développement en dérivées spatiales du champ de l'action moyenne effective (énergie libre de Gibbs à gros grain ("coarse-grained") dans le langage des systèmes magnétiques) qui consiste à tronquer la forme fonctionnelle de cette dernière en puissances des moments extérieurs ou, de manière équivalente, en gradients des champs. L'approximation par développement en dérivées se concentre sur les propriétés à grande longueur d'onde et, en termes de configurations "coarse-grained" du système, fonctionne comme un développement autour de configurations uniformes. On peut donc se demander si un tel schéma est capable de saisir la physique associée à des configurations non uniformes contenant, par exemple, des parois de domaine, des ondes de spin, ou des défauts localisés que l'on dans l'analyse des instantons du modèle d'Ising en 1 dimension.

Dans ce travail, nous évaluons la capacité du développement en dérivées du GRF à décrire quantitativement la physique à longue distance d'un modèle statistique sur toute la gamme des dimensions spatiales sans connaissance a priori des configurations "coarse-grained" pertinentes dans l'espace réel. Pour ce faire, nous examinons d'abord comment les ordres les plus bas du développement en dérivées décrivent l'approche de la dimension critique inférieure d_{lc} de la théorie scalaire ϕ^4 de type Ising qui est censée être contrôlée par la prolifération d'excitations localisées (instantons). Nous tenons à souligner que notre objectif n'est pas de fournir une autre description théorique de l'approche de la dimension critique inférieure pour les systèmes appartenant à la classe d'universalité du modèle d'Ising, une question qui est déjà bien comprise depuis plusieurs décennies. Notre intention avec cet exemple est de développer une approche générale, non perturbative (mais approximative) au sein du GRF qui servirait de référence pour des problèmes qui restent ouverts et dans lesquels on pense que des configurations non uniformes jouent un rôle significatif, tels que la phase à basse température des verres de spin d'Ising ou la dimension critique inférieure du modèle d'Ising en champ aléatoire (RFIM) forcé loin de l'équilibre. La dimension critique inférieure du RFIM à l'équilibre a été rigoureusement démontrée être $d_{lc} = 2$, mais celle du RFIM forcé loin de l'équilibre fait toujours l'objet de débats. Le GRF est bien adapté à cette tâche car même les ordres d'approximation les plus bas sont connus pour saisir des phénomènes non-perturbatifs non triviaux. Il présente l'avantage d'être une approche

générale, contrairement aux méthodes spécialisées auxquelles on doit généralement avoir recours pour saisir un tel comportement, comme la théorie des gouttelettes dans le cas du modèle d'Ising juste au-dessus de $d_{lc} = 1$, où des domaines fermés d'une orientation de spin dans l'autre (les gouttelettes) doivent être introduits explicitement. De plus, la dimension spatiale d est un paramètre de la théorie que nous pouvons faire varier continuellement au sein du GRF. Nous montrons que la convergence du potentiel effectif de point fixe décrivant le point critique du modèle est non-uniforme dans le champ lorsque la dimension d tend vers d_{lc} et se caractérise par l'émergence d'une couche limite autour des minima du potentiel.

Pour saisir le mécanisme de couche limite, il faut veiller à respecter la condition selon laquelle le champ dimensionnel ne se redimensionne pas (avec la coupure infrarouge du moment k introduite par la procédure GRF) à la dimension critique inférieure. Le fait que le champ ne se redimensionne pas signifie que la transition est détruite par des fluctuations dans la limite physique $k \to 0$. Cela peut également être vu sous un autre angle. Si une description correcte de la limite de la dimension critique inférieure peut être trouvée dans le GRF, elle devrait tenir compte de la disparition de la transition et de la phase ordonnée. Ces éléments sont représentés dans les équations de flot du GRF par un point fixe critique et un point fixe de température nulle, respectivement. Le point fixe critique est un point col avec autant de directions instables (pertinentes) qu'il y a de paramètres physiques pertinents à ajuster pour que le système atteigne la criticalité. Le point fixe de température nulle est un attracteur stable. La fusion des deux points fixes représente un événement de bifurcation au cours duquel les directions instables (pertinentes) du point col deviennent marginales. Il y a toujours une valeur propre triviale pertinente $\lambda = -(d - 2 + \eta)/2$ associée à la source appliquée (champ magnétique). La condition pour qu'elle devienne marginale est la même que pour le champ qui ne se remet pas à l'échelle.

Une autre caractéristique attendue de l'approche de la dimension critique inférieure, également liée à la fusion des points fixes critiques et à température nulle dans la limite $d \to d_{lc}$, est que le propagateur de la théorie devrait s'approcher d'une singularité. En effet, le point fixe à température nulle est associé à la phase ordonnée avec brisure de symétrie et le retour à la convexité du potentiel effectif dimensionné le long du flot de renormalisation du GRF est alors contrôlé par la présence d'une singularité dans le propagateur. (Les potentiels effectifs dans le contexte du GRF doivent être convexes uniquement dans la limite physique k→0, ou lorsque les flots de renormalisation se gèlent.)

Dans le chapitre 2, nous considérons le plus bas niveau du développement en dérivées qui soit applicable, l'Approximation du Potentiel Local légèrement modifiée (LPA'). L'approximation de potentiel local (ou LPA) elle-même ne peut pas être utilisée pour décrire la criticalité pour $d < 2$, car la dimension anormale du champ dans la LPA est fixée à $\eta = 0$ alors que l'exposant $d - 2 + \eta$ qui apparaît dans la fonction de corrélation doit être positif.

Après avoir introduit les équations de point fixe (qui décrivent le point critique) dans l'approximation LPA' dans la section 1, nous avons présenté dans la section 2 des résultats numériques obtenus dans cette approximation pour la théorie scalaire ϕ^4 au-dessus de la dimension critique inférieure (d_{lc}). Les données numériques pour la position du minimum du potentiel effectif, φ_{min}, indiquent qu'il ne varie pas comme $1/\sqrt{\tilde{\epsilon}}$, comme cela avait été supposé précédemment dans une étude antérieure du même problème par GRF, mais croît au contraire plus lentement (ici, nous définissons $\tilde{\epsilon} = (d - 2 + \eta)/[2(2 - \eta)]$). Nous trouvons également une divergence apparente de $u''(\varphi_{min})$ en $\frac{1}{\tilde{\epsilon}}$. Ces résultats numériques nous ont

poussés à utiliser la Théorie des Perturbations Singulières (ou SPT), car la limite en $\tilde{\epsilon}$ n'est pas uniforme dans le champ pour les fonctions au point fixe. La SPT traite des équations différentielles où la solution perturbée par un petit paramètre est qualitativement différente de la solution non-perturbée. La Théorie des Perturbations Singulières a des applications dans les oscillations non-linéaires, la mécanique de vol et la mécanique orbitale. Nous montrons dans la section 3.2 que la solution de la LPA' au point fixe est périodique lorsque $\tilde{\epsilon} = 0$ est naïvement implémenté. Ainsi, cette solution avec $\tilde{\epsilon} = 0$ ne peut pas être la solution à l'ordre dominant pour un potentiel effectif physique. La perturbation par un petit terme $\tilde{\epsilon} \to 0^+$ doit conduire à une image qualitativement différente. De ce fait, la Théorie des Perturbations Singulières peut être utilisée pour construire une solution pour le potentiel effectif à l'ordre dominant qui est uniformément valide sur toutes les échelles de champ.

Dans la section 3, nous avons étudié les propriétés de la solution du point fixe LPA' à l'ordre principal de la limite $\tilde{\epsilon} \to 0^+$. Pour ce faire (et appliquer la SPT), nous avons divisé le domaine de variation du champ en trois régions correspondant à des comportements qualitativement différents. Il était essentiel de reconnaître l'émergence d'une couche limite de largeur tendant vers zero comme une région intermédiaire, située entre une région interne entre les deux minima du potentiel $\pm\varphi_{min}$ et les régions où le potentiel $u(\varphi)$ et ses dérivées présentent un comportement en loi de puissance contrôlé par la partie d'échelle (scaling) de leurs équations de flot de renormalisation.

À partir des conditions de raccordement entre ces régions et d'une solution implicite dans la couche limite, nous avons trouvé analytiquement dans la section 3.4 que le propagateur développe une singularité en champ nul lors de l'approche de la dimension critique inférieure d_{lc}. Grâce à cela, nous avons déterminé le comportement du minimum φ_{min} et de la masse renormalisée au minimum $u''(\varphi_{min})$ lorsque $\tilde{\epsilon}$ tend vers zéro (comme $\varphi_{min} \propto \sqrt{\ln(1/\tilde{\epsilon})}$ et $u''(\varphi_{min}) \propto 1/(\tilde{\epsilon}\,\varphi_{min})$). L'identification de la singularité du propagateur comme cause de la divergence de $u''(\varphi_{min})$, pointée par les résultats numériques de la section 2, est une conséquence significative de la procédure de raccordement. Cette singularité du propagateur est en accord avec la fusion attendue du point fixe critique et du point fixe de température nulle contrôlant la phase ordonnée, et c'est l'une des caractéristiques attendues de l'approche de la dimension critique inférieure d_{lc}.

Les conditions de raccordement entre les solutions dans les différents domaines ont également été utilisées pour trouver la valeur de d_{lc} en fonction du pré-facteur du régulateur infrarouge dans la section 3.5. Nous soulignons que le raccordement à travers toutes les régions a été réalisé automatiquement, en ce sens qu'il peut être obtenu pour n'importe quelle paire (d_{lc}, α) - cela ne fixe aucune des valeurs. Il n'y a pas d'extremum pour les courbes $d_{lc}(\alpha)$ obtenues analytiquement, et donc le Principe de Sensibilité Minimale (PMS), une procédure d'optimisation du régulateur infrarouge, ne peut pas être appliqué.

Dans le chapitre 3, nous avons considéré le niveau suivant après la LPA' dans la hiérarchie des troncations du développement en dérivées du champ, afin de vérifier la stabilité voire une éventuelle amélioration des résultats lorsque l'on augmente l'ordre de l'approximation. Il s'agit du deuxième ordre du développement en dérivées, ∂_2. Nous n'avons pas pu progresser analytiquement autant que pour la LPA'. Cela n'est pas si surprenant car les équations de flot de renormalisation sont bien plus compliquées lorsque la fonction de renormalisation du champ $z(\varphi)$ varie avec le champ (comparé à la LPA' où $z(\varphi) = 1$). Le raccordement entre les solutions obtenues dans les différentes régions de la Théorie des Perturbations Singulières au

niveau du potentiel effectif $u(\varphi)$, ou de ses dérivées par rapport au champ, est analytiquement plus accessible car la divergence de la position du minimum φ_{min} vient de l'approche de la singularité du propagateur près de $\varphi = 0$, ce qui détermine le comportement $1/\delta(\tilde{\epsilon}) = \mathcal{O}(1/(\tilde{\epsilon}\,\varphi_{min}))$ de la seconde dérivée $u''(\varphi)$ dans la couche limite. En raison de l'équation hautement non-triviale pour $z(\varphi)$, il n'est cependant pas évident d'obtenir analytiquement son comportement et de réaliser un raccordement approprié des différentes régions de la Théorie des Perturbations Singulières. Cette ligne de recherche est toujours en cours.

Les équations de flot du GRF ont toutes un terme dépendant explicitement de $\tilde{\epsilon} = (d-2+\eta)/[2(2-\eta)]$, où le petit paramètre $\tilde{\epsilon}$ multiplie le champ lui-même et les dérivées par rapport au champ des fonctions du RG. Comme nous avons obtenu des observations numériques en faveur de la divergence de $u''(\varphi_{min})$ à partir des données au-dessus de d_{lc} (section 2), nous nous attendons à nouveau (comme dans LPA') que le terme en $\tilde{\epsilon}$ devienne pertinent plus tôt que ce à quoi on pourrait s'attendre lorsque toutes les fonctions du RG sont finies. L'équation pour $z(\varphi)$ est couplée à ce potentiel effectif singulier, et les résultats numériques montrent un pic de $z(\varphi)$ à proximité de φ_{min}. Nous nous attendons donc à ce qu'une couche limite émerge autour de φ_{min} au niveau ∂_2, de manière analogue à ce qui se passe dans la LPA', mais avec un comportement non-trivial de $z(\varphi)$ dans cette région. Les résultats numériques de la section 2 pour $d > d_{lc}$ nous ont encouragés à explorer un ansatz dans lequel la fonction de renormalisation du champ $z(\varphi)$ diverge dans une couche limite autour de φ_{min}, mais de manière sous-dominante par rapport à $u''(\varphi)$.

Avec cet ansatz, l'équation pour $u''(\varphi)$ dans la couche limite ne dépend plus de $z(\varphi)$ à l'ordre dominant, et nous avons trouvé analytiquement des solutions implicites à l'ordre dominant pour les deux fonctions, qui sont présentées dans la section 3. Ces équations peuvent également être re-mises à l'échelle sous une forme qui est indépendante du régulateur. Cependant, le couplage des équations pour $u''(\varphi)$ et $z(\varphi)$ dans la région interne nous a empêchés de décrire cette région aussi bien qu'en LPA', et nous n'avons pas encore réussi à trouver des conditions de raccordement appropriées entre les différentes régions. Nous pensons que ces conditions devraient déterminer le comportement de $z(\varphi_{min})$ avec $\tilde{\epsilon}$ et fournir des informations analytiques sur la valeur de la dimension critique inférieure $d_{lc}(\alpha)$. Dans la section 3.4, nous avons obtenu une évidence numérique qu'un extrémum de $d_{lc}(\alpha)$ pourrait être présent à ∂_2, ce qui alors permettrait une optimisation du régulateur infrarouge via le principe de Sensibilité Minimale, mais cela implique une extrapolation à partir des valeurs obtenues pour $d > d_{lc}$. Il est donc nécessaire de trouver des courbes $d_{lc}(\alpha)$ plus fiables.

Dans la section 3.4.1, nous avons présenté les raisons pour lesquelles nous nous attendons à ce que les résultats de la LPA' concernant la dépendance de φ_{min} en $\sqrt{\ln(1/\tilde{\epsilon})}$ et le développement d'une singularité dans le propagateur soient également présents dans l'approximation ∂_2, comme le suggèrent les tendances numériques pour $d > d_{lc}$ et en supposant que le raccordement est (en principe) possible au sein de la SPT.

Dans le chapitre 1, nous avons souligné que les points fixes critiques et de température nulle fusionnent à la dimension critique inférieure d_{lc}. Cela implique un certain nombre de conséquences concernant la température critique et les exposants critiques que nous explorons dans le chapitre 4, à la fois aux niveaux LPA' et ∂_2.

Dans la section 1, nous avons montré que la température critique T_c se comporte à l'approche de la dimension critique inférieure comme $T_c \propto 1/\ln(1/D_\varphi)$, où D_φ, la dimension

d'échelle du champ, est donnée par l'expression $D_\varphi \propto \tilde{\epsilon}$ qui avait été trouvée dans la théorie des gouttelettes en $d = 1 + \epsilon$. La théorie des gouttelettes est basée sur un traitement détaillé des parois de domaines de gouttelettes (bulles dans des régions de spins opposés) dans le modèle d'Ising près de la dimension critique inférieure exacte, $d_{lc} = 1$. Nous soulignons que $\tilde{\epsilon} \neq \epsilon$. De façon intéressante, à travers le mécanisme de la couche limite, le développement en dérivées tronqué dans le GRF semble donc capturer un comportement qui implique des fluctuations fortement non-uniformes (sous forme de gouttelettes).

En ce qui concerne les exposants critiques, nos résultats se limitent actuellement principalementà des données numériques pour $d > d_{lc}$, qui sont présentées dans la section 2.2. Concernant les tentatives analytiques, dans la section 3, nous avons proposé une discussion d'un mécanisme potentiel par lequel la valeur propre pertinente $\lambda_1 = -1/\nu$ pourrait devenir marginale dans la limite $d \to d_{lc}$, en nous basant sur les similitudes des résultats numériques avec les vecteurs propres de la valeur propre marginale triviale $\lambda_2 \propto \tilde{\epsilon}$ dans le voisinage du minimum du potentiel φ_{min}. Cependant, jusqu'à présent, notre travail ne donne pas de réponse concluante sur la question de savoir si le développement en dérivées tronqué prédit que $1/\nu$ tend vers zéro lorsque $\tilde{\epsilon} \to 0^+$. C'est un point qui mérite davantage d'attention dans les recherches futures. L'exposant critique ν de la longueur de corrélation doit diverger en d_{lc}, où une mise à l'échelle essentielle ("essential scaling" en Anglais) est obtenue pour le modèle d'Ising en relation avec la prolifération des instantons (kinks et anti-kinks) qui détruisent la transition à température finie. Strictement parlant, la divergence de l'exposant critique ν est une condition nécessaire mais pas suffisante pour retrouver un tel "essential scaling", c'est-à-dire une divergence exponentielle de la longueur de corrélation, mais nous travaillons toujours sur ce problème.

La conclusion que l'on peut tirer à ce stade est que les premiers ordres du développement en dérivées du champ au sein du GRF semblent au moins partiellement saisir l'effet des configurations fortement non-uniformes contenant des gouttelettes qui contrôlent le comportement critique des modèles purs de type Ising au voisinage de la dimension critique inférieure ($d_{lc} = 1$ dans le traitement exact). Ceci se produit à travers le mécanisme mathématique d'une couche limite dans les fonctions de point fixe et est décrit par la Théorie des Perturbations Singulières. Il reste à voir plus en détail si la prolifération des excitations localisées (gouttelettes ponctuelles) qui détruisent la transition à d_{lc} et conduisent à un "essential scaling" peut être effectivement décrite par des approximations basées sur un développement autour de configurations "coarse-grained" uniformes.

Dans les chapitres précédents, nous avons examiné si et comment le développement en dérivées du champ dans le cadre du GRF peut reproduire des situations où la physique à longue portée est dominée par des excitations spatialement localisées telles que les kinks et les anti-kinks qui prolifèrent à la dimension critique inférieure $d_{lc} = 1$ de la théorie scalaire ϕ^4 (qui est dans la classe d'universalité du modèle d'Ising) ou les gouttelettes qui contrôlent le comportement critique à mesure que nous nous approchons de d_{lc}. Dans le chapitre 5, nous traitons un problème différent où des configurations de champ fortement non-uniformes sont essentielles. Il s'agit de la phase ordonnée de la théorie scalaire ϕ^4. Dans ce cas, il est connu que la coexistence de phases (entre deux états ordonnés purs associés à la symétrie brisée) implique une configuration non-uniforme sous forme d'une paroi de domaine. De telles configurations non-uniformes permettent à la densité d'énergie libre ou au potentiel effectif d'être strictement convexe (c'est-à-dire plate) pour des valeurs du champ situées

entre les deux minima à la limite thermodynamique, comme l'exige leur définition par une transformation de Legendre.

Nous avons obtenu des résultats préliminaires concernant le potentiel effectif dépendant de l'échelle, la quantité centrale du GRF, dans la phase ordonnée de la théorie ϕ^4 quand $d > 1$. Dans ce cas, les configurations de champ qui contrôlent la thermodynamique et la coexistence de phases associée sont des configurations non-uniformes de parois de domaine. Ce qui est spécifique ici par rapport au point critique du même modèle en $d = 1 + \epsilon$ et au comportement à la dimension critique inférieure en $d = 1$, c'est que les excitations sont encore spatialement étendues (bien que seulement dans $\epsilon = d - 1$ dimensions) de sorte que leur coût les empêche de proliférer, contrairement aux gouttelettes près du point critique en $d = 1+\epsilon$ ou aux kinks en $d = 1$. Le calcul peut donc être effectué à travers une approximation de point col en présence d'un régulateur infrarouge, complété par des corrections à 1 boucle associées aux fluctuations gaussiennes autour du point col. Nous avons montré que l'excès d'énergie libre de la paroi de domaine associée à la tension de surface n'apparaît pas dans l'expression du potentiel effectif dépendant de l'échelle car ce dernier est considéré à la limite thermodynamique. La présence de la paroi de domaine est néanmoins nécessaire pour produire la forme spécifique en $k^2\varphi^2$ qui décrit le retour à la convexité quand $k \to 0$.

Il y a plusieurs aspects qui restent à compléter. Premièrement, nous devons terminer le calcul à 1 boucle pour vérifier si la contribution non nulle à la limite thermodynamique est proportionnelle à k^2 comme il semble naïvement, ou si la dépendance en k est modifiée pour devenir une loi de puissance plus faible, en particulier lorsque $d < 2$. Deuxièmement, nous voulons déterminer si et comment les troncations les plus basses du développement en dérivées du champ (LPA, LPA', second ordre ∂_2) sont capables de reproduire le comportement prédit de l'action effective dépendant de l'échelle. Comme déjà mentionné, cela a été démontré pour une large classe de régulateurs infrarouges pour $d > 2$. Cependant, nous sommes principalement intéressés ici par $d < 2$ et plus spécifiquement par la proximité de la dimension critique inférieure.

Pour résumer, dans ce travail, nous avons évalué comment la physique à longue portée de systèmes statistiques, lorsqu'elle est contrôlée par des fluctuations fortement non-uniformes, peut être décrite par le groupe de renormalisation fonctionnel avec un schéma d'approximation basé sur un développement autour de configurations "coarse-grained" uniformes (développement en dérivées spatiales). Nous nous sommes concentrés sur l'exemple bien étudié de la théorie ϕ^4 de type Ising au voisinage de sa dimension critique inférieure d_{lc} et avons utilisé une combinaison d'approches numériques et analytiques (Théorie des Perturbations Singulières, méthode du point col, etc.). Le principal résultat est que le mécanisme par lequel le comportement critique du modèle lorsque $d \to d_{lc}$ est qualitativement reproduit aux premiers niveaux de troncation du développement en dérivées est la convergence non-uniforme des fonctions de point fixe dans leur dépendance au champ, associée à l'émergence d'une couche limite. Des discussions supplémentaires et des perspectives sont également fournies dans le chapitre de conclusion et certains détails techniques additionnels sont décrits dans plusieurs annexes.

Dugi sažetak na hrvatskom jeziku

Od svog uvođenja, Renormalizacijska Grupa (RG) je preferirana teorija za razumijevanje i opis kolektivnog ponašanja karakteriziranog invarijantnošću na promjenu skale, kao npr. u blizini kontinuiranih faznih prijelaza. RG pruža snažan konceptualni okvir za istraživanje, no budući da su egzaktna rješenja uglavnom nedostupna, od samog početka vrlo je aktivna potraga za generičkim i efikasnim aproksimacijskim shemama. Jedna od modernijih linija istraživanja počinje od egzaktne formulacije Renormalizacijske Grupe, u obliku Funkcionalne Renormalizacijske Grupe (FRG) za funkcionale ovisne o skali koji su generatori korelacijskih funkcija, i uvodi potencijalno neperturbativne aproksimacije kroz "ansatze" za te funkcionale ovisne o skali. Pitanje kojim se bavimo je u kolikoj mjeri takve generičke aproksimacijske sheme mogu opisati specifične probleme u kojima na dugovalna svojstva znatno utječu neuniformne konfiguracije, npr. lokalizirana pobuđenja.

Primjer jedne takve aproksimacijske sheme u sklopu FRG-a je takozvani derivacijski razvoj efektivnog okrupnjenog djelovanja (okrupnjene /"coarse-grained" Gibsove slobodne energije u jeziku magnetskih sustava) koji odgovara razvoju tog djelovanja po vanjskom momentu ili ekvivalentno po gradijentima polja. FRG formalizam i derivacijski razvoj uvedeni su u poglavlju 1. Aproksimacija derivacijskim razvojem je primarno fokusirana na dugovalna svojstva i, u terminima okrupnjenih konfiguracija sustava, funkcionira kao razvoj oko uniformnih konfiguracija. Nameće se pitanje može li takva aproksimacijska shema ispravno opisati fiziku povezanu s neunifrmnim konfiguracijama koje sadrže, npr. domenske zidove, spinske valove ili lokalizirane defekte poput kinkova i anti-kinkova koji se javljaju u instantonskoj analizi jednodimenzionalnog Isingovog modela.

U ovoj tezi analiziramo može li derivacijski razvoj u sklopu Funkcionalne renormalizacijske Grupe opisati dugovalnu fiziku modela bez a priori poznavanja relevantnih okrupnjenih konfiguracija, čak i kad su one vrlo neuniformne. U tu svrhu istražujemo kako niski redovi derivacijskog razvoja opisuju prilazak donjoj kritičnoj dimenziji d_{lc} skalarne ϕ^4 teorije koja dijeli klasu univerzalnosti s Isingovim modelom i u kojoj se stoga očekuje da je fizika na d_{lc} dominirana proliferacijom lokaliziranih pobuđenja (instantona). Naglašavamo da nam nije cilj pružiti još jedan teorijski opis prilaska donjoj kritičnoj dimenziji za sustave u klasi univerzalnosti Isingovog modela, budući da je to pitanje prilično dobro objašnjeno već prije nekoliko desetljeća. Naša je namjera na ovom primjeru razviti općeniti, neperturbativni (ali aproksimativni) pristup unutar FRG-a koji bi služio za probleme koji su još otvoreni a u kojima se vjeruje da neuniformne konfiguracije igraju značajnu ulogu, poput npr. niskotemperaturne faze Isingovih spinskih stakala ili donje kritične dimenzje neravnotežnog, atermalno vođenog ("athermally driven") Isingovog modela s nasumičnim poljem (RFIM). Za ravnotežni RFIM, rigorozno je pokazano da je donja kritična dimenzija $d_{lc} = 2$, no za RFIM van ravnoteže sama vrijednost d_{lc} je i dalje upitna. FRG je vrlo pogodna metoda za takve sustave budući da se zna da i najniži stupnji aproksimacija u sklopu FRG-a mogu opisati netrivijalne neperturbativne pojave. Dodatna prednost FRG je i generalnost metode, u opreci sa specijaliziranim pristupima koji se obično moraju koristiti da bi se opisali ovakvi sustavi, poput kapljične teorije ("droplet theory") u slučaju Isingovog modela tik nad d_{lc} gdje je nužno zatvorene domene jedne spinske orijentacije uronjene u drugu orijentaciju (t.j., kapljice) eksplicitno uvesti i tretirati. Osim toga, prostorna dimenzija d je u FRG parametar koji se može kontinuirano varirati. Pokazali smo da je konvergencija efektivnog potencijala

u fiksnoj točki modela neuniformna u polju kad se dimenzija d približava d_{lc}, s pojavom graničnog sloja ("boundary layer") oko minimuma potencijala.

Kako bismo pronašli granični sloj i ispravno ga opisali, moramo paziti da je ispoštovan uvjet da se dimenzionalno okrupnjeno polje ne reskalira (s infracrvenim pragom, momentom k, uvedenim u FRG proceduri) na donjoj kritičnoj dimenziji. Prestanak reskaliranja polja kad nastupi d_{lc} znači da je prijelaz uništen fluktuacijama u fizikalnoj $k \to 0$ granici. Ovo se također može vidjeti i iz druge perspektive. Ako je moguće pronaći prikladan tretman donje kritične dimenzije FRG-om, on mora opisati nestajanje prijelaza i uređene faze. Ta dva režima su u FRG tokovima predstavljena kritičnom i niskotemperaturnom fiksnom točkom. Kritična fiksna točka je sedlo s toliko netabilnih (relevantnih) smjerova, koliko je fizikalno relevantnih parametara koje treba podesiti kako bi sustav postao kritičan. S druge strane, niskotemperaturna fiksna točka je stabilni atraktor. Stapanje te dvije fiksne točke predstavljalo bi bifurkaciju pri kojoj bi nestabilni (relevantni) smjerovi sedla postali marginalni. Postoji uvijek prisutna trivijalna relevantna svojstvena vrijednost $\lambda = -(d - 2 + \eta)/2$ povezana s vanjskim izvorom (magnetskim poljem). Uvjet njene marginalnosti istovjetan je s uvjetom da se dimenzionalno polje ne reskalira.

Drugo svojstvo koje se očekuje pri prilasku donjoj kritičnoj dimenziji, a koje je također povezano sa stapanjem kritične i niskotemperaturne fiksne točke u $d \to d_{lc}$ granici, je da bi propagator teorije trebao postati singularan. Tome je razlog što je niskotemperaturna fiksna točka povezana s uređenom fazom slomljene simetrije gdje je povratak ka konveksnosti dimenzionalnog efektivnog potencijala duž FRG tokova kontroliran prisutnošću singulariteta u propagatoru (efektivni potencijali u FRG-u moraju biti konveksni tek u fizikalnoj $k \to 0$ granici, ili na kraju tokova).

U poglavlju 2 razmatramo najniži primjenjiv red derivacijskog razvoja, minimalno modificiranu Aproksimaciju Lokalnim Potencijalom ("minimally modified Local Potential Approximation", LPA'). Nemodificirana LPA se ne može koristiti za opis kritičnosti u dimenzjama $d < 2$, budući da je anomalna dimenzija u LPA automatski postavljena na $\eta = 0$, a eksponent $d - 2 + \eta$ koji figurira u korelacijskoj funkciji mora biti pozitivan.

Nakon uvođenja jednadžbi fiksnih točaka (koje opisuju kritičnost) u LPA' u podpoglavlju 1, u podpoglavlju 2 predstavili smo numeričke LPA' račune za skalarnu ϕ^4 teoriju polja nad donjom kritičnom dimenzijom (d_{lc}). Numerički podatci o lokaciji minumuma efektivnog potencijala, φ_{min}, pokazuju da se ona ne skalira kao $1/\sqrt{\tilde{\epsilon}}$ (ovdje definiramo $\tilde{\epsilon} = (d - 2 + \eta)/[2(2 - \eta)]$), kao što je bilo pretpostavljeno u ranijem FRG istraživanju. Našli smo da φ_{min} raste znatno sporije s $1/\tilde{\epsilon}$. Također smo pronašli divergenciju druge derivacije u minimumu, $u''(\varphi_{min})$, kao $\sim 1/\tilde{\epsilon}$. Ovi numerički rezultati potaknuli su nas da koristimo Singularnu Perturbacijsku Teoriju (SPT), budući da $\tilde{\epsilon} \to 0^+$ granica RG funkcija u fiksnoj točki nije uniformna u polju. SPT se bavi aproksimacijama rješenja diferencijalnih jednadžbi čija su neperturbirana rješenja kvalitativno različita od onih perturbiranih nekom malom veličinom. Singularna Perturbacijska Teorija je uspješno primjenjiva na npr. nelinearne oscilatore, mehaniku letjelica i orbitalnu mehaniku. U podpoglavlju 3.2 smo pokazali da je rješenje LPA' jednadžbe fiksne točke (2.3) periodično u polju kad se naivno implementira $\tilde{\epsilon} = 0$. Takvo $\tilde{\epsilon} = 0$ rješenje je nefizikalno i ne može biti vodeći red rješenja za efektivni potencijal. Perturbacija malim $\tilde{\epsilon} \to 0^+$ članom mora dati kvalitativno drukčije, neperiodično rješenje. Zato koristimo Singularnu Perturbacijsku Teoriju kako bismo konstruirali vodeći red $\tilde{\epsilon} \to 0^+$ rješenja za efektivni potencijal koje je valjano i fizikalno na svim skalama polja.

U podpoglavlju 3 smo analitički istražili svojstva LPA' rješenja za fiksnu točku u vodećem redu $\tilde{\epsilon} \to 0^+$ granice. Kako bismo to učinili (i primijenili Singularnu Perturbacijsku Teoriju), podijelili smo domenu polja φ na tri kvalitativno različite regije. Pri tome je bilo ključno prepoznati razvoj graničnog sloja iščezavajuće širine kao srednje regije, locirane između unurašnje regije koja se nalazi među minimumima $\pm\varphi_{min}$ i regije repova RG funkcija gde se potencijal $u(\varphi)$ i njegove derivacije ponašaju kao potencije polja (što je kontrolirano skalirajućim dijelovima pripadnih jednadžbi toka).

Iz uvjeta za spajanje tih regija i implicinog rješenja koje smo našli unutar graničnog sloja, u podpoglavlju 3.4 smo analitički pokazali da propagator razvija singularitet u ishodištu polja, $\varphi = 0$, kad se približavamo donjoj kritičnoj dimenziji (d_{lc}). Iz toga smo pronašli kako se minimum φ_{min} i vrijednost renormalizirane mase u minimumu, $u''(\varphi_{min})$, skaliraju s $\tilde{\epsilon}$ (kao $\varphi_{min} \propto \sqrt{\ln(1/\tilde{\epsilon})}$ i $u''(\varphi_{min}) \propto 1/(\tilde{\epsilon}\,\varphi_{min})$). Identifikacija singulariteta propagatora kao uzrok divergencije $u''(\varphi_{min})$ na koju smo prvo posumnjali zbog numeričkih rješenja fiksne točke nad d_{lc} (podpoglavlje 2) je značajan rezultat analitički nađen procedurom asimptotskog spajanja različitih regija u okviru Singularne Perturbacijske Teorije. Ova singularnost propagatora u skladu je s očekivanim stapanjem kritične fiksne točke s niskotemepraturnom fiksnom točkom koja kontrolira uređenu fazu i jedna je od očekivanih obilježja prilaska donjoj kritičnoj dimenziji.

Uvjeti spajanja regija su korišteni i za pronalazak analitičkih krivulja ovisnosti iznosa donje kritične dimenzije d_{lc} ove aproksimativne FRG teorije o korištenom inracrvenom regulatoru, što je prezentirano u podpoglavlju 3.5. Naglašavamo da je spajanje kroz sve regije ostvareno automatski, u smislu da je provedivo za sve (d, α) parove (gdje je $\alpha = \mathcal{O}(1)$ prefaktor regulatora) - spajanje ne fiksira vrijednost ni d ni α. Također, analitičke $d_{lc}(\alpha)$ krivulje nemaju ekstrem, te stoga nije moguće koristiti ni Princip Minimalne Osjetljivosti (Principle of Minimal Sensitivity, PMS) kao proceduru optimizacije regulatora kojom bismo pronašli optimalni prefaktor α, te stoga i d_{lc}.

U poglavlju 3 smo razmotrili sljedeći korak nakon LPA' u hierarhiji derivacijskog razvoja, kako bismo provjerili stabilnost ili pronašli moguća poboljšanja rezultata s povećavanjem reda aproksimacije. Taj sljedeći korak je drugi red derivacijskog razvoja kojeg skraćeno nazivamo ∂_2. Analitički nismo ostvarili napredak na istoj razini kao u LPA'. To nije iznenađujuće, budući da su jednadžbe toka dane u podpoglavlju 1 puno kompliciranije kad funkcija renormalizacije polja $z(\varphi)$ ovisi o polju, u uspedbi s LPA' gdje je $z(\varphi)$=1. Asimptotsko spajanje rješenja među različitim regijama (u kontekstu Singularne Perturbacijske Teorije) na razini efektivnog potencijala $u(\varphi)$, ili njegovih derivacija po polju, je analitički puno jednostavnije nego za $z(\varphi)$ budući da je divergentno skaliranje minimuma φ_{min} u terminima $\tilde{\epsilon}$ posljedica prilasku singularitetu propagatora u okolini $\varphi = 0$, što određuje i skaliranje druge derivacije $u''(\varphi)$ u graničnom sloju s $1/\delta(\tilde{\epsilon}) = \mathcal{O}(1/(\tilde{\epsilon}\,\varphi_{min}))$. S druge strane, zbog vrlo netrivijalne jednadžbe za $z(\varphi)$, nije jasno kako analitički odrediti skaliranje te funkcije i posljedično nije moguće ostvariti prikladno spajanje različitih regija. Ovaj aspekt istraživanja je i dalje aktivan.

Sve jednadžbe toka i dalje imaju član koji eksplicitno ovisi o $\tilde{\epsilon} = (d - 2 + \eta)/[2(2 - \eta)]$, u kojem mali parametar $\tilde{\epsilon}$ množi samo polje, φ, i derivacije RG funkcija po polju. Budući da smo i u drugom redu derivacijskog razvoja našli pokazatelje divergencije $u''(\varphi_{min})$ iz numeričkih rješenja za fiksne točke nad donjom kritičnom dimenzijom (koja su prikazana u podpoglavlju 2), opet, kao i u LPA', očekujemo da $\tilde{\epsilon}$ član postane relevantan za manje

vrijednosti polja nego što bi se očekivalo da su sve RG funkcije konačne. Jednadžba za funkciju renormalizacije polja je spregnuta s takvim singularnim efektivnim potencijalom i u numeričkim rješenjima nad d_{lc} uočavamo da funkcija $z(\varphi)$ razvija vrhove ("peaks") u blizini minimuma, $\pm\varphi_{min}$. Stoga očekujemo da se i na razini ∂_2 razvije granični sloj oko φ_{min}, analogno LPA', ali s netrivijalnim ponašanjem $z(\varphi)$ u toj regiji. Numerički reultati podpoglavlja 2 za $d > d_{lc}$ su nas potakli da istražimo ansatz u kojem funkcija renormalizacije polja $z(\varphi)$ divergira u graničnom sloju oko φ_{min}, ali subdominantno u usporedbi s $u''(\varphi)$.

Korištenjem ovog ansatza, jednadžba za $u''(\varphi)$ u graničnom sloju i u vodećem redu u $\tilde{\epsilon} \to 0^+$ ne ovisi o $z(\varphi)$, te smo u podpoglavlju 3 analitički pronašli implicitna rješenja za obje funkcije (opet, u graničnom sloju i u vodećem redu). Jednadžbe se također mogu reskalirati u oblik koji ne ovisi o regulatoru. S druge strane, jednadžbe za $u''(\varphi)$ i $z(\varphi)$ su i dalje spregnute u unutarnjoj regiji. Zbog toga tu regiju nismo još uspjeli okarakterizirati tako temeljito kao u LPA', te još nismo našli primjerene uvjete spajanja među regijama (u kontekstu Singularne Perturbacijske Teorije). Vjerujemo da bi ti uvjeti spajanja trebali odrediti skaliranje $z(\varphi_{min})$ s $\tilde{\epsilon}$ i dati analitičke podatke o vrijednosti donje kritične dimenzije $d_{lc}(\alpha)$. U podpoglavlju 3.4 smo našli numeričke pokazatelje da bi krivulje $d_{lc}(\alpha)$ mogle imati ekstrem na razini ∂_2, što bi omogućilo korištenje Principa Minimalne Osjetljivosti (PMS), no to je uključivalo ekstrapolacije iz vrijednosti nad d_{lc}. Za korištenje PMS-a je stoga potrebno naći pouzdanije $d_{lc}(\alpha)$ krivulje.

U podpoglavlju 3.4.1 smo izložili razloge zbog kojih očekujemo da se LPA' rezultati o skaliranju φ_{min} kao $\sqrt{\ln(1/\tilde{\epsilon})}$ i razvoju singulariteta propagatora ponove i na ∂_2 razini, kao što sugeriraju numerički trendovi na $d > d_{lc}$ i uz pretpostavku da je spajanje regija (u principu) moguće.

U poglavlju 1 smo napomenuli da se kritična i niskotemperaturna fiksna točka stapaju na donjoj kritičnoj dimenziji, što daje određena predviđanja za ponašanje kritične temperature i kritičnih eksponenata koja istražujemo u poglavlju 4, na obje razine aproksimacije (LPA' i ∂_2).

U podpoglavlju 1 smo našli da se kritična temperatura skalira kao $T_c \propto 1/\ln(1/D_\varphi)$ s dimenzijom skaliranja polja $D_\varphi \propto \tilde{\epsilon}$. Ovaj izra se slaže s rezultatima kapljične teorije na $d = 1 + \epsilon$. Kapljična teorija se temelji na pažljivom tretmanu domenskih zidova kapljica (otoka jedne orijentacije spina u suprotnoj orijentaciji) u Isingovom modelu u blizini egzaktne donje kritične dimenzije, $d_{lc} = 1$. Naglašavamo da $\tilde{\epsilon} \neq \epsilon$. Interesantno je što ovaj rezultat ukazuje da, kroz mehanizam graničnog sloja, aproksimacijska shema derivacijskog razvoja u sklopu FRG-a naizgled uspjeva opisati ponašanje T_c povezano s vrlo neuniformnim konfiguracijama (u obliku kapljica).

Što se tiče kritičnih eksponenata, naši su rezultati trenutno uglavnom ograničeni na numeričke podatke nad donjom kritičnom dimenzijom, koji su dani u podpoglavlju 2.2. U vezi s analitičkim pristupom, u podpoglavlju 3 je raspravljen pretpostavljen mehanizam koji bi mogao voditi do marginalnosti inače relevantne svojstvene vrijednosti $\lambda_1 = -1/\nu$ u granici donje kritične dimenzije, gdje je ν kritični eksponent korelacijske duljine ξ. Argumenti za ovaj mehanizam bazirani su na sličnostima s numeričkim rezultatima za svojstvene vektore trivijalno marginalne svojstvene vrijednosti $\lambda_2 \propto \tilde{\epsilon}$, u okolini lokacije minimuma efektivnog potencijala φ_{min}. Ipak, ovaj rad u ovom trenutku ne daje definitivan odgovor na pitanje predviđa li derivacijski razvoj isčezavanje $1/\nu$ u granici $\tilde{\epsilon} \to 0^+$. Ovo pitanje je bitno i

zahtjeva daljnje istraživanje. Kritični eksponent ν korelacijske duljine ξ mora divergirati u donjoj kritičnoj dimenziji, gdje je u Isingovom modelu pronađeno esencijalno skaliranje ξ povezano s proliferacijom instantona (kinkova i anti-kinkova) koji uništavaju prijelaz pri svakoj konačnoj temperaturi. Strogo govoreći, divergencija kritičnog eksponenta je nužan (ali ne i dovoljan) uvjet za esencijalno skaliranje, t.j., eksponencijalnu divergenciju korelacijske duljine kao funkcije udaljenosti od kritičnosti u temperaturi, te stoga i dalje istražujemo ovaj problem.

Zaključak koji se može donjeti u ovom trenutku je da niski redovi derivacijskog razvoja u sklopu FRG-a naizgled barem donekle dobro opisuju efekte vrlo neuniformnih konfiguracija u obliku kapljica koje kontroliraju kritično ponašanje sustava u klasi univerzalnosti Isingovog modela kad se približavamo donjoj kritičnoj dimenziji (gdje je $d_{lc} = 1$ u egzaktnom tretmanu). Matematički mehanizam koji to omogućuje je granični sloj u funkcijama u fiksnoj točci, a opisan je Singularnom Perturbacijskom Teorijom. Preostaje detaljnije vidjeti može li se proliferacija lokaliziranih pobuđenja (točkastih kapljica) koja su odgovorna za uništenje prijelaza u d_{lc} i koja dovode do esencijalnog skaliranja efektivno opisati aproksimacijama baziranim na razvoju oko uniformnih okrupnjenih konfiguracija.

U prethodnim poglavljima razmatrali smo derivacijski razvoj u sklpu FRG-a te kako (i ako) isti može reproducirati fizikalne situacije u kojima je dugovalna fizika dominirana prostorno lokaliziranim pobuđenjima kao što su kinkovi i anti-kinkovi koji se proliferiraju na donjoj kritičnoj dimenziji skalarne ϕ^4 teorije (koja je u klasi univerzalnosti Isingovg modela) ili kapljice koje kontroliraju kritično ponašanje kako se približavamo d_{lc}. U poglavlju 5 se bavimo drukčijim problemom u kojem su bitne vrlo neuniformne konfiguracije polja. to je uređena faza skalarne ϕ^4 teorije. U ovom slučaju je poznato da koegzistencija faza (dva čista uređena stanja slomljene simetrije) uključuje neuniformnu konfiguraciju u obliku domenskog zida. Ovakve neuniformne konfiguracije omogućuju gustoći slobodne energije ili efektivnom djelovanju da bude strogo konveksno (t.j., ravno) u unutrašnjoj domeni srednjeg polja u termodinamičkoj granici, kao što i zahtijeva njihova definicija preko Legendreovog transformata.

Našli smo preliminarne rezultate o efektivnom djelovanju ovisnom o skali, koje je centalna veličina FRG-a, u uređenoj fazi ϕ^4 teorije za $d > 1$. U ovom su slučaju konfiguracije polja koje kontroliraju termodinamiku (i asociranu koegzistenciju faza) neunifromni domenski zidovi. Što je specifično u ovom slučaju u odnosu na kritičnu točku istog modela u $d = 1 + \epsilon$ i u odnosu na ponašanje na donjoj kritičnoj dimenziji $d = 1$ je da su pobuđenja i dalje ekstenzivna u prostoru (iako samo u $\epsilon = d - 1$ dimenzija). Zbog toga im se energija skalira s L^ϵ, što sprječava njihovu proliferaciju, za razliku od kapljica u blizini kritičnosti za $d = 1 + \epsilon$ ili instantona za $d = 1$. Stoga u računu možemo koristiti aproksimaciju sedlene točke u prisutnosti infracrvenog regulatora, komplementiranu "1-loop" korekcijama (korekcijama jedne petlje) koje proizlaze iz Gaussijanskih fluktuacija oko te sedlene točke. Dodatna (u odnosu na homogeno/konstantno rješenje) slobodna energija domenskog zida povezana s napetošću površine se ne javlja u izrazu za efektivni potencijal ovisan o skali, budući da je isti veličina koja je definirana u termodinamičkoj granici gdje linearna mjera veličine sustava L divergira, a ovaj doprinos se s njom skalira kao $1/L$. Ipak, u opis povrata ka konveksnom efektivnom potencijalu u fizikalnoj $k \to 0$ granici nužno je uključiti ovo nehomogeno rješenje (a ne samo homogena/konstantna stanja), budući da je domenski zid odgovoran za $\propto -k^2\varphi^2$ doprinos potencijalu.

Postoji još nekoliko aspekata ovog računa koje želimo dovršiti. Prvo, potrebno je do kraja provesti račune jedne petlje kako bismo provjerili je li njihov neiščezavajući doprinos u termodinamičkoj granici proporcionalan s k^2 kao što bi se naivno činilo, ili je ovisnost o k modificirana (u smislu nižeg potencijskog zakona, k^a, $a < 2$), pogotovo za $d < 2$. Drugo, želimo usporediti ako i kako niži redovi derivacijskog razvoja (LPA, LPA', drugi red ∂_2) mogu reproducirati time predviđeno ponašanje efektivnog djelovanja ovisnog o skali. Ovo je pokazano za velik broj infracrvenih regulatora i dimenzije $d > 2$, no mi smo uglavnom zainteresirani za $d < 2$ te, specifičnije, okolinu donje kritične dimenzije.

Da rezimiramo, u ovoj tezi smo razmatrali koliko dobro funkcionalna RG, koristeći aproksimacijsku shemu koja se oslanja na razvoj oko uniformnih okrupnjenih konfiguracija (derivacijski razvoj), može opisati dugovalnu fiziku statističkih sustavima u kojima je ona kontrolirana vrlo neuniformnim fluktuacijama. Usredotočili smo se na dobro proučen primjer skalarne ϕ^4 teorije, koja je u klasi univerzalnosti Isingovog modela, u režimu prilaska njenoj donjoj kritičnoj dimenziji d_{lc}. Koristili smo kombinaciju numeričkih i analitičkih (Singularna Perturbacijska Teorija, aproksimacija sedlene točke i.t.d.) pristupa. Glavni je rezultat pronađeni mehanizam kojim je reproducirano kvalitativno ponašanje ovog modlea u granici $d \to d_{lc}$ na niskim redovima derivativnog razvoja, za koji je presudna neuniformna konvergencija (u polju) funkcija u fiksnoj točci povezana s pojavom graničnog sloja. U zaključnom poglavlju su također ponuđene daljne rasprave i perspektive ovog istraživanja, a neki od tehničkih detalja obrađeni su u nekoliko dodataka.

Contents

Chapter 1

Introduction

Since its introduction, the Renormalization Group (RG) has been the theoretical tool of choice for understanding and describing collective behavior characterized by an emergent scale invariance as in the vicinity of a continuous phase transition. It provides a powerful conceptual framework but, exact results being scarce, the search for generic and efficient approximation schemes has been very active from the beginning [1–6]. One recent line of research starts from an exact formulation of the Renormalization Group, in the form of a functional Renormalization Group (FRG) for scale-dependent generating functionals of correlation functions [7–9], and introduces potentially nonperturbative approximations through ansatze for the scale-dependent generating functional under study. The question that we address is to what extent such generic approximation schemes are able to describe specific problems in which the long-distance behavior involves strongly nonuniform configurations with, e.g., localized excitations.

An example of such an approximation scheme within the FRG is the so-called derivative expansion of the effective average action (coarse-grained Gibbs free energy in the language of magnetic systems) which amounts to truncating the functional form of the latter in powers of the external momenta or equivalently in gradients of the fields [10, 11]. The derivative-expansion approximation focuses on the long-wavelength properties and, in terms of coarse-grained configurations of the system, works as an expansion about uniform configurations. One may therefore wonder if such a scheme is able to capture the physics associated with nonuniform configurations containing, e.g., domain walls, spin waves, or localized defects such as the kinks and anti-kinks found in the instanton analysis of the 1-dimensional Ising model.

In this work we assess the ability of the derivative expansion of the FRG to quantitatively describe the long-distance physics of a model without a priori knowledge of the relevant real-space coarse-grained configurations, even when they are strongly nonuniform. To do so we investigate how low orders of the derivative expansion describe the approach to the lower critical dimension d_{lc} of the Ising-like scalar ϕ^4 theory which is expected to be controlled by the proliferation of localized excitations (instantons) [12–14]. FRG is well suited for this task since even the lowest orders of approximations are known to capture nontrivial nonperturbative phenomena [15, 16], and it has an advantage of being a general approach, unlike specialized approaches one must usually resort to capturing such behavior, like the droplet

theory in the case of the Ising model just above d_{lc}, where enclosed domains of one spin-orientation in the other (the droplets) must be introduced explicitly [12–14]. Additionally, the spatial dimension d is a parameter of the theory that we can vary. We show that the convergence of the fixed-point effective potential describing the critical point of the model is nonuniform in the field when the dimension d approaches d_{lc}, with the emergence of a boundary layer around the minimum of the potential. < At the lowest nontrivial approximation level (known as LPA') this allows us to make analytical predictions for the value of the lower critical dimension d_{lc} and for the behavior of the critical temperature as $d \to d_{lc}$, which are both found in fair agreement with the known exact results. We check the stability of the results upon increasing the approximation order by studying the second order of the derivative expansion (∂_2). The ∂_2 investigation is still in progress. As of yet, less has been found analytically due to the complexity coming from the nontrivial field renormalization function $z(\varphi)$ ($z(\varphi) = 1$ in LPA'). Numerical results above the d_{lc} show strong indications that the boundary layer persists, tentatively with the same behavior of the critical temperature in the d_{lc} limit. However, predictions of the value of the lower critical dimension require matching the boundary layer solution with the rest of the field domain, which we have not achieved at the present moment. We also consider for the same Ising-like scalar ϕ^4 model the ordered phase in the limit where $d \to d_{lc}$. We focus on the way the effective potential in the FRG becomes convex as the proper spatial fluctuations, which now involve nonuniform configurations with a domain wall separating two phases, are included in the calculation.

1 Functional Renormalization Group

1.1 General Renormalization Group Principles

Consider a macroscopic system, composed of an arbitrarily large number of constituents that interact. A correlation length ξ can be defined. This length scale is taken so that constituents separated by distances larger than $\mathcal{O}(\xi)$ interact weakly, while those inside a volume of $\mathcal{O}\left(\xi^d\right)$ are strongly correlated and exhibit collective behaviors. Here, d is the spatial dimension. One can then imagine building new, composite constituents from strongly correlated ones to describe long-range physics.

We have described a fundamental idea behind Renormalization Group (RG) methods [17–19]. Practically implementing such a scheme that builds an effective theory taking into account the strong correlations is challenging. Nevertheless, RG is conceptually and computationally powerful. As it is based mostly on scaling arguments not relying on specificities of the system, it is versatile and has proven its usefulness in many areas such as condensed matter (e.g., many-particle fermionic [20] or bosonic [21] systems, density functional theory [22–26]), cold atoms [27], high-energy physics [28–32] and quantum gravity [33, 34]. It deals with quantum and classical systems in and out of equilibrium. We continue the discussion in the context of equilibrium continuous phase transitions.

At criticality ξ diverges and one would have to integrate out *all* of the fluctuations in the system, making the procedure no less complicated than calculating a partition function from a microscopic theory. Surprisingly, a simplification occurs instead. As we coarse-grain the microscopic details out, the only relevant length scale left in an arbitrarily large system is the correlation length ξ. When ξ diverges we are left with scale invariance. This makes

critical systems statistically self-similar when examined at different length scales. L. Kadanoff [35, 36] realised that Widom's conjecture [37] about the singular part of the free energy being a homogeneous function of parameters which describe the deviation from the critical point is a consequence of scale invariance. This self-similarity at different scales thus means that the fluctuations coarse-grained up to some arbitrary length scale must be governed by effective actions close to the one we start from, to maintain the probability distribution across scales. Let us make this idea a bit more tangible, on a still abstract example where an approximate RG procedure can be used (a similar discussion can be found in, e.g., [38]). We start from a system that has one microscopic scale a (e.g., the lattice constant), and is described by an action S.[1] We coarse grain its possible configurations under the length scale ba, where $1 < b \ll \xi/a$. In the next step we re-scale all the length scales by b. The coarse-graining also changed the scale of the configurations (e.g., the field). We want to be able to map to a statistically self-similar set of configurations, so we can also allow for the re-scaling of the field by some scale ζ, which is generally different from b. This allows us to toggle the ζ with regards to b, to keep the effective action of the approximately same form through this transformation. We have roughly described some Renormalization Group transformation of the action S, which we term R_b, consisting of coarse-graining, rescaling the lenght-scales (by b) and renormalizing the fields (by ζ). We stress that these steps can alternatively be done in Fourier (momentum) space, as will be done in the FRG.

Iterative applications of the $S_{i+1} = R_b S_i$ transformation allows us to move in the space of actions S_i. The term "flow" is often used to describe this. The effective actions of self-similar systems describing their long-range physical properties should not change at all under this transformation, representing fixed points S^* of the R_b operator that satisfy $S^* = R_b S^*$. If a system exhibits fluctuations below the scale at which it is strongly correlated, e.g., if we start from a bare action, multiple RG steps might be necessary before a critical fixed point describing long-range universal behavior is reached, $S_c^* = \lim_{n\to\infty} R_b^n S_0$. We stress that critical fixed points are not the only fixed points that exist. The correlation length is a physically relevant scale and between $S_{i+1} = R_b S_i$ it is transformed as $\xi_{i+1} = \xi_i/b$. If we start from a finite ξ_0, RG steps make it smaller. We move away from the critical fixed point, meaning that this fixed point is not fully attractive, but a saddle [41, 42] with as many unstable directions as there are physical parameters needing to be fine-tuned to make the system critical. These unstable directions are called relevant in the RG language. In a stereotypical example, systems that move away from the fixed point that describes criticality flow towards either the ordered phase (zero-temperature attractor/fixed point) or the disordered phase (high-temperature attractor/fixed point) [17, 18, 38].

Contrary to the name, the R_b transformations (for different b's) form a semi-group and not a group: $R_{b=1}$ is an identity, taking two steps consecutively leads to the same result as taking them simultaneously or $R_{b_1} R_{b_2} = R_{b_1+b_2}$, but we cannot restore the information about the system under the scale we coarse-grained, so there is no invertibility.

It is convenient to calculate how physical quantities change under an infinitesimal rescaling $b \to b + db$. This results in differential flow equations. The fixed points of these equations

[1] Many different formalisms exist. E.g, in Wilson's RG [1, 39, 40] one builds an effective action S by coarse-graining in momentum space and then rescaling the UV cutoff to match the original Λ. In FRG an analogue of the Gibbs energy Γ is considered, also in momentum space, but an infrared (IR) momentum scale is introduced and varied instead [8].

conceptually correspond to the fixed points of the R_b operators, $S^* = R_b S^*$.

Not all actions will flow into a critical fixed point S_c^*, even if it exists. This is apparent, as not all systems are critical. But if a system exhibits a continuous phase transition, varying some relevant parameters, e.g., the temperature, can of course make it critical. To see how this translates into the language of RG flows, we look at a system that is perturbed by some arbitrarily small δS away from the critical fixed point, $S = S_c^* + \delta S$.[2] One can then linearize the effect of the Renormalization Group transformations R_b on S (or the flow equations themselves), in δS. In the language of nonlinear phenomena [41, 42], this gives the stability matrix of the fixed point S_c^*. The eigenvalues and eigendirections in the parameter space of S_i of this matrix are a crucial result of the RG. If the perturbed system given by S is away from a fixed point along some of these directions, it will either flow into or away from S_c^*, depending on the corresponding eigenvalue. The stable directions along which the flow ends up in the fixed point are called irrelevant, and they span the critical surface. It is named a surface because it is of lower dimensionality than the space of the flows, allowing for unstable directions. This is schematically presented in Fig. 1.1. In contrast, the fixed points describing the ordered and disordered phase are usually fully stable (attractors). The unstable directions that lead away from the fixed point are relevant, and moving along them (i.e., parallel to linear combinations of the relevant eigenvectors) corresponds in principle to the change of relevant physical parameters in an experimental setting. If there are n physical parameters that need to be fine-tuned to achieve a transition, there must be n relevant eigenvalues. Directions that are neither relevant or irrelevant are called marginal. Their qualification requires going beyond linearization.

Due to scale invariance, near criticality, physical quantities display power-law dependence on deviations of the values of these relevant physical parameters away from their critical values [17–19, 43], for example on temperature with $t = |1 - T/T_c|$ or magnetic field with h (away from $h = 0$) . Exponents of those power-laws are called critical exponents.

To see how this connects to scale invariance, we can consider the free energy density of a system with two unstable (relevant) directions t and h, given by

$$f(t, h) = \frac{F(t, h)}{V}, \tag{1.1}$$

where $V = L^d$ is the volume of the d-dimensional system under consideration. This corresponds to a conventional critical point (a higher number of relevant directions is associated with multi-critical points). Consider the coarse-graining and rescaling steps under which there is a $L \to bL$ transformation. When near criticality, the system is scale invariant, so the energy density is to remain the same:

$$f(t, h) = b^{-d} f(b^{y_t} t, b^{y_h} h). \tag{1.2}$$

Here $t \to b^{y_t} t$ (and analogously for h) has been used. This is due to the fact that rescaling with $b = b_1 b_2$ is the same as first rescaling by b_2 and then b_1, and that at criticality $t = h = 0$.

[2] For example, in many cases, it is enough to consider the space of actions S_i to be spanned by a set of couplings $C = \{C_1, ..., C_N\}$ allowed by the symmetry of the problem in question. Actually, all couplings allowed by symmetry must be considered, as they can be generated along the RG flow even if not present in the initial condition of the flow. This seems formidable but usually most couplings turn out to be irrelevant [17]. Then our perturbed system $S = S_c^* + \delta S$ would be given by couplings $\{C_1^* + \delta C_1, ..., C_N^* + \delta C_N\}$, with $\delta C_i \ll 1$ and C_i^* being their values in criticality.

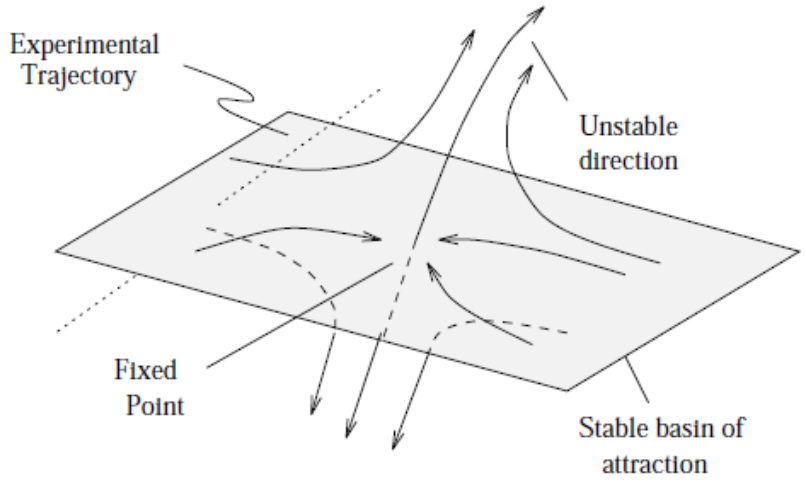

Figure 1.1 – Schematic representation of RG flows (picture taken from [38]). The stable basin of attraction is the critical surface.

Minding that t and h are relevant directions, as we rescale we must move away from criticality, so $y_t, y_h > 0$. These are the corresponding relevant eigenvalues. As an illustration of how critical power-law scaling is recovered from Eq. (1.2), we can choose to rescale by such b that $b^{y_t} t = 1$:

$$f(t,h) = t^{d/y_t} f\Big(1, h/t^{y_h/y_t}\Big). \tag{1.3}$$

To connect to a standardly defined critical exponent, we can recall that the magnetization $m(t,h)$ is obtainable by differentiating f with respect to h, directly giving the scaling:

$$m(t,h) = t^{(d-y_h)/y_t} m\Big(1, h/h/t^{y_h/y_t}\Big). \tag{1.4}$$

The critical exponent of interest, β, is defined as $m(t, h=0) \propto t^{-\beta}$, and we directly recover $\beta = -(d-y_h)/y_t$, connecting the eigenvalues of the unstable (relevant) directions with the critical exponents. Exponents for the susceptibility (γ), the heat capacity (α) or the source h with respect to magnetization (δ) can be similarly connected to the eigenvalues y_t and y_h as these physical quantities can be calculated from $f(t,h)$. At the same time this also reproduces and explains identities relating different exponents to each other (e.g., Rushbrooke's identity, $\alpha + 2\beta + \gamma = 2$ [19]), which were often first noticed in experiments.

The correlation length is similarly obtained as

$$\xi(t,h) = b\xi(b^{y_t} t, b^{y_h} h) = t^{-1/y_t} \xi\Big(1, h/t^{y_h/y_t}\Big), \tag{1.5}$$

relating the relevant eigenvalue y_t to the critical exponent ν, $\xi \propto t^{-\nu}$, as $y_t = 1/\nu$.

Concepts and ideas of this general RG introduction can be found elaborated in more detail in standard textbooks, lecture notes and reviews, like [15, 17–19, 38, 43–47].

1.2 Functional Renormalization Group methodology

Many perturbative RG approaches in condensed matter physics are based on the Wilsonian renormalization group [1, 39, 40]. Approaching RG in momentum space and separating low- and high-momentum (compared to some introduced momentum scale k) fluctuations, it is the first form of FRG. The implementation of schemes beyond perturbative RG is technically complicated in the Willsonian RG. Due to the nonperturbative nature of the fluctuations that are of interest to us, we turn to a more modern formulation of FRG, where the separation between low- and high-momenta is smooth and one deals with the generating functional of 1-particle irreducible (1-PI) correlation functions instead of the action.

Functional RG (FRG) is used when the functional form of quantities (like, e.g., the effective potential) are relevant, or when one needs to treat the problem at hand nonperturbatively [16]. FRG is an exact formulation of the RG ideas and as such it offers an exact flow equation for the scale-dependent generating functional of 1-PI correlation functions (which is, in the language of magnetism, the scale-dependent Gibbs free energy). This flow equation, known as the Wetterich equation [8, 16], is a complicated integro-differential equation and it generally cannot be solved. Its remarkable usefulness lies in the fact that such a formulation permits and suggests the use of nonperturbative approximation schemes, and the search for generic and efficient approximation schemes has been very active from the beginning [2–6, 39]. One of such nonperturbative schemes is the Derivative Expansion (DE), which we will consider in this thesis.

In Section 1.1 we introduced general concepts necessary to discuss any RG procedure. Now we can present a more formal picture for the FRG, starting from the partition function.

A general partition function $Z[J]$ for a system described by the action $S[\boldsymbol{\phi}]$ is given by the expression[3]

$$Z[\mathbf{J}] = \int_{\mathbf{x}} \mathcal{D}\boldsymbol{\phi} \exp\left(-S[\boldsymbol{\phi}] + \mathbf{J}\cdot\boldsymbol{\phi}\right), \tag{1.6}$$

where $\mathbf{J}$ is the source field, and the integral goes over all possible configurations of the field $\boldsymbol{\phi}$. All energy-related quantities in Eq. (1.6) are *reduced*, meaning that the thermodynamic $\beta = 1/k_B T$ is absorbed in $S[\boldsymbol{\phi}]$.

Following the general RG idea, we want to treat the microscopic fluctuations separately from the long-range ones. We do this in the momentum space for practical reasons. In this picture the microscopic fluctuations are the field modes with relatively large momenta, the "fast" ones. What is called fast is up to our choice. We artificially introduce a scale k into the system, and regard the modes with momenta $|\mathbf{q}| \gtrapprox k$ as fast, microscopic fluctuations.

To proceed, we need to decouple the fast from the slow modes in the partition function. We do that by "weighing down" the slow modes by a k-dependent change in the effective action $\Delta S_k[\boldsymbol{\phi}]$:

$$Z_k[\mathbf{J}] = \int \mathcal{D}\phi \exp\left(-S[\boldsymbol{\phi}] - \Delta S_k[\boldsymbol{\phi}] + \mathbf{J}\cdot\boldsymbol{\phi}\right), \tag{1.7}$$

[3] We use the conventions where $\int_{\mathbf{x}} = \int d^d x$, $\int_{\mathbf{q}} = \int d^d q/(2\pi)^d$ and "$\cdot$" stands for the scalar product, in the sense of $\mathbf{A}\cdot\mathbf{B} = \sum_i \int_{\mathbf{x}} A_i(\mathbf{x}) B_i(\mathbf{x})$, and analogously for products of vectors and operators represented by matrices. Bold quantities, like $\mathbf{J}$, stand for N-component vectors, $\mathbf{J}(\mathbf{x}) = (J_1(\mathbf{x}), ..., J_N(\mathbf{x}))$.

The concrete construction of $\Delta S_k[\boldsymbol{\phi}]$ involves an infrared (IR) regulator function R_k:

$$\Delta S_k[\boldsymbol{\phi}] = \frac{1}{2}\boldsymbol{\phi}\cdot\mathbf{R_k}\cdot\boldsymbol{\phi} = \frac{1}{2}\int_{\mathbf{q}} R_k\left(\mathbf{q}^2\right)|\boldsymbol{\phi}(\mathbf{q})|^2 \tag{1.8}$$

The scale-dependent action $S_k[\boldsymbol{\phi}]$ should respect the same symmetries as the starting action $S[\boldsymbol{\phi}]$ [16, 44]; so, when the problem is $O(N>1)$ or Z_2 symmetric, we have $R_{i,j}(\mathbf{q}) = R_k(\mathbf{q}^2)\delta_{i,j}$ as was already taken into consideration in Eq. (1.8). More on the regulator will be said in Section 1.2.2.

The $\Delta S_k[\boldsymbol{\phi}]$ is constructed so that it has minimal effect on the fast modes. The scale-dependent partition function $Z_k[\mathbf{J}]$ is then effectively the partition function including only the microscopic, fast modes. Te k scale is the IR cutoff of such a system, in the sense that fluctuations with momenta $|\mathbf{q}| \lesssim k$ are frozen out. This cutoff is constructed to be smooth. By changing the IR cutoff k, we change the scale of the problem and move along the RG flows. In the limit $k \to 0$ all of the fluctuations are integrated over and $Z_k[\mathbf{J}]$ corresponds to the physical partition function in Eq. (1.6):

$$Z_{k=0}[\mathbf{J}] = Z[\mathbf{J}], \tag{1.9}$$

hence $k = 0$ is the physical limit of this procedure.

1.2.1 Effective action formalism

The free energy $W[\mathbf{J}]$ is defined from the partition function according to

$$W[\mathbf{J}] = \ln\left(Z[\mathbf{J}]\right) \tag{1.10}$$

The ensemble average of the field

$$\varphi_i(\mathbf{x}) := \langle\phi_i(\mathbf{x})\rangle = \frac{\partial W[\mathbf{J}]}{\partial J_i(\mathbf{x})}. \tag{1.11}$$

is the most probable state of the system [16]. More generally, $W[\mathbf{J}]$ is the generating functional of the connected correlation functions [44]. Instead of the free energy $W[\mathbf{J}]$, which is a function of the source field $\mathbf{J}(\mathbf{x})$, one can work in terms of its Legendre transform $\Gamma[\boldsymbol{\varphi}]$, the effective action given by

$$\Gamma[\boldsymbol{\varphi}] + W[\mathbf{J}] = \mathbf{J}\cdot\boldsymbol{\varphi}, \tag{1.12}$$

whose natural variable is the average field $\boldsymbol{\varphi}(\mathbf{x})$ itself. As already mentioned, $\Gamma[\boldsymbol{\varphi}]$ is the generating functional of the 1-PI correlation functions [44]. In the language of magnetism, $W[\mathbf{J}]$ is an analogue of the Helmholtz and $\Gamma[\boldsymbol{\varphi}]$ of the Gibbs free energy, and $\boldsymbol{\varphi}(\mathbf{x})$ is the magnetization that can be used as an order parameter. In this picture, the source field $\mathbf{J}(\mathbf{x})$ is a function of $\boldsymbol{\varphi}(\mathbf{x})$:

$$J_i(\mathbf{x}) = \frac{\delta\Gamma[\boldsymbol{\varphi}]}{\delta\varphi_i(\mathbf{x})}. \tag{1.13}$$

We can define the scale-dependent equivalent of these quantities by using the scale-dependent partition function $Z_k[\mathbf{J}]$ (see Eq. (1.7)), starting with the free energy

$$W_k[\mathbf{J}] = \ln\left(Z_k[\mathbf{J}]\right). \tag{1.14}$$

We want to construct a running effective action $\Gamma_k[\boldsymbol{\varphi}]$ which would interpolate between the $k = \Lambda$ limit, where all fluctuations are frozen, and mean-field theory is exact:

$$\Gamma_\Lambda[\boldsymbol{\varphi}] = S[\boldsymbol{\phi} = \boldsymbol{\varphi}], \tag{1.15}$$

and the Gibbs free energy $\Gamma[\boldsymbol{\varphi}]$ at $k \to 0$, where all fluctuations are formally integrated into the theory:

$$\Gamma_{k=0}[\boldsymbol{\varphi}] = \Gamma[\boldsymbol{\varphi}]. \tag{1.16}$$

Notice that Eq. (1.15) holds for $\Delta S_\Lambda \to +\infty$, where it enforces the exactness of the saddle-point approximation, and is approximate in practice where ΔS_Λ is large but finite.

We modify the Legendre transform to reflect this [16]:

$$\Gamma_k[\boldsymbol{\varphi}] + W_k[\mathbf{J}] = \mathbf{J}\cdot\boldsymbol{\varphi} - \frac{1}{2}\boldsymbol{\varphi}\cdot\mathbf{R_k}\cdot\boldsymbol{\varphi}. \tag{1.17}$$

A consequence of this modification of the Legendre transform is that as long as not all of the fluctuations are integrated out, i.e., for $k \neq 0$, the effective action $\Gamma_k[\boldsymbol{\varphi}]$ does not need to be convex. Convexity is instead expected for the quantity $\Gamma_k[\boldsymbol{\varphi}] + \boldsymbol{\varphi}\cdot\mathbf{R_k}\cdot\boldsymbol{\varphi}/2$. In the limit $k \to 0$ the regulator term vanishes and $\Gamma_{k=0}[\boldsymbol{\varphi}]$ is convex, as it must be to match the Gibbs free energy.

1.2.2 Regulator

To achieve the decoupling of fast and slow modes, the regulator function $R_k(\mathbf{q}^2)$ must have certain generic properties. The modifier of the action $\Delta S_k[\boldsymbol{\phi}]$ vanishes in $k = 0$ by construction, so that $\Gamma_{k=0}$ corresponds to the Gibbs free energy. Therefore we put $R_{k=0}(\mathbf{q^2}) = 0$. In the opposite limit, Γ_Λ is to correspond to the bare action S. Therefore, $R_\Lambda(\mathbf{q}^2)$ must be much larger than any bare-action energy scale, so that all of the modes are "frozen" out by $\Delta S_\Lambda \gg 1$. Between these two limits, the function $R_k(\mathbf{q}^2)$ must suppress the slow modes with $|\mathbf{q}| < k$, and not affect the fast ones. So a generic $R_k(\mathbf{q}^2)$ function is a monotonously decreasing function. It is usually of $\mathcal{O}(k^2)$ for low momenta up to somewhat of a step at $|q| = k$, after which it tends to rapidly vanish. A sketch of this is given in Fig. 1.2

The choice of the regulator function would have no effect on universal quantities in fixed points, if one could do practical calculations exactly. Once approximation schemes are used in the exact FRG flow equation, this introduces dependence on $R_k(\mathbf{q^2})$. For the results to be useful, this dependence must not be significant and should also be understood. In practice, we will use two different regulator functions and allow for a regulator prefactor α to be adjustable to account for this. These are the Theta regulator and the exponential regulator, respectively:

$$R_k\left(\mathbf{q}^2\right) \propto \alpha\left(k^2 - \mathbf{q}^2\right)\Theta\left(k^2 - \mathbf{q}^2\right), \qquad R_k(\mathbf{q}) \propto \alpha k^2 e^{-\mathbf{q}^2/k^2}, \tag{1.18}$$

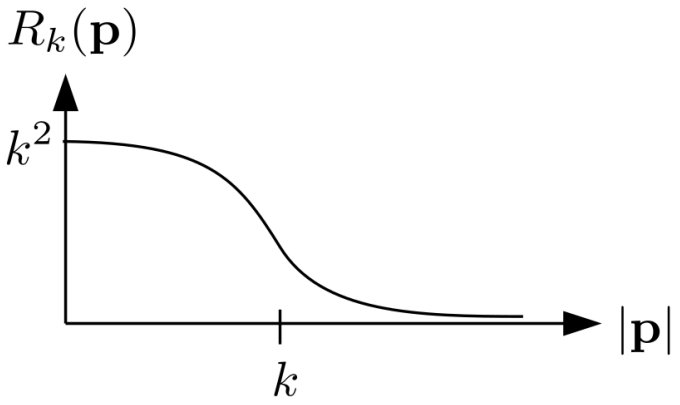

Figure 1.2 – Typical shape of the IR regulator function in dependence of momentum (picture taken from [16]).

where Θ denotes the Heaviside step function. The proportionality constant that has not been explicitly included in the above expressions pertains to the scaling of the regulator with k and will be clear when we introduce the field renormalization and the so-called dimensionless quantities in Section 1.2.5.

There exist several established ways of optimizing the choice of the regulator for the use in the DE approximation scheme. The Litim-Pawlowski optimization method [48–51] aims to maximize the convergence of a truncated flow (expanded in the field variable). The Principle of Minimal Sensitivity (PMS) compares different prefactors α for a same regulator function (it cannot compare across functional forms of the reguulator). It takes as optimal the value of α at which the physical quantities, e.g., the critical exponents, are least sensitive to its change (e.g., the value of α where the exponent $\eta(\alpha)$ admits an extremum) [16, 52, 53]. A third method is applicable to conformally invariant problems. This invariance results in identities for the effective action, and a regulator is chosen to minimize the deviations from these identities [54]. Good agreement has then been found with the prefactors optimized by PMS.

1.2.3 Exact flow equation for the effective action Γ_k

We seek flow equations for an effective action describing the universality class of a scalar ϕ^4 theory, as has been announced in the introduction to this chapter and will also be discussed in Section 2. This means that the field φ is a scalar, and $\Gamma_k[\varphi]$ is Z_2-symmetric.

To see how the scale-dependent quantities change with k, we directly take the derivative of the partition function, $\partial_k Z_k[J]$. When we express this in the terms of the scale-dependent free energy $W_k[J] = \ln(Z_k[J])$; it is termed the Polchinski equation [7] and it reads:

$$\partial_k W_k[J] = -\frac{1}{2}\int_{\mathbf{x}}\int_{\mathbf{y}} \partial_k R_k(\mathbf{x}-\mathbf{y})\left(\frac{\delta^2 W_k[J]}{\delta J(\mathbf{y})\delta J(\mathbf{x})} + \frac{\delta W_k[J]}{\delta J(\mathbf{y})}\frac{\delta W_k[J]}{\delta J(\mathbf{x})}\right). \tag{1.19}$$

To arrive at the equation for $\Gamma_k[\varphi]$, the Legendre transform relation Eq. (1.17) is partially differentiated with respect to k. Care must be taken to switch from ∂_k with the source J

held constant, to the same derivative with a constant average field $\varphi(\mathbf{x})$. One needs to use the identity

$$\int_{\mathbf{z}} \frac{\delta^2 W_k[J]}{\delta J(\mathbf{x})\delta J(\mathbf{z})}\left[\frac{\delta^2 \Gamma_k[J]}{\delta\varphi(\mathbf{z})\delta\varphi(\mathbf{y})} + R_k(\mathbf{x}-\mathbf{y})\right] = \delta(\mathbf{x}-\mathbf{y}) \tag{1.20}$$

to express the propagator in the RHS of Eq. (1.19) in terms of the effective action $\Gamma_k[\varphi]$:

$$G_k(\mathbf{x},\mathbf{y}) = \frac{\delta^2 W_k[J]}{\delta J(\mathbf{x})\delta J(\mathbf{y})} = \left[\frac{\delta^2 \Gamma_k[\varphi]}{\delta\varphi(\mathbf{y})\delta\varphi(\mathbf{x})} + R_k(\mathbf{x}-\mathbf{y})\right]^{-1}. \tag{1.21}$$

Here $[\cdots]^{-1}$ stands for the inverse of the operator. The propagator identity Eq. (1.20) is found directly form taking a functional derivative of the expression for the source $J(\mathbf{x})$,

$$J(\mathbf{x}) = \frac{\delta\Gamma[\boldsymbol{\varphi}]}{\delta\varphi(\mathbf{x})} + [R_k \cdot \varphi](\mathbf{x}), \tag{1.22}$$

with respect to the source itself, $J(\mathbf{y})$, and using:

$$\frac{\delta J(\mathbf{x})}{\delta J(\mathbf{y})} = \delta(\mathbf{x}-\mathbf{y}). \tag{1.23}$$

The result is the exact Wetterich flow equation [8]:

$$\partial_k \Gamma_k[\varphi] = \frac{1}{2}\int_{\mathbf{x}}\int_{\mathbf{y}} \partial_k R_k(\mathbf{x}-\mathbf{y})\left[\frac{\delta^2 \Gamma_k[\varphi]}{\delta\varphi(\mathbf{y})\delta\varphi(\mathbf{x})} + R_k(\mathbf{x}-\mathbf{y})\right]^{-1} \tag{1.24}$$

We note that the regulator function $R_k(\mathbf{q}^2)$ is constructed so that the derivative $\partial_k R_k$ in the flow equation decays fast enough for large momenta so that there is convergence in the UV limit.

The flows are often tracked in the so-called renormalizaton time $t = \ln(k/\Lambda) < 0$ where Λ is some momentum scale larger than any of the physical scales in the problem. The change of scale is then expressed by $\partial_t = k\partial_k$.

The flow Eq. (1.24) can be written in compact form, representing the space-integrals by a trace:

$$\partial_t \Gamma_k[\varphi] = \frac{1}{2}\,\mathrm{Tr}\left[\partial_t R_k\left(\Gamma_k^{(2)}[\varphi] + R_k\right)^{-1}\right], \tag{1.25}$$

with $\Gamma_k^{(2)}[\varphi]$ denoting the second (functional) derivative of the effective action with respect to φ. As we are considering the universality class of the scalar ϕ^4 theory, we have taken $\varphi(\mathbf{x})$ to be a scalar. In the case of an N-component vector field $\varphi(\mathbf{x}) = (\varphi_1(\mathbf{x}), ..., \varphi_N(\mathbf{x}))$, a trace over the components must also be taken in the RHS of the flow equation, Eq. (1.25) [16].

Defining an operator that only acts on the renormalization time dependence of the regulator function, $\tilde{\partial}_t = (\partial_t R_k)\partial_{R_k}$, Eq. (1.25) can be recast in a form that is often more practical for further algebraic manipulations:

$$\partial_t \Gamma_k[\varphi] = \frac{1}{2}\tilde{\partial}_t\,\mathrm{Tr}\left[\ln\left(\Gamma_k^{(2)}[\varphi] + R_k\right)\right]. \tag{1.26}$$

This makes apparent the 1-loop structure of the flow equation [55, 56]. If one uses the mean-field value $\Gamma^{(2)}[\varphi] = S^{(2)}[\varphi]$ in the RHS of Eq. (1.26), the 1-loop result [44, 57]

$$\Gamma^{1-\text{loop}}[\varphi] = S[\varphi] + \frac{1}{2}\,\text{Tr}\left[\ln\left(S^{(2)}[\varphi]\right)\right] \tag{1.27}$$

is recovered. This means that sensible approximation schemes for the FRG always reproduce one-loop results.

1.2.4 Derivative expansion

The Derivative Expansion (DE) is an ansatz for the effective action $\Gamma_k[\varphi]$. It is a series in the spatial derivatives of the average field, $\nabla\varphi(\mathbf{x})$, or equally in the momenta.

We are going to use the DE up to the second order (shortened to DE2 or ∂_2), where the ansatz is given by:

$$\Gamma_k[\varphi] = \int_{\mathbf{x}} \left\{ U_k[\varphi(\mathbf{x})] + \frac{1}{2} Z_k[\varphi(\mathbf{x})](\nabla_{\mathbf{x}}\varphi(\mathbf{x}))^2 \right\}. \tag{1.28}$$

The full field dependence of the functionals $U_k[\varphi]$ (the effective potential) and $Z_k[\varphi]$ (the field renormalization function) is kept, meaning that this approach is nonperturbative in the couplings. $U_k[\varphi]$ and $Z_k[\varphi]$ (and their field-derivatives) are in this text sometimes referred to as *RG functions*.

To move forward with the Wetterich Eq. (1.24), we must find the ∂_2 expression for the propagator, and thus the second field derivative of the ∂_2 effective-action ansatz from Eq. (1.28):

$$\begin{aligned}\Gamma^{(2)}_{\mathbf{x},\mathbf{y}}[\varphi] := \frac{\delta^2\Gamma_k[\varphi]}{\delta\varphi(\mathbf{y})\delta\varphi(\mathbf{x})} =& \left\{ U_k''[\varphi] - \frac{1}{2} Z_k''[\varphi](\nabla\varphi)^2 - Z_k'[\varphi]\nabla^2\varphi(\mathbf{x}) \right\}\delta(\mathbf{x}-\mathbf{y}) + \\ &- Z_k'[\varphi]\nabla\varphi(\mathbf{x})\nabla\delta(\mathbf{x}-\mathbf{y}) - Z_k[\varphi]\nabla^2\delta(\mathbf{x}-\mathbf{y}).\end{aligned} \tag{1.29}$$

We are showing this expression to underline the fact that ∂_2 is constructed with long-wave fluctuations and physics in mind. One can note conceptual similarities with the Ginzburg-Landau approach [58] from the ansatz in Eq. (1.28) itself, and indeed, the DE is best suited to describe configurations with smooth, long-wavelength deviations from a uniform coarse-grained field $\varphi(\mathbf{x}) = \varphi$. This is made even clearer in the next step, where after computing the necessary field derivatives, i.e., Eq. (1.29), we take $\varphi(\mathbf{x})$ to be uniform. In addition, it has been identified that the corrections to second order and higher in the DE are suppressed by a factor η [53, 59], which is not a small quantity in the ϕ^4 theory when one nears the lower critical dimension d_{lc}, where strongly nonuniform fluctuations proliferate.[4] A natural and still open question arises. How well can the derivative expansion deal with nonuniform fluctuations? This is especially relevant for systems with complicated microscopic physics, e.g., in the presence of quenched disorder, where such configurations are expected but unknown, so that it is not always feasible to tailor theoretical treatments where nonuniform fluctuations are introduced by hand.

[4] In fact, it is found to be $\eta = 1$ at $d_{lc} = 1$ in the exact treatment of the Ising model [60, 61].

We use round brackets for the φ dependence when it is taken uniform, for emphasis. The effective potential is then given by

$$U_k(\varphi) = \frac{\Gamma_k(\varphi)}{V}, \tag{1.30}$$

and the flow equation for $U_k(\varphi)$ is trivially inherited from the Wetterich equation Eq. (1.24) for the effective action, evaluated with a uniform φ after all of the functional derivatives involved have been carried out, like in Eq. (1.29).

To find the flow equation for the field renormalization function, we note that for a uniform configuration, the second derivative of the action $\Gamma^{(2)}_{\mathbf{x},\mathbf{y}}[\varphi]$ given by Eq. (1.29) reduces to:

$$\Gamma^{(2)}_{\mathbf{q}}(\varphi) = U_k''(\varphi) + \mathbf{q}^2 Z_k(\varphi), \tag{1.31}$$

where a Fourier transform has been performed. The function $Z_k(\varphi)$ can then be obtained as

$$Z_k(\varphi) = \left.\frac{\partial \Gamma^{(2)}_{\mathbf{q}}(\varphi)}{\partial(\mathbf{q}^2)}\right|_{\mathbf{q}^2=0}, \tag{1.32}$$

which allows us to find its flow equation by twice (functionally) differentiating the Wetterich Eq. (1.24) with respect to the field, evaluating the outcome in a uniform configuration, taking a Fourier transform of the result, and identifying the term $\propto \mathbf{q}^2$.

With φ taken uniform in Eq. (1.29), the otherwise complicated problem of inverting the functional on the RHS of Eq. (1.21) becomes algebraic in the momentum space, giving the following expression for the propagator:

$$G_k\left(\mathbf{q}^2\right) = \frac{1}{U_k''(\varphi) + R_k(\mathbf{q}^2) + \mathbf{q}^2 Z_k(\varphi)}, \tag{1.33}$$

a final ingredient needed in the Wetterich equation. Before proceeding with the expressions for the ∂_2 flow equations, we introduce dimensionless quantities.

1.2.5 Scale invariance at criticality and dimensionless quantities

We are interested in criticality, where scale invariance emerges due to the divergence of the correlation length [17, 18, 43]. This invariance to changes in scale prompts us to consider fixed points of the flow equations; yet, the use of an IR regulator explicitly introduces a scale k, breaking down scale invariance. To get a clearer picture of the scale-invariant behavior, it is common and practical [15, 16] to work with *dimensionless* (as opposed to *dimensionful*) RG functions. We move from dimensionful to dimensionless (marked by a tilde) quantities and *vice versa* by multiplying them with appropriate powers of the momentum cutoff k, which is analogous to re-scaling after coarse-graining.

The scaling of momenta and lengths with k is simply

$$y = \mathbf{q}^2/k^2 \quad \text{and} \quad \tilde{\mathbf{x}} = k\mathbf{x}, \tag{1.34}$$

and the scaling of the rest of the relevant variables and functions that comes form dimensional analysis of the effective-action ansatz Eq. (1.28) is given by:

$$\begin{aligned} &U_k(\varphi) = k^d \tilde{u}_k(\tilde{\varphi}); \\ &\varphi^2 = Z_k^{-1} k^{(d-2)} \tilde{\varphi}^2, \quad Z_k(\varphi) = Z_k \tilde{z}_k(\tilde{\varphi}), \quad R_k\left(\mathbf{q}^2\right) = Z_k k^2 y \tilde{r}(y). \end{aligned} \tag{1.35}$$

In the second row of Eq. (1.35) a constant Z_k is introduced, as from $\Gamma_k(\varphi)$ we can infer the scaling of, e.g., $\varphi^2 Z_k(\varphi)$, but not φ or $Z_k(\varphi)$ separately. For this, we look at the propagator expression, Eq. (1.33), in combination with Eq. (1.35):

$$G_k^{-1}\left(\mathbf{q}^2\right) = Z_k k^2 [\tilde{u}_k''(\tilde{\varphi}) + y(\tilde{r}(y) + \tilde{z}_k(\tilde{\varphi}))], \tag{1.36}$$

where the expression in the square brackets is dimensionless. For small momenta and near criticality we expect the propagator to behave as $G^{-1}(\mathbf{q}^2) \sim |\mathbf{q}|^{2-\eta}$ [17], with η being the anomalous dimension. The regulated $G_k^{-1}(\mathbf{q}^2)$ has a mass term as long as $k \neq 0$ and we do not expect this behavior for $|\mathbf{q}| \ll k$, so we introduce a scale-dependent anomalous dimension

$$\eta_k = -\partial_t \ln(Z_k), \tag{1.37}$$

with the physical limit $\eta_{k\to 0} \to \eta$. To calculate it, we define Z_k by imposing a *renormalization condition*

$$\tilde{z}_k(\tilde{\varphi}_r) = 1 \quad \Longrightarrow \quad Z_k = Z_k(\varphi_r) \tag{1.38}$$

at some renormalization point φ_r which may be scale (k) dependent. Now, the anomalous dimension can be calculated from

$$\eta_k = -\partial_t [\ln(Z_k(\varphi_r))]. \tag{1.39}$$

If we could work with the exact Wetterich equation without approximations, the choice of φ_r would be irrelevant. However, as with the regulator, once approximations are introduced, one must consider the choice of φ_r. In the lowest order of the derivative expansion which is called the Local Potential Approximation (LPA), $Z_k(\varphi)$ is taken as a constant and $\eta_k = 0$ by construction. We do not use LPA as $\eta = 0$ prevents us from studying the criticl behavior below $d = 2$ (see Chapter 2). At the next order, the minimally modified LPA', $Z_k(\varphi)$ is a constant in the field but not in k so that it scales with the scaling dimension $-\eta_k$. It has been found that for LPA' it is best to renormalize at the location of the minimum of the effective potential $\varphi_{min,k}$ [62, 63], and this is what we use. The next order is ∂_2 itself, where the specific choice of φ_r is less relevant. As it is more practical to enforce the Z_2 symmetry, at ∂_2 we will renormalize in the origin, $\varphi = 0$.

The flow of a dimensionless function $\tilde{F}(\tilde{\varphi})$ is connected to the flow of the dimensionful function $F(\varphi)$ over the corresponding scaling dimension D_F:

$$\begin{aligned} &\partial_t|_\varphi F(\varphi) = \beta_F \quad \text{and} \quad F(\varphi) = k^{D_F} \tilde{F}(\tilde{\varphi}) \quad \Longrightarrow \\ &\Longrightarrow \quad \partial_t|_{\tilde{\varphi}} \tilde{F}(\tilde{\varphi}) = -D_F \tilde{F}(\tilde{\varphi}) + D_\varphi \tilde{\varphi} F'(\tilde{\varphi}) + \beta_{\tilde{F}}, \quad \text{with} \quad \beta_{\tilde{F}} = k^{-D_F} \beta_F, \end{aligned} \tag{1.40}$$

where the β-functions represent the nontrivial part of the flow (which can be found from the Wetterich Eq. (1.24)), and the rest is dubbed the scaling part of the flow (found by the

standard chain rule for derivatives and switching from fixed φ to fixed $\tilde{\varphi}$). The β-functions are actually functionals and depend on RG functions, the anomalous dimension η and contain the regulator, as can be seen in Section 1.3.

In the rest of the chapters we drop the tilde from the dimensionless quantities to avoid cluttering the notation, as we do not discuss their tilde-less dimensionful versions, unless otherwise stated.

1.3 Flow equations in the second order of the derivative expansion

Directly following the above explained procedure leads to the flow equations for the dimensionless effective potential and field renormalization function, given by

$$\partial_t u_k(\varphi) = -du_k(\varphi) + (2-\eta_k)\,\tilde{\epsilon}_k\,\varphi u_k'(\varphi) + 2v_d \ell_0^{(d)}(\varphi;\eta_k), \tag{1.41}$$

$$\begin{aligned}\partial_t z_k(\varphi) =& \eta_k z_k(\varphi) + (2-\eta_k)\,\tilde{\epsilon}_k\,\varphi\; z_k'(\varphi) + \\ &+ \frac{2}{d} v_d \Big\{ \left(z_k'(\varphi)\right)^2 \left[(2d+1)\,\ell_2^{(d+2)}(\varphi;\eta_k) - 2m_{4,0}^{(d+4)}(\varphi;\eta_k)\right] - d z_k''(\varphi)\,\ell_1^{(d+2)}(\varphi;\eta_k) + \\ &+ 2z_k'(\varphi)\,u_k'''(\varphi)\left(d\ell_2^{(d)}(\varphi;\eta_k) - 2m_{4,0}^{(d+2)}(\varphi;\eta_k)\right) - 2\left(u_k'''(\varphi)\right)^2 m_{4,0}^{(d)}(\varphi;\eta_k)\Big\}.\end{aligned} \tag{1.42}$$

The constant v_d is the surface of a d-dimensional unit sphere, given by:

$$v_d = \frac{1}{2^{d+1}\sqrt{\pi}^d \Gamma(d/2)}. \tag{1.43}$$

It comes from the momentum integration on the RHS of the Fourier transform of the Wetterich Eq. (1.24), and so do the threshold functions $\ell_n^{(d)}$ and $m_{n,0}^{(d)}$:

$$\ell_{n\geqslant 0}^{(d)}(\varphi;\eta_k) = -\frac{1}{2}\int_0^{+\infty} dy\, y^{d/2-1}\tilde{\partial}_y \begin{Bmatrix} g_k^n(y,\varphi), & n>0 \\ \ln\left(g_k(y,\varphi)\right), & n=0 \end{Bmatrix}, \tag{1.44}$$

$$m_{n,0}^{(d)}(\varphi;\eta_k) = -\frac{1}{2}\int_0^{+\infty} dy\, y^{d/2}\tilde{\partial}_y\Big\{\left(\partial_y g_k(y,\varphi)\right)^2 \left(g(y,\varphi)\right)^{n-4}\Big\}. \tag{1.45}$$

Here $g(y,\varphi) = k^{-(2-\eta_k)}G_k(\mathbf{q}^2)$ is the dimensionless propagator and the derivation operator $\tilde{\partial}_y$ marked by a tilde only acts on the dimensionless regulator $r(y)$, such that

$$\tilde{\partial}_y r(y) = -\left(\eta_k r(y) + 2y r'(y)\right). \tag{1.46}$$

This is because $\tilde{\partial}_y$ comes from the flow of the dimensionful regulator, $\partial_t R_k(\mathbf{q}^2)$, and applies to dimensionless quantities. Explicit expressions for the threshold functions are given in Appendix A. We stress that the threshold functions are functionals of the Renormalization Group functions and they also depend on the anomalous dimension η_k:

$$\ell_n^{(d)}(\varphi;\eta_k) = \ell_n^{(d)}\left(u_k''(\varphi), z_k(\varphi);\eta_k\right), \qquad m_{n,0}^{(d)}(\varphi;\eta_k) = m_{n,0}^{(d)}\left(u_k''(\varphi), z_k(\varphi);\eta_k\right). \tag{1.47}$$

In the flow equations Eqs. (3.2) and (3.3) we did not write out these dependences explicitly to make the expressions less cluttered.

The full expressions for the relevant flow equations will also be given in Chapter 2 for the minimally modified Local Potential Approximation (LPA') and Chapter 3 for ∂_2, where they will be used.

2 Strongly nonuniform fluctuations

There are systems which are both theoretically interesting and relevant to the description of real physical problems whose important qualitative and quantitative properties at long distance are dominated by the effects of nonuniform fluctuations.

In the following we list a few examples of such systems and briefly touch on how they are treated in the framework of the derivative expansion scheme for FRG.

First we consider the return to convexity of the scale-dependent effective action in the ordered low-temperature phase of the $O(N)$ model. The effective action Γ (corresponding to the Gibbs free energy of a magnetic system) is a Legendre transform of the free energy (defined as the logarithm of the partition function), and must thus be convex. It is not simple to build an adequate description of the low temperature phase. One has to account for the possible coexistence of different phases, meaning that even small changes in external conditions can cause significant changes in the configurations the system can adopt. This means that the convexity results from strongly nonuniform fluctuations in configuration space which are hard to handle by perturbative methods. However, the return to convexity in the ordered phase of the $O(N)$ model can already be captured at the lowest order (LPA) of the nonperturbative derivative expansion scheme of FRG, as discussed in [15, 64, 65] and especially [66]. In the case of the ordered phase of $O(N)$ treated by the FRG, one starts from some nonconvex Landau action that has a double well shape which is regarded as the (mean-field) initial condition, and the convexity is restored along the RG flows by integrating all the fluctuations into the effective action. The fluctuations that are responsible for the return to convexity are nonuniform configurations such as spin waves or domain walls [15, 65, 67], and it is interesting that the LPA and ∂_2 reproduce this property.

Another famous example, recently revisited in the FRG context in [68], is localized excitiations (vortices) dominating the mechanism of the Berezinskii-Kosterlitz-Thouless (BKT) transition. The BKT transition is observed in the $O(N = 2)$ model in $d = 2$ [69–72], and is found in other two-dimensional systems with global $O(2)$ symmetry such as liquid helium films [73–76], trapped $2d$ atomic gasses [77–80], $2d$ superconductors [81] and others. While the Mermin-Wagner theorem [82] states that there can be no spontaneous symmetry breaking in $d = 2$ (which is the lower critical dimension for $O(N > 2)$ models), a transition to algebraic order (power-law decay of correlations with distance) happens due to the binding of vortex-antivortex pairs. This is of interest to us as the vortices are localized topological defects, as evident from their mapping to the $2d$ Coulomb gas of point charges [45, 71, 72] or to the sine-Gordon model where vortices are conceptually connected to the soliton solutions the model admits [72, 83], solitons being localized (and stable) wave solutions [84]. An FRG description of the BKT transition using the second order of the derivative expansion was first attempted about twenty years ago [85], and has been improved on in the last There

is another recent study [86] whose interest is whether FRG can capture genuine topological defects. The authors benchmark this starting from a one-dimensional anharmonic oscillator (a quartic correction to the harmonic case is added). They aim to calculate the gap between the ground state and the first excited state using FRG. It is clear that with a change of sign of the mass term, they can switch to our double-well potential of the scalar ϕ^4 theory. However, their interest lies in the description of tunneling, which is a direction we plan to undertake in the future and is out of the scope of this text. It is still interesting and fitting to resent their results here, as they work in the regime where instantons (or kinks, described in Section 2.2) rule the phyisics of the problem. The authors deal with a quantum mechanical double well potential, so their results are given as a comparison of numerically obtained average estimates of different formulations of the flow equations with the accurate results coming from the Schrödinger equation approach to the problem. The agreement of most FRG treatments used is excellent for the anharmonic oscillator, but in the case of the double-well potential, this is not the case for relatively small values of the quartic coupling, showing that the problem we are undertaking is once more not well, in full, represented in the existing literature.

Another interesting system involving strongly nonuniform configurations is the Random Field Ising Model (RFIM). The random field represents a quenched (static) disorder that couples linearly with the local order parameter. This makes the RFIM a challenging problem and an interesting example of collective behavior due to the competition between order (from the interactions) and disorder (from the random fields). The long-distance physics is controlled by nonuniform configurations in the form of avalanches and droplet excitations that become scale-free at criticality. Their effect has been shown to be properly accounted for by the truncated DE even at ∂_2 and LPA' thanks to a careful account of the functional character of the RG [87–93]. The equilibrium RFIM has a lower critical dimension of $d_{lc} = 2$ [94, 95], at which the fluctuations destroy the transition. The equilibrium and out-of-equilibrium RFIM's are not in the same universality class below $d \approx 5.1$ [92, 96] even though their critical exponents are numerically very close [97–99]. It is however not yet clear whether they share the same lower critical dimension $d_{lc} = 2$, with arguments both for [100] and against [101]. The physics of in- and out-of-equilibrium cases is different. In equilibrium, there is a critical fixed point for $d > 2$ corresponding to a paramagnetic-to-ferromagnetic transition [102–104]. The out-of-equilibrium case describes a hysteresis transition that appears when the RFIM is athermally driven by an external magnetic field. In the limit of quasistatic changes of the applied field, a critical point is found on both branches of the hysteresis curve (magnetization vs. field, with the field either increasing or decreasing) [105–108]. The "phases" at play are a high-disorder phase with a smooth hysteresis curve in the thermodynamic limit and a low-disorder phase with a discontinuous jump. Even though they appear quite different, the two situations at criticality are characterized by the presence of scale-free avalanches (which are discontinuous collective events) in the relevant coarse-grained configurations. The FRG (and its generic approximation schemes, such as DE) is especially relevant here as the avalanches cause nonanaliticities in the functional dependence of the fixed-point effective action that cannot be treated perturbatively [92].

In all of these systems it is crucial to consider and appropriately account for nonuniform fluctuations, and the DE seems to fare well with the task (even though still not everything is clear about the FRG description of these systems). Yet, the jury is still out when the

relevant coarse-grained configurations that control the large-scale behavior involve localized excitations such as the kinks and anti-kinks found in the instanton analysis of the $1d$ Ising model [109] or in the $1d$ sine-Gordon model [110, 111]. We therefore choose to investigate the scalar ϕ^4 theory near its lower critical dimension. It is the field-theoretical continuum version of the Ising model [18, 19], as can be heuristically shown by using auxiliary-field Hubbard-Stratonovich transformations [44, 112]. This makes it a paradigmatic model of a discrete-symmetry system where the transition is destroyed by localized excitations - the kinks and anti-kinks described in Section 2.2 in the context of the Ising model. The action of the scalar ϕ^4 theory is given by

$$S[\phi] = \int d^d x \left\{ \frac{1}{2}(\nabla\phi(\mathbf{x}))^2 + \frac{r}{2}\phi^2(\mathbf{x}) + \frac{g}{4!}\phi^4(\mathbf{x}) \right\} \tag{1.48}$$

and can be found in most textbooks on critical phenomena, e.g., [18, 19, 44, 113]. Here, d is the spatial dimension and the constant g is the coupling constant for the interaction term, which becomes irrelevant in the RG sense above the upper critical dimension $d_{uc} = 4$ [44, 114]. At and above $d_{uc} = 4$, depending on the sign of the coupling r, there can be spontaneous symmetry breaking ($r < 0$) or just the disordered phase ($r > 0$), with $r = 0$ being the critical value leading to the identification $r \sim T - T_c$.

We stress that, eventually, our interest lies in systems where the nature and existence of suspected strongly nonuniform fluctuations is not simply accessible through a saddle-point approximation, e.g., droplets of all kinds in glassy systems such as spin glasses [115–117]. When the nature of the the nonuniform fluctuations is unknown, one cannot use specifically tailored approaches to capture the related physics. A possible path would then be to use a generic approximation scheme such as DE, as one does not have to put in by hand the putative nonuniform fluctuations. We are interested in the ϕ^4 theory in this light.

2.1 Lower critical dimension

The effects of fluctuations at the critical point are not equally important in every spatial dimension d. Take a system that exhibits a continuous phase transition and whose constituents have short-range interactions. In higher dimensions, each constituent has many neighbors to interact with. These interactions favor ordering, which minimizes the energy contribution to the free energy. When we go down in d there are less and less neighbors to interact with, and the entropic contribution in the free energy becomes more and more significant compared to the energy. This opposes ordering. The critical temperature is then pushed to progressively lower values, until at some $d = d_{lc}$ ordering at finite temperatures becomes impossible. This defines the lower critical dimension.

Take the ϕ^4 theory as an example. Above the upper critical dimension, $d_{uc} = 4$, the impact of the fluctuations on the critical behavior is negligible and the mean-field exponents describe the criticality exactly [18, 118]. In the RG language, the quartic coupling becomes irrelevant [17, 44]. Criticality is then described by the Gaussian fixed point, corresponding to a non-interacting field theory described by quadratic fluctuations. Below d_{uc} this fixed point becomes unstable, because the quartic interaction becomes relevant and grows under RG transformations [17, 44]. This means that flows started near the Gaussian fixed point move away from it as we coarse-grain and consider larger scales. Another critical fixed point, the Wilson-fisher fixed point, emerges as the stable attractor of *critical* flows in $d = 4 - \epsilon$,

$\epsilon > 0$ [2]. This is a nontrivial critical fixed point that accounts for interactions and gives nontrivial critical exponents different from the mean-field ones. The perturbative predictions given in terms of an expansion in $\epsilon = 4 - d$ have been been found to give good results (even for $\epsilon = 1$ when resummation schemes are used) [118, 119]. However, as we go down towards the lower critical dimension d_{lc}, the role of the fluctuations becomes even more pronounced and they have to be treated nonperturbatively in the coupling constant. For the $O(N > 2)$ models the second order ∂_2 of the derivative expansion gives good results down to the lower crtitical dimension $d_{lc} = 2$ [16]. The fluctuations that destroy this transition, though, are the Goldstone modes [82] which are in essence long-wavelength, extended fluctuations and are properly captured by the derivative expansion.

Exact results for the Ising model in zero external field tell us that there is a continuous transition at a finite temperature in $d = 2$ [120], but not in $d = 1$ [60]. Thus the exact lower critical dimension is $d_{lc} = 1$.

2.2 Peierls argument

While in this thesis we do calculations for the Ising universality class, our goal is not to provide another characterization of this problem but to assess how approximations of the FRG can describe the events that destroy ordering at d_{lc}, which are kinks (or instantons [84, 109]).

The Peierls argument states that proliferation of these localized excitations in a $1d$ Ising-like system is due to their finite energetic cost and comes with an entropic gain that destroys long-range order. The argument is detailed by Peierls in [121] and revisited in textbooks such as [43, 45]. The essence of the argument can be demonstrated by considering the contribution of one kink to the free energy of the ordered phase of the Ising model in $d = 1$.

The Hamiltonian for the Ising model with nearest-neighbor ferromagnetic interactions is given by [60, 61]

$$H = -J \sum_{\langle i,j \rangle} s_i s_j, \qquad J > 0, \quad s_i = \pm 1, \tag{1.49}$$

where $\langle i, j \rangle$ denotes nearest neighbors on the lattice. The energy for the $1d$ chain is minimized by the ordered configuration where all of the spins point in the same direction (i.e., all s_i have the same sign).

If we now choose a location along an ordered spin chain after which we flip all the spins to the opposite sign, like in Fig. 1.3, there is a finite energetic cost of $2J$ associated with this kink configuration.

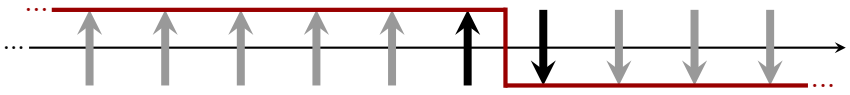

Figure 1.3 – Example of an Ising chain configuration with one kink.

At finite temperatures, such excitations represent thermal fluctuations. For a thermalized system, we need to consider the free energy F and account for their entropic contribution. If there are N spins, there are $\sim N$ locations for the kink, and the entropic contribution of

one kink is then $\propto \ln(N)$:

$$\Delta F = \Delta E - T\Delta S \quad \approx \quad 2J - \beta^{-1} \ln N \quad \overset{N\to\infty}{\longrightarrow} \quad -\infty. \tag{1.50}$$

In the thermodynamic limit $N \to +\infty$ it is obviously more favorable to have a kink than not to, and this only becomes more pronounced with more and more kinks which therefore destroys any order (associated with a nonzero spontaneous magnetization).

The destruction of the transition in $d = 1$ by the proliferation of localized defects can also be seen for example in the sine-Gordon model [110, 111] where the instantons connect neighboring minima of the periodic potential (instead of across a double-well potential of the ϕ^4 theory).

As we want to assess the ability of the derivative expansion to describe the long distance physics without *a priori* knowledge of the relevant real-space coarse-grained configurations, kinks in a Z_2-symmetric system are a better benchmark than the Goldstone modes that destroy long-range ordering in models with a continuous symmetry.

2.2.1 In the context of FRG

At criticality and for the physical $k \to 0$ limit, the dimensionful effective potential $U_k(\varphi)$ is convex and has a minimum in the origin, $\varphi_{min} = 0$, reflecting the fact that the coarse-grained dimensionful order-parameter field vanishes at the continuous phase transition. However, this is not the case for the dimensionless effective potential. The fixed point solution for the dimensionless effective potential $\tilde{u}(\tilde{\varphi})$ has a nonconvex double-well shape [15, 16], with finite dimensionless minima in $\pm\tilde{\varphi}_{min}$.

Looking at the scaling of the field with the momentum cutoff k

$$\varphi_{min} = k^{(d-2+\eta)/2}\tilde{\varphi}_{min}, \tag{1.51}$$

we see that as long as $d - 2 + \eta > 0$, it is possible to have a finite dimensionless field with the dimensionful one vanishing when $k \to 0$, which describes a continuous transition. Even for $k > 0$ and a finite dimensionfull φ, for $d - 2 + \eta > 0$ we have $\tilde{\varphi} \gg \varphi$. The dimensionless perspective "magnifies" critical fluctuations around the origin. These fluctuations are small and well controlled for $k \ll 1$ as long as $d - 2 + \eta > 0$. This is not the case when $d - 2 + \eta = 0$. The transition is destroyed by fluctuations. We see conceptual agreement with the Peierls argument, which is then reflected in FRG as the field not rescaling or the condition $d_{lc} - 2 + \eta(d_{lc}) = 0$, at the lower critical dimension.

This can also be seen from another perspective. If a correct description of the lower critical dimension limit can be found in the FRG, it should account for the disappearance of the transition and of the ordered phase. These are represented in FRG flows by a critical fixed point and a zero-temperature fixed point, respectively. The critical fixed point is a saddle with as many unstable (relevant) directions as there are physical relevant parameters to be adjusted for the system to reach criticality. The zero-temperature fixed point is a stable attractor (a sink for flows of dimensionfull quantities). The merging of the two fixed points would represent a bifurcation event [41, 42] in which the unstable (relevant) directions of the saddle become marginal. There is an always present trivial[5] relevant eigenvalue $\lambda =$

[5] This will be discussed in Chapter 4, Section 3.

$-(d-2+\eta)/2$ associated with the applied source (magnetic field). The condition for it becoming marginal is the same as for the field not rescaling.

Another anticipated feature of the approach to the lower critical dimension, also related to the merging of the critical and zero-temperature fixed points in the $d \to d_{lc}$ limit, is that the propagator of the theory should approach a singularity. This is because the zero-temperature fixed point is associated with the symmetry-broken ordered phase and the return to convexity of the dimensionful effective potential along the FRG flow is then controlled[6] by the presence of a singularity in the propagator [15, 65, 66].

For practical reasons, we introduce the parameter

$$\tilde{\epsilon} = \frac{d-2+\eta}{2(2-\eta)}. \tag{1.52}$$

This parameter vanishes at the lower critical dimension. We choose it instead of the scaling dimension of the field $D_\phi = (d-2+\eta)/2$ itself to simplify the fixed point equation for $u''(\varphi)$ but the two are simply proportional when $d-2+\eta \to 0$.

In the following chapters we will use the FRG framework and flow equations as developed for the description of critical phenomena. The phase transition does not exist at and below $\tilde{\epsilon} = 0$. Hence, we focus on the $\tilde{\epsilon} \to 0^+$ limit, and take that we are in principle arbitrarily close to it, but just above. This also means that we work in dimensions below $d = 2$, as a negative $\eta_{d_{lc}} = 2 - d_{lc}$ would be unphysical.

Not much literature explicitly deals with the lower critical dimension of the scalar ϕ^4 theory in the FRG derivative expansion. The paper by H. Ballhausen, J. Berges and C. Wetterich (BBW) [122] is the most relevant for the issues we want to tackle in our research. We have however found that they overlooked a key aspect of the approach to the lower critical dimension, and this will be discussed in the next chapters.

3 Conclusion

In this introduction we have described how Renomalization Group (RG) methods in principle build effective actions for long-wave degrees of freedom that describe criticality, where microscopic details of the system are irrelevant and we encounter universality. We have introduced the Functional RG (Section 1.2) and the derivative expansion (DE) approximation scheme (Section 1.2.4) which we consider in this thesis. We want to see if DE descriptions can be built for systems where strongly nonuniform fluctuations play a major role in the long-distance physics. This is unclear as the DE is in essence an expansion in small momenta around uniform configurations of the coarse-grained field. Still, the DE has proven to be fruitful and versatile down to $d = 2$ [16], quite away from the upper critical dimension (e.g., $d_{uc} = 4$ for the $O(N)$ model) [16]. We will investigate how the lowest nontrivial DE scheme (LPA') and the next order in the DE hierarchy (the second order of DE, ∂_2) handle strongly nonuniform configurations in the case of the scalar ϕ^4 theory near its lower critical dimension, where the proliferation of localized kinks destroy the transition (the Peierls argument, Section 2.2). Special care must be taken in this limit to respect the condition

[6] As shown in [66] for the LPA, for some regulator choices the singularity may actually not work as a barrier to the flow which then blows up at a finite scale $k \neq 0$.

that the dimensionful field does not rescale at the lower critical dimension, as was discussed in Section 2.2.1. We will also consider other possible signatures of the d_{lc} limit, like the relevant RG eigenvalues becoming marginal, the critical temperature approaching zero and the propagator developing a singularity.

Chapter 2

Approach to the lower critical dimension within the modified Local Potential Approximation (LPA')

The Local Potential Approximation, or LPA in short, is the lowest step in the hierarchy of the derivative expansion (DE) scheme. The DE scheme has been presented in Section 1.2.4 of Chapter 1. In LPA one takes the dimensionfull field renormalization function $Z_k(\varphi)$ to be a constant in k and φ [10, 123]. The higher order terms in the derivative expansion are neglected.

However, the choice of $Z_k(\varphi)$ being constant in k is synonymous with putting the anomalous dimension of the field $\eta = 0$. With this choice one cannot explore spatial dimensions below $d = 2$. Looking at the generic shape of the propagator one expects near criticality [44]:

$$G(\mathbf{x} - \mathbf{y}) \propto \frac{1}{|\mathbf{x} - \mathbf{y}|^{d-2+\eta}}, \tag{2.1}$$

one immediately sees that in the case of $\eta = 0$, the behavior for dimensions less than 2 would be unphysical.

Hence, as we are interested in the limit of the lower critical dimension, we cannot start at LPA but at LPA' - the minimally modified Local Potential Approximation, where $Z_k(\varphi)$ scales with $k^{-\eta}$, but the dimensionless field renormalization function $z_k(\varphi)$ is a constant in φ, which can be chosen to be 1.

1 Flow equations

The flow equations in LPA' are obtained by using $z_k(\varphi) = 1$ in the flow equations for the second order of the derivative expansion (see Chapter 1, Section 1.3). The resulting equations

are

$$\begin{aligned}\partial_t u_k(\varphi) &= -d u_k(\varphi) + (2-\eta_k)\,\tilde{\epsilon}\,\varphi u_k'(\varphi) + 2 v_d \ell_0^{(d)}(u_k''(\varphi), 1; \eta_k),\\ \partial_t z_k(\varphi) &= 0.\end{aligned} \tag{2.2}$$

We remind of the definition of the renormalization "time" $t = \ln(k/\Lambda)$, and the renormalization choice $\varphi_r = \varphi_{min,k}$, with $u_k'(\varphi_{min,k}) = 0$, for the LPA'. The shorthand v_d stands for the surface of a d-dimensional unit sphere and comes from integration over the momentum, and so do the threshold functions $\ell_n^{(d)}$ and $m_{n,0}^{(\varphi)}$. For explicit expressions for the threshold functions see Appendix A. They involve the propagator and its derivatives. The right-hand sides of the flow equations are usually called beta (β) functions and comprise a scaling contribution (the two first terms of the equation for $u_k(\varphi)$) and a nontrivial contribution expressed in terms of threshold functions.

To describe criticality, we need to solve the fixed-point equation for the effective potential, $\partial_t u_k(\varphi) = 0$, while simultaneously satisfying the condition put on the anomalous dimension by the renormalization condition $z_k(\varphi_{min,k}) = 1$. To mark fixed-point quantities, we simply drop the k index to avoid cluttering the notation, e.g., $u_k(\varphi) \to u(\varphi)$ and $\eta_k \to \eta$. The fixed-point equation is then given by:

$$\begin{aligned}0 &= -d u(\varphi) + (2-\eta)\,\tilde{\epsilon}\,\varphi u'(\varphi) + 2 v_d \ell_0^{(d)}(u''(\varphi), 1; \eta),\\ \text{with}\quad \eta &= \frac{4 v_d}{d} m_{4,0}^{(d)}(u''(\varphi_{min}), 1; \eta)^2 (u'''(\varphi_{min}))^4.\end{aligned} \tag{2.3}$$

It is, however, often more practical to work in terms of $u''(\varphi)$ than $u(\varphi)$ as will be seen in this chapter, and $u(\varphi)$ can be recovered from $u''(\varphi)$ by twice integrating, up to a physically irrelevant constant. Hence we also give here the fixed-point equation for $u''(\varphi)$, which is obtained by taking the second field-derivative of Eq. (2.3):

$$\begin{aligned}0 =& -(2-\eta)\,u''(\varphi) + (2-\eta)\,\tilde{\epsilon}\,\varphi u'''(\varphi) +\\ &- 2 v_d \big[u^{(iv)}(\varphi)\,\ell_1^{(d)}(u''(\varphi), 1; \eta) - (u'''(\varphi))^2\,\ell_2^{(d)}(u''(\varphi), 1; \eta)\big].\end{aligned} \tag{2.4}$$

Note that it only involves $u''(\varphi)$ and its derivatives.

2 Numerical results above the lower critical dimension

We start by solving numerically for the fixed-point solutions at dimensions d above d_{lc} (done in FORTRAN90 [124]), where we do not expect any singular behavior. We subsequently diminish the dimension d as much as the numerical procedure allows. This numerical investigation is meant to guide and complement analytical calculations, which give the main results and are the focus of this chapter.

The conceptual steps of the computation can be outlined as follows. We look for the zeros of the smooth function $\partial_t u_k''(\varphi)$ using a modified Newton-Raphson method and evaluating the right-hand side of Eq. (2.2), at the same time self-consistently calculating the anomalous dimension η from Eq. (2.3). As initial conditions, we use known fixed points at higher dimensions for calculations at the lower ones. Starting from, e.g., the nontrivial fixed point in $d \lesssim 4$, where we found it easier to estimate a usable numerical ansatz, we run the procedure

until a fixed point in some lower dimension is found. This new fixed point is then used as a new initial condition for solving at a lower dimension. This is how, in steps, we reach relevantly low dimensions.

To avoid divergencies that are expected in the profile of the effective potential, we actually conduct numerical calculations in terms of the susceptibility $\chi(\varphi) = (u''(\varphi) + \alpha)^{-1}$, and its flow equation, $\partial_t \chi_k(\varphi) = -\chi_k^2(\varphi)\, \partial_\varphi^2 [\partial_t u_k(\varphi)]$. The $\chi(\varphi)$ is always bounded from above with a maximum at $\varphi = 0$. For $|\varphi| \to +\infty$ the susceptibility has a power-law vanishing tail[1], unlike $u(\varphi)$ or any of its derivatives, which diverge, rendering numerics useless in this region. However, this is not conceptually relevant and we find that discussing $u''(\varphi)$ is more intuitive.

From its role in the correlation function, we expect the anomalous dimension η to be a monotonically decreasing function of the dimension d. This is the case, as can be seen from numerical results in Fig. 2.1a. In this section we refer to numerical results obtained with the exponential regulator, as we found no qualitative difference when we used r_Θ.

The parameter $\tilde{\epsilon}$ that we have defined in Chapter 1,

$$\tilde{\epsilon} = \frac{D_\phi}{2-\eta} = \frac{d-2+\eta}{2(2-\eta)}, \tag{2.5}$$

is then monotonically increasing with the spatial dimension d, as can be seen from Fig. 2.1b.

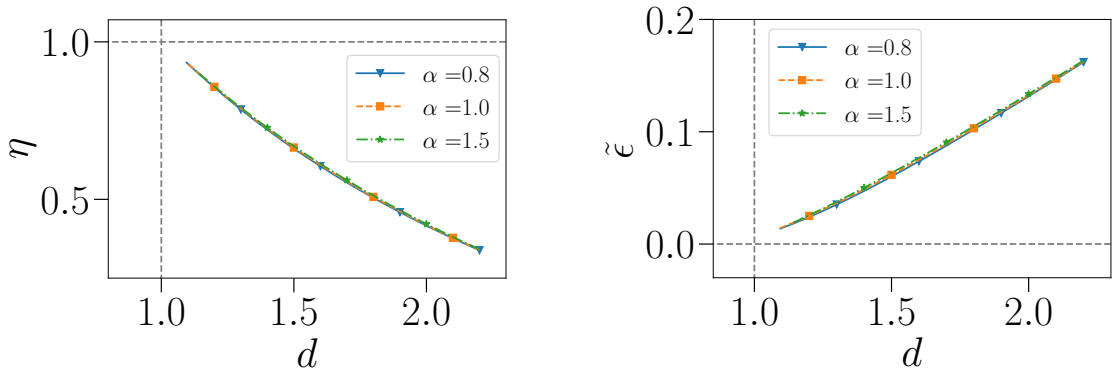

(a) (b)

Figure 2.1 – Dependence of the anomalous dimension η and the $\tilde{\epsilon}$-parameter on the spatial dimension d. Data plotted from numerically determined fixed-point solutions above d_{lc}, with the exponential regulator and three different regulator prefactor choices α. The dashed grey lines are visual guides. Markers are plotted for every 30th data point.

The fixed-point solutions for the effective potential $u(\varphi)$ and its second derivative $u''(\varphi)$ are plotted for a range of dimensions above d_{lc} and regulator prefactor choices α in Fig. 2.2.

These solutions reach at lowest $\tilde{\epsilon} \approx 0.0138$, or $d \approx 1.095$ before they break. The nature of the difficulties in the numerics is evident from the solutions themselves, before the procedure breaks. The second derivative becomes very large near the location of the minimum of the

[1]The tail behavior is determined by the scaling part of the flow, as for $|\varphi| \to +\infty$ the threshold functions vanish due to $u''(\varphi)$ strongly diverging which causes the propagator itself to vanish.

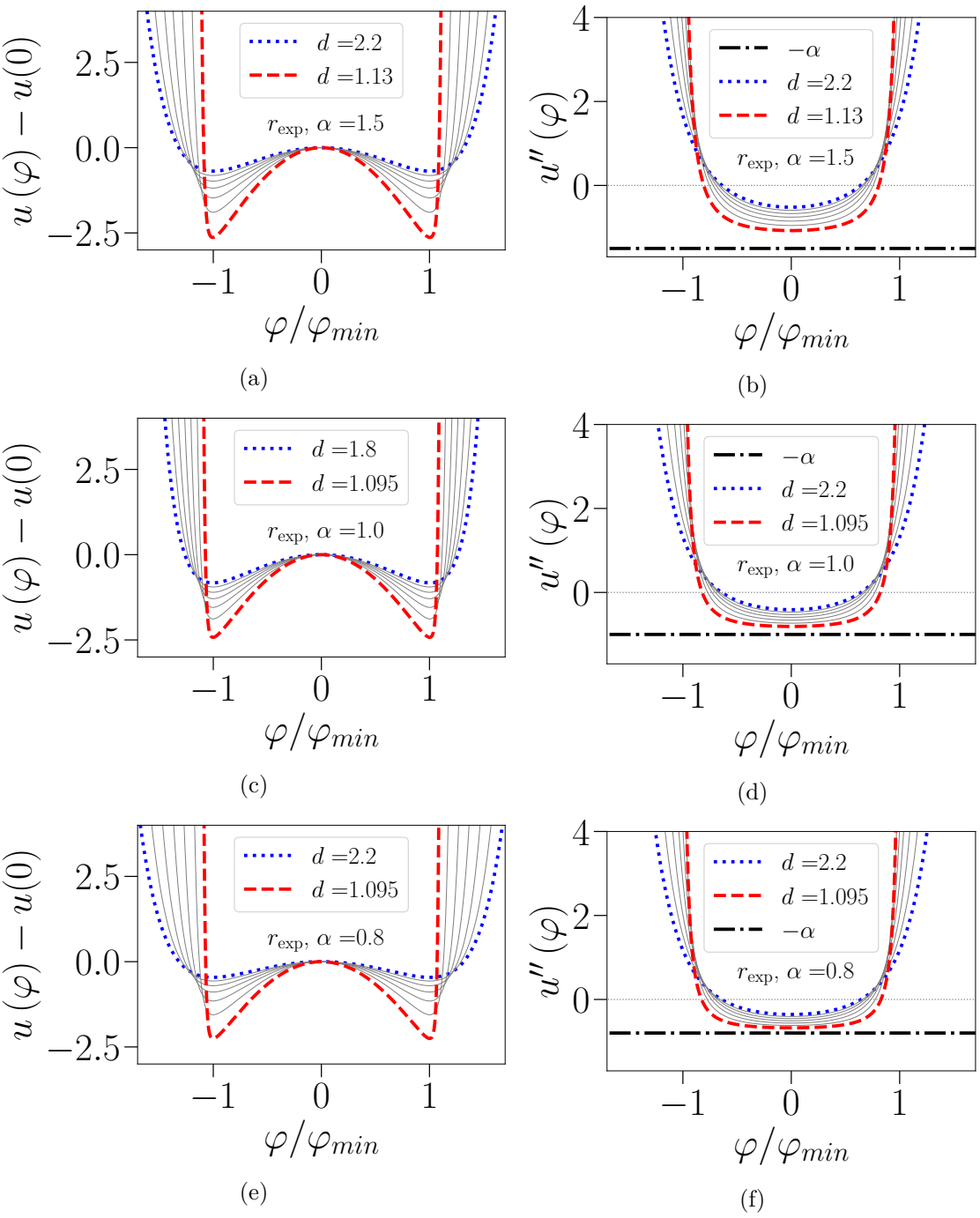

Figure 2.2 – Numerical fixed-point solutions for the effective potential $u(\varphi)$ and its second derivative $u''(\varphi)$ calculated with r_{exp} for a range of dimensions and regulator prefactors.

effective potential, and this means that it starts rapidly changing. The associated loss of precision in any grid mesh makes finding a solution impossible. Aside from this, we can see that $u''(0)$ tends to $-\alpha$, which signals another expected singularity - that of the propagator.

The second derivatives of the fixed-point effective potentials presented in Fig. 2.2 and their tendency to diverge in φ_{min} is especially interesting.

From the numerical results in the same Fig. 2.2 one can obtain the values of the location of the minimum of the effective potential φ_{min}. In $O(N > 2)$ models, one has $\varphi_{min} \propto 1/\sqrt{d-2} = 1/\sqrt{d-d_{lc}}$ [16], but from the numerical data, it is not clear how φ_{min} scales with $\tilde{\epsilon}$ in our case. Power-law fits of $\varphi_{min}(\tilde{\epsilon})$, which are shown in Fig. 2.3b, give the following exponents:

$$\varphi_{min} \overset{fit}{\propto} \frac{1}{\tilde{\epsilon}^{a}}, \qquad a = \begin{cases} (0.1245 \pm 0.0001) & r_{exp}, \quad \alpha = 0.8 \\ (0.10301 \pm 0.0002) & r_{exp}, \quad \alpha = 1.0 \\ (0.0661 \pm 0.0005) & r_{exp}, \quad \alpha = 1.5 \end{cases} \tag{2.6}$$

From such low numerically obtained exponents we can only conclude that if φ_{min} diverges, it must do so very slowly.

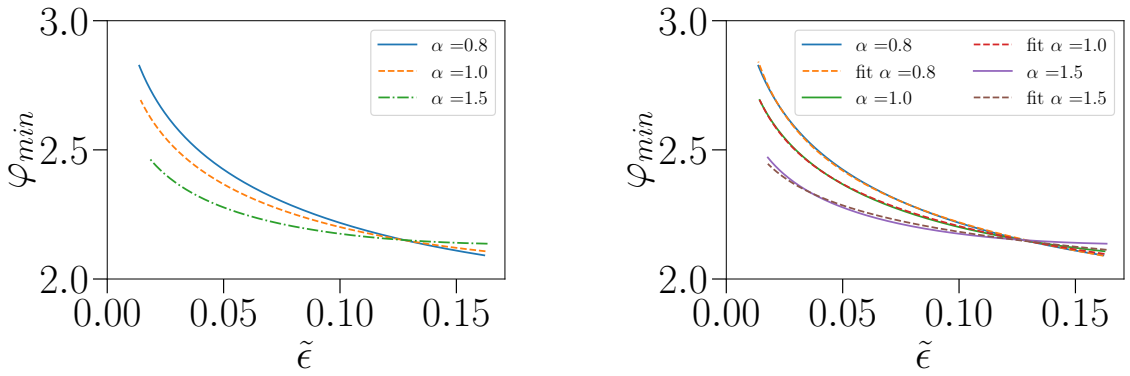

(a) Numerical data.

(b) Data with superimposed power-law fits.

Figure 2.3 – Location of the minimum of the effective potential, φ_{min}, obtained from numerical fixed points in Fig. 2.2.

We turn to the data in Fig. 2.2 and discuss how the values of $u''(\varphi_{min})$ depend on $\tilde{\epsilon}\,(d)$. The accompanying power-law fits are shown in Fig. 2.4. The fitted exponents are as follows:

$$u''\left(\varphi_{min}\right) \overset{fit}{\propto} \frac{1}{\tilde{\epsilon}^{b}}, \qquad b = \begin{cases} (1.009 \pm 0.003) & r_{exp}, \quad \alpha = 0.8 \\ (1.023 \pm 0.003) & r_{exp}, \quad \alpha = 1.0 \\ (1.059 \pm 0.003) & r_{exp}, \quad \alpha = 1.5 \end{cases} \tag{2.7}$$

and they indicate that we should expect $u''(\varphi_{min})$ to diverge essentially as $1/\,\tilde{\epsilon}$.

As mentioned, due to this divergence, the susceptibility $\chi\,(\varphi)$ becomes so small around φ_{min} as we lower d that we lose the necessary precision, which makes this procedure fail at low $\tilde{\epsilon}\,(d)$.

We found a way to analytically interpret and understand these results, as is laid out in the following sections.

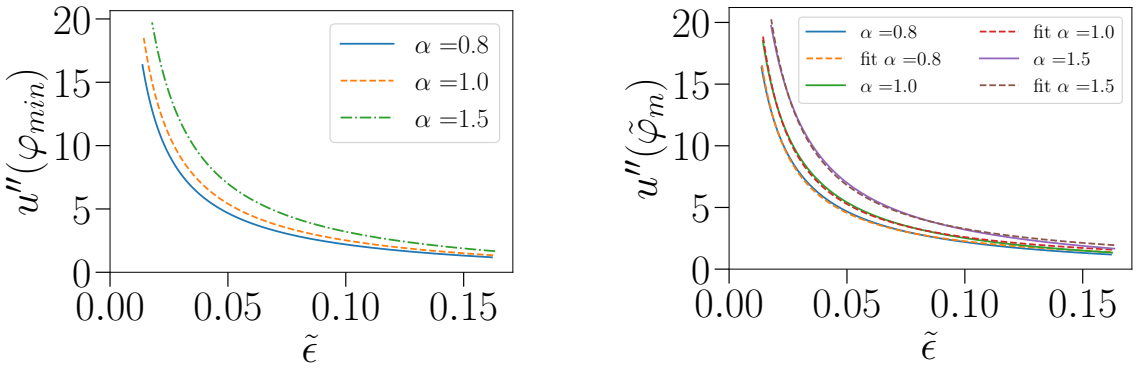

(a) Numerical data.

(b) Data with superimposed power-law fits.

Figure 2.4 – Value of the second derivative $u''(\varphi_{min})$ in the location of the minimum of the effective potential, φ_{min}, obtained from numerical fixed points in Fig. 2.2.

3 Constructing the analytical solution

In the preceding Section 2 we have found that numerical results above d_{lc} signal divergence of the second derivative of the effective potential $u''(\varphi)$ in the vicinity of the minimum φ_{min}. While because of this we cannot reach the d_{lc} limit numerically, we shift it in our favor by using the divergence in the $\varphi \approx \varphi_{min}$ neighborhood to simplify the flow equations in this region. This allows us to construct an analytical solution when $\tilde{\epsilon} \to 0$.

The fixed-point equation for the first derivative $u'(\varphi)$, which is obtained by taking a field-derivative of Eq. (2.3), is given by

$$0 = -\frac{1}{2}(d+2-\eta)u'(\varphi) + (2-\eta)\,\tilde{\epsilon}\,u_k''(\varphi)' + \beta_{u'(\varphi)}(u''(\varphi), z(\varphi) = 1; \eta), \tag{2.8}$$

where $\beta_{u'(\varphi)}$ stands for the nontrivial part. We turn our attention to the $\tilde{\epsilon}$ term, as we are interested in the $\tilde{\epsilon} \to 0$ limit. We ask ourselves when does it become relevant, as for small φ we expect it to be small compared to the rest of the equation. It is clear that if $u''(\varphi)$ diverges, the $\tilde{\epsilon}$-term is significant at smaller fields than what we would assume for an analytical potential. This means that we must be careful when assessing the $\tilde{\epsilon}$-terms in the flow equations. We need to use a method that allows for the different regions in φ to be treated separately based on the relevance or irrelevance of the $\tilde{\epsilon}$-term and provides a way to match them into one continuous solution. This is the realm of the Singular Perturbation Theory [125–129]. In this chapter we will show that it will allow us to build a physical fixed-point solution in the leading order in $\tilde{\epsilon}$, qualitatively different from the solution of the $\tilde{\epsilon} = 0$ equation which we will show cannot be valid for fields with $|\varphi| \geqslant \varphi_{min}$.

In the BBW reference [122] the subtlety of how the $\tilde{\epsilon}$ term becomes relevant for fields $|\varphi| \ll 1/\sqrt{\tilde{\epsilon}}$ has been missed.

3.1 Singular Perturbation Theory analysis

Singular Perturbation Theory (SPT) deals with differential equations where the solution perturbed by a small parameter is qualitatively different from the unperturbed solution. SPT

has successful applications to nonlinear oscillations, flight mechanics and orbital mechanics [125, 127]. We will show in Section 3.2 that the solution to the fixed-point Eq. (2.3) is periodic when $\tilde{\epsilon} = 0$ is directly used. As such, the $\tilde{\epsilon} = 0$ solution cannot be the leading-order solution for a physical effective potential. The perturbation by a small $\tilde{\epsilon} \to 0^+$ term must lead to a qualitatively different picture. Because of this, we use SPT to construct a leading-order solution for the effective potential which is uniformly valid over all field scales.

In SPT one divides the domain of the problem (in φ) into qualitatively different regimes. In each of the regimes, different simplifications occur in the leading order for $\tilde{\epsilon} \to 0^+$. The solutions of those simplified equations then need to be matched by requiring their asymptotic limits to coincide in the matching regions between these regimes. In our problem there are three different regions (or field scales) in which the effective potential has qualitatively different behavior and the behavior of $u''(\varphi)$ is driven by a different part of the fixed-point Eq. (2.4):

- In the innermost region, between the two minima $\pm\varphi_{min}$, $u''(\varphi)$ cannot diverge on physical grounds and thus cannot make the propagator, and consequently the nontrivial parts of the flows, small. We take $\varphi_{min} > 0$ in the following. With φ being finite the $\tilde{\epsilon}$ term in the flow equation Eq. (2.3) is a nonsingular perturbation in the d_{lc} limit. This region is therefore described in the leading order in $\tilde{\epsilon}$ by the flow Eq. (2.4) with $\tilde{\epsilon}$ set to zero:
$$u(\varphi) = \frac{2v_d}{d}\ell_0^{(d)}(u(\varphi), 1; \eta) \tag{2.9}$$
We call this the inner region.
- In the outermost region, where $|\varphi| > \varphi_{min}$ and $|\varphi| \to +\infty$, the nontrivial parts of the flow must vanish due to the strong $u''(\varphi)$ divergence. The behavior of the tails of the RG functions is hence guided by the scaling parts of their flow equations. For instance, the effective potential here follows the power law
$$0 = -du(\varphi) + (2-\eta)\,\tilde{\epsilon}\,\varphi u'(\varphi) \quad \Longrightarrow \quad u(\varphi) \propto |\varphi|^{d/(2-\eta)/\tilde{\epsilon}}. \tag{2.10}$$
We call this the tail region.
- Between the inner and the tail regions, a boundary layer of vanishing width emerges around φ_{min} as $\tilde{\epsilon} \to 0^+$, where $u''(\varphi)$ diverges but the threshold functions still need to be considered. The rest of this subsection contains the qualification of this boundary layer. (Due to the Z_2 symmetry, a similar boundary layer takes place around $-\varphi_{min}$.)

For a schematic illustration of these regions see Fig. 2.5.

A standard SPT problem would have predefined boundary conditions (e.g., the value of $u''(\varphi = 0)$), which we clearly do not have, and the locations where the regimes change would be readily evident from the parameters of the equation. From the numerical data of Section 2 above d_{lc}, showing the divergence of $u''(\varphi_{min})$, we expect there to be a boundary layer situated around the location of the minimum of the effective potential φ_{min}, but we do not know where φ_{min} is in advance. We cannot determine where it is from numerical results of Section 2, and we also wish to find the scaling of φ_{min} with $\tilde{\epsilon}$ analytically. Instead of concrete values for the boundary conditions, we are guided by the fact that a physical dimensionless effective potential for our problem should be of the double-well shape [16].

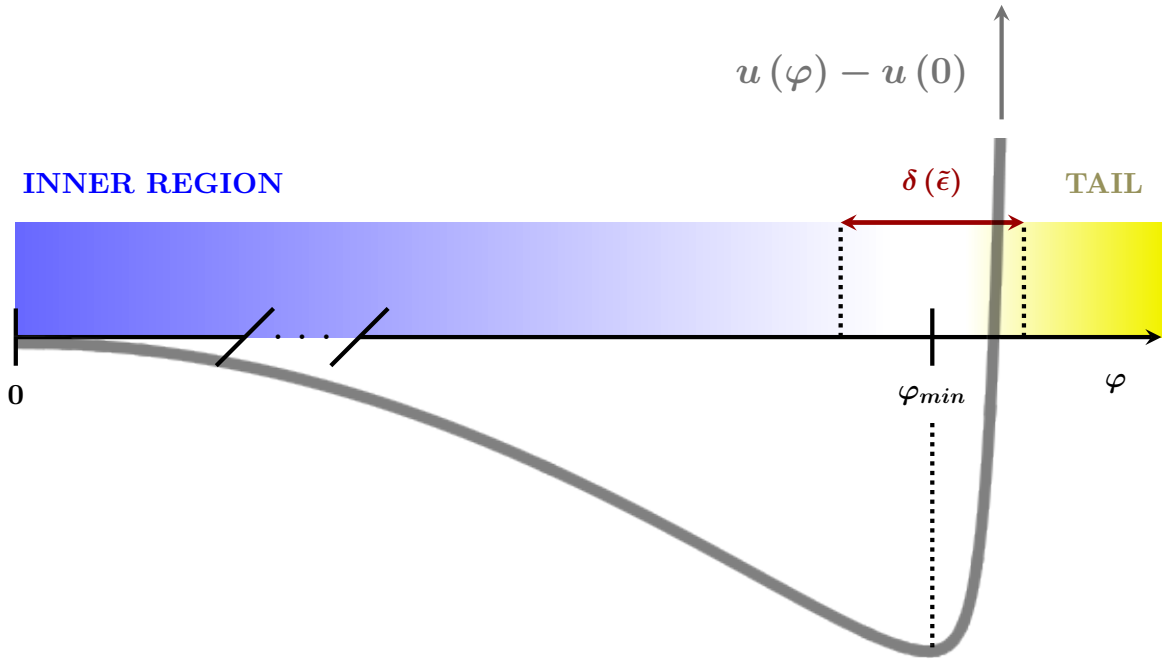

Figure 2.5 – Schematic representation of the different relevant field-scales, including the boundary layer of width $\delta(\tilde{\epsilon})$ around the location of the minimum of the effective potential φ_{min}, with the curve of the effective potential sketched.

What we know about the boundary layer from the divergence of $u''(\varphi_{min})$ is that it must form somewhere around the minimum of the effective potential φ_{min}, where $u''(\varphi)$ is very large but the terms involving threshold functions should be comparable to the $\tilde{\epsilon}$-term, so that we are not in the tail region. Thus, per Singular Perturbation Theory, we introduce two δ-scales that qualitatively describe this situation:

$$\begin{aligned} &\varphi = \varphi_{min} + \delta_\varphi(\tilde{\epsilon})\, x \quad \text{and} \quad u''(\varphi) = \frac{g(x)}{\delta_g(\tilde{\epsilon})}, \\ &\text{where} \quad \delta_\varphi(\tilde{\epsilon}), \delta_g(\tilde{\epsilon}) \overset{\tilde{\epsilon}\to 0^+}{\longrightarrow} 0 \quad \text{and} \quad x, g(x) = \mathcal{O}(1). \end{aligned} \tag{2.11}$$

In the following we show that for a nontrivial boundary layer regime, these scales must "balance" (also known as the *principle of dominant balance* [126]) in the following way:

$$\delta(\tilde{\epsilon}) := \delta_\varphi(\tilde{\epsilon}) = \delta_g(\tilde{\epsilon}) \quad \text{and} \quad \tilde{\epsilon}\,\varphi_{min} = \mathcal{O}(\delta(\tilde{\epsilon})). \tag{2.12}$$

The $\delta_\varphi(\tilde{\epsilon})$ is the boundary layer width, as fields with $|\varphi| \gg \varphi_{min} + \mathcal{O}(\delta_\varphi(\tilde{\epsilon}))$ give a diverging boundary-layer field x. Wen we speak about being in the boundary layer, it is taken that $x = \mathcal{O}(1)$. This makes the definition of the boundary layer in the effective potential (and its derivatives) more precise: it is the range of fields φ for which $x = \mathcal{O}(1)$, with a $\delta_\varphi(\tilde{\epsilon})$ we will calculate. Equally, $g(x)$ is by construction of $\mathcal{O}(1)$, and so are its derivatives.

Making the boundary layer regime from Eq. (2.11) explicit in the fixed-point equation for the second derivative $u''(\varphi)$, Eq. (2.4), and multiplying it by $-\delta_g(\tilde{\epsilon})/(2-\eta)$, we get

term-by-term:

$$\begin{aligned} 0 =& g(x) - \tilde{\epsilon}\left(\frac{\varphi_{min}}{\delta_\varphi(\tilde{\epsilon})} + x\right) g'(x) + \\ &+ \frac{2v_d}{2-\eta}\left[\frac{g''(x)}{\delta_\varphi^2(\tilde{\epsilon})}\ell_1^{(d)}\left(\frac{g(x)}{\delta_g(\tilde{\epsilon})}, 1; \eta\right) - \delta_g(\tilde{\epsilon})\left(\frac{g'(x)}{\delta_g(\tilde{\epsilon})\,\delta_\varphi(\tilde{\epsilon})}\right)^2 \ell_2^{(d)}\left(\frac{g(x)}{\delta_g(\tilde{\epsilon})}, 1; \eta\right)\right]. \end{aligned} \tag{2.13}$$

The proposed divergence of $u''(\varphi)$ as $1/\delta_g(\tilde{\epsilon})$ simplifies the propagator and hence also the threshold functions $\ell_n^{(d)}$. In Appendix A we show that in this case they scale as $\ell_n^{(d)} \propto (\delta_g(\tilde{\epsilon}))^{-(n+1)}$. This makes all the terms in the second row of Eq. (2.13) of $\mathcal{O}\Big((\delta_g(\tilde{\epsilon})/\delta_\varphi(\tilde{\epsilon}))^2\Big)$.

The chief lesson of SPT is that one needs to balance the δ-scales in a way that leaves the remaining equation non-trivial. This way, even if we were to start with no knowledge of the shape of fixed-point solutions above d_{lc}, the SPT would recognize that the fixed-point Eq. (2.4) has a potential to produce all three regimes in Fig. 2.5. In general the SPT shows what regimes can occur in a differential equation and boundary conditions would determine whether a certain regime emerges in the solution, and where in the field to place it. Here physical arguments play that role, like the double-well shape of the effective potential that we have already mentioned.

To see the regime that is neither the inner nor the tail region, the following conditions must apply to the δ-scales and terms of Eq. (2.13):

- The terms involving threshold functions $\ell_n^{(d)}$ should not vanish (this would be the tail region). They should also not diverge as that would mean a propagator singularity.[2] If we are to expect a propagator singularity, we know from $u''(\varphi)$ having a minimum in $\varphi = 0$ that it is to be in the inner region, and not in the boundary layer. Hence we have $\delta(\tilde{\epsilon}) := \delta_\varphi(\tilde{\epsilon}) = \delta_g(\tilde{\epsilon})$.
- The quantity $\tilde{\epsilon}\,\varphi_{min}/\delta(\tilde{\epsilon})$ must not diverge, as no other term in Eq. (2.11) diverges. In the boundary layer, it also must be relevant, i.e., not vanish. This directly gives that $\tilde{\epsilon}\,\varphi_{min}$ is of $\mathcal{O}(\delta(\tilde{\epsilon}))$.
- The $\tilde{\epsilon}\,x g'(x)$ term drops out in the lowest order in $\tilde{\epsilon}$, as it is by order of $\mathcal{O}(\tilde{\epsilon})$ smaller than the first term, i.e., $g(x)$.

If we wanted to do an analogous analysis for the inner or tail region, we would have to allow, e.g., for some of the $\delta(\tilde{\epsilon})$-scales not to vanish, depending on the case.

It follows that between the inner region and the tail region, a boundary layer emerges with

$$\tilde{\epsilon}\varphi_{min} = \mathcal{O}(\delta(\tilde{\epsilon})) \quad \text{and} \quad u''(\varphi) = \mathcal{O}\left(\frac{1}{\delta(\tilde{\epsilon})}\right). \tag{2.14}$$

From this analysis of the scales we expect $\tilde{\epsilon}\varphi_{min}$ to vanish in the lower critical dimension. Later in the text we will show that $\tilde{\epsilon}\varphi_{min}$ does indeed vanish and φ_{min} still diverges, but much more weakly than the $1/\sqrt{\tilde{\epsilon}}$ predicted by [122] and in agreement with numerical results in Section 2.

[2] This whole term, including the $u^{(iv)}(\varphi)$ and $(u'''(\varphi))^2$ prefactors, comes from $\partial_\varphi^2 \ell_0^{(d)}$. It being singular would mean that $\ell_0^{(d)}$ is nonanalytic, which would come from a propagator singularity.

We continue by investigating the nontrivial regimes - the inner region and the boundary layer. (Note that in SPT one usually speaks of "inner" and "outer" to characterize the solution within the boundary layer (inner) and outside it (outer). Here we use a different convention because it seems more appropriate for describing the various domains.)

3.2 Inner region and the $\tilde{\epsilon} = 0$ fixed-point solution

By inspecting the $\tilde{\epsilon} = 0$ fixed-point equation for $u(\varphi)$ we will show that its solution is periodic. If it were taken as a leading order solution at all field scales, this would be unphysical. Instead, we find conditions for this solution (in its limit towards large fields) to be compatible with the emergence of the boundary layer. It turns out that for this matching to be possible, the propagator must develop a singularity in the field-origin $\varphi = 0$. As matching to a boundary layer is crucial in building a physical fixed-point solution, so is the propagator singularity.

We restate the $\tilde{\epsilon} = 0$ version of Eq. (2.3) for clarity:

$$u(\varphi) = \frac{2v_d}{d}\ell_0^{(d)}(u''(\varphi), 1; \eta = 2 - d). \tag{2.15}$$

We set $\eta = 2 - d$ in the threshold function as we are dealing with the $\tilde{\epsilon} = 0$ equation. On the RHS is the positive[3] threshold function $\ell_0^{(d)}$:

$$\frac{d}{2v_d}L(u''(\varphi)) \equiv \ell_0^{(d)}(u''(\varphi), 1; \eta) = -\frac{1}{2}\int_0^{+\infty} dy y^{d/2}\frac{\eta r(y) + 2yr'(y)}{u''(\varphi) + y(1 + r(y))} > 0, \tag{2.16}$$

where we have introduced the shorthand L, to make the following Section 3.2.1 clearer, where we will map this problem onto an anharmonic oscillator using general, abstract properties of $L(u''(\varphi))$. This is to be followed by a more specific discussion in Section 3.2.2 focusing on a practically revealing regulator choice r_Θ and $\alpha = 1$, making the issue more tangible.

3.2.1 Periodicity of the $\tilde{\epsilon} = 0$ solution

We start from Eq. (2.15), the $\tilde{\epsilon} = 0$ equation for the effective potential:

$$u(\varphi) = \frac{2v_d}{d}\ell_0^{(d)}(u''(\varphi), 1; \eta = 2 - d) := L(u''(\varphi)), \tag{2.17}$$

and we take its second derivative, to treat L as a function of $u''(\varphi)$:

$$\partial_\varphi^2 L(u''(\varphi)) = u''(\varphi). \tag{2.18}$$

The right hand side of Eq. (2.17) (the function L), is a monotonically decreasing function of its argument $u''(\varphi)$, which is readily shown from the properties of the threshold function:

$$\frac{\partial \ell_0^{(d)}(u''(\varphi), 1; \eta)}{\partial u''(\varphi)} = -\ell_1^{(d)}(u''(\varphi), 1; \eta) < 0 \quad \Longrightarrow \quad L'(u''(\varphi)) = -\frac{2v_d}{d}\ell_1^{(d)}(u''(\varphi), 1; \eta) < 0. \tag{2.19}$$

[3] This comes from the properties of the regulator.

The monotonicity of $L(u''(\varphi))$ means that the $L - u''(\varphi)$ relation can be inverted for any regulator choice, albeit not explicitly, and we can express everything in terms of L as a variable. When we choose to view L as an independent variable, we emphasize that by naming it Φ, and in inverse we treat $u''(\varphi)$ as a function of Φ:

$$L(u''(\varphi)) := \Phi(\varphi), \qquad u''(\varphi) := F(\Phi). \tag{2.20}$$

The choice of shorthand F is purposeful, as the Eq. (2.18) for $u''(\varphi)$ can now be expressed in a shape reminiscent of an equation of motion for a dynamical variable Φ where φ plays the role of time and F of force, with a potential V:

$$\ddot{\Phi}(\varphi) = F(\Phi), \quad V(\Phi) - V(\Phi_0) = -\int_{\Phi_0}^{\Phi} d\tilde{\Phi} F\left(\tilde{\Phi}\right), \quad \Phi_0 = \Phi(\varphi = 0). \tag{2.21}$$

Here we introduced the shorthand $\partial_\varphi \Phi(\varphi) = \dot{\Phi}(\varphi)$.

As $L(u''(\varphi)) := \Phi$ monotonically decreases with $u''(\varphi)$, so must its inverse, the force

$$u''(\varphi) = L^{-1}(L(u''(\varphi))) = L^{-1}(\Phi) := F(\Phi) \tag{2.22}$$

monotonically decrease too, as a function of the dynamical variable Φ. This means that its derivative is not positive, $F'(\Phi) \leqslant 0$, showing the convexity of the potential $V(\Phi)$:

$$\frac{dV(\Phi)}{d\Phi} = -F(\Phi) \quad \text{(by definition)} \quad \Longrightarrow \quad \frac{d^2V(\Phi)}{d\Phi^2} = -\frac{dF(\Phi)}{d\Phi} \geqslant 0. \tag{2.23}$$

As a physical effective potential $u(\varphi)$ has a double-well shape, we expect any reasonable effective potential to have an inflection point φ_i before φ_{min} in which the second derivative $u''(\varphi_i) = F(\Phi_i)$ vanishes. From Eq. (2.23), we see that the potential V then has a minimum at Φ_i. This makes $V(\Phi)$ convex with a minimum: a potential well.

Due to the parity condition $u'''(0) = 0$, starting from the origin of "time" $\varphi = 0$, this "particle" has velocity 0:

$$\dot{\Phi}(0) = -\frac{2v_d}{d} u'''(0) \ell_1^{(1)}(u''(0), 1; 2 - d) = 0, \tag{2.24}$$

After "time" φ_* has elapsed, the "particles" velocity $\dot{\Phi}(\varphi_*)$ is again 0 after which it gets turned around. Thus φ_* is the half-period and can be implicitly calculated from the equation of motion, Eq. (2.21), utilizing the fact that the velocity $\dot{\Phi}(\varphi)$ must vanish at both turnaround points, those being $\varphi = 0$ and φ_*:

$$0 = \dot{\Phi}(\varphi_*) - \dot{\Phi}(0) = \int_{\Phi(\varphi=0)}^{\Phi(\varphi_*)} d\tilde{\Phi}\ F\left(\tilde{\Phi}\right) = \int_0^{\varphi_*} d\tilde{\varphi}\ \dot{\Phi}(\tilde{\varphi})\ F(\Phi(\tilde{\varphi})). \tag{2.25}$$

In this subsection we have shown that the function $\ell_0^{(d)}(u''(\varphi), 1; d - 2)$ describes an orbit $\Phi(\varphi)$ of a $1d$ particle in a convex potential well $V(\Phi)$ defined in Eq. (2.20) (an anharmonic oscillator [130]). As such, $\ell_0^{(d)}(u''(\varphi), 1; d - 2)$ must be periodic in the field φ. This means that the $\tilde{\epsilon} = 0$ solution for $u(\varphi)$, which is by Eq. (2.15) proportional to this periodic threshold function, must be periodic in the field φ too, with the same half-period φ_* (for any regulator

choice). The second derivative $u''(\varphi)$ oscillates between its minimal value $u''(0)$ and the maximal value $u''(\varphi_*)$.

In any dimension above the lower critical dimension d_{lc}, no matter how small the positive $\tilde{\epsilon}$, a continuous phase transition exists. The periodic $\tilde{\epsilon} = 0$ fixed-point solutions *by themselves* are not physically sound descriptions of a critical system. However, until the $\tilde{\epsilon}$-term becomes commensurate to other terms in Eqs. (2.3) and (2.4), the periodic solution is the leading-order description of the inner region. This must end somewhere between $\varphi = 0$ and the location of the first minimum of the periodic solution φ_*, because φ_* is the half-period and the Z_2 symmetry tells us that the situation must be the same for the $-\varphi_* < \varphi < 0$ fields. Outside of this first period everything simply repeats and if the $\tilde{\epsilon}$-term is to have any effect anywhere it would have to have it in the first period too. When the $\tilde{\epsilon}$-term becomes relevant, the boundary layer soon develops around φ_{min}. In the vicinity of φ_{min}, $u''(\varphi)$ is very large. To make the matching possible, the maximum of the periodic solution $u''(\varphi_*)$ must then be very large too, and the matching should take place at fields φ_M so that $\varphi_M < \varphi_{min} \lesssim \varphi_*$. What comes from this will be discussed in Section 3.4 about the matching arguments, once the boundary layer solution has been introduced.

3.2.2 An illustrative example of periodicity

We present the arguments of Section 3.2.1 on the choice of the Theta regulator with the prefactor $\alpha = 1$. This regulator choice is motivated by the simplicity of the resulting relevant threshold function:

$$\ell_0^{(d)}\left(u''(\varphi), 1; \eta\right) = \frac{2(d+2-\eta)}{d(d+2)} \frac{1}{1+u''(\varphi)} \overset{\tilde{\epsilon}=0}{=} \frac{4}{(d+2)} \frac{1}{1+u''(\varphi)}. \tag{2.26}$$

This expression is calculated directly from using r_Θ, $\alpha = 1$ in the LPA' expression for ℓ_n^{d} given in Appendix A, and it serves well in elucidating the concepts which we developed in the universal, regulator independent discussion in Section 3.2.1.

One starts by taking the second field-derivative of Eq. (2.15):

$$u''(\varphi) = \frac{\partial^2 L(u''(\varphi))}{\partial \varphi^2} \tag{2.27}$$

This line of derivation is not the most practical for the sake of the current calculation, but the step reflects Eq. (2.18) in the general case. With our regulator choice, the starting equation Eq. (2.15) simplifies to

$$u(\varphi) = \frac{8v_d}{d(d+2)} \frac{1}{1+u''(\varphi)}. \tag{2.28}$$

Before proceeding we re-scale the field as $\tilde{\varphi} = \sqrt{d(d+2)/8v_d}\,\varphi$ and the potential as $\tilde{u} = d(d+2)u/8v_d$, forsaking the tilde for simplicity:

$$u(\varphi) = \frac{1}{1+u''(\varphi)} = L(u''(\varphi)). \tag{2.29}$$

We now invert the $L - u''(\varphi)$ relation, to express everything in terms of L as a variable, which we have named Φ when conceptually used in the free-variable capacity:

$$L(u''(\varphi)) := \Phi(\varphi), \qquad u''(\varphi) := F(\Phi). \tag{2.30}$$

giving the same equation of motion as Eq. (2.21):

$$\ddot{\Phi}(\varphi) = F(\Phi) \tag{2.31}$$

The simplicity of Eq. (2.28) makes it possible to invert the $L - u''(\varphi)$ dependence explicitly (for this specific regulator choice):

$$u''(\varphi) = \frac{1}{L(u''(\varphi))} - 1 \quad \text{or} \quad F(\Phi) = \frac{1}{\Phi} - 1, \tag{2.32}$$

and as such we can plot this "force" in Fig. 2.6a.

The most pertinent part of this discussion is the corresponding "potential" for this $1d$ dynamical variable Φ:

$$F(\Phi) = -\frac{dV(\Phi)}{d\Phi} \quad \overset{Eq.\ (2.32)}{\Longrightarrow} \quad V(\Phi) - V(\Phi_{\text{init.}}) = \Phi - \ln(\Phi) - (\Phi_{\text{init.}} - \ln(\Phi_{\text{init.}})). \tag{2.33}$$

In the process of integrating to get the potential, we used as the lower boundary any finite (both not diverging and not vanishing) value of the dynamical variable, which we marked $\Phi_{\text{init.}}$. We are interested solely in the shape of this function, for which this integration constant is irrelevant. From Fig. 2.6b and $V''(\Phi) = 1/\Phi^2 \geqslant 0$, we see that the "particle" is in a convex potential well, and as such its trajectory Φ must be an orbit.

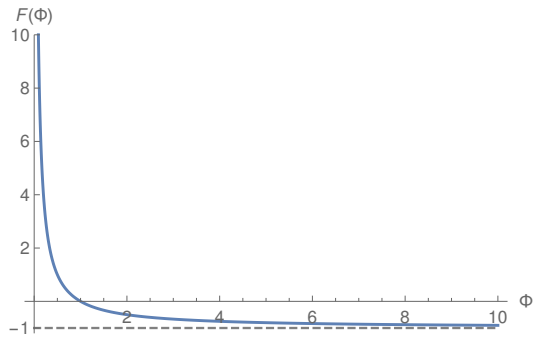

(a) $F(\Phi) = 1/\Phi - 1$

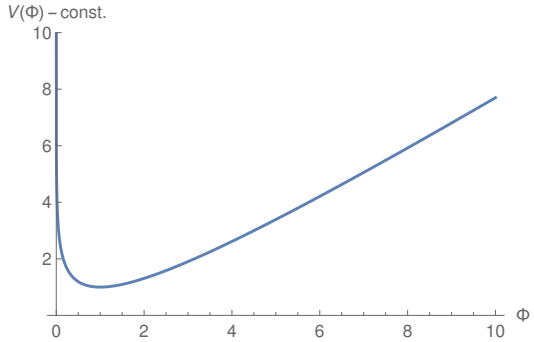

(b) $V(\Phi) - \text{const.} = \Phi - \ln(\Phi)$

Figure 2.6 – The "force" F and the "potential" V of te $\tilde{\epsilon} = 0$ solution for $u(\varphi)$ as mapped to the anharmonic oscillator, for $r(y) = (1/y - 1)\Theta(1 - y)$. In the left panel, the dashed line at $F(\Phi) = -1$ is a visual guide. We note that Φ, by its definition over the threshold function $\ell_0^{(d)}$, must always be positive.

For this specific regulator choice, we solve the equation Eq. (2.29) numerically and plot these periodic solutions for the potential in Fig. 2.7 to further underline the point that we made analytically.

3.3 Boundary layer

We proceed by investigating the next regime, the boundary layer. In this section we will find an implicit boundary layer solution for $u'''(\varphi)$ expressed in terms of $u''(\varphi)$. In later sections this will allow us to consider the asymptotic behavior towards the tail and the matching

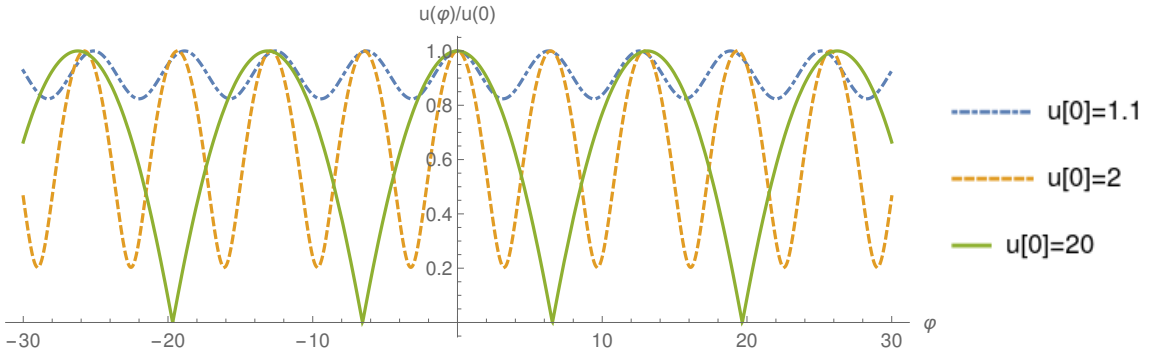

Figure 2.7 – Periodic $\tilde{\epsilon} = 0$ solutions for the fixed-point effective potential with r_Θ and $\alpha = 1$. We note that the field and the potential have been rescaled by dimension-dependent constants to yield the simple shape of Eq. (2.29). The solutions are parametrized solely by $u(0)$, as $u'(0)$ vanishes from parity. In these units $u(0)$ must be $\geqslant 1$, as $u''(\varphi) = 1/u(\varphi) - 1$ and $u(\varphi)$ starts off concavely. For $u(0) \gtrapprox 23$ the system becomes stiff and no solutions can be found, a numerical artifact of the adaptive Runge-Kutta method offered in Wolfram Mathematica v12.1 [131]. Between these two $u(0)$ values, the solutions are robustly periodic, as we have shown analytically that they must be. We stress that $u(\varphi)$ is defined up to a physically irrelevant constant.

with the periodic solution. This information will allow us to analytically find the scaling of φ_{min} and $u''(\varphi_{min})$ with $\tilde{\epsilon}$ from matching with the solution for the inner region, and also the value of the lower critical dimension itself, as a function of the IR regulator characteristics, from joining with the tail region.

3.3.1 Boundary layer equations

We know from Section 3.1 on Singular Perturbation Theory that the boundary layer regime is given by:

$$\begin{aligned} &x = \frac{\varphi - \varphi_{min}}{\delta(\tilde{\epsilon})}, \quad u''(\varphi) = \frac{g(x)}{\delta(\tilde{\epsilon})}, \\ &\text{with} \quad \delta(\tilde{\epsilon}) \overset{\tilde{\epsilon}\to 0^+}{\longrightarrow} 0 \quad \text{and} \quad x, g(x) = \mathcal{O}(1). \end{aligned} \tag{2.34}$$

Concerning the nontrivial parts of the flow, we have found the expressions for the threshold functions in the boundary layer regime in Appendix A. They scale with the width of the boundary layer $\delta(\tilde{\epsilon})$ as

$$\begin{aligned} &\ell_n^{(d)}(u''(\varphi), 1; \eta) = (\delta(\tilde{\epsilon}))^{n+1}\, L_n^{(d)}(g(x)) + \mathcal{O}\Big((\delta(\tilde{\epsilon}))^{n+2}\Big), \quad L_n^{(d)}(g(x)) = \mathcal{O}(1); \\ &m_{n,0}^{(d)}(u''(\varphi), 1; \eta) = (\delta(\tilde{\epsilon}))^{n}\, M_n^{(d)}(g(x)) + \mathcal{O}\Big((\delta(\tilde{\epsilon}))^{n+1}\Big), \quad M_n^{(d)}(g(x)) = \mathcal{O}(1). \end{aligned} \tag{2.35}$$

The auxiliary functions $L_n^{(d)}$ and $M_n^{(d)}$ are defined as follows:

$$L_n^{(d)}(g(x)) = (n + \delta_{n,0})\frac{\alpha A^{(d)}(\eta)}{(g(x))^{n+1}}, \quad M_n^{(d)}(g(x)) = \frac{\alpha d A^{(d)}(\eta) - \alpha^2 B^{(d)}(\eta)}{(g(x))^{n}}, \tag{2.36}$$

where we introduced the positive regulator dependent constants $A^{(d)}(\eta)$ and $B^{(d)}(\eta)$:

$$\begin{aligned} A^{(d)}(\eta) =& \left(\frac{d+2-\eta}{2}\right) \int_0^{+\infty} dy y^{d/2} \left[\frac{r(y)}{\alpha}\right] > 0, \\ B^{(d)}(\eta) =& \left(\frac{d+2-2\eta}{2}\right) \int_0^{+\infty} dy y^{d/2} \left[\frac{(yr(y))'}{\alpha}\right]^2 > 0. \end{aligned} \tag{2.37}$$

From the considerations of the scaling parts of the flow in Eq. (2.13) we predict that we will encounter a $\tilde{\epsilon}\,\varphi_{min}/\delta\,(\tilde{\epsilon})$ term in the boundary layer equations. It is practical to substitute it for the following:

$$\frac{\tilde{\epsilon}\,\varphi_{min}}{\delta\,(\tilde{\epsilon})} = \frac{2\alpha v_d A^{(d)}(\eta)}{(2-\eta)} \frac{g'(0)}{(g(0))^3} = \mathcal{O}(1). \tag{2.38}$$

This expression for the location of the minimum φ_{min} is found from the fixed-point equation for $u'(\varphi_{min}) = 0$ (see Appendix A).

By using Eq. (2.34) to Eq. (2.38) in the fixed-point equation for $u''\,(\varphi)$, Eq. (2.4), we arrive at the boundary-layer fixed-point equation:

$$0 = -\,(2-\eta)g(x) + 2\alpha v_d A^{(d)}(\eta)\left(\frac{g'(0)g'(x)}{(g(0))^3} + 2\frac{(g'(x))^2}{(g(x))^3} - \frac{g''(x)}{(g(x))^2}\right). \tag{2.39}$$

3.3.2 Boundary layer solution

We found an analytical implicit solution for the dependence of $g'(x)$ on $g(x)$ itself, as announced on the beginning of Section 3.3.

We start by simplifying the equations using a reparametrization for φ (and consequently x) which we call *canonical field rescaling*:

$$\varphi_c = \frac{\varphi}{\sqrt{\dfrac{2\alpha v_d A^{(d)}(\eta)}{(2-\eta)}}}. \tag{2.40}$$

We named this field canonical for the usual reason - because the *canonical equation*, Eq. (2.41), is the simplest form of the boundary-layer fixed-point equation. This rescaling is useful at both the LPA' and ∂_2 level. The labels x and $g(x)$ are kept to avoid cluttering the notation (see Appendix B).

Looking at the canonical equation for fixed-point $g\,(x)$:

$$0 = g\,(x) - \frac{g'(0)g'\,(x)}{(g(0))^3} - 2\frac{(g'\,(x))^2}{(g\,(x))^3} + \frac{g''(x)}{(g\,(x))^2}, \tag{2.41}$$

one recognizes a part that is a total derivative. In the following equation we emphasize this by writing out the derivation operator d/dx explicitly:

$$0 = g\,(x) - \frac{d}{dx}\left[\frac{g'(0)g\,(x)}{(g(0))^3} - \frac{g'\,(x)}{(g\,(x))^2}\right]. \tag{2.42}$$

To find a solution for Eq. (2.42), we take the function in the square brackets as an independent variable $Y(x)$:

$$Y(x) := g(x)\left(\frac{g'(0)}{(g(0))^3} - \frac{g'(x)}{(g(x))^3}\right), \tag{2.43}$$

and view $g(x)$ as a function of it, $G(Y(x)) := g(x)$, an identification that allows for this differential equation to be once-integrated. The result follows:

$$\frac{G(Y)}{G(0)} = \frac{e^{-Y^2/2}}{1 - \sqrt{\frac{\pi}{2}}\frac{g'(0)}{(g(0))^2}\,\mathrm{erf}\left(Y/\sqrt{2}\right)} \tag{2.44}$$

and represents an implicit solution for $g'(x)$ in terms of $g(x)$:

$$\frac{g(x)}{g(0)} = \frac{\exp\left[-\frac{(g(x))^2}{2}\left(\frac{g'(0)}{(g(0))^3} - \frac{g'(x)}{(g(x))^3}\right)^2\right]}{1 - \sqrt{\frac{\pi}{2}}\frac{g'(0)}{(g(0))^2}\,\mathrm{erf}\left[\frac{g(x)}{\sqrt{2}}\left(\frac{g'(0)}{(g(0))^3} - \frac{g'(x)}{(g(x))^3}\right)\right]}. \tag{2.45}$$

Going to large boundary layer fields x, the boundary layer regime must continuously transform into the tail region. In the tail region, $u''(\varphi)$ must diverge stronger than in the boundary layer where it does so as $1/\delta(\tilde{\epsilon})$. This means that $g(x) = \delta(\tilde{\epsilon})\,u''(\varphi)$ must diverge in the $x \to +\infty$ limit.

To make use of this asymptotic argument in the boundary layer solution Eq. (2.45), we need to also find the behavior of $Y(x)$ in the same (tail) limit:

$$\begin{aligned} &u''(\varphi) \propto |\varphi|^{1/\tilde{\epsilon}} \quad \Longrightarrow \quad u'''(\varphi) \propto |\varphi|^{1/\tilde{\epsilon}-1}: \\ &Y(x) = \frac{g'(0)}{(g(0))^3}|\varphi|^{1/\tilde{\epsilon}} + \mathcal{O}\left(|\varphi|^{-1-2/\tilde{\epsilon}}\right) \quad \Longrightarrow \quad Y(x) \propto |\varphi|^{1/\tilde{\epsilon}}, \end{aligned} \tag{2.46}$$

where we used that the quantities in $x = 0$ must be of $\mathcal{O}(1)$ by definition of the boundary-layer function $g(x)$. We now use this limit of $G(Y) := g(x)$ diverging when $Y(x)$ diverges to pinpoint the value of $g'(0)/(g(0))^3$, the only parameter on the right-hand side of Eq. (2.44). It is more practical to express this in terms of $1/G(Y)$:

$$\begin{aligned} \frac{G(0)}{G(Y)} =& e^{Y^2/2}\left[1 - \sqrt{\frac{\pi}{2}}\frac{g'(0)}{(g(0))^2}\,\mathrm{erf}\left(Y/\sqrt{2}\right)\right] = \\ =& e^{Y^2/2}\left[1 - \sqrt{\frac{\pi}{2}}\frac{g'(0)}{(g(0))^2}\right] + \frac{(g(0))^2}{g'(0)}\frac{1}{Y} + \mathcal{O}\left(\frac{1}{Y^2}\right). \end{aligned} \tag{2.47}$$

For this expression to vanish in the $Y(x) \to +\infty$ limit, the combination of $\mathcal{O}(1)$-terms multiplying the exponential divergence must be zero, leading to the following identification:

$$\frac{g'(0)}{(g(0))^2} = \sqrt{\frac{2}{\pi}}. \tag{2.48}$$

The canonical solution in the boundary layer we arrived at through this asymptotic matching of the tail to the boundary layer is given by:

$$\frac{g\left(x\right)}{g(0)}=\frac{e^{-Y^{2}/2}}{\operatorname{erfc}\left(Y/\sqrt{2}\right)}=\frac{\exp\left[-\frac{\left(g\left(x\right)\right)^{2}}{2}\left(\frac{\sqrt{2/\pi}}{g(0)}-\frac{g'\left(x\right)}{\left(g\left(x\right)\right)^{3}}\right)^{2}\right]}{\operatorname{erfc}\left[\frac{g\left(x\right)}{\sqrt{2}}\left(\frac{\sqrt{2/\pi}}{g(0)}-\frac{g'\left(x\right)}{\left(g\left(x\right)\right)^{3}}\right)\right]}. \tag{2.49}$$

For purposes of visualizing this solution, we do some more rescaling:

$$\begin{aligned} x\rightarrow\tilde{\mathrm{x}}=g(0)x,\quad g\left(x\right)\rightarrow\tilde{\mathrm{g}}\left(\tilde{\mathrm{x}}\right)=\frac{g\left(x\right)}{g(0)}:\\ \tilde{\mathrm{g}}\left(\tilde{\mathrm{x}}\right)=\frac{\exp\left[-\frac{\left(\tilde{\mathrm{g}}\left(\tilde{\mathrm{x}}\right)\right)^{2}}{2}\left(\sqrt{\frac{2}{\pi}}-\frac{\tilde{\mathrm{g}}'\left(\tilde{\mathrm{x}}\right)}{\left(\tilde{\mathrm{g}}\left(\tilde{\mathrm{x}}\right)\right)^{3}}\right)^{2}\right]}{\operatorname{erfc}\left[\frac{\tilde{\mathrm{g}}\left(\tilde{\mathrm{x}}\right)}{\sqrt{2}}\left(\sqrt{\frac{2}{\pi}}-\frac{\tilde{\mathrm{g}}'\left(\tilde{\mathrm{x}}\right)}{\left(\tilde{\mathrm{g}}\left(\tilde{\mathrm{x}}\right)\right)^{3}}\right)\right]}. \end{aligned} \tag{2.50}$$

We plot the parameter-free function $\tilde{\mathrm{g}}\left(\tilde{\mathrm{x}}\right)$ in Fig. 2.8.

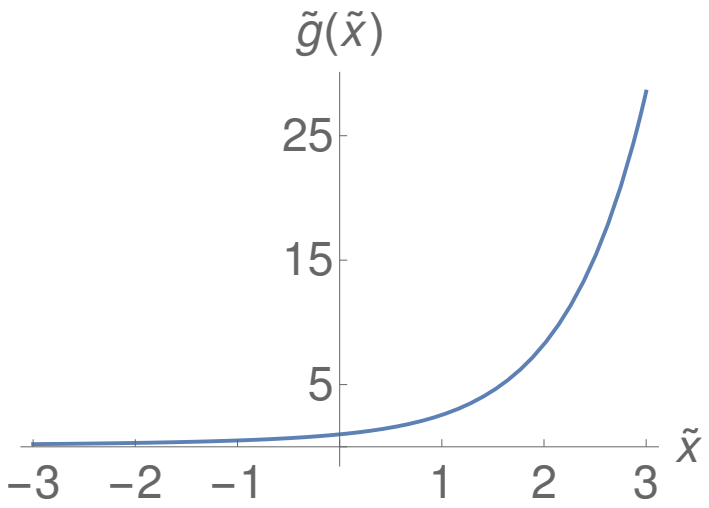

Figure 2.8 – Fixed-point solution for the boundary layer function $\tilde{\mathrm{g}}\left(\tilde{\mathrm{x}}\right)$ which describes the second derivative of the effective potential in the boundary layer. For the definition and implicit solution for $\tilde{\mathrm{g}}\left(\tilde{\mathrm{x}}\right)$ see Eq. (2.50).

3.4 Matching arguments for the inner region and the boundary layer

The boundary layer solution and the periodic solution of the $\tilde{\epsilon}=0$ equation are leading-order solutions in their respective regions. It is crucial to check that matching between these two solutions can be enforced, so that a solution can be constructed for all field values. The matching arguments at this leading order give us the scaling of the location of the minimum φ_{min} and of the second derivative $u''\left(\varphi_{min}\right)$ of the effective potential in φ_{min} with $\tilde{\epsilon}$.

In Section 3.2.1 we have found $u_0''(\varphi)$ to be periodic, where the index 0 stands for the solution of the $\tilde{\epsilon} = 0$ equation (exceptionally in this subsection). The periodic solution $u_0''(\varphi)$ describes the inner regon in the leading order. In Section 3.2.1 we have argued that the matching is to be done at such φ_M fields so that $1 \ll u_0''(\varphi_M) \ll u''(\varphi_{min}), u_0''(\varphi_*)$, or $\varphi_M < \varphi_{min} \lesssim \varphi_*$. The reason φ_{min} must be less than φ_* is that while doing the scale-balancing of SPT, we assumed that the width of the boundary layer (i.e., $\delta(\tilde{\epsilon})$) around φ_{min} vanishes as we approach $\tilde{\epsilon} \to 0^+$. Because of this, we know that for the boundary layer to be able to emerge before φ_*, φ_{min} must come before φ_*, as the boundary layer can be made arbitrarily narrow around φ_{min} by lowering the spatial dimension. All in all, the matching happens at fields φ_M that are less than the minimum (in the positive φ region), but for which the second derivative of the effective potential is very large (although less than the boundary layer divergence of $u''(\varphi)$). This means that we can choose an interval of matching field φ_M, where both the periodic and the boundary layer solution are valid (in an asymptotic sense), to be described by:

$$\varphi_{min} - \varphi_M = \mathcal{O}((\delta(\tilde{\epsilon}))^a), \quad 0 < a < 1, \quad \delta(\tilde{\epsilon}) \to 0^+, \tag{2.51}$$

or in the terms of the boundary layer field x:

$$x_M = \frac{\varphi_M - \varphi_{min}}{\delta(\tilde{\epsilon})} \propto -(\delta(\tilde{\epsilon}))^{a-1} = \frac{-1}{(\delta(\tilde{\epsilon}))^{|1-a|}} \to -\infty. \tag{2.52}$$

This is then a region in which we cannot anymore say that $u''(\varphi_M)$ is of $\mathcal{O}(1)$ (or even finite), but it still does not diverge as fast as $1/\delta(\tilde{\epsilon})$. Note that φ_M denotes a range of fields for which Eq. (2.51) holds and not a specific "boundary field", as the asymptotic matching between different filed scales is functional and not in a single value only.

We can show how $u''(\varphi_M)$ (and $u_0''(\varphi_M)$, as they must behave the same) scales in the leading order from the asymptotic behavior of the boundary layer solution in the matching region. Here $g(x) \ll 1$, so that $u''(\varphi)$ does not diverge as strongly as in the boundary layer. The implicit expression Eq. (2.49) then reduces to:

$$\frac{g(0)}{2g(x)} = \exp\left(\frac{(g'(x))^2}{2(g(x))^4}\right), \tag{2.53}$$

with a solution of the form:

$$-\frac{g(0)}{\sqrt{\pi}}x \approx \operatorname{erfi}\left(\sqrt{\ln\left(\frac{g(0)}{2g(x)}\right)}\right) \tag{2.54}$$

Inverting Eq. (2.54) we obtain the needed asymptotic limit:

$$\frac{g(0)}{g(x)} = \tilde{x}\sqrt{\ln(\tilde{x})}\left\{2 + \frac{1}{2}\frac{\ln[\ln(\tilde{x})]}{\ln(\tilde{x})} + \cdots\right\}, \qquad \tilde{x} := \frac{|x|\, g(0)}{\sqrt{2}}. \tag{2.55}$$

Finally, by using the fact that $u''(\varphi) = g(x)/\delta(\tilde{\epsilon})$ in the boundary layer and inserting φ_M, we arrive at

$$u_0''(\varphi_*) \gg u''(\varphi_M) = \mathcal{O}\left(\frac{1}{(\delta(\tilde{\epsilon}))^a\sqrt{\ln(1/\delta(\tilde{\epsilon}))}}\right) \overset{\delta(\tilde{\epsilon})\to 0}{\longrightarrow} +\infty. \tag{2.56}$$

3.4.1 Propagator singularity

We discuss an important consequence of the divergence of $u''(\varphi_*)$, namely that for the periodic solution to be matchable to the boundary layer solution, the propagator must develop a singularity.

The only way for the $\ell_n^{(d)}$ functions to diverge is through the propagator singularity (visible from heir defining expressions in Appendix A). In the following we find this divergence of the threshold functions by connecting, as before, $\ell_0^{(d)}(u''(\varphi), 1; \eta)$ to the dynamical variable $\Phi(\varphi)$ of the mapped-to anharmonic oscillator (see Section 3.2.1).

Starting from the energy-balance Eq. (2.25) for the anharmonic oscillator, we can write

$$\frac{1}{2}\dot{\Phi}^2(\varphi) = \int_{\Phi_0}^{\Phi(\varphi)} d\tilde{\Phi} F\Big(\tilde{\Phi}\Big), \qquad \dot{\Phi}(\varphi) = \partial_\varphi \Phi(\varphi), \quad \Phi_0 = \Phi(\varphi = 0). \tag{2.57}$$

We have dropped the index 0 from the periodic solution to simplify the notation. We remind the reader that $F(\Phi)$ is actually the second derivative $u''(\varphi)$. Then inside one half-period from 0 to φ_*, one has

$$0 = \int_{u''(0)}^{u''(\varphi_*)} dw w \partial_w \Phi(w). \tag{2.58}$$

where we have switched the measure from $\Phi(\varphi)$ to $F(\Phi) = u''(\varphi)$. Using partial integration, Eq. (2.58) can be rewritten as:

$$0 = u''(\varphi_*)\Phi(u''(\varphi_*)) - u''(0)\Phi(u''(0)) - \int_{u''(0)}^{u''(\varphi_*)} dw \Phi(w). \tag{2.59}$$

The function $\Phi(\varphi) = (2v_d/d)\ell_0^{(d)}(u''(\varphi), 1; \eta)$ is monotonically decreasing with $u''(\varphi)$. When $u''(\varphi)$ diverges, as is the case for $u''(\varphi_*)$, $\ell_0^{(d)}$ asymptotically goes to zero as $\propto 1/u''(\varphi_*)$ (see Appendix A), which means that $u''(\varphi_*)\Phi(u''(\varphi_*))$ is of $\mathcal{O}(1)$. We again take advantage of knowing this asymptotic limit of $\ell_0^{(d)}$ by dividing the domain of the remaining integral in Eq. (2.59) at some intermediate $u''(\varphi_c)$, which we choose positive and of $\mathcal{O}(1)$. Then, we estimate the part of the integral from φ_c to φ_* by

$$\int_{u''(\varphi_c)}^{u''(\varphi_*)} dw \Phi(w) \approx \int_{u''(\varphi_c)}^{u''(\varphi_*)} dw \frac{2\alpha v_d A^{(d)}(2-d)/d}{w} = \frac{2\alpha v_d A^{(d)}(2-d)}{d} \ln\left(u''(\varphi_*)\right) + \mathcal{O}(1). \tag{2.60}$$

Inserting this result in Eq. (2.59) and reverting to $\ell_0^{(d)}$ for clarity, we obtain

$$\alpha A_d \ln\left(u''(\varphi_*)\right) = -u''(0)\ell_0^{(d)}(u''(0), 1; \eta) - \int_{u''(0)}^{u''(\varphi_c)} dw\ \ell_0^{(d)}(w, 1; \eta) + \mathcal{O}(1). \tag{2.61}$$

The left-hand side diverges, so the right-hand side must diverge too. Since both $u''(\varphi_c)$ and $u''(0)$ are finite, the threshold function $\ell_0^{(d)}$ must carry this divergence. This threshold function can only diverge if the propagator develops a singularity. The dimensionless propagator at the LPA' level is given by:

$$g\Big(\varphi; y = \mathbf{q}^2/k^2\Big) = \frac{1}{u''(\varphi) + y(1 + r(y))}, \tag{2.62}$$

where y is the dimensionless momentum squared and must be positive. The pole is approached whenever the denominator vanishes. This can happen for different momenta, depending on the regulator. For the Theta regulator there are two ways to approach the pole, depending on α:

$$\left(y_{pole}, u''_{pole}\right) = \begin{cases} (0, -\alpha), & \alpha < 1 \\ (1, -1), & \alpha > 1, \end{cases} \tag{2.63}$$

as there is for the exponential regulator:

$$\left(y_{pole}, u''_{pole}\right) = \begin{cases} (0, -\alpha), & \alpha < 1 \\ (\ln(\alpha), -(1 + \ln(\alpha))), & \alpha > 1. \end{cases} \tag{2.64}$$

The singularity develops with the lowering of d towards d_{lc}, and $u''_{pole} < 0$ is first approached in $\varphi = 0$, as $u''(\varphi)$ has a minimum there. In the limiting process, while $\tilde{\epsilon} \ll 1$ but not 0, the value of $u''(0)$ must always stay slightly, but strictly, above the singular value u''_{pole}. This qualitative picture is general (regulator independent). It has been found from the matching conditions, meaning that it is connected to the divergence of $u''(\varphi_{min})$.

As the singularity is approached in the origin, we can estimate the threshold function $\ell_0^{(d)}$ in $\varphi = 0$, from Eq. (2.61):

$$\Phi(\varphi = 0) = \frac{2v_d}{d}\ell_0(d)\left(u''(0) \to u''_{pole}, 1; 2 - d\right) \sim \frac{2\alpha v_d A^{(d)}(2 - \eta)}{d\left|u''_{pole}\right|} \ln\left(u''(\varphi_*)\right) \to +\infty. \tag{2.65}$$

3.4.2 Divergence of the period of the $\tilde{\epsilon} = 0$ solution

The singularity of the propagator in the origin manifests itself in pushing the half-period φ_* to infinity. To show the divergence of φ_*, we will use the fact that the inflection point φ_i of $u(\varphi)$ happens before the minimum, $\varphi_i < \varphi_*$. We will first estimate the leading order behavior of φ_i, and then show that it is the same for φ_*.

We use the energy balance equation for the dynamical variable Φ (see Section 3.2.1),

$$\frac{1}{2}\left(\dot{\Phi}(\varphi)\right)^2 = \int_{\Phi_0}^{\Phi(\varphi)} d\tilde{\Phi} F(\tilde{v}), \quad \Phi_0 = \Phi(\varphi = 0), \tag{2.66}$$

to express the field as

$$\varphi(\Phi) = -\int_{\Phi_0}^{\Phi} \frac{d\tilde{\Phi}}{\sqrt{\int_{\Phi_0}^{\tilde{\Phi}} d\hat{\Phi} F\left(\hat{\Phi}\right)}}. \tag{2.67}$$

We have chosen to first investigate the inflection point φ_i (and $\Phi_i = \Phi(\varphi_i)$). This is because we know that $F(\Phi) = u''(\varphi)$ is a monotonically decreasing and negative convex function of Φ for for $\Phi_i < \Phi < \Phi_0$. The fact that $F(\Phi)$ is convex can be shown using the properties of the threshold functions. For start we expand $F''(\Phi)$:

$$F'(\Phi) = \frac{1}{\partial_F \Phi} \quad \Longrightarrow \quad F''(\Phi) = F'(\Phi)\partial_\Phi\left(\frac{1}{\partial_F \Phi}\right) = -\frac{\partial_F^2 \Phi}{(\partial_F \Phi)^2}. \tag{2.68}$$

We use the fact that $\Phi \propto \ell_0^{(d)}$ to evaluate its derivatives,

$$\partial_F^n \Phi = \frac{2v_d}{d} \partial_{u''(\varphi)}^n \ell_0^{(d)}(u''(\varphi), 1; \eta) = (-1)^n \frac{2v_d}{d} \ell_n^{(d)}(u''(\varphi), 1; \eta), \tag{2.69}$$

which, when introduced into Eq. (2.68), gives

$$F''(\Phi) = \frac{d}{2v_d} \frac{\ell_2^{(d)}(u''(\varphi), 1; \eta)}{\left(\ell_1^{(d)}(u''(\varphi), 1; \eta)\right)^3} > 0, \tag{2.70}$$

showing that $F(\Phi)$ is indeed convex. The explicit expressions for the threshold functions are given in Appendix A, and the fact that they are positive comes from the general properties of the regulator function.

Convexity tells us that any of its secants lays above the $F(\Phi)$ curve [132]. Choosing the intersection points to be at the origin $\varphi = 0$ and the inflection point φ_i, where the force $F(\Phi(\varphi)) = u''(\varphi)$ vanishes, gives us an estimate of the intermediate values:

$$|F(\Phi(\varphi = 0))| \geqslant |F(\Phi(\varphi))| \geqslant |F(\Phi(\varphi = 0))| \frac{\Phi(\varphi) - \Phi_i}{\Phi_0 - \Phi_i}, \quad \text{for} \quad 0 \leqslant \varphi \leqslant \varphi_i. \tag{2.71}$$

The first inequality comes from the monotonic decrease of Φ with $u''(\varphi) = F$ which then also holds for the inverse $F(\Phi)$, and we also account for $u''(\varphi)$ being negative before the inflection occurs. We use Eq. (2.71) estimates for the $F(\Phi)$ in the integral expression for φ, Eq. (2.67), to put limits on the inflection field φ_i from both above and below. The asymptotic behavior of Φ_0 (given in Eq. (2.65)) is utilized in Eq. (2.71) while integrating and combined with some algebra, gives the following analytic estimate of the leading order for the location of the inflection point:

$$\frac{\pi}{\sqrt{2}} \sqrt{\frac{\alpha v_d A_d}{d\left(u''_{pole}\right)^2}} \sqrt{\ln\left(u''(\varphi_*)\right)} \geqslant \varphi_i \geqslant 2 \sqrt{\frac{\alpha v_d A_d}{d\left(u''_{pole}\right)^2}} \sqrt{\ln\left(u''(\varphi_*)\right)}, \tag{2.72}$$

showing that the inflection point φ_i diverges with the logarithm of $u''(\varphi_*)$:

$$\varphi_* \geqslant \varphi_i \sim \sqrt{\ln\left(u''(\varphi_*)\right)}. \tag{2.73}$$

This already shows that the half period φ_* diverges, but in Appendix C we also find that the distance between the inflection point and the half-period vanishes, due to similar monotony and convexity (in this case concavity) arguments:

$$\varphi_* - \varphi_i \lesssim \mathcal{O}\left(\frac{1}{\sqrt{\ln\left(u''(\varphi_*)\right)}}\right) \to 0^+, \tag{2.74}$$

directly pinpointing the order of magnitude of the half-period of the periodic solution, in terms of the second derivative in that field, $u''(\varphi_*)$:

$$\mathcal{O}(\varphi_*) = \mathcal{O}(\varphi_i) \quad \overset{Eq.\ (2.73)}{\Longrightarrow} \quad \varphi_* \propto \sqrt{\ln\left(u''(\varphi_*)\right)}. \tag{2.75}$$

3.4.3 Scaling of the physical minimum φ_{min} with $\tilde{\epsilon}$

We have already noted that the matching of solutions from different SPT regions is not a boundary-value problem, but that the matching must be done on the level of functions, between the asymptotic forms.

Let us rewrite Eq. (2.4) in the following way:

$$u''(\varphi) = \tilde{\epsilon}\,\varphi u'''(\varphi) + \frac{2v_d}{(2-\eta)}\partial_\varphi^2\left[\ell_0^{(d)}(u''(\varphi), 1; \eta)\right]. \tag{2.76}$$

In the matching region, the $u''(\varphi)$ has to start to diverge in the $\tilde{\epsilon} = 0$ equation, so we can take $\ell_0^{(d)} \propto 1/u''(\varphi)$ (see Appendix A). On the other hand, the $\tilde{\epsilon}$-term has to stop being relevant in the BL equation for the match to be possible. In the region where we match them, both the boundary layer and the $\tilde{\epsilon} = 0$ equation for the second derivative of the potential thus have the same shape at the leading order,

$$u''(\varphi) = \frac{2\alpha v_d A^{(d)}(\eta)}{(2-\eta)}\partial_\varphi^2\left[\frac{1}{u''(\varphi)}\right], \tag{2.77}$$

or, reparametrized into the canonical form (see Appendix B),

$$u''(\varphi) = \partial_\varphi^2\left[\frac{1}{u''(\varphi)}\right]. \tag{2.78}$$

We proceed by integrating Eq. (2.78) in the matching region φ_M (see Eq. (2.51)). We can do this with the periodic solution

$$\varphi_* - \varphi_M \approx \frac{1}{u''(\varphi_M)\sqrt{2\ln\left(\dfrac{u''(\varphi_*)}{u''(\varphi_M)}\right)}}, \tag{2.79}$$

or we can find the same φ_M from integrating with the boundary layer asymptotics in mind:

$$\varphi_{min} - \varphi_M \approx \frac{1}{u''(\varphi_M)\sqrt{2\ln\left(\dfrac{u''(\varphi_{min})}{u''(\varphi_M)}\right)}} \approx \frac{1}{u''(\varphi_M)\sqrt{2\ln\left(\dfrac{1}{\tilde{\epsilon}\,\varphi_{min}u''(\varphi_M)}\right)}}. \tag{2.80}$$

Taking into account that both Eqs. (2.79) and (2.80) hold for any φ_M, the location of the actual minimum must obey

$$\varphi_{min} \sim \varphi_* \tag{2.81}$$

and the second derivatives must also match in the leading order:

$$u''(\varphi_*) \sim u''(\varphi_{min}) \sim \frac{1}{\delta(\tilde{\epsilon})} = \mathcal{O}\left(\frac{1}{\tilde{\epsilon}\,\varphi_{min}}\right) \overset{Eq.\ (2.81)}{=} \mathcal{O}\left(\frac{1}{\tilde{\epsilon}\,\varphi_*}\right). \tag{2.82}$$

Using results of Section 3.4.2 elucidating the divergence of the half-period φ_*, we arrive at:

$$\begin{aligned} &\varphi_{min} \sim \varphi_* \sim \sqrt{\ln\left(\frac{1}{\tilde{\epsilon}}\right)}, \\ &u''(\varphi_{min}) \sim u''(\varphi_*) \sim \frac{1}{\tilde{\epsilon}\sqrt{\ln\left(\dfrac{1}{\tilde{\epsilon}}\right)}}. \end{aligned} \tag{2.83}$$

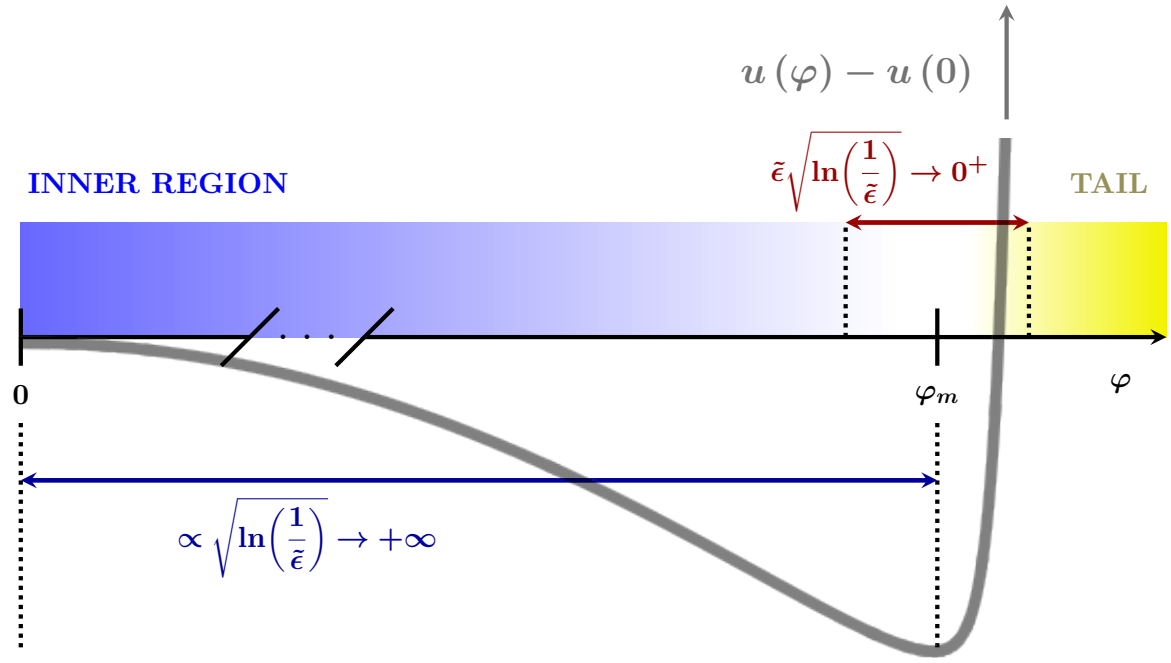

Figure 2.9 – The sketch of the SPT regions. We indicated the scales of the minimum φ_{min} and the width of the boundary layer $\delta(\tilde{\epsilon})$ that we have found from the leading-order fixed-point solution constructed across the regions.

This scaling of φ_{min} given in Eq. (2.83) agrees with the assumption of the boundary layer width $\delta(\tilde{\epsilon})$ vanishing in the $\tilde{\epsilon} \to 0$ limit:

$$\delta(\tilde{\epsilon}) \sim \tilde{\epsilon}\sqrt{\ln\left(\frac{1}{\tilde{\epsilon}}\right)}. \tag{2.84}$$

We note that $\delta(\tilde{\epsilon})$ describes the divergence of $u''(\varphi) \propto 1/\delta(\tilde{\epsilon})$ in the boundary layer. A very significant result of matching is then that we have found how the approach to the singularity of the propagator in $\varphi = 0$ is reflected in the divergent scaling of φ_{min} and $u''(\varphi_{min})$.

We can now complement the sketch of the SPT regions given in Fig. 2.5 with the actual scales. The result is given in Fig. 2.9.

We now comment on the numerical results above the lower critical dimension presented in Section 2. From them, we expected that if the location of the minimum φ_{min} diverges, it must do so very slowly, and that the value of the second derivative $u''(\varphi_{min})$ should diverge as $1/\tilde{\epsilon}$.

Our numerical calculations cannot identify the logarithmic scalings that we have found analytically, as those diverge very weakly when $\tilde{\epsilon} \to 0^+$. Nevertheless, from Fig. 2.10 we can see that the numerical results are compatible with

$$\varphi_{min}/\sqrt{\ln(1/\tilde{\epsilon})} = \mathcal{O}(1), \qquad \tilde{\epsilon}\sqrt{\ln(1/\tilde{\epsilon})}\, u''(\varphi_{min}) = \mathcal{O}(1). \tag{2.85}$$

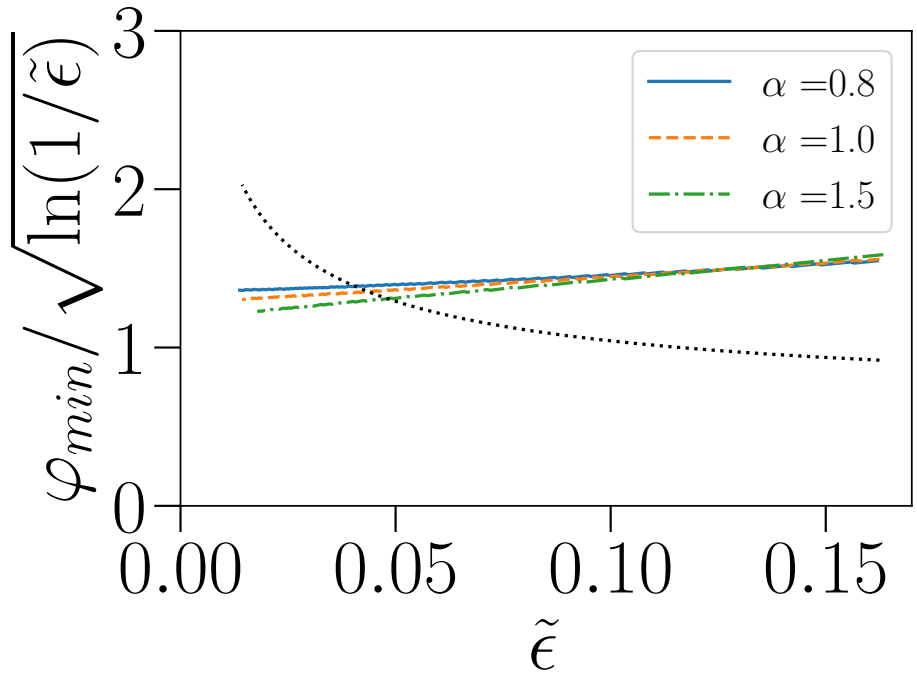

(a) Scaling of the location of the minimum of the effective potential φ_{min}. The black dotted line is illustrative and shows how the dependence would look if $\varphi_{min} \propto 1/\sqrt{\tilde{\epsilon}}$.

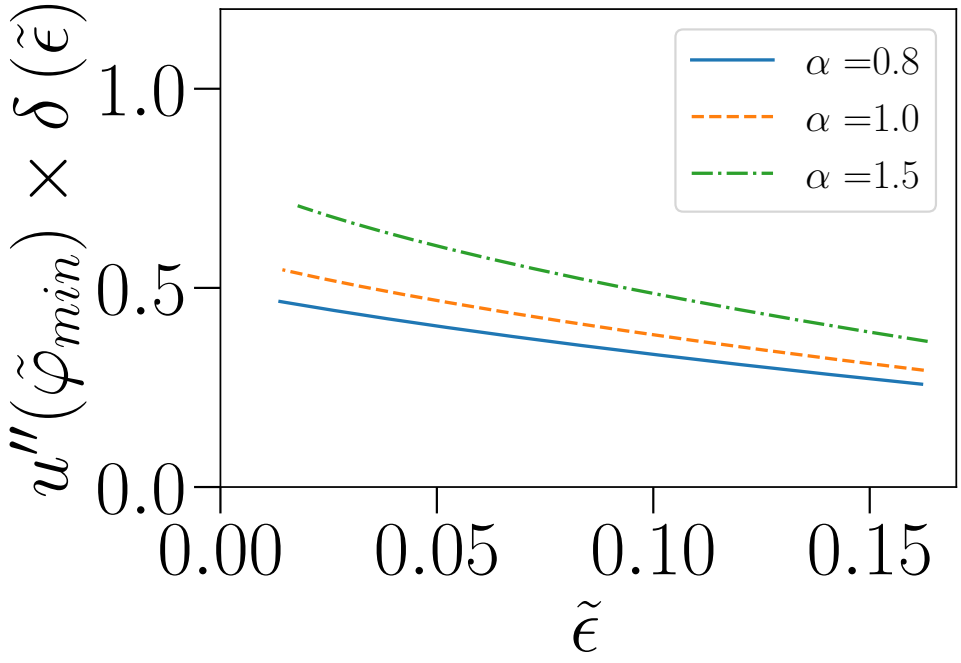

(b) Scaling of the second derivative in φ_{min}, $u''(\varphi_{min})$, with $\delta(\tilde{\epsilon}) = \tilde{\epsilon}\sqrt{\ln(1/\tilde{\epsilon})}$.

Figure 2.10 – Numerical fixed-point results obtained above the lower critical dimension from solving for the fixed point using a Newton-Rhapson method (see Section 2), compared to scaling obtained analytically in Section 3.4.3.

3.5 Determination of the value of the lower critical dimension

While solving the boundary-layer equations in Section 3.3.2, we have found the value of $g'(0)/(g(0))^2$. The boundary-layer solution for $u''(\varphi)$ is not the only place this parameter occurs. We turn our attention to the expression for the anomalous dimension η as given by the fixed-point equation, Eq. (2.3):

$$\begin{aligned}\eta =& \frac{4v_d}{d} m_{4,0}^{(d)}(u''(\varphi_{min}),1;\eta)\left(u'''(\varphi_{min})\right)^2 = \\ =& 4v_d\alpha\left[A^{(d)}(\eta) - \frac{\alpha}{d}B^{(d)}(\eta)\right]\left[\frac{g'(0)}{(g(0))^2}\right]^2 = \frac{8v_d\alpha}{\pi}\left[A^{(d)}(\eta) - \frac{\alpha}{d}B^{(d)}(\eta)\right],\end{aligned} \tag{2.86}$$

where we have used the boundary-layer function $g(x)$ and the fact that $x = 0$ for $\varphi = \varphi_{min}$. The boundary-layer expression for the threshold function $m_{4,0}^{(d)}$ is listed in Eqs. (2.35) to (2.37).

At the lower critical dimension itself, $\tilde{\epsilon}$ vanishes. This gives $\eta = 2 - d_{lc}$ for the anomalous dimension. Combining this with the expression for the anomalous dimension given by Eq. (2.86), we find the expression for the value of the lower critical dimension:

$$d_{lc} = \frac{2(\pi - \alpha_*(d_{lc}))}{\pi + 4 - 3\alpha_*(d_{lc})}, \qquad \alpha_*(d) = \begin{cases}\alpha, & r_\Theta(y) \\ \alpha 2^{-(1+d/2)}, & r_{\exp}(y).\end{cases} \tag{2.87}$$

This dependence is plotted in Fig. 2.11. We observe that reasonable values are obtained

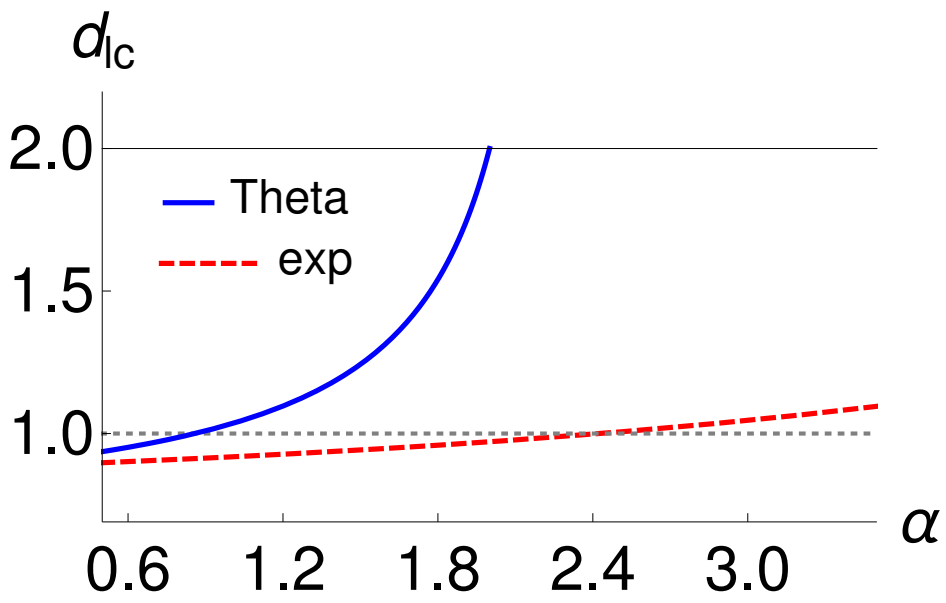

Figure 2.11 – Dependence of the value of the lower critical dimension d_{lc} on the regulator prefactor α. The $d_{lc} = 1$, $d_{lc} = 2$ lines are included as a visual guide. We remind that due to $\eta_{d_{lc}} = 2 - d_{lc}$, we work below $d = 2$.

for the exponential regulator with the usual $\mathcal{O}(1)$ prefactors, where they are within 10% of

the exact value, $d_{lc} = 1$. The Theta regulator deviates more significantly. Unfortunately, d_{lc} does not display an extremum as a function of α which would allow us to determine an optimal value by the use of the aforementioned principle of minimal sensitivity (PMS) (see Chapter 1, Section 1.2.2). PMS tells us that the α which produces the best solutions can be found by demanding that a small change in α around its optimal value minimally changes the critical exponents or other universal physical quantities, such as d_{lc}.

Knowing the dependence of d_{lc} on the regulator prefactor, we turn back to the numerical results above d_{lc}. As an illustration, we plot extrapolated results for d_{lc} for the r_{exp} and several prefactor choices. The extrapolations are done from the $\tilde{\epsilon}\,(d)$ curves down to the $\tilde{\epsilon}\,(d_{lc}) = 0$ value. These results are displayed in Fig. 2.12. We can see that these extrapolations are in good agreement with the analytical curve, speaking in favor of numerics capturing the echoes of the singular $d \to d_{lc}$ limit at finite $\tilde{\epsilon}$.

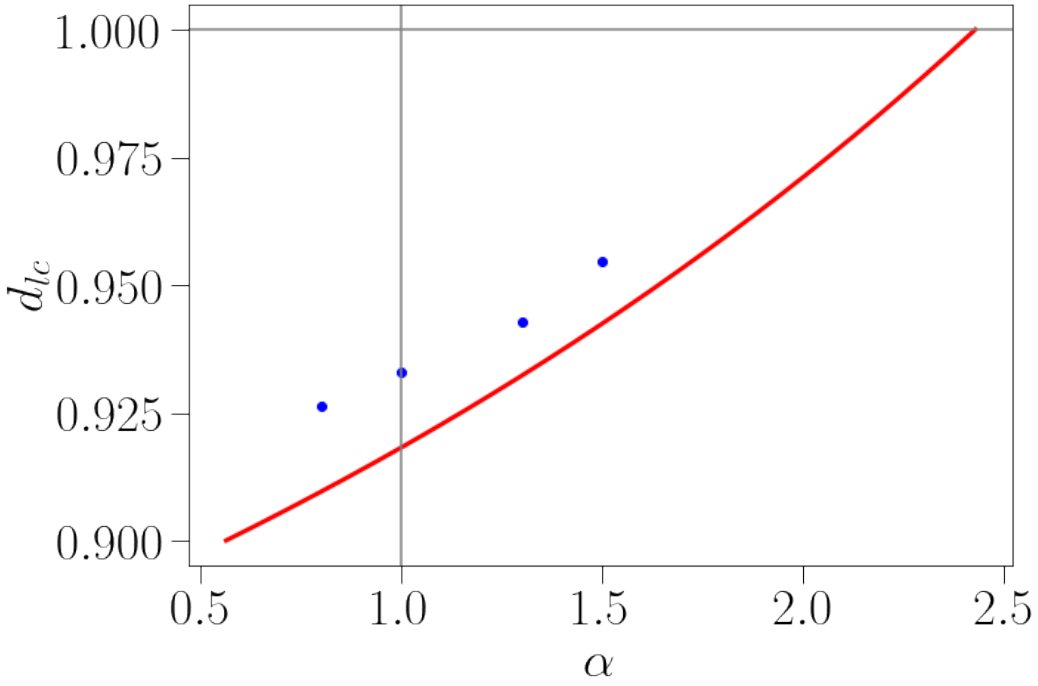

Figure 2.12 – Extrapolations (blue dots) for the value of the lower critical dimension for the exponential regulator and several prefactors α compared to the analytical curve shown in red. The gray lines $d_{lc} = 1$ and $\alpha = 1$ are included as visual guides.

4 Conclusion

After introducing the LPA' fixed-point equations in Section 1, in Section 2 we have presented numerical results in the LPA' approximation for the scalar ϕ^4 theory above the lower critical dimension (d_{lc}). The result for the location of the minimum of the effective potential, φ_{min}, indicates that it does not scale as $1/\sqrt{\tilde{\epsilon}}$, as is assumed in [122], but grows instead more slowly (here, $\tilde{\epsilon} = (d - 2 + \eta)/[2(2 - \eta)]$). We also find a divergence of $u''(\varphi_{min})$ similar to $1/\tilde{\epsilon}$. These numerical results drove us to use the Singular Perturbation Theory (SPT), as

the $\tilde{\epsilon}$ limit for the fixed-point functions is not uniform in the field.

Through the use of SPT in Section 3, we have investigated the properties of the fixed-point LPA' solution at the leading order of the $\tilde{\epsilon} \to 0^+$ limit. To do so, we have separated the field domain into three qualitatively different regions. It was essential to recognize the emergence of a boundary layer of vanishing width as an intermediate region, located between an inner region situated between the two minima $\pm\varphi_{min}$ and the tail region where the potential $u(\varphi)$ and its derivatives exhibit power-law behavior controlled by the scaling part of their flow equations.

From the matching conditions between these regions and an implicit solution in the boundary layer, we have analytically found in Section 3.4 that the propagator develops a singularity in the origin of the field in the limit of the lower critical dimension. From this, we have found the scaling of the φ_{min} and $u''(\varphi_{min})$ with $\tilde{\epsilon}$ (as $\varphi_{min} \propto \sqrt{\ln(1/\tilde{\epsilon})}$ and $u''(\varphi_{min}) \propto 1/(\tilde{\epsilon}\,\varphi_{min})$). The identification of the propagator singularity as the cause of the divergence of $u''(\varphi_{min})$ signaled by numerical results of Section 2 is a significant consequence of the matching procedure. This singularity of the propagator is in agreement with the expected merging of the critical fixed point and the zero-temperature fixed point controlling the ordered phase and it is one of the anticipated hallmarks of the approach to the lower critical dimension (d_{lc}).

Matching conditions have also been used to find the value of d_{lc} as a function of the regulator prefactor in Section 3.5. We stress that matching through all of the regions has been achieved automatically, in the sense that it can be done for any (d_{lc}, α) pair - it does not fix either of the values. There is no extremum for the analytical $d_{lc}(\alpha)$ curves, so the Principle of Minimal Sensitivity can also not be applied.

The critical temperature and critical exponents will be discussed in Chapter 4.

In the next chapter, we first investigate the same $\tilde{\epsilon} \to 0^+$ limit at the second order of the derivative expansion.

Chapter 3

Approach to the lower critical dimension within the second order of the derivative expansion (∂_2)

In Chapter 2 we have provided a picture of the approach to the lower critical dimension of the scalar ϕ^4 theory in the minimally modified Local Potential Approximation (LPA'). LPA' is the lowest approximation in the derivative expansion scheme of FRG that one can use to reach systems at low spatial dimensions, $d < 2$. Here we check the stability of the results upon increasing the approximation order. Some of the LPA' results were also unsatisfactory, as for example the lack of an optimal regulator prefactor α that would more crisply pinpoint the value of the lower critical dimension. Hence, in this chapter we work in the second order of the derivative expansion, ∂_2. This is a line of research that we are still actively pursuing, as the coupling of the equations for the effective potential and the field renormalization function $z_k(\varphi)$ make the problem much more complicated than in LPA' where $z_k(\varphi) = 1$.

1 Flow equations

The flow equations are given in Chapter 1, Section 1.3. For completeness, we repeat here the results for the flow of the dimensionless effective potential and field renormalization function:

$$\partial_t u_k(\varphi) = -d u_k(\varphi) + (2-\eta_k)\,\tilde{\epsilon}_k\,\varphi u_k'(\varphi) + 2 v_d \ell_0^{(d)}, \tag{3.1}$$

$$\begin{aligned}\partial_t z_k(\varphi) =& \eta_k z_k(\varphi) + (2-\eta_k)\,\tilde{\epsilon}_k\,\varphi\, z_k'(\varphi) + \\ &+ \frac{2}{d} v_d \Big\{ \left(z_k'(\varphi)\right)^2 \left[(2d+1)\,\ell_2^{(d+2)} - 2 m_{4,0}^{(d+4)}\right] - d z_k''(\varphi)\,\ell_1^{(d+2)} + \\ &+ 2 z_k'(\varphi)\, u_k'''(\varphi)\left(d\ell_2^{(d)} - 2 m_{4,0}^{(d+2)}\right) - 2\left(u_k'''(\varphi)\right)^2 m_{4,0}^{(d)}\Big\},\end{aligned} \tag{3.2}$$

where $t = \ln(k/\Lambda)$.

We also use the flow equation for the second derivative $u_k''(\varphi)$, which is derived by twice differentiating $\partial_t u_k(\varphi)$ with respect to the field:

$$\begin{aligned}\partial_t u_k''(\varphi) = &-(2-\eta_k)\,u_k''(\varphi) + (2-\eta_k)\,\tilde{\epsilon}_k\,\varphi u_k'''(\varphi) + \\ &- 2v_d\big[u_k^{iv}(\varphi)\,\ell_1^{(d)} + z_k''(\varphi)\,\ell_1^{(d+2)} - \left(u'''(\varphi)\right)^2\ell_2^{(d)} + \\ &\qquad - z_k'(\varphi)\,u_k'''(\varphi)\,\ell_2^{(d+2)} - \left(z_k'(\varphi)\right)^2\ell_2^{(d+4)}\big],\end{aligned} \tag{3.3}$$

The flow equation for the second derivative of the effective potential $u_k''(\varphi)$ is included here because this function is present in the propagator of the theory and, consequently, in the nontrivial parts of the flow of all the other RG functions. Its conceptual relevance and operational practicality are also evident from the LPA' calculations of Chapter 2. The equation for $\partial_t u_k''(\varphi)$ together with $\partial_t z_k(\varphi)$ form a closed system of partial differential equations, and $u(\varphi)$ can be recovered by twice integrating $u''(\varphi)$, up to a physically irrelevant constant. We continue to work in $u''(\varphi)$ instead of $u(\varphi)$.

We proceed by searching for the fixed-point solutions of these equations which satisfy $\partial_t u_k''(\varphi) = 0$ and $\partial_t z_k(\varphi) = 0$. The anomalous dimension η is calculated from $\partial_t z_k(\varphi) = 0$ evaluated at the renormalization field φ_r for which $z_k(\varphi_r) = 1$. At the approximation level ∂_2 we choose $\varphi_r = 0$.

In the following section we present numerical ∂_2 results above d_{lc}. In Chapter 2 on LPA', the numerical data was largely complemented and explained by analytical results, which will unfortunately not be the case here. The ∂_2 level is significantly more complicated than the LPA' equivalent due to the coupling between the $u''(\varphi)$ and $z(\varphi)$ equations, and we have not been able to do as much analytically at the present moment. For instance, an important difference is that we have found no way to properly determine the leading-order solutions in the inner region as we did in Chapter 2, Section 3.2. Therefore, after a numerical investigation at $d > d_{lc}$, we will focus on the boundary layer region.

2 Numerical fixed-point results above the lower critical dimension

As in Chapter 2 Section 2 on LPA', we solve for fixed points above the lower critical dimension using a modified Newton-Rhapson method (done in FORTRAN90 [124]), until the procedure fails at some $d > d_{lc}$, for the same reason as in LPA' - the problem is singular and we saturate the precision. With Fig. 3.1 we illustrate solutions for the effective potential at the LPA' and ∂_2 approximation level. The solutions do not differ qualitatively for other choices of the regulator function or prefactor, save for difficulties with r_Θ for $\alpha \geqslant z(0) = 1$ (for examples of difficutiles, see Fig. E.1 in Appendix E), and we include some examples of different choices in Appendix E.

In Fig. 3.1 we can see that the ∂_2 fixed-point effective potential has the same apparent features as in LPA', including indications of a possible singular $d \to d_{lc}^+$ limit. This is more evident in the second derivative $u''(\varphi)$. Comparing Fig. 3.1c and Fig. 3.1d we see in both approximations the tendency of $u''(0)$ to diminish as the dimension is lowered, possibly toward the propagator singularity, and a trend pointing toward the divergence of $u''(\varphi)$ in the neighborhood of φ_{min}.

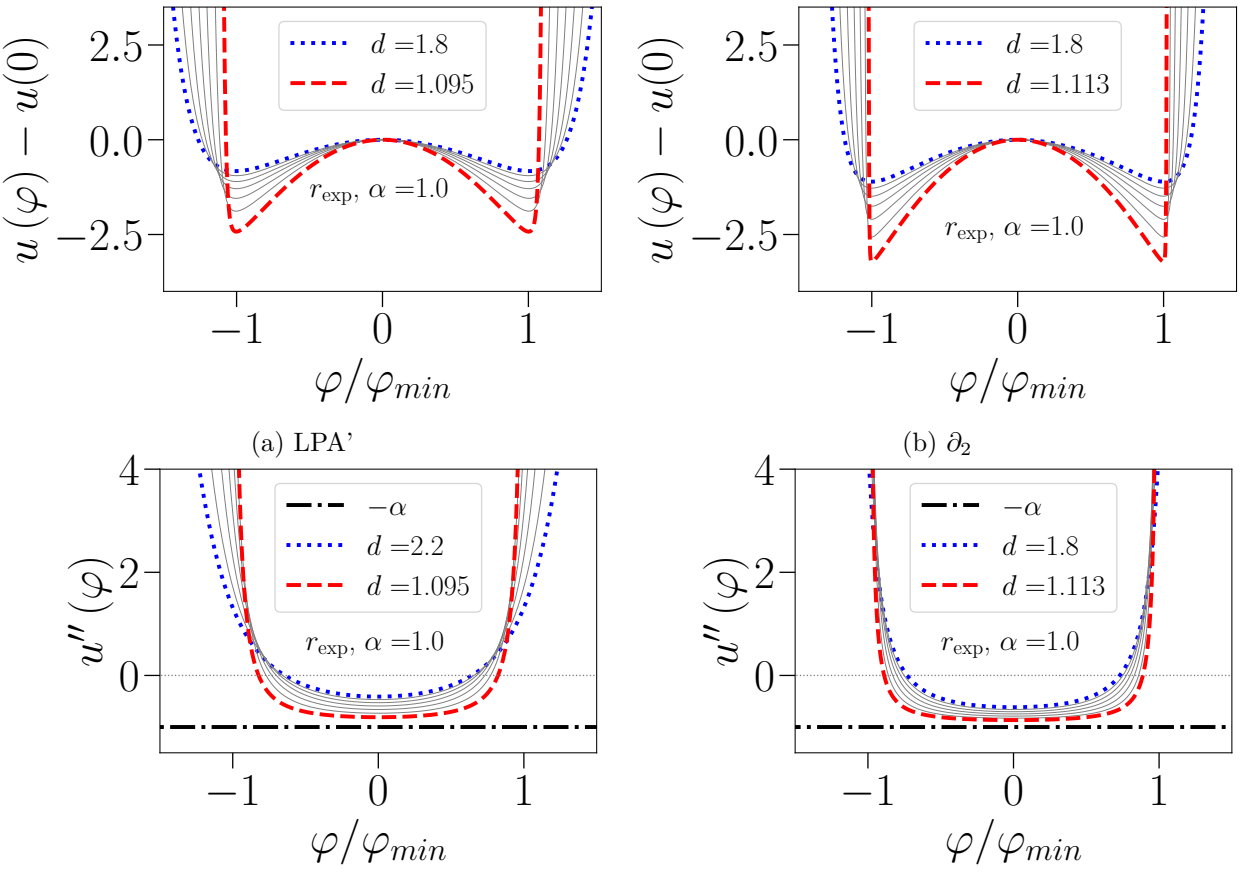

(a) LPA' (b) ∂_2

(c) LPA' (d) ∂_2

Figure 3.1 – Numerical results for the fixed-point effective potential $u(\varphi)$ and its second field-derivative $u''(\varphi)$ in the two lowest applicable consecutive orders of the derivative expansion. In LPA' the prescription for the field renormalization was done in $\varphi_r = \varphi_{min}$, while at ∂_2, we used $\varphi_r = 0$.

These shared qualitative propensities of the effective potential in both LPA' and ∂_2 lead us to check for an analogous boundary layer in the second order of the derivative expansion.

Another clear indication of the need to investigate the φ_{min} neighborhood separately and with special care is the tendency of the field renormalization function to spike there as the dimension is lowered, as seen in Fig. 3.2.

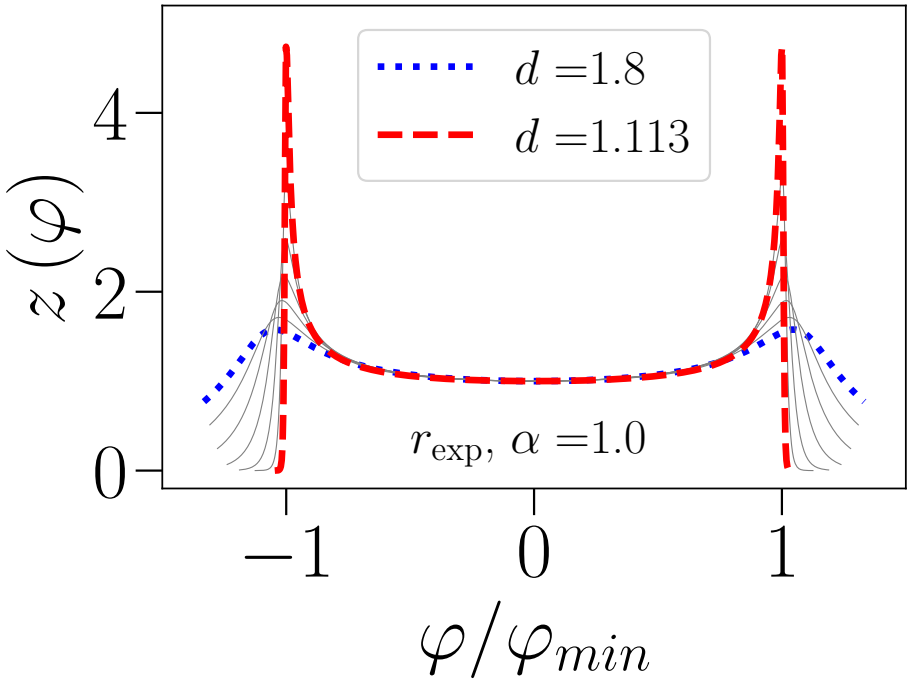

Figure 3.2 – Field renormalization function for $d > d_{lc}$.

In Fig. 3.3 we compare the scaling of φ_{min} and $u''(\varphi_{min})$ in LPA' with the ∂_2 results. We see that the scaling analytically obtained at LPA' is compatible with the numerical results in ∂_2. This is of course not a rigorous confirmation, and we do not treat it as such.

To underline this, we also plot the second derivative $\chi''(\varphi)$ of the dimensionless susceptibility $\chi(\varphi) = (\alpha + u''(\varphi))^{-1}$ in φ_{min} (as seen in Fig. 3.5). We chose this function out of operational practicality.[1] We see that the results seem to be in agreement with $\delta(\tilde{\epsilon})\,\chi''(\varphi_{min}) = \mathcal{O}(1)$ for $\delta(\tilde{\epsilon}) \propto \tilde{\epsilon}\sqrt{\ln(1/\tilde{\epsilon})}$, which is the analytical LPA' result for the scaling. We note that in the reminder of this chapter we only assume $\delta(\tilde{\epsilon}) \to 0$ and do not use the analytical result from LPA' on how $\delta(\tilde{\epsilon})$ scales with $\tilde{\epsilon}$.

The difference between LPA' and ∂_2 is the field renormalization function. In LPA', it is taken that $z(\varphi) = 1$, but in ∂_2 the fixed-point field renormalization function must be calculated. A numerical result of such a calculation has already been shown in Fig. 3.2. Other regulator choices are shown in Appendix E for plots of fixed-point solutions, Figs. E.2

[1] We remind that the numerics is actually carried out for the susceptibility $\chi(\varphi) = 1/(u''(\varphi) + \alpha)$ as this is a function bounded from above for $|\varphi| \to +\infty$, with a maximum in $\varphi = 0$, unlike $u(\varphi)$ or any of its field-derivatives, which have divergent tails with power law behavior determined by the scaling parts of their flow equations.

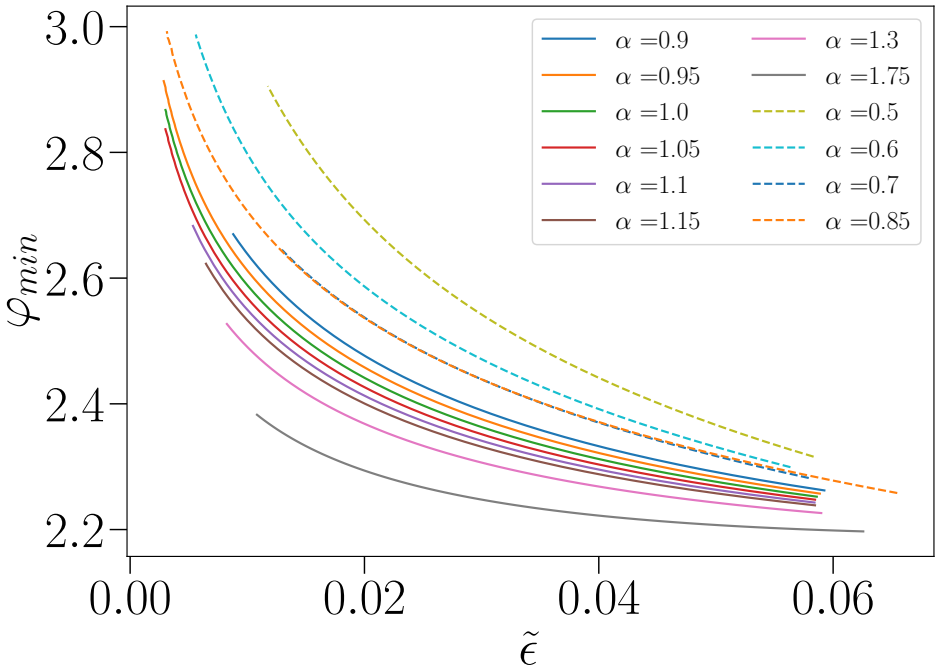

(a) Numerical data for φ_{min} obtained from fixed-point solutions above d_{lc}.

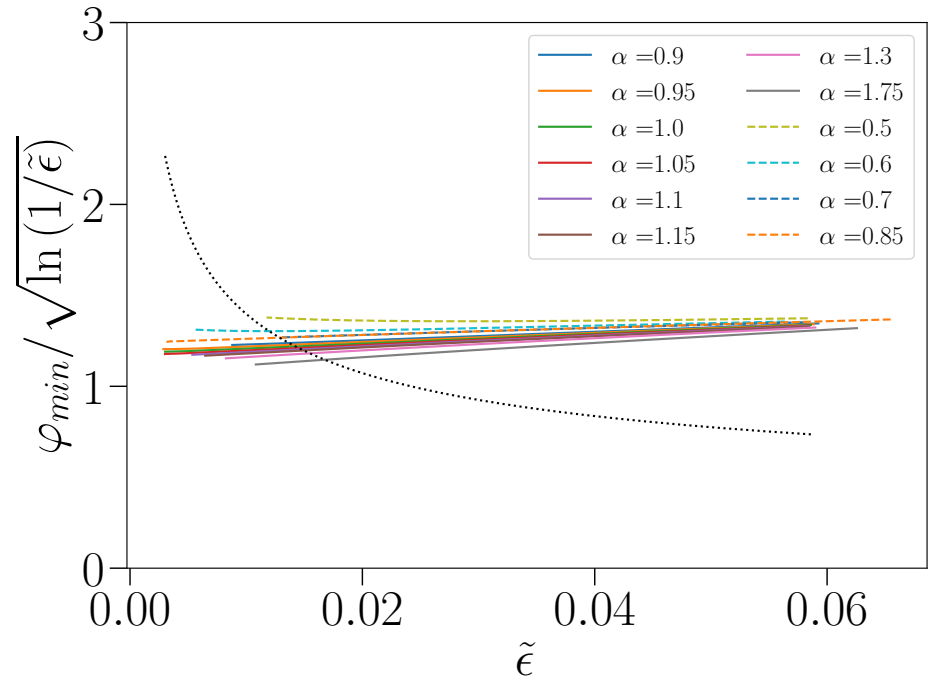

(b) We expect the same scaling of the data for φ_{min} as in LPA'. The black dotted line is illustrative and shows how the dependence would look if $\varphi_{min} \propto 1/\sqrt{\tilde{\epsilon}}$.

Figure 3.3 – Numerical results for the location of the minimum of the fixed-point effective potential, φ_{min}, in the ∂_2 order, compared with the boundary layer scaling analytically obtained for LPA'.
Full lines: r_{exp}, dashed lines: r_Θ.

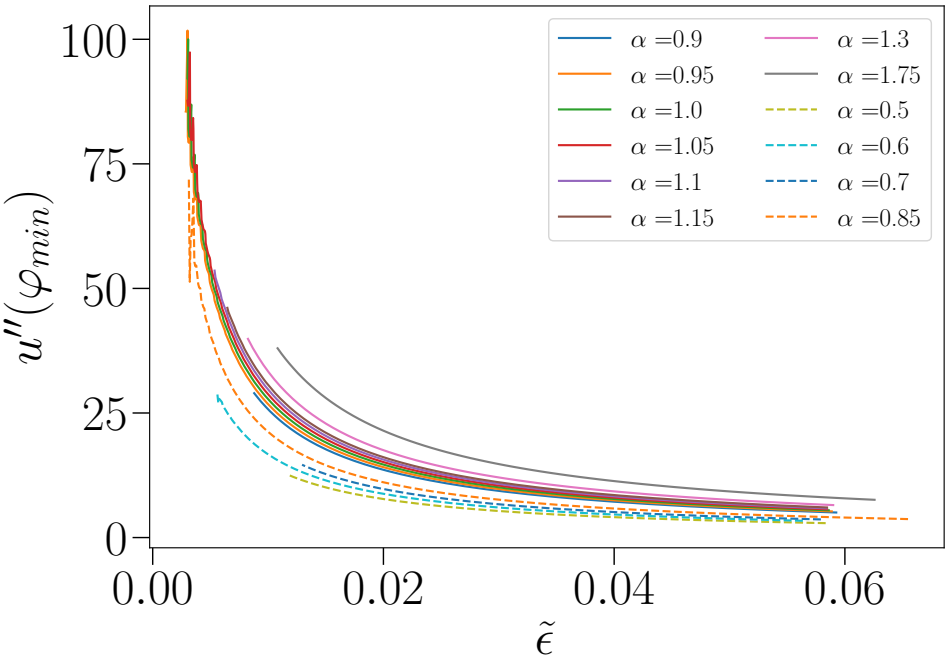

(a) Numerical data for $u''(\varphi_{min})$ obtained from fixed-point solutions above d_{lc}.

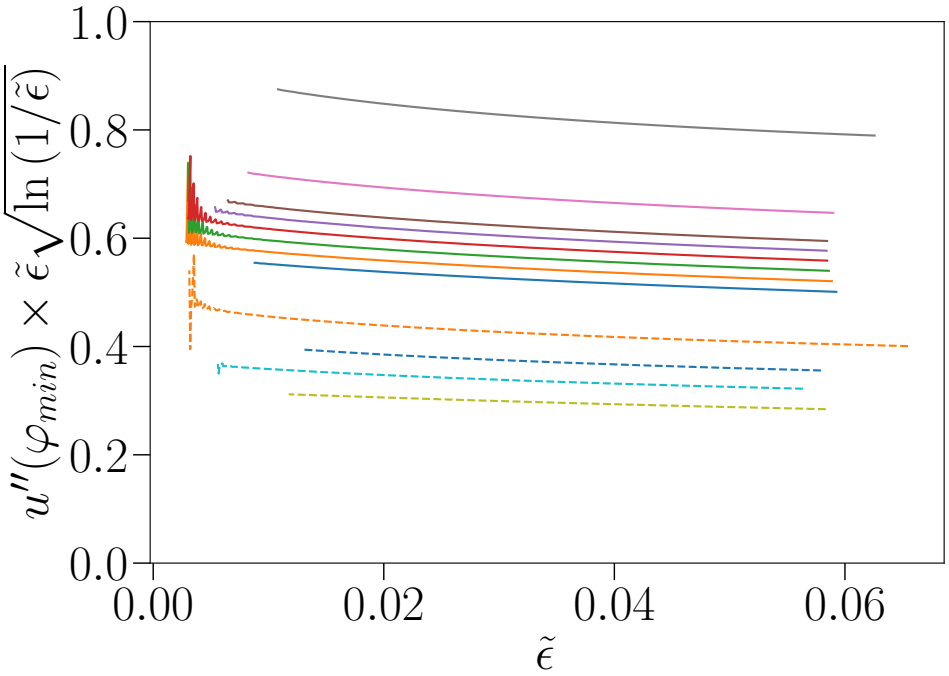

(b) Scaling of the same data for $u''(\varphi_{min})$ with $\delta(\tilde{\epsilon}) \propto \tilde{\epsilon}\sqrt{\ln(1/\tilde{\epsilon})}$.

Figure 3.4 – Numerical results for the fixed-point value of the second field-derivative in the location of the minimum, $u''(\varphi_{min})$, for the ∂_2 order, compared with the boundary layer scaling analytically obtained for LPA'.
Full lines: r_{exp}, dashed lines: r_Θ. Regulator prefactors α specified on the upper plot are valid for both plots.

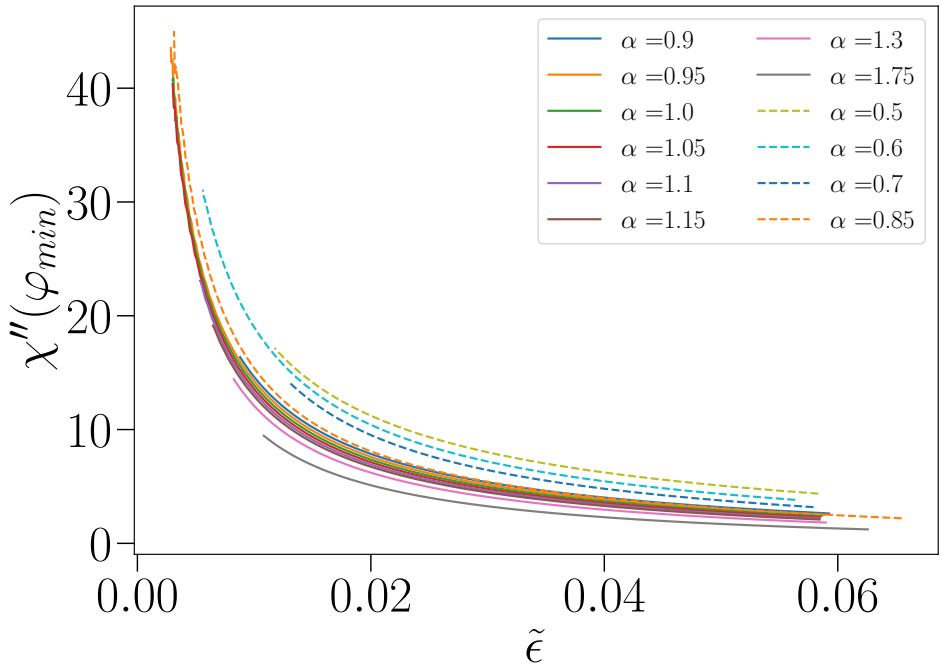

(a) Numerical data for $\chi''(\varphi_{min})$.

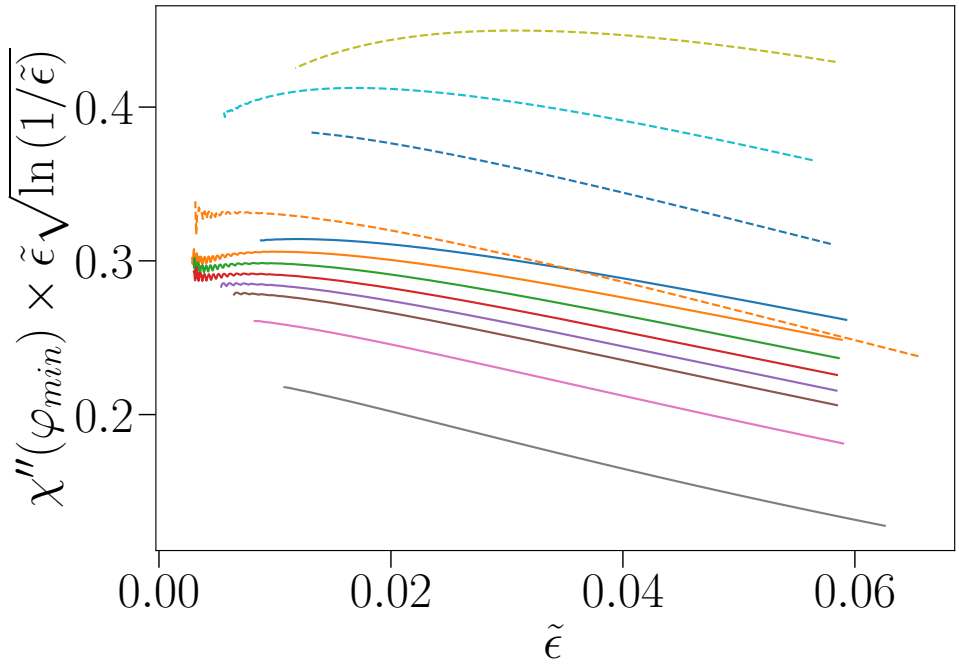

(b) The comparison of scaling of the same data for $\chi''(\varphi_{min})$ with $\delta(\tilde{\epsilon}) \propto \tilde{\epsilon}\sqrt{\ln(1/\tilde{\epsilon})}$.

Figure 3.5 – Numerical results for the fixed-point value of the second derivative of the susceptibility in the location of the minimum, $\chi''(\varphi_{min})$, for the ∂_2 order, compared with the boundary layer scaling analytically obtained for LPA'.
Full lines: r_{exp}, dashed lines: r_{Θ}. Regulator prefactors α specified on the upper plot are valid for both plots.

and E.3, but there is no qualitative difference from what can be seen in Fig. 3.2 (r_Θ, $\alpha \geqslant 1$ results excluded). When calculating for $d > d_{lc}$, we chose $z(0) = 1$, meaning that we used the prescription $\varphi_r = 0$ for the field renormalization, as already stated. We remind that in LPA' it was optimal to renormalize at $\varphi_r = \varphi_{min}$, but in ∂_2 the choice is less relevant and $\varphi_r = 0$ simplifies numerical calculations.

It is evident from Fig. 3.2 that $z(\varphi)$ peaks in the vicinity of the location of the minimum φ_{min}. This makes it doubtful that we can take $z(\varphi)$ to be of $\mathcal{O}(1)$ in the boundary layer, as it was with $z(\varphi) = 1$ in LPA'. The question of the maximal value of $z(\varphi)$ is especially interesting as analytical arguments of SPT do not pinpoint the boundary layer scaling, and we will have to use numerical indicators to form an ansatz for the behavior of the field renormalization function in the boundary layer. With this in mind, we focus on the value of $z(\varphi_{z\max})$ in its maximum, $\varphi_{z\max}$. From the shape of $z(\varphi)$ in Fig. 3.2, we expect $\varphi_{z\max}$ to be in the boundary layer. We stress that we cannot claim with certainty that we are numerically close enough to the d_{lc} limit to capture the asymptotic behavior of the fixed-point solutions, and one can in general not speak about a boundary layer in numerics. What we are investigating are the trends in the vicinity of φ_{min} as the dimension (or $(\tilde{\epsilon})$) is lowered. We plot the results for $z(\varphi_{z\max})$ in Fig. 3.6.

We see from Fig. 3.6 that the maximum of $z(\varphi)$ grows as we lower the dimension, and we cannot exclude that it might diverge in the $\tilde{\epsilon} \to 0$ limit. To better qualify this tentative divergence, we define a scale $\kappa(\tilde{\epsilon})$ as the measure of the ratio of $z(\varphi)$ and $u''(\varphi)$ in the boundary layer:

$$\begin{aligned} &\frac{z(\varphi)}{u''(\varphi)} \propto \kappa(\tilde{\epsilon}) \quad \text{in the boundary layer :} \quad z(\varphi) = \frac{\kappa(\tilde{\epsilon})}{\delta(\tilde{\epsilon})}\zeta(x), \\ &\text{with} \quad x = \frac{\varphi - \varphi_{min}}{\delta(\tilde{\epsilon})} = \mathcal{O}(1) \quad \text{leading to} \quad \zeta(x) = \mathcal{O}(1). \end{aligned} \tag{3.4}$$

However, if $z(\varphi)$ diverges, from the comparison of the numerical data for $z(\varphi_{z\max})$ with the LPA' scaling $\delta(\tilde{\epsilon})$ shown in Fig. 3.6b, we expect it to do so more slowly than $u''(\varphi_{min})$. (Yet, we do not have firm proof of $\delta(\tilde{\epsilon})$ scaling the same in ∂_2 as in LPA', and we are above d_{lc}.) In Fig. 3.7 we show that the numerical results could possibly be compatible with

$$\kappa(\tilde{\epsilon}) \approx \frac{1}{\sqrt{\ln(1/(\tilde{\epsilon}))^5}}. \tag{3.5}$$

This is of course not a strict determination and we do not use the actual scaling in Eq. (3.5) in the following. We just use the compatibility of the $d > d_{lc}$ numerical results with $z(\varphi)$ diverging (but more slowly than $u''(\varphi)$) to justify the boundary-layer ansatz. We find the spiking of $z(\varphi)$ around the location of the minimum φ_{min} instructive and we choose to focus on a regime where $\delta(\tilde{\epsilon}) \ll \kappa(\tilde{\epsilon}) \to 0^+$.

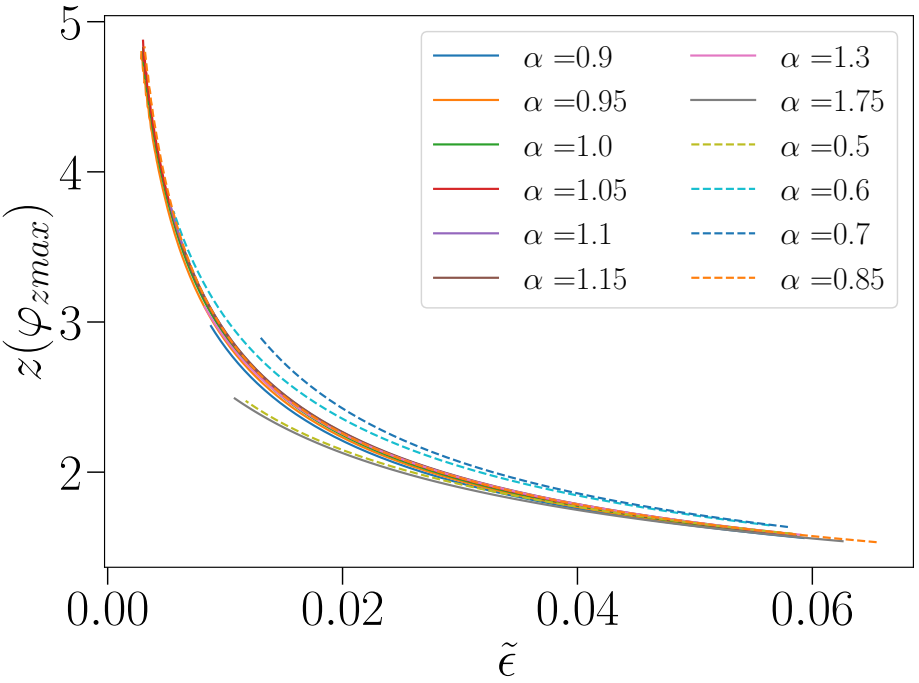

(a) Numerical data.

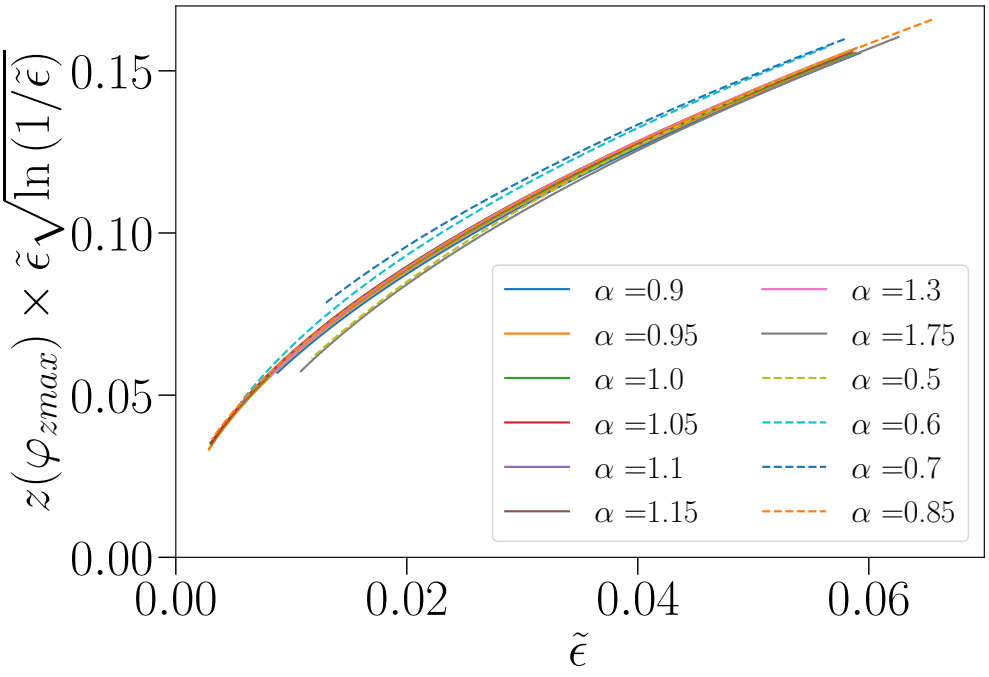

(b) Compared with the boundary layer scaling of $u''(\varphi_{min})$ analytically obtained for LPA'.

Figure 3.6 – Numerical results for the fixed-point value of the field renormalization function in its maximum, $z(\varphi_{z\max})$, for the ∂_2 order.
Full lines: $r_{\exp}$, dashed lines: r_Θ.

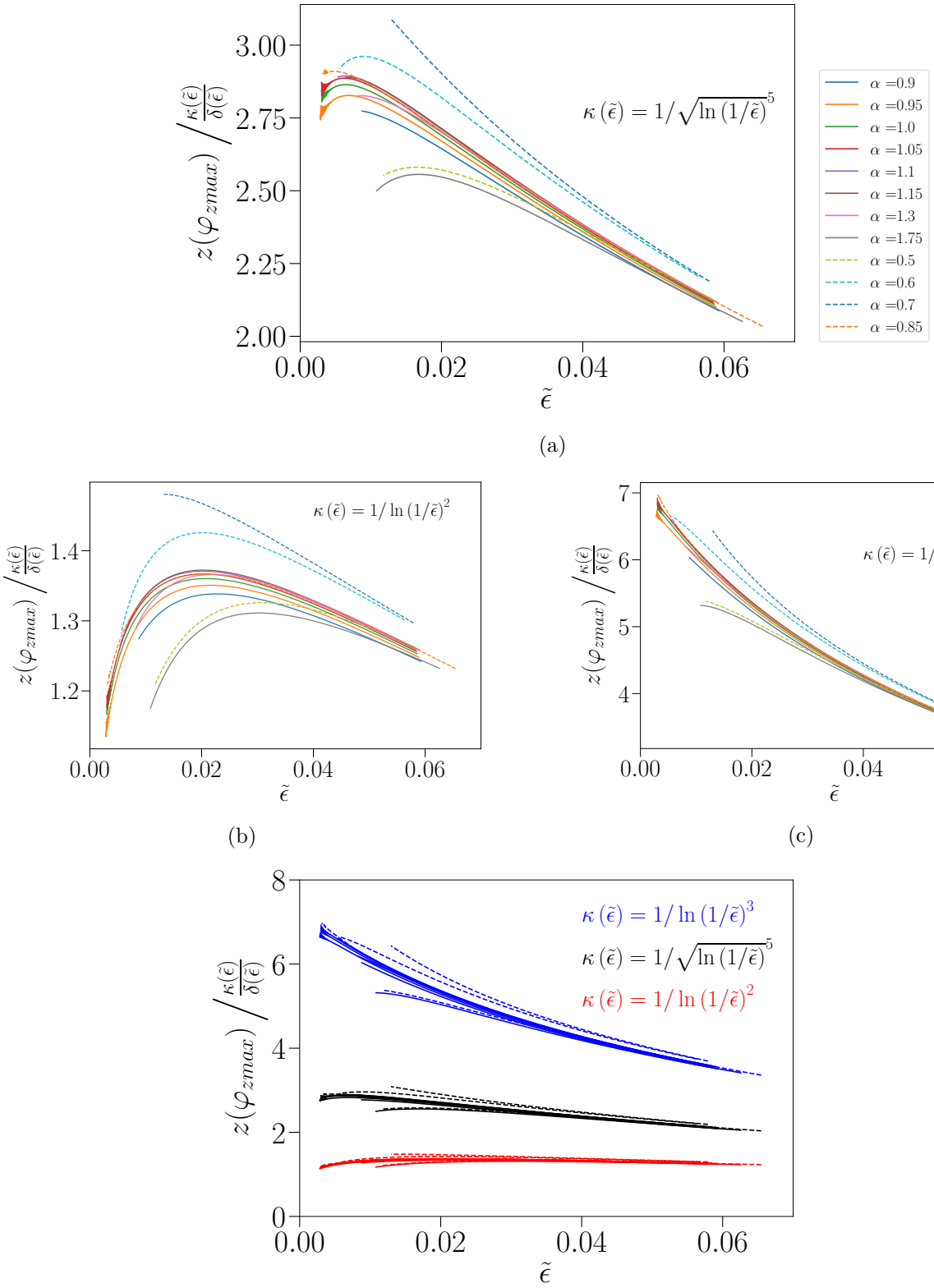

(a)

(b)

(c)

(d) Figs. 3.7a to 3.7c compared.

Figure 3.7 – Numerical results for the fixed-point value of the field renormalization function in its maximum, $z(\varphi_{z\max})$, for the ∂_2 order. The first panel, Fig. 3.7a, shows that $\kappa(\tilde{\epsilon}) \approx \mathcal{O}\left(1/\sqrt{\ln(1/\tilde{\epsilon})}^5\right)$ is compatible $z(\varphi_{z\max}) \times \delta(\tilde{\epsilon})/\kappa(\tilde{\epsilon}) = \mathcal{O}(1)$, while the second row illustrates what happens when we deviate from this scaling.
Full lines: $r_{\exp}$, dashed lines: r_Θ. Regulator prefactors α specified on the upper plot are valid for all plots.

3 Boundary layer

From the numerical insight obtained from results above the lower critical dimension in Section 2 , we choose the following ansatz for the scaling of the field renormalization function $z(\varphi)$ in the boundary layer:

$$u''(\varphi) \gg z(\varphi) \to +\infty \quad \Longrightarrow \quad \frac{1}{\delta(\tilde{\epsilon})} \gg \frac{\kappa(\tilde{\epsilon})}{\delta(\tilde{\epsilon})} \to +\infty \quad \Longrightarrow \quad \delta(\tilde{\epsilon}) \ll \kappa(\tilde{\epsilon}) \to 0^+, \tag{3.6}$$

which describes a field renormalization function that diverges in the boundary layer, but subdominantly with respect to the second derivative $u''(\varphi)$.

The boundary layer regime is then given in full by

$$\begin{aligned} &x = \frac{\varphi - \varphi_{min}}{\delta(\tilde{\epsilon})}: \quad u''(\varphi) = \frac{1}{\delta(\tilde{\epsilon})} g(x), \quad z(\varphi) = \frac{\kappa(\tilde{\epsilon})}{\delta(\tilde{\epsilon})} \zeta(x), \\ &\text{where} \quad x = \mathcal{O}(1) \quad \text{means that} \quad g(x), \zeta(x) = \mathcal{O}(1) \quad \text{and} \quad \delta(\tilde{\epsilon}) \ll \kappa(\tilde{\epsilon}) \overset{\tilde{\epsilon}\to 0^+}{\longrightarrow} 0^+. \end{aligned} \tag{3.7}$$

3.1 Boundary layer equations

From the considerations of the scaling parts of the flow we predict that we will encounter a $\tilde{\epsilon}\,\varphi_{min}/\delta(\tilde{\epsilon})$ term in the BL equations. It is convenient to substitute it for the following:

$$\frac{\tilde{\epsilon}\,\varphi_{min}}{\delta(\tilde{\epsilon})} = \frac{2\alpha v_d A^{(d)}(\eta)}{(2-\eta)} \frac{g'(0)}{(g(0))^3} = \mathcal{O}(1). \tag{3.8}$$

The supporting expression for the location of the minimum φ_{min} is found in Appendix C from the fixed-point equation for $u'(\varphi_{min}) = 0$. This step is analogous to LPA'.

Moving on to the nontrivial parts of the flow, we have found in Appendix A the threshold functions to behave as:

$$\begin{aligned} \ell_n^{(d)}(u''(\varphi), z(\varphi); \eta) &= (\delta(\tilde{\epsilon}))^{n+1} L_n^{(d)}(g(x)) + \mathcal{O}\Big(\kappa(\tilde{\epsilon})\,(\delta(\tilde{\epsilon}))^{n+1}\Big), \\ m_{n,0}^{(d)}(u''(\varphi), z(\varphi); \eta) &= \kappa(\tilde{\epsilon})\,(\delta(\tilde{\epsilon}))^{n-1} M_n^{(d)}(g(x), \zeta(x)) + \\ &\quad + \mathcal{O}\Big(\max\Big\{(\delta(\tilde{\epsilon}))^n, (\kappa(\tilde{\epsilon}))^2 (\delta(\tilde{\epsilon}))^{n-1}\Big\}\Big). \end{aligned} \tag{3.9}$$

The auxiliary functions $L_n^{(d)}$ and $M_n^{(d)}$ are given by:

$$L_n^{(d)}(g(x)) = (n + \delta_{n,0}) \frac{\alpha A^{(d)}(\eta)}{(g(x))^{n+1}}, \quad M_n^{(d)}(g(x), \zeta(x)) = \zeta(x) \frac{\alpha d A^{(d)}(\eta)}{(g(x))^n}, \tag{3.10}$$

with the regulator-dependent constant $A^{(\varphi)}(\eta)$ defined as in LPA' (see Chapter 2, Eq. (2.37)):

$$A^{(d)}(\eta) = \left(\frac{d+2-\eta}{2}\right) \int_0^{+\infty} dy y^{d/2} \left[\frac{r(y)}{\alpha}\right] > 0. \tag{3.11}$$

Inserting Eq. (3.7) to Eq. (3.11) in the fixed-point equations Eqs. (3.2) and (3.3), we arrive at the boundary-layer fixed-point equations in the $\tilde{\epsilon} \to 0^+$ limit:

$$0 = -(2-\eta) g(x) + 2\alpha v_d A^{(d)}(\eta) \left(\frac{g'(0) g'(x)}{(g(0))^3} + 2 \frac{(g'(x))^2}{(g(x))^3} - \frac{g''(x)}{(g(x))^2} \right), \tag{3.12}$$

$$0=\eta\zeta\left(x\right)-2\alpha v_{d}A^{(d)}(\eta)\left[2\frac{\left(g'\left(x\right)\right)^{2}}{\left(g\left(x\right)\right)^{4}}\zeta\left(x\right)-\left(\frac{g'(0)}{\left(g(0)\right)^{3}}+\frac{4g'\left(x\right)}{\left(g\left(x\right)\right)^{3}}\right)\zeta'\left(x\right)+\frac{1}{\left(g\left(x\right)\right)^{2}}\zeta''\left(x\right)\right]. \tag{3.13}$$

3.2 Boundary layer solution

When the field is rescaled to absorb constants and the boundary layer equations are cast in their canonical form (see Appendix B), they are universal (regulator-independent):

$$0=g\left(x\right)-\frac{g'(0)g'\left(x\right)}{\left(g(0)\right)^{3}}-2\frac{\left(g'\left(x\right)\right)^{2}}{\left(g\left(x\right)\right)^{3}}+\frac{g''\left(x\right)}{\left(g\left(x\right)\right)^{2}}, \tag{3.14}$$

$$0=\eta\zeta\left(x\right)-(2-\eta)\left[2\frac{\left(g'\left(x\right)\right)^{2}}{\left(g\left(x\right)\right)^{4}}\zeta\left(x\right)-\left(\frac{g'(0)}{\left(g(0)\right)^{3}}+\frac{4g'\left(x\right)}{\left(g\left(x\right)\right)^{3}}\right)\zeta'\left(x\right)+\frac{1}{\left(g\left(x\right)\right)^{2}}\zeta''\left(x\right)\right], \tag{3.15}$$

Save for the aforementioned universality, another specificity of the $\delta\left(\tilde{\epsilon}\right)\ll\kappa\left(\tilde{\epsilon}\right)\to 0^{+}$ regime is the complete decoupling of the Eq. (3.14) for $g\left(x\right)$ from the function $\zeta\left(x\right)$. Neither the universality nor the decoupling is present if $z\left(\varphi\right)$ is taken to behave differently in the boundary layer, but we stress that this did not inform our choice of ansatz.

Due to this decoupling, the implicit boundary layer solution for $u''\left(\varphi\right)=g\left(x\right)/\delta\left(\tilde{\epsilon}\right)$ is the same at the ∂_2 approximation level as it is in LPA'. This solution is found in Chapter 2, Section 3.3.2, and we restate the final canonical result here for completeness:

$$\frac{g(0)}{g\left(x\right)}=\exp\left(\frac{\left(Y\left(x\right)\right)^{2}}{2}\right)\operatorname{erfc}\left(\frac{Y\left(x\right)}{\sqrt{2}}\right),\qquad Y\left(x\right):=g\left(x\right)\left(\frac{g'(0)}{\left(g(0)\right)^{3}}-\frac{g'\left(x\right)}{\left(g\left(x\right)\right)^{3}}\right). \tag{3.16}$$

The canonical equation for $\zeta\left(x\right)$ can be further simplified by introducing the auxiliary function $f\left(x\right)=\zeta\left(x\right)/\left(g\left(x\right)\right)^{2}$:

$$Eq.\ (3.15)\quad\Longrightarrow\quad 0=f(x)+\left(\frac{2-\eta}{4-\eta}\right)\left[\frac{g'(0)}{\left(g(0)\right)^{3}}f'(x)-\frac{1}{\left(g(x)\right)^{2}}f''(x)\right], \tag{3.17}$$

where we also used the equation Eq. (3.14) for $g(x)$ to maximally simplify Eq. (3.17).

If we use the same auxiliary function $Y(x)$ in the canonical fixed-point Eq. (3.17) for $F(Y(x)):=f(x)$, we arrive at an integrable differential equation:

$$0=F''(Y)-YF'(Y)-nF(Y),\quad n=\frac{4-\eta}{2-\eta}\ \in\ \mathbb{R}^{+}. \tag{3.18}$$

There are two different classes of functions whose linear combinations constitute a full solution of Eq. (3.18) - hypergeometric functions of the ${}_1F_1$ type and Hermite functions $\mathcal{H}$:

$$F_n(Y)=c_F(n)\ {}_1F_1\left(\frac{n}{2},\frac{1}{2},\frac{Y^2}{2}\right)+c_{\mathcal{H}}(n)\ \mathcal{H}\left(-n,\frac{Y}{\sqrt{2}}\right),\quad c_F(n),c_{\mathcal{H}}(n)=\text{const. in } Y. \tag{3.19}$$

The hypergeometric functions that solve Eq. (3.18) diverge as $\exp\left(Y^2/2\right)$ when Y diverges [133]:

$$ {}_1F_1\left(\frac{n}{2},\frac{1}{2},\frac{Y^2}{2}\right)=\frac{\sqrt{2\pi}}{\sqrt{2}^n\Gamma(n/2)}Y^{n-1}e^{Y^2/2}+\mathcal{O}\left(\frac{1}{Y^n}\right). \tag{3.20} $$

This is a relevant section of the domain in Y, as Y diverges towards the tail region, $Y(x\to+\infty)\to+\infty$.[2] The $F(Y)=\zeta(x)/(g(x))^2\propto z\left(\varphi\right)/\left(u''\left(\varphi\right)\right)^2$ vanishes in this limit due to the tail behavor of the RG functions $z\left(\varphi\right)$ and $u''\left(\varphi\right)$. Thus the hypergeometric functions do not figure in a physical solution.

This leaves for the solution the Hermite functions:

$$ F_n(Y)\propto\mathcal{H}\left(-n,\frac{Y}{\sqrt{2}}\right)\quad\Longrightarrow\quad\begin{cases}\zeta_\eta(x)\propto\left(g(x)\right)^2\,\mathcal{H}\left(-\dfrac{4-\eta}{2-\eta},\dfrac{Y(x)}{\sqrt{2}}\right),\\[2ex] \text{with}\quad Y(x):=g(x)\left(\dfrac{g'(0)}{\left(g(0)\right)^3}-\dfrac{g'(x)}{\left(g(x)\right)^3}\right).\end{cases} \tag{3.21} $$

The numerical value of the proportionality constant is of no relevance, as Eq. (3.18) is linear in $F(Y)$. These Hermite functions are well-behaved in all physical limits of Y for any parameter n, including the tail limit. Thus, no n is pinpointed, and there is still a freedom in the anomalous dimension $\eta=2(n-2)/(n-1)$. Therefore, finding the implicit boundary layer solutions for $g(x)$ (Eq. (3.16)) and $\zeta(x)$ (Eq. (3.21)) does not lead to a unique value of the lower critical dimension d_{lc}. This is in contrast with LPA', where η was fixed from the conditions on the asymptotic behavior of $g(x)$ towards the tail region, and the d_{lc} value could be analytically found from $\tilde{\epsilon}\to0^+$.

3.3 Expression for d_{lc} in canonical boundary layer quantities

This freedom in d_{lc} comes form the fact that different solutions exist for the boundary layer field renormalization function $\zeta(x)$ for different values of the anomalous dimension η, all of them seemingly physical.

The multiplicative freedom in $\zeta\left(x\right)$ due to the relevant equation being linear in it is not what is at play here. These $\zeta_\eta\left(x\right)$ solutions vary in shape for different η, as one can see from the implicit solution in Eq. (3.21). The value of d_{lc} is parametrized by an invariant of the boundary-layer symmetry (reparametrizing $\delta\left(\tilde{\epsilon}\right)$ by and $\mathcal{O}(1)$ prefactor would not change it, see Appendix B), $\zeta'(0)/g(0)$:

$$ \frac{\zeta'(0)}{g(0)}=2\sqrt{\frac{2}{\pi}}-\sqrt{2}\frac{\Gamma\left(1+\dfrac{1}{d_{lc}}\right)}{\Gamma\left(\dfrac{1}{2}+\dfrac{1}{d_{lc}}\right)} \tag{3.22} $$

where we have used the canonical boundary layer equations, Eqs. (3.16) and (3.21), for $g\left(x\right)$ and $\zeta\left(x\right)$, together with $\eta_{d_{lc}}=2-d_{lc}$. For the full procedure, see Appendix D. We set $\zeta(0)=1$, which we can choose as all equations are linear in $\zeta(x)$.

[2] $Y(x)$ is built form the function $g(x)$ and its derivatives, which are decoupled from $\zeta(x)$. Hence, the arguments for its behavior can be inherited directly from LPA'.

With this we have shown that we cannot determine the value of the lower critical dimension from the implicit boundary-layer solutions for the renormalization functions alone. In obtaining these solutions we have already considered the necessary matching with the tail region. Hence, information about the value of d_{lc} should come form the matching conditions of the boundary layer solutions to the inner region, which needs to fix the parameter $\zeta'(0)/g(0)$. Hopefully this could be achieved from matching $z(\varphi)$ at the leading order, but at the present moment we do not know how to do this analytically. Numerical attempts have also not yet solved the matching issue, due to what we suspect to be a problem of extreme sensitivity to boundary conditions.

As a consequence of the d_{lc} relation in Eq. (3.22), if the location of the maximum of $z(\varphi)$ happens to coincide with that of the minimum of the effective potential, $\varphi_{z\max} = \varphi_{min}$, we would have $\zeta'(0) = 0$ and the value of the lower critical dimension would be precisely 1, which is the value for the exact theory.

3.4 Extrapolations of the d_{lc} value in ∂_2 from numerical results at $d > d_{lc}$

Being unable at this point to make progress with the matching between the boundary layer and the inner region, we have proceeded to investigate the possible values of the lower critical dimension d_{lc} from results for $\tilde{\epsilon}(d)$ at $d \geqslant d_{lc}$, using the fact that $\tilde{\epsilon}$ vanishes at d_{lc}. The dependence of the values of the lower critical dimension on the IR regulator function and its prefactor are shown in Fig. 3.8. Extrapolations are by construction shaky. There are nonetheless some signs that they might still produce interesting results, like the fact that the numerical results for the scaling of φ_{min} and $u''(\varphi_{min})$ above d_{lc} are already consistent with the scaling one would expect in the $\tilde{\epsilon} \to 0^+$ limit, which speaks in favor of the effects of the boundary layer already being felt at the finite $\tilde{\epsilon}$ that we can reach numerically, or the good agreement of the extrapolations with the analytical curve of $d_{lc}(\alpha)$ in LPA' (see Chapter 2, Fig. 2.12).

The results in Fig. 3.8 point to physical inadequacy of fixed-point solutions where the Theta regulator is used with $\alpha \geqslant z(0) = 1$. We suspect that this is an atypical and singular situation with the Theta regulator, as the problem does not exist for the analytical exponential regulator. Furthermore, one can see the problematic $\tilde{\epsilon}(d)$ curves in Fig. E.1 of Appendix E.

Looking at the dependence of the extrapolated values of d_{lc} on the prefactor α in Fig. 3.8, we observe that the $d_{lc}(\alpha)$ function has an extremum. This would allow for the use of PMS, if more reliable $d_{lc}(\alpha)$ curves were found in the future. This is in contrast with LPA', where no extrema are present and therefore no optimization can be carried out. Results of such an optimization procedure are shown in Fig. 3.9, for illustrative purposes only. At each d, the prefactor α is varied and the extremum of $d(\alpha)$ is found, after which the dimension is lowered. However, as the same algorithm is used for the calculation of the fixed-point solutions as in Section 2, this procedure also fails for finite $\tilde{\epsilon}$.

3.4.1 About the scaling of φ_{min} with $\tilde{\epsilon}$ and the propagator singularity

Save for the analytical $d_{lc}(\alpha)$ curves, the results we have derived from matching at the level of LPA' are the scaling of the location of the minimum of the effective potential φ_{min} with $\tilde{\epsilon}$ and the fact that the propagator develops a singularity in $\varphi = 0$. We have been able to

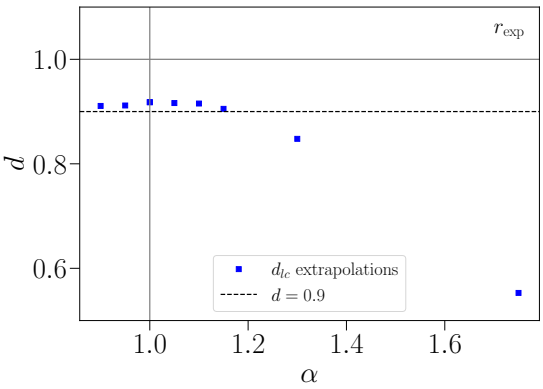

(a) Exponential regulator

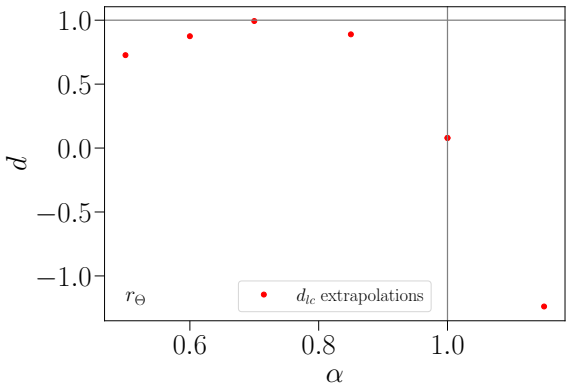

(b) Theta regulator

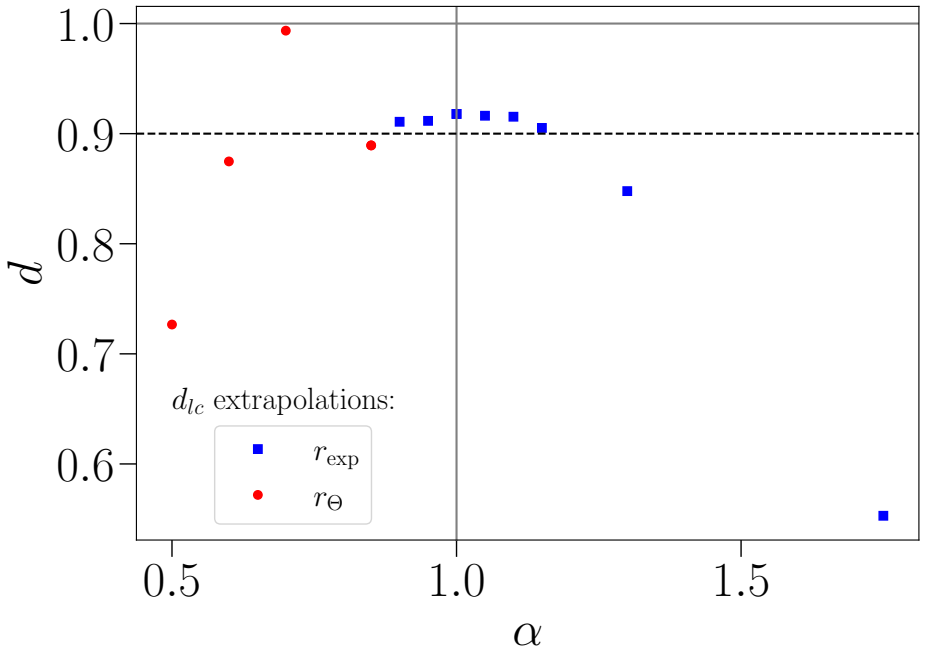

(c) Combined results, with $\alpha \geqslant z(0) = 1$ removed for the Theta regulator.

Figure 3.8 – Extrapolations of the value of the lower critical dimension for different regulator function r and prefactor α choices. We again note the problematic $\alpha \geqslant z(0) = 1$ solutions for the Theta regulator. Lines $\alpha = 1$ and $d = 1.0$ (and $d = 0.9$ for r_{exp}) are included as visual guides.

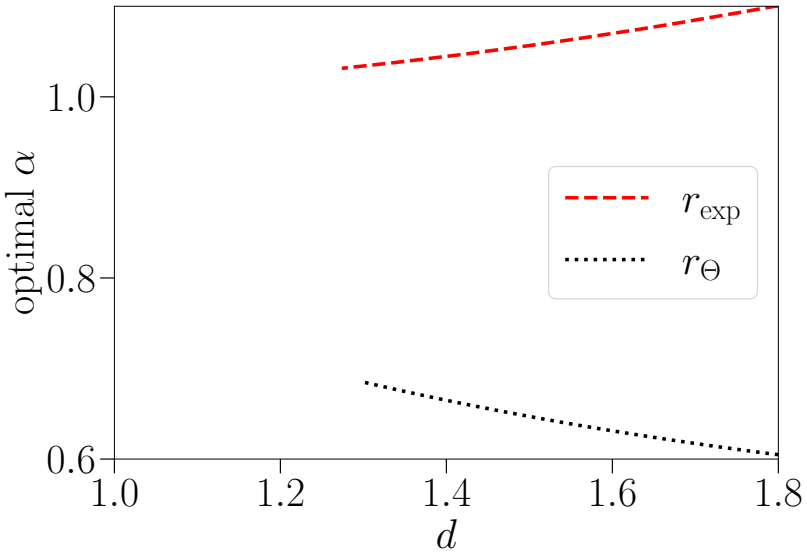

Figure 3.9 – Numerical results for the optimal regulator prefactor α in the second order of the derivative expansion ∂_2 for the two regulator functions - exponential and Theta.

establish a maching and find the scaling of $u''(\varphi) \propto 1/\delta(\tilde{\epsilon})$ with $\tilde{\epsilon}$, as $\delta(\tilde{\epsilon}) = \mathcal{O}(\tilde{\epsilon}\,\varphi_{min})$, and we have connected how the approach to the regulator singularity in $\varphi = 0$ determines the scaling of φ_{min}. However, the equation for $z(\varphi)$ is highly nontrivial, and we do not see how information on the scaling of $z(\varphi)$ (i.e., $\kappa(\tilde{\epsilon})$) can be obtained from the vicinity of $\varphi = 0$ or any other intermediate $0 < \varphi < \varphi_{min}$ field. As we have not found analytical matching criteria or established a numerical procedure for matching, in this section we limit ourselves to considerations requiring only a few minimal assumptions. We stress that without matching conditions, one cannot make crisp conclusions about the scaling of φ_{min} or about the propagator developing a singularity.

From the numerical data above d_{lc} presented in Fig. 3.3, we see that if φ_{min} diverges, it must again do so very slowly. Furthermore, the second derivative $u''(\varphi)$ diverges in the vicinity of φ_{min}, as seen in Fig. 3.4.

Still, the integral of $u''(\varphi)$ from 0 to φ_{min} must vanish:

$$\int_0^{\varphi_{min}} d\varphi u''(\varphi) = u'(0) - u'(\varphi_{min}) = 0. \tag{3.23}$$

This implies that φ_{min} should diverge. As $u''(\varphi)$ diverges in the neighborhood of φ_{min}, this has to be somehow compensated by integrating negative values $u''(\varphi) < 0$ over a divergent field-domain up to the neighborhood of φ_{min}.

To elaborate, this integral can be separated along the SPT regions, so that one can use the appropriate form of the leading-order solution to estimate it. We do so at some field φ_M

in the matching region between the inner region and the boundary layer:

$$\begin{aligned} 0 &= \int_0^{\varphi_{min}} d\varphi u''(\varphi) = I_{IN} + I_{BL}: \\ I_{IN} &= \int_0^{\varphi_M} u''(\tilde{\varphi}) d\tilde{\varphi}, \\ I_{BL} &= \int_{\varphi_M}^{\varphi_{min}} u''(\tilde{\varphi}) d\tilde{\varphi}. \end{aligned} \tag{3.24}$$

From Fig. 3.3, it is clear that if φ_{min} diverges (and we just argued that it does), it does so more slowly than, e.g., $1/\sqrt{\tilde{\epsilon}}$. We can then find some finite exponent a, so that the matching field defined as

$$\varphi_M = \varphi_{min} - b\,\tilde{\epsilon}^{1-a}, \quad 0 < a < 1, \quad b > 0, \tag{3.25}$$

corresponds to the "left limit" of the boundary layer, where the boundary-layer field x is negative and diverges:

$$x_M = \frac{\varphi_m - \varphi_{min}}{\delta(\tilde{\epsilon})} = -b\frac{\tilde{\epsilon}^{1-a}}{\delta(\tilde{\epsilon})} \propto \frac{-b}{\tilde{\epsilon}^a\,\varphi_{min}} \to -\infty, \tag{3.26}$$

where we have used the SPT result that $\delta(\tilde{\epsilon}) = \mathcal{O}(\tilde{\epsilon}\,\varphi_{min})$. In the case where $z(\varphi) \ll u''(\varphi)$ in the boundary layer (even if $z(\varphi)$ diverges), the argumentation for $\delta(\tilde{\epsilon}) = \mathcal{O}(\tilde{\epsilon}\,\varphi_{min})$ is the same as in LPA' due to the decoupling of the equation for $g(x) = \delta(\tilde{\epsilon})\,u''(\varphi)$.

We continue by evaluating I_{BL} at the leading order. Conveniently for this argument, the function that we need to integrate in the boundary layer is $u''(\varphi) = g(x)/\delta(\tilde{\epsilon})$, and from its canonical boundary layer equation in Eq. (3.14) we see that $g(x)$ is a total derivative:

$$\begin{aligned} I_{BL} &= \int_{\varphi_M}^{\varphi_{min}} u''(\varphi)\,d\varphi = \frac{1}{\delta(\tilde{\epsilon})}\int_{\varphi_M}^{\varphi_{min}} g(x) d(\varphi_{min} + \delta(\tilde{\epsilon})\,x) = \\ &= \int_{x_M}^{0} g(x)\,dx = g(x_M)\left[\frac{g'(0)}{(g(0))^3} - \frac{g'(x_M)}{(g(x_M))^3}\right]. \end{aligned} \tag{3.27}$$

Using the asymptotic form of $g(x)$ for $x \to -\infty$ (Chapter 2, Eq. (2.55)) and evaluating it in φ_M, we arrive at

$$I_{BL} \approx \sqrt{2a\ln(1/\tilde{\epsilon})} + \mathcal{O}\left(\tilde{\epsilon}^0\right). \tag{3.28}$$

We stress that the asymptotic form in Eq. (2.55) gives for the second derivative $u''(\varphi) = g(x)/\delta(\tilde{\epsilon})$ in the matching region

$$u''(\varphi_M) = \mathcal{O}\left(\frac{1}{\tilde{\epsilon}^{1-a}\sqrt{\ln(1/\tilde{\epsilon})}}\right), \tag{3.29}$$

which diverges more slowly than the inverse of $\delta(\tilde{\epsilon}) \propto \tilde{\epsilon}\,\varphi_{min}$, as it must in φ_M:

$$\frac{\tilde{\epsilon}\,\varphi_{min}}{\tilde{\epsilon}^{1-a}\sqrt{\ln(1/\tilde{\epsilon})}} = \frac{\tilde{\epsilon}^a\,\varphi_{min}}{\sqrt{\ln(1/\tilde{\epsilon})}} \to 0. \tag{3.30}$$

Now, if we take that in principle there is matching, we can use Eq. (3.29) to put an upper bound to the contribution of the matching region to the integral in the inner region, I_{IN}. The matching region is at most of width $\tilde{\epsilon}^{1-a}$ in the φ field, and $u''(\varphi)$ is there at most of $\mathcal{O}\left(1/\left(\tilde{\epsilon}^{1-a}\sqrt{\ln(1/\tilde{\epsilon})}\right)\right)$, so that by using Jordan's estimation lemma [134], this contribution can at worse be of $\mathcal{O}\left(1/\sqrt{\ln(1/\tilde{\epsilon})}\right) \to 0$, which is negligible compared to the I_{BL} integral. For the inner integral to compensate for the divergence of the boundary layer one, i.e.,

$$I_{IN} = -I_{BL} \approx -\sqrt{2a\ln(1/\tilde{\epsilon})}, \tag{3.31}$$

the divergence must come from the domain of integration (as outside of the matching region we integrate finite $u''(\varphi)$) which is up to the matching region, in the leading order, of $\mathcal{O}(\varphi_{min})$, i.e.,

$$\varphi_{min} \propto \sqrt{\ln(1/\tilde{\epsilon})}, \tag{3.32}$$

as in the LPA'. This again accounts for the slow divergence of φ_{min}, which can in the $d > d_{lc}$ numerical results be mistaken for φ_{min} going to a constant in the $\tilde{\epsilon} \to 0^+$ limit.

In this discussion we have used that $u''(\varphi_{min})$ diverges and that a value of a can be found such that $\tilde{\epsilon}^a \varphi_{min}$ vanishes in the $\tilde{\epsilon} \to 0^+$ limit, both of which are strongly suggested by the $d > d_{lc}$ numerical results presented in Section 2. Apart from this, only the assumption that matching is in principle possible has been used. This can be translated into saying that we have assumed that the coupling of the fixed-point equations for $z(\varphi)$ and $u''(\varphi)$ in the inner region does not affect the behavior of $u''(\varphi_M)$, nor the result for $u'(\varphi_M)$, in the matching region. This is compatible with the numerical results of Section 2, where $u''(\varphi)$ can be seen to be qualitatively the same as in LPA', but it should ideally be checked from the matching conditions (which we presently do not have). While this makes the argument not a rigorous demonstration, the assumptions that we have used are not very demanding and are supported by numerical trends when $d > d_{lc}$. We will use this scaling of φ_{min} (and consequently $\delta(\tilde{\epsilon})$) in the following, e.g., in Chapter 4 when we will be discussing the critical temperature and the critical exponents.

We also want to discuss the pole singularity, as it is what we expect in the $\tilde{\epsilon} \to 0^+$ limit from the merging of the critical and the zero-temperature fixed points. We note that when the propagator is singular, the threshold functions diverge. Consider then the value of the effective potential in the origin, obtained from the flow equation Eq. (3.1) at the fixed point:

$$u(0) = \frac{2v_d}{d}\ell_0^{(d)}(u''(0), z(0) = 1; \eta). \tag{3.33}$$

If the propagator has a singularity, $u(0)$ diverges. As $u(\varphi)$ is defined up to some physically irrelevant constant, for this to be significant we must compare $u(0)$ to $u(\varphi)$ (defined up to the same constant) evalutaed at some other φ. If we evaluate the same Eq. (3.1) (in the fixed point) in φ_{min}, we find it to be $u(\varphi_{min}) \propto \delta(\tilde{\epsilon}) \to 0$ (as $u'(\varphi_{min}) = 0$ makes it proportional to $\ell_0^{(d)} \propto 1/u''(\varphi) \propto \delta(\tilde{\epsilon})$, see Appendix A). This means that the depth of the minima compared to $u(0)$, i.e., $u(0) - u(\varphi_{min})$, diverges. This deepening of the minima as the dimension is lowered can be seen in Fig. 3.1 for both ∂_2 and LPA', where in LPA' we have indeed found analytically that the propagator develops a singularity.

We give a rough argument of how the propagator singularity is connected to the divergence of φ_{min}. When we have evaluated the integrals I_{BL} and I_{IN}, we have found them to be of $\mathcal{O}\left(\sqrt{\ln\left(1/\tilde{\epsilon}\right)}\right) = \mathcal{O}(\varphi_{min})$ (with matching assumed). From the definition of these integrals in Eq. (3.24), it is clear that $I_{IN} = -I_{BL} = u'(\varphi_M)$. The first derivative $u'(\varphi)$ for the expected double-well shape of $u(\varphi)$ is negative on the whole interval $0 < \varphi < \varphi_{min}$ (so no cancellation between negative and positive values of $u'(\varphi)$ can happen there, if we were to integrate $u'(\varphi)$ to get $u(\varphi)$).

We now take another argument from numerical data at $d > d_{lc}$. Looking at the shape of $u'(\varphi)$ shown in Fig. 3.10, we see that $u'(\varphi)$ does grow before φ_{min}, and we see no significant narrowing or peaking which would suggest that $u'(\varphi)$ becomes negligible on a substantial fraction of the $0 < \varphi < \varphi_{min}$ domain. If we assume that this persists to the $\tilde{\epsilon} \to 0^+$ limit, the integral $\int_{\varphi_{min}}^{0} u'(\varphi)\, d\varphi = u(0) - u(\varphi_{min})$ would consist of contributions of always the same (negative) sign that are not negligible on a substantial part of a diverging domain, making the integral divergent too. This connects the propagator singularity with φ_{min} being pushed to infinity.

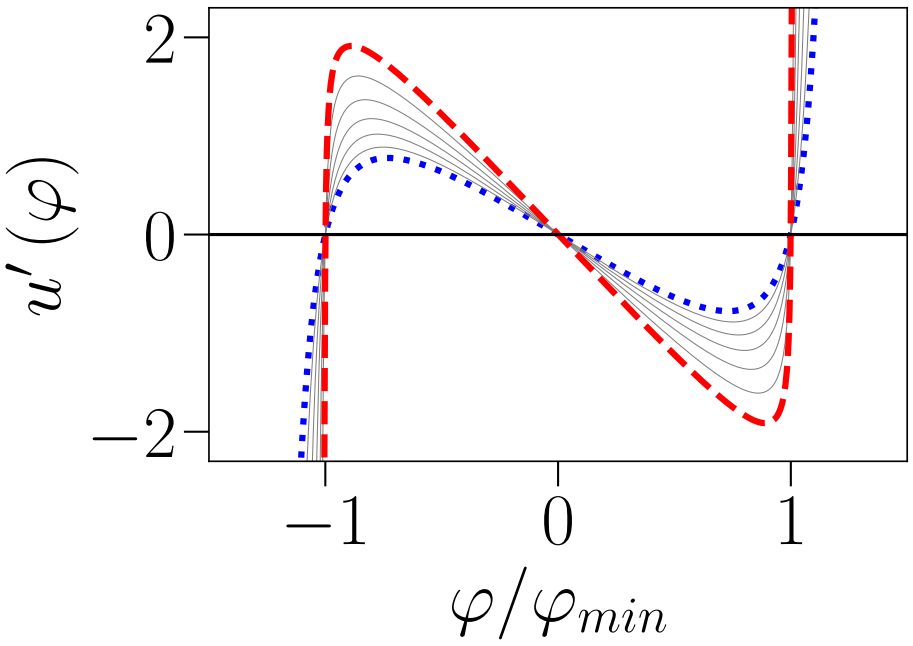

Figure 3.10 – Derivative $u'(\varphi)$ for $d > d_{lc}$ in the range $1.113 < d < 1.8$, calculated with r_{exp} and $\alpha = 1$. A horizontal black line at $u'(\varphi) = 0$ is added as a visual guide.

The most reckless assessment based on the arguments that we have presented, and which can be reduced to $u(\varphi) = \int d\varphi \int d\varphi u''(\varphi)$ and $u''(\varphi)$ being mostly $\mathcal{O}(1)$ between the matching region and the origin, would give $u(0) = \mathcal{O}(\varphi_{min}^2)$. This, though, agrees with a leading-order estimate one can find from the inner region at LPA' level, for example with

the r_Θ, $\alpha = 1$ choice giving[3] Eq. (2.29) of Chapter 2, Section 3.2.2, which we twice integrate:

$$\begin{aligned} &Eq.\ (3.34): \quad u(\varphi) = \frac{1}{1+u''(\varphi)} \implies \\ &\implies \varphi_M = \varphi_{\min} + \mathcal{O}\left(\tilde{\epsilon}^{1-a}\right) = -\frac{1}{\sqrt{2}} \int_{u(0)\gg 1}^{u(\varphi_M)\ll 1} \frac{du}{\sqrt{\ln\left(u/u(0)\right) - \left(u-u(0)\right)}} = \\ &= \sqrt{\frac{u(0)}{2}} \int_{u(\varphi_M)/u(0)}^{1} \frac{dx}{\sqrt{1-x+\ln(x)/u(0)}} \overset{u(0)\to+\infty}{\longrightarrow} \sqrt{\frac{u(0)}{2}} \int_0^1 \frac{dx}{\sqrt{1-x}} = \sqrt{2u(0)}. \end{aligned} \tag{3.34}$$

4 Conclusion

In this chapter we have considered the next step after LPA' in the hierarchy of derivative expansion truncations. This is the second order of the derivative expansion, ∂_2. We have not been able to advance analytically as far as in LPA'. This is not so surprising as the flow equations shown in Section 1 are much more complicated when $z(\varphi)$ is field-dependent (v.s LPA', where $z(\varphi) = 1$). The matching between solutions in different SPT regions at the level of $u(\varphi)$, or its field derivatives, is analytically more accessible since the divergent scaling of φ_{min} comes from the approach to the propagator singularity near $\varphi = 0$, determining the scaling $1/\delta(\tilde{\epsilon}) = \mathcal{O}(1/(\tilde{\epsilon}\,\varphi_{min}))$ of the second derivative $u''(\varphi)$ in the boundary layer. Because of the highly nontrivial equation for $z(\varphi)$, it is however not clear how to analytically obtain its scaling. This line of research is still in progress.

The flow equations have an $\tilde{\epsilon} = (d-2+\eta)/[2(2-\eta)]$-term, where the small parameter $\tilde{\epsilon}$ multiplies the field itself and the field derivatives of the RG functions. As we have found numerical evidence of $u''(\varphi_{min})$ diverging from data above d_{lc} (shown in Section 2), we again expect that the $\tilde{\epsilon}$ term becomes relevant earlier than one would expect when all the RG functions are finite. The equation for $z(\varphi)$ is coupled to this singular effective potential, and the numerical results show spiking of $z(\varphi)$ in the vicinity of $\pm\varphi_{min}$. We expect a boundary layer to emerge around φ_{min} also at the ∂_2 level, analogously to LPA', but with a nontrivial behavior of $z(\varphi)$ in this region. The numerical results of Section 2 for $d > d_{lc}$ have encouraged us to explore the ansatz in which the field renormalization function $z(\varphi)$ diverges in a boundary layer around φ_{min}, but subdominantly to $u''(\varphi)$.

With this ansatz the equation for $u''(\varphi)$ in the boundary layer does not depend on $z(\varphi)$ at leading order, and we have analytically found implicit leading-order boundary-layer solutions for both functions in Section 3. However, the coupling of the equations for $u''(\varphi)$ and $z(\varphi)$ in the inner region has prevented us from characterizing this region as well as in LPA', and we have not yet managed to find proper matching conditions between the different regions. We believe that these conditions should determine the scaling of $z(\varphi_{min})$ with $\tilde{\epsilon}$ (or in the language of this chapter, $\kappa(\tilde{\epsilon})$), and give analytical information on the value of the lower critical dimension $d_{lc}(\alpha)$. In Section 3.4 we have found numerical evidence that an extremum of $d_{lc}(\alpha)$ might be present at ∂_2, which would allow for PMS, but this involves an extrapolation from values above d_{lc}. Finding more reliable $d_{lc}(\alpha)$ curves is needed to possibly use PMS in the future.

In Section 3.4.1 we have presented reasons why we expect the LPA' results about the

[3] Up to some rescaling by $\mathcal{O}(1)$ constants, given in Chapter 2, Section 3.2.2.

scaling of φ_{min} like $\sqrt{\ln(1/\tilde{\epsilon})}$ and the propagator developing a singularity to be carried over to ∂_2, as suggested by the numerical trends at $d > d_{lc}$ and assuming that matching is (in principle) possible.

In the next chapter we will discuss the behavior of the critical temperature and of the critical exponents as one approaches the lower critical dimension at the level of both LPA' and ∂_2.

Chapter 4

Critical temperature and critical exponents in LPA' and ∂_2

In Chapter 1, Section 2.2.1 where we introduced the $\tilde{\epsilon} \to 0^+$ criterion for the lower critical dimension d_{lc}, we also stressed that the critical and zero-temperature fixed points merge in d_{lc}. This brought certain expectations for the critical temperature and the critical exponents which we explore in this chapter.

1 Critical temperature

We expect the critical temperature to vanish at d_{lc}, as T_c is progressively pushed to lower values when decreasing the spatial dimension by the entropic contribution of the fluctuations becoming more relevant. While the actual value of T_c is connected to the microscopic properties of a system and as such is not a universal property, if we know the scaling of the location of the minimum with $\tilde{\epsilon}$, we can show how T_c vanishes in the $\tilde{\epsilon} \to 0^+$ limit for this universality class.

Going down toward $T = 0K$, there are less and less thermal fluctuations, and the value of the uniform coarse-grained order parameter field is bound to be in the neighborhood of the location of the minima of the effective potential, $\pm\varphi_{min}$. The problem is Z_2 symmetric and we continue with $\varphi > 0$ fields without loss of generality. These $\varphi \approx \varphi_{min}$ configurations in the first approximation see the well of the effective potential as parabolic, $\propto (\varphi_{min} - \varphi)^2/2$. Their Boltzmann weights in the corresponding probability distribution are then given by

$$\approx \exp\left(-\frac{\varphi_{min}^2}{2}\left(1 - \frac{\varphi}{\varphi_{min}}\right)^2\right). \tag{4.1}$$

Here we remind that the energy related quantities obtained from the FRG, like the effective action Γ or the free energy W, are all reduced, by which we mean that they have a factor of thermodynamic $\beta = 1/k_B T$ absorbed. This can be seen for instance from the definition of the free energy, $W[J] = \ln(Z[J])$. We can then interpret Eq. (4.1) as some finite potential term $\propto (1 - \varphi/\varphi_{\min})^2/2$ multiplied by a diverging critical β_c:

$$\beta_c \sim \varphi_{\min}^2 \sim \ln\left(\frac{1}{\tilde{\epsilon}}\right) \quad \Longrightarrow \quad T_c \sim \frac{1}{\ln(1/\tilde{\epsilon})} \xrightarrow{\tilde{\epsilon}\to 0} 0. \tag{4.2}$$

The scaling we used for φ_{min} in Eq. (4.2) has been shown in Chapter 2 analytically for LPA', and has been tentatively argued for ∂_2 in Chapter 3.

The relation $T_c \sim 1/\varphi_{\min}^2$ is also respected in the $O(N > 2)$ case at $d_{lc} = 2$, where $T_c \propto d - d_{lc}$ and $\varphi_{\min} \propto 1/\sqrt{d - d_{lc}}$ are found from equivalence with the nonlinear sigma model near $d = 2$ [16]. This situation is however dominated by long-wave Goldstone modes, and our interest lies with localized, strongly nonuniform kinks.

This is why it is more relevant to compare our finding with the results obtained by A. D. Bruce and D. J Wallace (B&W) in their work on a droplet theory for the Ising model close to its lower critical dimension $d_{lc} = 1$. [12–14]. Their investigation is done as an expansion in $\epsilon = d - 1$ (note that $\epsilon \neq \tilde{\epsilon}$). That is not the only conceptual difference in our approaches. B&W build a theory of the critical behavior by focusing on the statistical mechanics of droplet configurations (droplets being bubbles of one phase enclosed by a domain wall) entirely controlled by the surface tension. They obtain the following result for the critical temperature:

$$T_c \sim \epsilon = d - 1. \tag{4.3}$$

The results Eq. (4.2) and Eq. (4.3) for the critical temperature can be linked to the scaling dimension of the field, D_φ. In our FRG approach, $D_\varphi = (2 - \eta)\,\tilde{\epsilon}$ and we have:

$$D_\varphi = \frac{d - 2 + \eta}{2}, \quad T_c \sim \frac{1}{\ln\left(1/D_\varphi\right)}, \tag{4.4}$$

at the leading order. The key result of the B&W approach [12–14] is the behavior of D_φ itself, which is nontrivial as a function of $\epsilon = d - 1$ and is given by

$$D_\varphi \sim \frac{e^{-2/(d-1)}}{d-1} \quad \Longrightarrow \quad d - 1 \propto \frac{1}{\ln\left(1/D_\varphi\right)}. \tag{4.5}$$

Combining Eqs. (4.3) and (4.5) gives $T_c \propto 1/\ln\left(1/D_\varphi\right)$ in the leading order, which is reproduced by our result, Eq. (4.4). We have thus recovered from FRG the correct scaling of T_c with $\tilde{\epsilon}$, without a priori knowing the value of d_{lc} at which $\tilde{\epsilon} = 0$. This agreement with a configuration-based theory is encouraging.

We stress that this scaling of T_c has been missed in the reference [122] which is the only comparative FRG literature. Results there gave $T_c \propto D_\varphi \propto \tilde{\epsilon}$.

2 Stability of the critical fixed point

The expectation derived from the merging of fixed points regarding the values of the critical exponents is that the relevant eigenvalues, from which we calculate them, should become marginal (i.e., vanish) in the $\tilde{\epsilon} \to 0^+$ limit. This would allow the critical fixed point to merge with the zero-temperature stable attractor.

For the critical fixed point of the scalar ϕ^4 theory, we expect two relevant eigenvalues corresponding to its unstable directions. One of the directions is conceptually connected to the temperature. The critical exponent ν of the correlation length is calculated from the related eigenvalue as $\lambda_1 = -1/\nu$. The eigenvector $e_1(\varphi)$ is even in φ [17]. The critical

exponent ν should diverge at the lower critical dimension leading to the essential (as opposed to the usual power law [17, 44, 45]) scaling of the correlation length with the temperature distance from the transition, $T - T_c$ (with $T_c \to 0$). This essential scaling is for instance present in the $1d$ Ising model, as can be seen from its exact solution [60, 61], where

$$\xi \propto e^{2\beta J}, \qquad \beta = k_B T \quad \text{and} \quad 2J \text{ is the "energy cost" of one kink.} \tag{4.6}$$

This also agrees with λ_1 becoming marginal, as we expect from the fixed-point merging. The other relevant eigenvalue, λ_2, is associated with an odd eigenvector $e_2(\varphi)$, and it gives the scaling dimension of the magnetic field as $d+\lambda_2$, with $\lambda_2 = -D_\varphi$. The rest of the eigenvalues are expected to be irrelevant (positive) and of $\mathcal{O}(1)$ [17, 44].

2.1 Linearized flow equations

To analyze the stability of a fixed point, i.e., find and interpret the eigenvalues of the stability matrix, we must investigate the flow in its neighborhood. For the case of the second order of the derivative expansion, the FRG flows move in the space spanned by all possible functions $u_k(\varphi)$ and $z_k(\varphi)$, while for LPA' we have $z_k(\varphi) = 1$. For practical reasons, in this work we often speak in terms of $u_k''(\varphi)$ instead of $u_k(\varphi)$. We use the shorthand $F_{i,k}(\varphi)$ for all of these functions (or their field-derivatives), while y_i stands for their respective scaling dimensions.[1] With this, we can write down a generic flow equation as

$$\partial_t F_{i,k}(\varphi) = -y_i F_{i,k}(\varphi) + \frac{1}{2}(d - 2 + \eta_k)\varphi F'_{i,k}(\varphi) + \beta_{F_{i,k}(\varphi);k}\big(u_k''(\varphi), z_k(\varphi); \eta_k\big), \tag{4.7}$$

where the β-function is here the nontrivial part of the flow. The explicit LPA' flow equations are given in Chapter 2, Section 1, and the ∂_2 ones are in Chapter 3, Section 1.

To investigate the flow in the vicinity of the fixed point, we must allow for small perturbations of the RG functions away from the fixed point:

$$F_{i,k}(\varphi) = F_i(\varphi) + \delta F_i(\varphi), \quad \delta F_i(\varphi) \ll 1, \tag{4.8}$$

where we have again dropped the k-index to mark fixed-point quantities for which $\partial_t F_i(\varphi) = 0$. The flow equation for the arbitrarily small perturbation $\delta F_i(\varphi)$ is given from Eq. (4.7) by

$$\begin{aligned}\partial_t \delta F_i(\varphi) = &\left[-y_i + \frac{1}{2}(d - 2 + \eta_k)\varphi\partial_\varphi\right]\delta F_i(\varphi) + \sum_j \frac{\delta\beta_{F_i(\varphi)}(u''(\varphi), z(\varphi); \eta)}{\delta F_j(\varphi)}\delta F_j(\varphi) + \\ &+ \left[-\partial_\eta y_i + \frac{1}{2}\varphi F_i'(\varphi) + \partial_\eta \beta_{F_i(\varphi)}\big(u''(\varphi), z(\varphi); \eta\big)\right]\delta\eta + \mathcal{O}\left(\delta^2\right).\end{aligned} \tag{4.9}$$

If we neglect all but linear terms in the perturbations, noted here by $\mathcal{O}(\delta^2)$[2], the equations $\{\partial_t \delta F_i(\varphi)\}$ form the stability matrix of the fixed point [41, 42]. The question of stability is now posed as an eigenproblem of this matrix. The flow-derivatives ∂_t are here taken with respect to the renormalization time $t = \ln(k/\Lambda)$, where Λ is some large momentum scale, larger than all of the energy scales in the system (for instance the UV cutoff). As one takes flows from the microscopic $k = \Lambda$ limit to the physical limit $k \to 0$ in which all

[1] E.g., the dimensionfull $Z_k(\varphi)$ scales as $k^{-\eta}$, so the corresponding scaling dimension is $y_z = -\eta$.

[2] The δ standing for perturbations should not be confused with the boundary layer width $\delta(\bar{\epsilon})$.

of the fluctuations are integrated, the t starts from 0 and becomes more and more negative. Therefore, the relevant eigenvalues calculated form $\{\partial_t \delta F_i(\varphi)\}$ are the negative ones, $\lambda_i < 0$. To reiterate, in the problem at hand, the scalar ϕ^4 theory, we expect two such eigenvalues. One is the relevant temperature-related eigenvalue $\lambda_1 = -1/\nu$, associated with an even eigenvector $e_1(\varphi)$. The other is the trivial eigenvalue for which $\lambda_2 = -D_\varphi$ can be found analytically, where $D_\varphi = (d-2+\eta_k)/2 = (2-\eta_k)\,\tilde{\epsilon}_k$ is the scaling dimension of the field. The components of the corresponding eigenvector $e_2(\varphi)$ projected on $\delta F_{i,k}(\varphi)$ are given by the derivatives of the corresponding fixed-point functions

$$\delta F_{i,k}(\varphi) \propto F_i'(\varphi), \tag{4.10}$$

and thus when the space in which we calculate the stability matrix is spanned by $\delta u''(\varphi)$ (or $\delta\chi(\varphi)$) and $\delta z(\varphi)$, e_2 is odd. This is presented in Section 2.1.1

We clarify two conventions we tacitly introduced in Eq. (4.9). First, the sum in Eq. (4.9) only goes over the RG functions that figure in the β functions:

$$\sum_j : \quad F_j(\varphi) \in \{u''(\varphi), z(\varphi)\}. \tag{4.11}$$

Second, the functional derivatives by a function $F_i(\varphi)$, of field derivatives of the same function marked by $F_i^{(n)}(\varphi)$, stand for derivative operators:

$$\frac{\delta F_j^{(n)}(\varphi)}{\delta F_i(\varphi)} = \delta_{i,j}\partial_\varphi^{(n)}. \tag{4.12}$$

In the case of Eq. (4.9), these field-derivative operators act on the perturbations $\delta F_j(\varphi)$ to their right in the β-function related sum.

The anomalous dimension is calculated by evaluating the flow equation for the field renormalization function $z_k(\varphi)$, in a suitably selected[3] renormalization filed φ_r. By construction, the $z_k(\varphi_r)$ does not change during the flow. Thus, we have the renormalization condition:

$$0 = \frac{dz_k(\varphi_r)}{dt} = \partial_t z_k(\varphi)|_{\varphi_r} + z_k'(\varphi_r)(\partial_t \varphi_r). \tag{4.13}$$

Here, the $\partial_t z_k(\varphi)|_{\varphi_r}$ term is the flow with fixed φ post-factum evaluated in φ_r, which can be chosen such that it flows, e.g., $\varphi_r = \varphi_{\min,k}$. The value of η_k is calculated from Eq. (4.13), and $\delta\eta = \eta_k[\{F_{i,k}(\varphi_r)\}] - \eta$, with η_k linearized in the perturbations of $F_{i,k}(\varphi_r)$. In numerical calculations for $d > d_{lc}$ in Section 2.2, we choose $\varphi_r = \varphi_{min}$ (the fixed-point value, but when the anomalous dimension is calculated interpolations are used to find the best φ_{min} values that need not be on the grid) for the LPA', and $\varphi_r = 0$ for ∂_2.

It is unclear whether analytical results (save for the trivial eigenvalue $\lambda_2 = -D_\varphi$) can be obtained from this set of complicated partial differential equations which represent our eigenvalue problem. The numerical results in Section 2.2 are currently the best FRG results

[3] On the LPA' level, the best results are obtained at $\varphi_r = \varphi_{min,k}$, the running minimum of the effective potential [135, 136], which is what we use. On the ∂_2 level this is less relevant and for simplicity we renormalize in the origin, $\varphi_r = 0$.

we have found about ν. Regarding analytical challenges, in Section 3 we discuss limitations of using the leading-order fixed-point solutions we found using SPT to evaluate the fixed-point terms in the perturbation equations Eq. (4.9). In the same section, while acknowledging those limitations, we speculate on a mechanism that could give a marginal $\lambda_1 = -1/\nu$. The discussion of such a mechanism is instigated by the numerical results for the components of e_1 in the boundary layer range.

2.1.1 The λ_2 eigenvalue

Before we proceed, we show how the trivial λ_2 eigenvalue is obtained, as we refer to its value and its eigenvectors in Section 2.2 on numerical results above d_{lc}, and in Section 3 to discuss possible marginality of $\lambda_1 = -1/\nu$. We stress that we are primarily interested in the λ_1 eigenvalue as it gives the critical exponent ν of the correlation length.

We start solving for λ_2 by examining the Eq. (4.9) for the flow of a general RG function perturbation. We compare its form to the flow equation of the field-derivative of the same function (the one we perturbed in Eq. (4.9)):

$$\begin{aligned}\partial_t(\partial_\varphi F_{i,k}(\varphi)) = \partial_\varphi(\partial_t F_{i,k}(\varphi)) = &\left[-y_i + \frac{1}{2}(d+2-\eta_k)\right]F'_{i,k}(\varphi) + \frac{1}{2}(d+2-\eta_k)\varphi F''_{i,k}(\varphi) + \\ &+ \sum_j \frac{\delta\beta_{F_{i,k}(\varphi)}(u''_k(\varphi), z_k(\varphi); \eta_k)}{\delta F_{j,k}(\varphi)} F'_{j,k}(\varphi)\,.\end{aligned} \tag{4.14}$$

We now rewrite Eq. (4.9) to reflect the fact that when we are conducting functional derivatives by $\delta F_j(\varphi)$, this induces a similar structure as do field derivatives in Eq. (4.14):

$$\begin{aligned}\partial_t \delta F_i(\varphi) = &-\frac{1}{2}(d-2+\eta)\delta F_i(\varphi) + \left[-\partial_\eta y_i + \frac{1}{2}\varphi F'_i(\varphi) + \partial_\eta \beta_{F_i(\varphi)}(u''(\varphi), z(\varphi); \eta)\right]\delta\eta + \\ &+ \left[-y_i + \frac{1}{2}(d-2+\eta_k)\right]\delta F_i(\varphi) + \frac{1}{2}(d+2-\eta_k)\varphi\delta F'_i(\varphi) + \\ &+ \sum_j \frac{\delta\beta_{F_i(\varphi)}(u''(\varphi), z(\varphi); \eta)}{\delta F_j(\varphi)}\delta F_j(\varphi)\,.\end{aligned} \tag{4.15}$$

An ansatz for the eigenvector components imposes itself from this comparison of Eqs. (4.14) and (4.15):

$$\delta F_j(\varphi) = c k^{\lambda_2} F'_j(\varphi), \tag{4.16}$$

with the same constant c for every j, taken arbitrarily small to allow for linearization.

It is now trivial to see that this ansatz reduces Eq. (4.15) to the following expression, as then the last two rows of Eq. (4.15) correspond to RHS of the flow equation Eq. (4.14) evaluated in the fixed point, and $\partial_t \delta F_i(\varphi) = \lambda_2 c k^{\lambda_2} F'_i(\varphi)$:

$$\begin{aligned}\lambda_2 c k^{\lambda_2} F'_i(\varphi) = &-\frac{1}{2}(d-2+\eta)c k^{\lambda_2} F'_i(\varphi) + \\ &+ \left[-\partial_\eta y_i + \frac{1}{2}\varphi F'_i(\varphi) + \partial_\eta \beta_{F_i(\varphi)}(u''(\varphi), z(\varphi); \eta)\right]\delta\eta.\end{aligned} \tag{4.17}$$

The proper result, $\lambda_2 = -(d-2+\eta)/2 = -D_\varphi$, is thus obtained if $\delta\eta = 0$. As the running anomalous dimension η_k is defined from the flow equation of $z_k(\varphi)$ (see Eq. (4.13)), one must check that the linearized equation indeed leads to $\delta\eta = 0$. It is easy to see that with Eq. (4.16) this is realized at the LPA' level with the choice of renormalization prescription $\varphi_r = \varphi_{min,k}$ and at the ∂_2 level (and higher-order ones) with the choice $\varphi_r = 0$.

2.2 Numerical results above d_{lc} for the relevant eigenvalues

In the numerical procedure (done in FORTRAN90 [124]), one pointwise (on the discrete field-grid) perturbs the numerical fixed-point solutions by values as small as 10^{-10}, then calculates the resulting flow. This is how a stability matrix is built. It is then diagonalized using methods native to LAPACK (Linear Algebra PACKage, written in FORTRAN90, available at [137]).

We have appropriately found all but two of the eigenvalues to be irrelevant (positive and of $\mathcal{O}(1)$). As mentioned, the remaining two eigenvalues are relevant and identified by the parity of their eigenvectors as $\lambda_1 = -1/\nu$ (even) and $\lambda_2 = -D_\varphi$ (odd). The results for λ_1 and λ_2 in the LPA' and ∂_2 approximation are presented in Figs. 4.1 and 4.2 respectively. From Figs. 4.1 and 4.2 it is evident that λ_2 is in perfect agreement with the analytical prediction, $\lambda_2 = -(2-\eta)\,\tilde{\epsilon}$, for both LPA' and ∂_2.

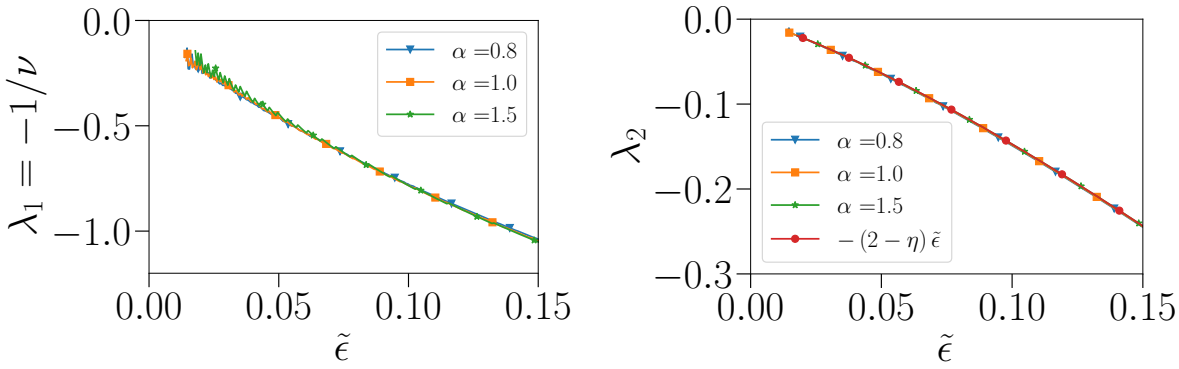

(a) (b)

Figure 4.1 – LPA': Numerical results above d_{lc} for the two relevant eigenvalues, calculated with the exponential regulator. The prediction $\lambda_2 = -(2-\eta)\,\tilde{\epsilon}$ is also displayed in the right panel. Markers are plotted for every 30th data point.

The tendency of $\lambda_1 = -1/\nu$ to vanish in LPA' as the d_{lc} limit is approached is evident in Fig. 4.1. Due to the logarithmic scales in $\tilde{\epsilon}$ that we have analytically discovered in the problem, parametric fitting to explore this unknown dependence would not be feasible.

The results for this eigenvalue are less conclusive at the level of ∂_2. As we could be dealing with logarithmic scaling in $\tilde{\epsilon}$, λ_1 might be vanishing, albeit very slowly, perhaps with some power of $1/\ln(1/\tilde{\epsilon})$. However, the results in Fig. 4.2 are also compatible with λ_1 going to a finite negative constant as $\tilde{\epsilon} \to 0^+$.

If we consider the droplet theory results [12–14], such a slow possible vanishing of $1/\nu$ is not so surprising. B&W indeed find $1/\nu \propto \epsilon + \mathcal{O}(\epsilon^2)$ (recall that $\epsilon = d - 1 \neq \tilde{\epsilon}$). If we look

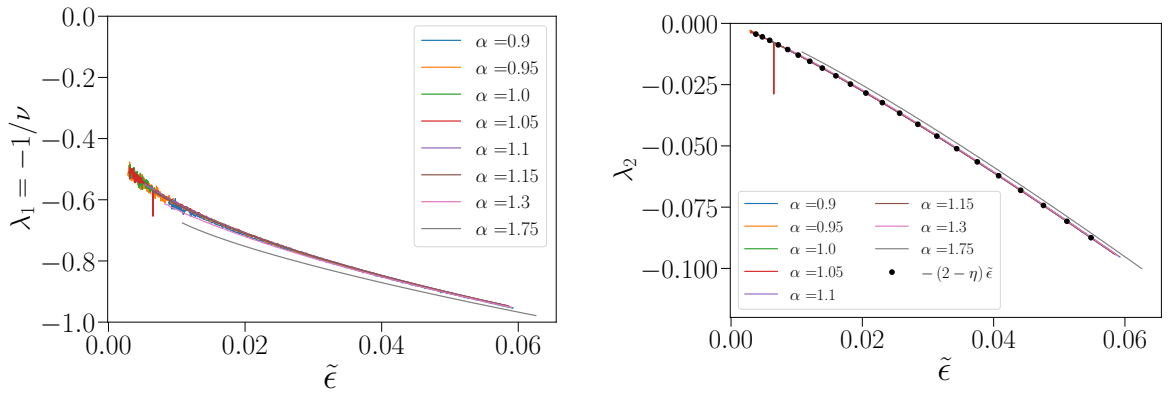

(a) (b)

Figure 4.2 – ∂_2: Numerical results above d_{lc} for the two relevant eigenvalues, calculated with the exponential regulator. The prediction $\lambda_2 = -(2-\eta)\,\tilde{\epsilon}$ is also displayed in the right panel.

at the leading order in ϵ in the expression for D_φ in the droplet theory, we have

$$\epsilon \propto \frac{1}{\ln(1/\tilde{\epsilon})}. \tag{4.18}$$

This would translate into $1/\nu \propto 1/\ln(1/\tilde{\epsilon})$ in our approach. In Fig. 4.3 we plot the LPA' and ∂_2 results for λ_1 as a function of $1/\ln(1/\tilde{\epsilon})$. We see that the LPA' results are not compatible with the slow, logarithmic vanishing of ν. If λ_1 vanishes at the ∂_2 level, however, it seems that it must vanish even slower than $1/\ln(1/\tilde{\epsilon})$.

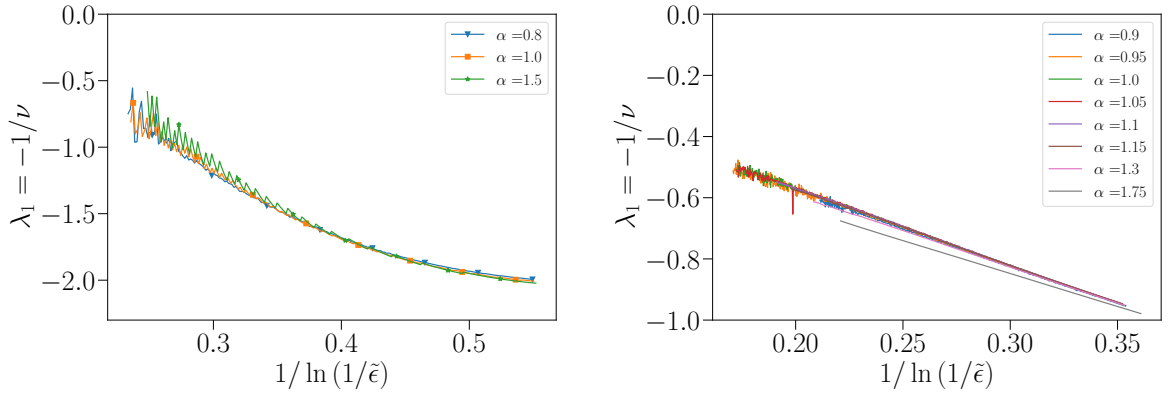

(a) LPA' (b) ∂_2

Figure 4.3 – Comparison of the scaling of ν obtained from FRG by numerical means at $d > d_{lc}$ with the logarithmic scaling expected from droplet theory [12–14]. Note the different ranges in $\tilde{\epsilon}$ for the LPA' and ∂_2 data. For LPA', markers are plotted for every 30th data point.

In the hope of interpreting these results better, we have also investigated the eigenvectors. The space in which the FRG flows unfurl in the case of the ∂_2 ansatz is spanned by all possible

functions $u_k''(\varphi)$ and $z_k(\varphi)$, as previously stated. The diverging tails of the effective potential and of its field derivatives $u_k^{(n)}(\varphi)$ are problematic from the numerical standpoint, so in the case of numerical investigations, we perform the calculation by using $\chi_k(\varphi) = 1/(\alpha + u_k''(\varphi))$, the dimensionless susceptibility that has a vanishing tail. Therefore, our results which are presented in Fig. 4.4 to Fig. 4.8 will be for the eigenvector components as projected onto the perturbations $\delta\chi(\varphi)$ and $\delta z(\varphi)$. The calculations shown are for the IR regulator r_{exp} with $\alpha = 1$, but other choices did not give qualitatively different results. As expected, the ∂_2 components given in Fig. 4.5 in relation to eigenvalue λ_1 are even and those for λ_2 are odd. In LPA' renormalizing at $\varphi_{min} > 0$ introduces asymmetry, as seen in Fig. 4.4.

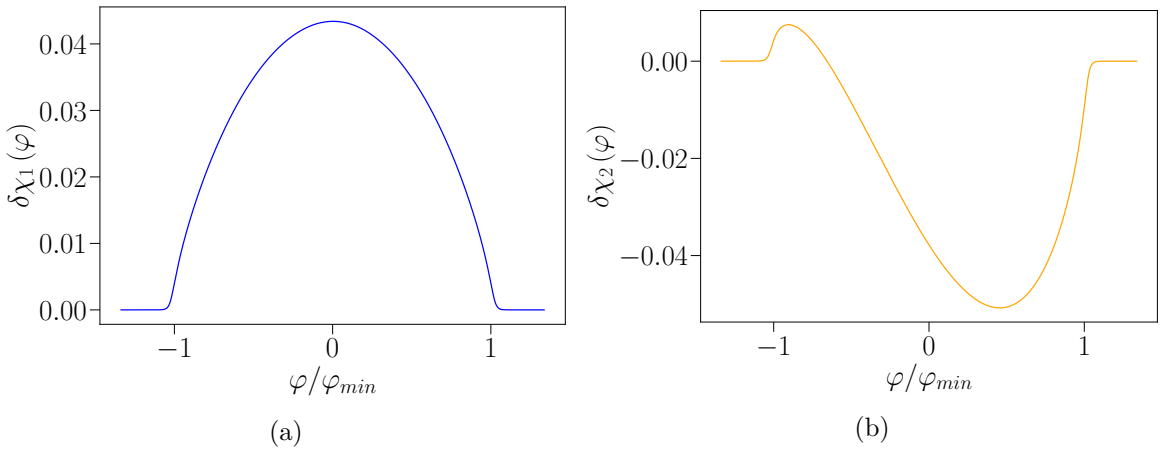

Figure 4.4 – LPA': Numerical results above d_{lc} for the eigenvectors e_1 and e_2, corresponding to eigenvalues $\lambda_1 = -1/\nu$ and $\lambda_2 = -(2-\eta)\,\tilde{\epsilon}$ respectively. The data is obtained for r_{exp} with $\alpha = 1$ at $d = 1.095$ (and $\tilde{\epsilon} = 0.014$). This shape is generic for the dimensions between $d = 2.200$ and $d = 1.095$, which is the range that was calculated. The eigenvectors are asymmetric in φ (e_1 should be even and e_2 odd), as is more evident in Fig. 4.4b. We suspect that this is due to the asymmetry of the stability matrix induced by renormalization in the location of the right minimum, $\varphi_{min} > 0$.

We expect that the existence of the boundary layer in the fixed-point solution and the related divergent scaling of the RG functions would lead to some nontrivial behavior of the eigenvectors in this field range, as fixed-point solutions factor in the linearized eigenequations. This brought us to more closely inspect the numerical eigenvector data around φ_{min}. The results make it more natural to start this discussion from the ∂_2.

The results of interest at the level of ∂_2 are shown in Fig. 4.6. The figures show a "zoom" on the boundary layer region. We stress that the boundary layer develops as we progress towards the $\tilde{\epsilon} \to 0^+$ limit, while the numerical calculations are done for finite $\tilde{\epsilon}$ and we cannot say with certainty that they already capture the quality of the limit of the lower critical dimension. When we speak of the boundary layer in the context of numerical calculations above d_{lc}, we refer to the range of fields where $x = \mathcal{O}(1)$ for $x = (\varphi - \varphi_{min})/\delta(\tilde{\epsilon})$ and $\delta(\tilde{\epsilon}) = \tilde{\epsilon}\sqrt{\ln(1/\tilde{\epsilon})}$ is evaluated at the $\tilde{\epsilon}$ we work in. We are nonetheless interested in the trends the solutions exhibit as we diminish d. In the case of the $\delta z(\varphi)$ component, the field scale is centered around $\varphi_{z\text{max}}$, the location of the maximum of $z(\varphi)$. We expect that in

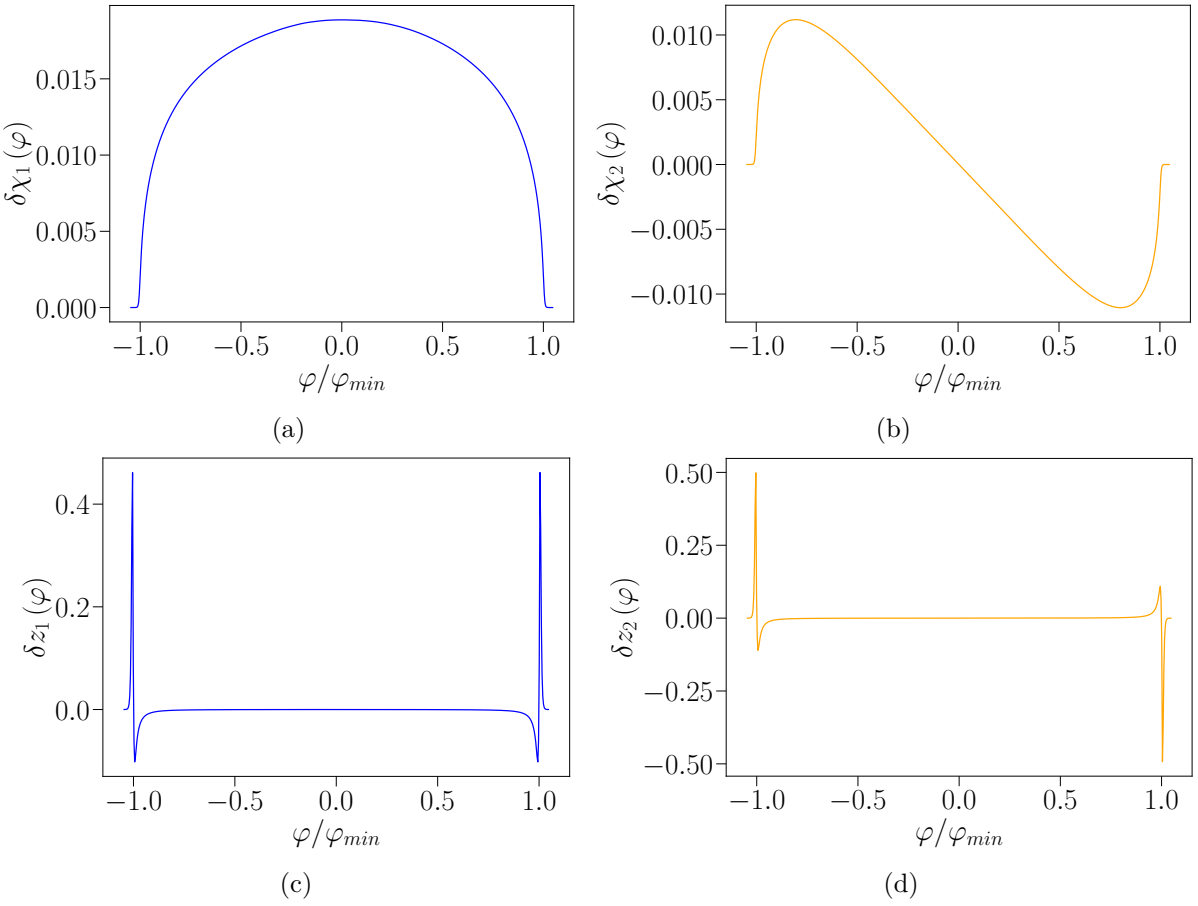

Figure 4.5 – ∂_2 : Numerical results above d_{lc} for the components of the eigenvectors e_1 and e_2, corresponding to eigenvalues $\lambda_1 = -1/\nu$ and $\lambda_2 = -(2-\eta)\,\tilde{\epsilon}$ respectively. The data is obtained for r_{exp} with $\alpha = 1$ at $d = 1.113$ (and $\tilde{\epsilon} = 0.003$). The rapid diminishing of the $\delta\chi$ component and the nontrivial peaks of the δz component happen in the vicinity of φ_{min}, which is "zoomed in" in Fig. 4.6.

the limit of the lower critical dimension $\varphi_{z\max}$ is in the boundary layer, and from the nature of the $\delta z(\varphi)$ eigenvector component, it is useful to include the maximum in the "zoomed" plots.

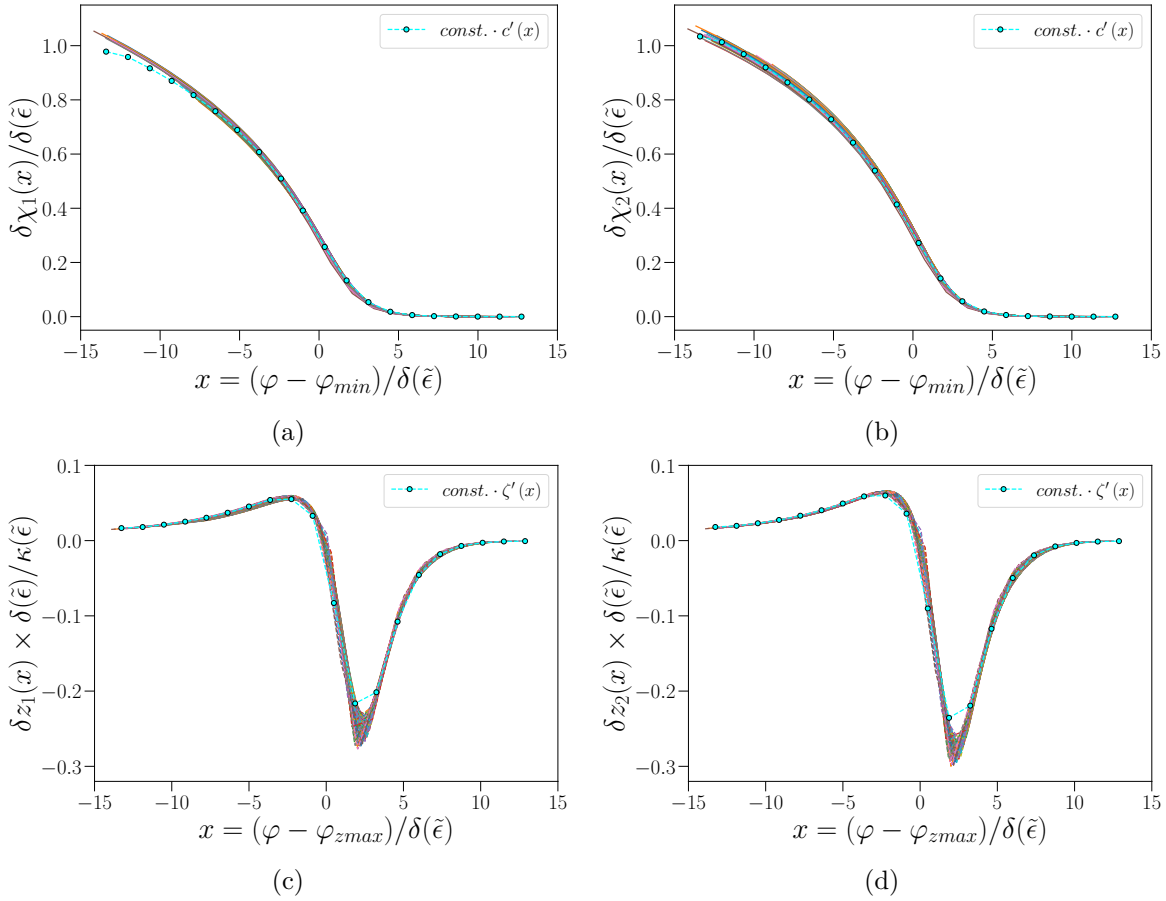

Figure 4.6 – ∂_2 : Numerical results above d_{lc} for the components $\delta\chi_i$ and δz_i of the eigenvectors $e_{i=1,2}$. The data is obtained for $r_{\exp}$ with $\alpha = 1$ in the range of dimensions from $d = 1.2$ down to 1.113. The boundary layer range of fields is zoomed in. For each d we plot the same number of points around the minimum. The components of the e_i as projected to $\delta\chi_i$ and δz_i are plotted scaled accordingly to the labels of the respective y axes. The data points for $c'(x) = \chi'(\varphi)$ and $\zeta'(x) = z(\varphi)\,\delta(\tilde{\epsilon})/\kappa(\tilde{\epsilon})$ are given for $d = 1.113$.

The nature we speak of is the observation from numerical data above d_{lc} that in the boundary layer, the e_1 eigenvector projected on the perturbations $\delta\chi(\varphi)$ and $\delta z(\varphi)$ resembles in shape the functions $\chi'(\varphi)$ and $z'(\varphi)$ respectively. For comparison, in Fig. 4.6 we have also plotted the e_2 components, for which we know that they truly correspond to the mentioned derivatives of the RG functions. We see good agreement, both of the e_2 with the derivatives, and between e_1 and e_2. Note that the e_2 corresponds to the derivatives in all fields, while for e_1 this is only observed in the neighborhood of φ_{min}. We believe this is why, e.g., we see better agreement with $\chi'(\varphi)$ in the limit of negative x in Fig. 4.6b than in Fig. 4.6a. To collapse the eigenvector plots onto the derivatives of the fixed-point functions, it seems

that we must rescale them by the boundary layer scaling of $\chi(\varphi)$ and $z(\varphi)$, namely we must plot $\delta\chi(\varphi)/\delta(\tilde{\epsilon})$ and $\delta z(\varphi)\times\delta(\tilde{\epsilon})/\kappa(\tilde{\epsilon})$. We note that this is to be taken as an illustration and that we use the scaling $\delta(\tilde{\epsilon}) = \tilde{\epsilon}\sqrt{\ln(1/\tilde{\epsilon})}$ strictly proven only in LPA' and $\kappa(\tilde{\epsilon}) = 1/\sqrt{\ln(1/\tilde{\epsilon})}^5$, which is a rough estimate. The main takeaway of this numerical data is that the eigenvector components have a nontrivial structure in the field range around φ_{min}, and that it resembles derivatives of the RG functions.

While the overall scale of an eigenvector component is not relevant due to the linearity of the equations, two things are. First, the ratio of amplitudes of the same eigenvector for different values of the field. In this case, the full field plots in Fig. 4.6 already invite attention to the boundary layer range, especially the $\delta z(\varphi)$ component. Secondly, the ratio of amplitudes in the same field for eigenvectors calculated for different dimensions, but with the same value of numerical pointwise-perturbation when building the stability matrix. Here collapses at different d, in a range from 1.2 down to 1.113, seem to happen for the same scaling (as a function of $\tilde{\epsilon}(d)$), as can be seen in Fig. 4.6. Both of these observations encourage investigations of the eigenproblem in the context of possible boundary layer simplifications. This is not without difficulties and limitations, as will be discussed in Section 3.

For the case of LPA', the results around φ_{min} are less clear. In Fig. 4.7 we give the tracking (as the $\tilde{\epsilon}$ lowers) of the amplitude of the eigenpertubation evaluated in the location of the minimum φ_{min}. We reiterate that the overall amplitude of an eigenvector, which is by construction a solution to a linear problem, is generally not relevant, but here we track how the same numerical pointwise-perturbation builds into the value of $\delta\chi(\varphi_{min})$ at different dimensions. We see form Fig. 4.7 that this value decreases monotonically, but from Fig. 4.7b it is clear that it happens slower than the decrease of $\delta(\tilde{\epsilon})$, a scaling one might expect if ∂_2 results are consulted, or if $\delta\chi(\varphi)$ scaled the same as $\chi(\varphi)$. Still, we show in Fig. 4.7 an illustrative plot with a scaling of $1/\ln(1/\tilde{\epsilon})$, to show the similarity in shape with $\chi'(\varphi)$. This similarity is less distinct than in ∂_2, but we put more weight on the ∂_2 results. LPA' is the lower approximation order, and additionally it is possible that this lack of clarity in scaling of $\delta\chi_1$ in the vicinity of φ_{min}, along with Fig. 4.8b showing a "weaker" collapse of the $\delta\chi_2$ eigenvector known to be $\propto \chi'(\varphi)$, indicates that the LPA' might not reach the asymptotic limit as fast as ∂_2. We must also be aware that the renormalization done in φ_{min} might carry some problems, like the aforementioned asymmetry of Fig. 4.4, and that results in LPA' depend on the renormalization point [62, 63].

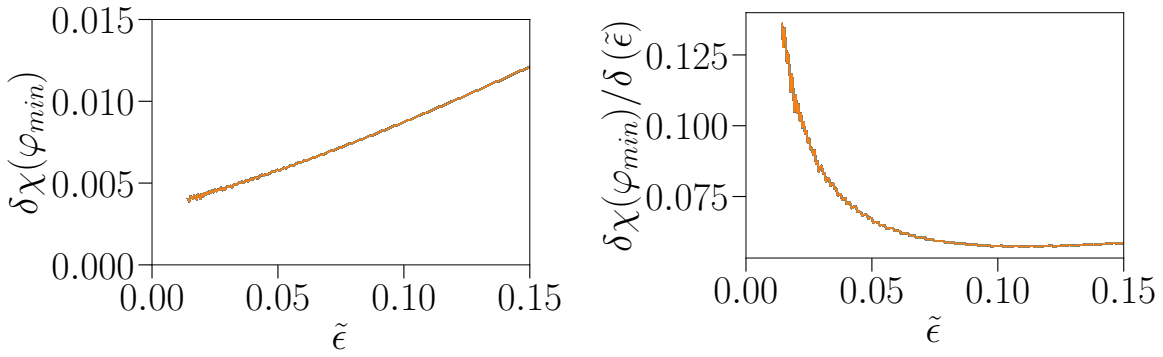

(a) Numerical data.

(b) Scaled with $\delta(\tilde{\epsilon})$.

Figure 4.7 – LPA': Numerical results above d_{lc} for the value o the eigenvector e_1 in the location of the minimum of the effective potential φ_{min}. While a prefactor of the eigenvector is irrelevant due to the eigenproblem inherently being linear, this amplitude is not to be seen in that context, as it is achieved with the same numerical pointwise perturbation of 10^{-10} for all of the $\tilde{\epsilon}$ we plot, so the ratios of the values are relevant.

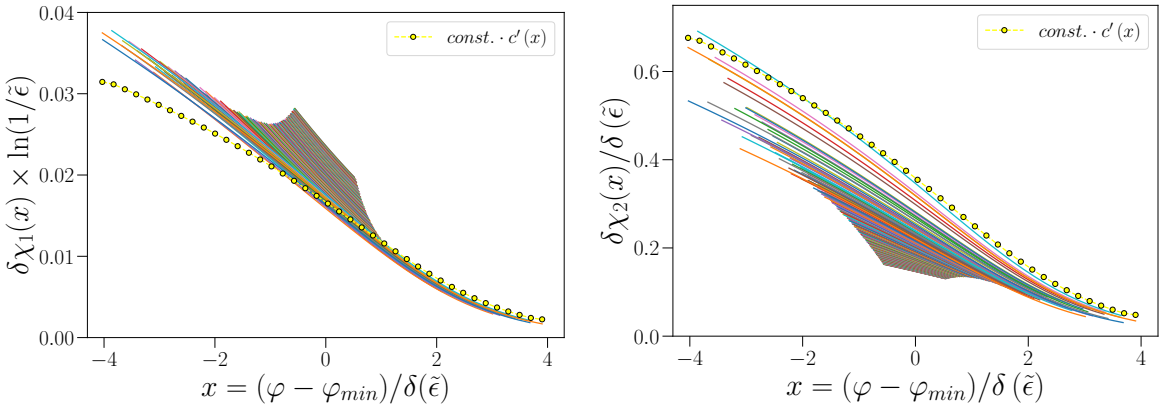

(a)

(b)

Figure 4.8 – LPA': Numerical results above d_{lc} for $e_{1,2}$. The data is obtained for $r_{\exp}$ with $\alpha = 1$ in the range of dimensions from $d = 2.2$ down to 1.095. The boundary layer range of fields is zoomed in. For each d we plot the same number of points around the minimum. The data for smaller $\tilde{\epsilon}$ thus seemingly has a wider domain, which is more noticeable here than in the ∂_2 plots in Fig. 4.6. The data points for $c'(x) = \chi'(\varphi)$ are given for $d = 1.095$.

3 The open question of the marginality of $\lambda_1 = -1/\nu$

The merging of the zero-temperature fixed point with the critical fixed point requires the relevant eigenvalues of the critical fixed point to become marginal. This is because the zero-temperature fixed point is an attractor and the critical fixed point is a saddle, as it has unstable directions which are physically relevant for the transition. This means that the eigenvalues $\lambda_1 = -1/\nu$ and $\lambda_2 = -D_\varphi \propto \tilde{\epsilon}$ should vanish in a proper description of d_{lc}, which must be checked.

The trivial eigenvalue $\lambda_2 \propto \tilde{\epsilon}$ does indeed vanish in the d_{lc} limit, as can be seen both analytically in Section 2.1.1 and from numerical results in Section 2.2. We obtained numerical results for λ_1 above d_{lc}, presented in Section 2.2 that are congruent with marginality, but are not conclusive.

As the results for the values of λ_1 are inconclusive, we turn our attention to the corresponding eigenvector e_1. In the previous section we found that e_1 projected onto $\delta\chi$ (and δz at ∂_2) seems to be very similar to the derivatives of the respective fixed-point RG functions, $\chi'(\varphi)$ and $z'(\varphi)$, in the vicinity of φ_{min}. We continue with a tentative discussion based on this. First, we take that a boundary layer around $\varphi_{min,k}$ persists after perturbation. Second, we established previously that the fixed-point solutions inside the boundary layer can be understood as an expansion in the orders of the correction ($\delta(\tilde{\epsilon})$ for LPA' and $\kappa(\tilde{\epsilon})$ for ∂_2). We analogously assume that in this boundary layer, the e_1 components $\delta\chi_1$ and δz_1 can be expanded too, and are in the leading order given by the derivatives:

$$\begin{aligned} &\delta F_i(\varphi) \propto k^{\lambda_1} f_{i,0}(x) + \mu_i(\tilde{\epsilon})\, f_{i,1}(x) + ..., \\ &\text{with some} \quad \mu_i(\tilde{\epsilon}) \to 0 \quad \text{when} \quad \tilde{\epsilon} \to 0^+ \quad \text{and} \quad f_{i,0}(x) = f_i'(x), \end{aligned} \tag{4.19}$$

where the lowercase f_i represent the boundary layer functions (e.g., $c(x) = \chi(\varphi)/\delta(\tilde{\epsilon})$ and $\zeta(x) = z(\varphi)\,\delta(\tilde{\epsilon})/\kappa(\tilde{\epsilon})$) of the corresponding uppercase F_i. Thirdly, the proportionality constants in Eq. (4.19) must be such that in the boundary layer $\delta z/\delta\chi = \mathcal{O}(\chi'(\varphi)/z'(\varphi)) = \kappa(\tilde{\epsilon})/(\delta(\tilde{\epsilon}))^2$. All three of these points are strongly indicated by the numerical results of Section 2.2 (moreso by the ∂_2 data).

It is important to note that we take Eq. (4.19) only in the boundary layer, for two very clear reasons. Firstly, the numerical agreement of e_1 components with the derivatives is only found in the neighborhood of φ_{min}. Secondly, $\chi'(\varphi)$ and $z'(\varphi)$, the derivatives in question, are odd functions. While e_1 components might correspond to them in the leading order in the boundary layer, in the rest of the regions one must match to such forms that the full eigenvector e_1 across all φ is even.

Let us recall λ_2. Its eigenvector e_2 has components that were *in the leading order* same as the assumed Eq. (4.19) form, as they are the derivatives of the corresponding RG functions everywhere in the field.

Looking at the boundary layer, the same cancelations then must happen *in the leading order* for the e_1 as for the e_2 components in Section 2.2 (choosing the renormalization procedure with $\delta\eta = 0$). We stress that this does not mean that $\lambda_1 \propto \tilde{\epsilon}$. On the contrary, we expect the corrections to the leading order to put an upper limit on the value of $\lambda_1 = -1/\nu$. The calculations of these corrections is a formidable task we have not done in the present moment. If the fixed-point solutions are consulted, we might expect some slow logarithmic behavior, which could account for the inconclusiveness of the λ_1 numerical results in Section 2.2. The most this approach could show without explicitly finding the corrections is that $\lambda_1 \to 0$ in the leading order in the $\tilde{\epsilon} \to 0^+$ limit, where the boundary layer develops. However, we believe that the assumptions about the boundary layer shape of e_1 are strongly backed by the numerical results of Section 2.2, and we aim to further explore this mechanism of λ_1 becoming marginal in future research.

4 Conclusion

In this chapter we have discussed LPA' and ∂_2 results for the critical temperature T_c and the critical exponents.

In Section 1 we have recovered the scaling of the critical temperature $T_c \propto 1/\ln(1/D_\varphi)$ with the scaling dimension of the field $D_\varphi \propto \tilde{\epsilon}$ that had been found in the droplet theory in $d = 1 + \epsilon$ [12–14]. The droplet theory is based on a careful treatment of domain walls of droplets (bubbles in regions of opposite spins) in the Ising model near the exact lower critical dimension of $d_{lc} = 1$. We stress that $\tilde{\epsilon} \neq \epsilon$. Interestingly, through the boundary layer mechanism the truncated derivative expansion in the FRG appears to capture a behavior that involves strongly nonuniform fluctuations (in the form of droplets).

Concerning the critical exponents, our results are currently mostly limited to numerical data for $d > d_{lc}$, which are presented in Section 2.2. Regarding analytical attempts, in Section 3 we have offered a discussion of a tentative mechanism by which λ_1 could become marginal in the $d \to d_{lc}$ limit, based on the similarities of the numerical results with the eigenvectors of the trivially marginal eigenvalue $\lambda_2 \propto \tilde{\epsilon}$ in the vicinity of the location of the minimum of the potential φ_{min}.

However, our research does not give a conclusive answer whether the truncated derivative expansion predicts $1/\nu$ to vanish when $\tilde{\epsilon} \to 0^+$. This is something that deserves more attention in future research. The critical exponent ν of the correlation length must diverge in d_{lc}, where essential scaling has been found for the Ising model in connection with the proliferation of instantons (kinks and anti-kinks) that destroy the finite-temperature transition. Strictly speaking, the critical exponent ν diverging is a necessary but not sufficient condition to recover essential scaling. It might however be sufficient for the $\lambda_1 = -1/\nu$ eigenvalue to be marginal, as in generic cases of marginal variables logarithmic corrections can occur [17, 44]. We plan to investigate whether this can be translated into an exponential divergence of the correlation length, i.e., essential scaling.

Chapter 5

The ordered phase of the ϕ^4 theory in the FRG when approaching the lower critical dimension

In the previous chapters we have studied how the FRG within the truncated derivative expansion can reproduce physical situations in which the long-distance physics is dominated by spatially localized excitations such as the kinks and anti-kinks that proliferate at the lower critical dimension of the Ising-like scalar ϕ^4 theory or the droplets that control the critical behavior when approaching this dimension. We now consider a different problem where strongly nonuniform configurations of the field are important, the ordered phase of the scalar ϕ^4 theory. In this case indeed it is known that phase coexistence between the two symmetry-broken pure states involves a nonuniform configuration that has the form of a domain wall. This is what allows the free-energy density or effective action in the inner domain of average field values to be strictly convex, i.e, flat, in the thermodynamic limit, as required by its definition as a Legendre transform. The conventional mean-field description misses this point and predicts a nonconvex Landau effective potential with a maximum in zero field. The return to convexity under the influence of spatial fluctuations therefore requires taking into account the domain-wall configurations. Compared to the localized instanton and the droplets previously discussed, such configurations are spatially extended. They appear as a kink in one dimension but are uniform in the remaining $(d-1)$ dimensions. As a result their contribution to the free energy above the minimum scales as L^{d-1} in a large but finite system of linear size L. On the other hand their contribution to the free-energy density or effective action goes as $1/L$ and vanishes in the thermodynamic limit, leading to a flat inner part of the effective action as a function of the average field.

We are interested in the way one can keep track of the nonuniform domain-wall configurations within the FRG. It is known that low orders of the derivative expansion, even the lowest one (the LPA), describe the fluctuation-induced return to convexity of the effective average potential for a large class of infrared regulators [15, 16, 65, 66]. Mathematically, this takes place through the approach of the singularity (usually a pole) in the renormalized propagator of the theory, and the inner part of the scale-dependent effective potential

behaves at small IR cutoff k as [15, 16]

$$U_k(\varphi) = V(k) - \frac{b}{2}k^2\varphi^2 + \mathcal{O}(k^{2(d-2)}) \tag{5.1}$$

with $b > 0$ a constant of $\mathcal{O}(1)$. The inner part of the potential thus becomes flat in the limit $k \to 0$, as it should. The above expression has been established for $d > 2$ [15, 16, 65] and no analogous expression has been derived when $d < 2$, which is the case of interest for us. Furthermore, it is unclear how the above form of the scale-dependent effective potential relates to the presence of domain-wall configurations. We therefore want to address this point and derive the generic form of the scale-dependent effective potential $U_k(\varphi)$ in the phase coexistence region where a domain-wall configuration dominates the physics. Deep enough in the ordered phase, i.e., physically, at low enough temperature, this amounts to computing the scale-dependent generating functional through a saddle-point method in the presence of an IR regulator. The calculation in the absence of regulator is standard and indeed selects the proper domain-wall configurations and the Gaussian fluctuations around it. A calculation in the presence of an IR regulator was done by Ringwald and Wetterich in the case of the $\mathcal{O}(N \geq 3)$ model [67]. There, the dominant nonuniform configuration is not a domain wall but a spin wave. The study of the $N = 1$ case has never been undertaken and this is what we do below. Another motivation is to investigate how the ordered fixed point behaves in the limit $d = 1 + \epsilon$ with $\epsilon \to 0$ because one knows that it should then merge with the critical fixed point that we have studied earlier.

1 Formalism: saddle-point approximation

We consider the Ising-like scalar ϕ^4 theory in a large system of linear size L in dimension $d = 1 + \epsilon$ and $0 < \epsilon < 1$. The scale-dependent effective average action $\Gamma_k[\varphi]$ can be obtained from the functional integral

$$\begin{aligned} e^{-\Gamma_k[\varphi]} &= \\ &= \int \mathcal{D}\phi \exp\Big(- S[\phi] + \int_{\mathbf{x}} \Gamma^{(1)}_{k,\mathbf{x}}[\varphi][\phi(\mathbf{x}) - \varphi(\mathbf{x})] + \\ &\qquad - \frac{1}{2}\int_{\mathbf{xy}} [\phi(\mathbf{x}) - \varphi(\mathbf{x})] R_k(\mathbf{x} - \mathbf{y})[\phi(\mathbf{y}) - \varphi(\mathbf{y})]\Big) \end{aligned} \tag{5.2}$$

where the action of the ϕ^4 theory in the ordered phase can be rewritten as

$$S[\phi] = \int_{\mathbf{x}} \left\{ \frac{1}{2}[\nabla_{\mathbf{x}}\phi(\mathbf{x})]^2 - \frac{1}{\xi^2}\phi(\mathbf{x})^2 + \frac{1}{2\xi^2\phi_0^2}\phi(\mathbf{x})^4 \right\}, \tag{5.3}$$

where ϕ_0 is the minimum of the bare potential and ξ the bare correlation length.

We consider the system deep in the ordered phase where the correlation length is small. Making the temperature explicit by rescaling the field by a factor $\sqrt{T}$ so that the integrand now has a $1/T$ prefactor as in a Boltzmann distribution, this amounts to considering the limit of low temperature. One can then calculate the functional integral by the Laplace method (or method of steepest descent), looking for saddle points.

We are primarily interested in the scale dependent effective potential $U_k(\varphi)$ which is obtained from the effective average action when the average field configuration is uniform, i.e., $U_k(\varphi) = \Gamma_k(\varphi)/L^d$. From Eq. (5.2) we then derive

$$e^{-L^d U_k(\varphi)} = \\ = \int \mathcal{D}\phi \exp\left(-S[\phi] + U_k'(\varphi)[\int_{\mathbf{x}} \phi(\mathbf{x}) - L^d\varphi] - \frac{1}{2}\int_{\mathbf{xy}} [\phi(\mathbf{x})-\varphi]R_k(\mathbf{x}-\mathbf{y})[\phi(\mathbf{y})-\varphi]\right). \tag{5.4}$$

The saddle-point approximation selects the classical configurations of the field $\phi(\mathbf{x})$ that dominate the functional integral. One needs to solve

$$\frac{\delta S[\phi]}{\delta\phi(\mathbf{x})} = -\nabla^2_{\mathbf{x}}\phi(\mathbf{x}) - \frac{2}{\xi^2}\phi(\mathbf{x})\left(1 - \frac{\phi(\mathbf{x})^2}{\phi_0^2}\right) = U_k'(\varphi) - \int_{\mathbf{y}} R_k(\mathbf{x}-\mathbf{y})[\phi(\mathbf{y})-\varphi] \tag{5.5}$$

where $U_k(\varphi)$ is given at leading order by

$$U_k(\varphi) = U_k^{\rm SP}(\varphi) = \\ = \frac{S[\phi_{*k}]}{L^d} - U_k'(\varphi)\left[\frac{1}{L^d}\int_{\mathbf{x}} \phi_{*k}(\mathbf{x}) - \varphi\right] + \frac{1}{2L^d}\int_{\mathbf{xy}} [\phi_{*k}(\mathbf{x})-\varphi]R_k(\mathbf{x}-\mathbf{y})[\phi_{*k}(\mathbf{y})-\varphi]\,. \tag{5.6}$$

with $\phi_{*k}(\mathbf{x})$ the φ-dependent saddle-point solution. When deriving the above expression for $U_k(\varphi)$ with respect to φ and using the saddle-point equation one obtains a self-consistency equation, $0 = [U_k''(\varphi) + R_k(q^2=0)][\frac{1}{L^d}\int_{\mathbf{x}} \phi_{*k}(\mathbf{x}) - \varphi]$, which implies that

$$\frac{1}{L^d}\int_{\mathbf{x}} \phi_{*k}(\mathbf{x}) = \varphi \tag{5.7}$$

in the limit of large L, and the effective potential in the saddle-point approximation can be rewritten in this limit as

$$U_k^{\rm SP}(\varphi) = \frac{S[\phi_{*k}]}{L^d} + \frac{1}{2L^d}\int_{\mathbf{xy}} \phi_{*k}(\mathbf{x})R_k(\mathbf{x}-\mathbf{y})\phi_{*k}(\mathbf{y}) - (\varphi^2/2)R_k(q^2=0). \tag{5.8}$$

The uniform solution of the above equation which leads to the standard mean-field (Landau) description is simply $\phi_{*k} = \varphi$ (from Eq. (5.7)) and $U_k^{\rm SP}(\varphi) = S(\varphi)/L^d = \varphi^2[-2 + (\varphi^2/\phi_0^2)]/(2\xi^2)$, which indeed satisfies Eqs. (5.5) and (5.6). As is well known, the Landau effective action is nonconvex even in the limit $k \to 0$ and this solution cannot be valid for all fields. Indeed, the Hessian matrix around the saddle point can be diagonalized in Fourier space and is equal to

$$\Gamma_k^{(2)}[\varphi] = q^2 + R_k(q^2) - \frac{2}{\xi^2}\left(1 - 3\frac{\varphi^2}{\phi_0^2}\right). \tag{5.9}$$

Obviously when φ^2 is small enough ($\varphi^2 \leq (\phi_0^2/3)[1-(\xi^2k^2/2)\min_q(q^2+R_k(q^2))]$), the uniform saddle point is unstable and is not an acceptable solution (the 1-loop correction due to the integration over the Gaussian fluctuations around the saddle-point then becomes imaginary). As is known for $k = 0$, the proper saddle-point is a nonuniform configuration in the form of a domain wall which leads to a more stable solution in a whole inner region of the field (away from the minima), where the effective potential is now flat, hence convex. We expect that the same is true in the presence of an IR regulator, at least for small k.

2 Domain-wall saddle-point solution

We now look for a nonuniform solution of the saddle-point equation. We anticipate that the relevant solution is a domain wall which has a kink-like shape in one dimension, which we simply denote as x, and is uniform in the $(d-1)$ remaining dimensions, labelled by $\mathbf{x}_\perp$ (x can of course equally well be chosen in any of the d directions of space but this degeneracy does not affect the results). In the following we set ξ and ϕ_0 to 1 (so that U_k is then expressed in units of ϕ_0^2/ξ^2) and we search for a solution $\phi_{*k}(\mathbf{x}) = f_k(x_\parallel = x)$ with $f_k(x)$ approaching plus or minus a constant at large distance $|x|$. Eq. (5.5) can be reexpressed as

$$f_k''(x) + 2f_k(x)[1 - f_k^2(x)] = k^3 \int_{-L/2}^{L/2} dy\, r(k(x-y)) f(y) + [-U_k'(\varphi) + k^2 \int_{-L/2}^{L/2} dy\, r(x-y)\, \varphi] \tag{5.10}$$

where we have defined $\int_{\mathbf{x}_\perp} R_k(\mathbf{x}) = k^3 r(kx)$ (so that $R_k(q^2 = 0) = \int dx k^3 r(kx) = \mathcal{O}(k^2)$), neglecting subdominant terms that go to zero when the system size L is large. One also has the condition (see Eq. (5.7))

$$\frac{1}{L} \int_{L/2}^{L/2} dx f_k(x) = \varphi. \tag{5.11}$$

We anticipate that $U_k'(\varphi)$ goes to zero as k^2 when $k \to 0$ (see Eq. (5.1) and we define $b\varphi = U_k'(\varphi)/k^2$ (where b is a constant to be determined below). As a consequence, the whole right-hand side of Eq. (5.10) goes to 0 as k^2. In the absence of a regulator, when $k = 0$, one recovers the standard instantonic equation for a kink,[84] $f_0''(x) + 2f_0(x)[1 - f_0^2(x)] = 0$ with boundary conditions such that f_0 approaches $+1$ (the minimum of the bare potential in reduced units) when x is large and -1 when $-x$ is large. The well-known solution is a hyperbolic tangent,

$$f_0(x) = \tanh(x - a) \tag{5.12}$$

where $a \equiv a(\varphi)$ is fixed by Eq. (5.11), i.e., at the zeroth order, $a = a_0 \approx -(L/2)\varphi$ plus terms that decay exponentially with L, provided φ stays away from ± 1.

We then look for a solution of the form

$$f_k(x) = f_0(x) + k^2 f_1(x) + \cdots, \tag{5.13}$$

where the ellipses denote subdominant terms when $k \to 0$ and $L \to \infty$ (the order of the limits may be important and will be discussed below). The function $f_1(x)$ is the solution of

$$f_1''(x) + 2f_1(x)[1 - 3f_0^2(x)] = k \int_{-L/2}^{L/2} dy\, r(k(x-y)) f_0(y) - [b - \int_{-k(L/2+x)}^{k(L/2-x)} dy\, r(y)]\varphi. \tag{5.14}$$

Some care is needed to take into account different domains of values of x: $|x-a| < \mathcal{O}(1/k)$, $|x-a| \sim \mathcal{O}(1/k)$, and near the boundaries where $L/2 - |x| \sim \mathcal{O}(L^0)$. Details on the derivation are given in Appendix F. The final result reads

$$f_1(x) = \frac{f_1(0)}{\cosh^2(x-a)} - \frac{\alpha}{4} g(k(x-a)) + \frac{\alpha}{8}[-\varphi + \mathrm{sgn}(x-a)]\left[1 - g\left(k\left(\frac{L}{2} - |x|\right)\right)\right], \tag{5.15}$$

where $g(x) = 2\int_0^x dy\, r(y)/\alpha$ and $\alpha = \int_{-\infty}^{+\infty} dy\, r(y)$. For instance, for a Gaussian regulator, $r(y) = \alpha \exp(-y^2/2)/\sqrt{2\pi}$ (we called it the exponential regulator in the previous chapters

because it is exponential in the variable q^2), $g(x) = \mathrm{erf}(x/\sqrt{2})$. The last term of the above expression helps enforcing the boundary conditions when $x \to \pm L/2$. Note that for consistency one must have $b = \alpha$.

The location of the kink, $a \equiv a_k(\varphi)$, is corrected from its zeroth-order value as the solution must satisfy Eq. (5.11). One obtains

$$a_k(\varphi) = -\varphi \frac{L}{2}\left(1 + \frac{\alpha}{4}k^2 + \cdots\right) \tag{5.16}$$

up to subdominant terms when $k \to 0$ and $L \to \infty$.

Reinstalling ξ and ϕ_0 we can finally express the kink-like saddle-point solution in the presence of an IR regulator as

$$\begin{aligned}\frac{\phi_{*k}(\mathbf{x})}{\phi_0} =& \tanh((x-a_k)/\xi) + \\ &+ k^2\xi^2\Bigg\{\frac{f_1(0)}{\cosh^2((x-a_0)/\xi)} - \frac{\alpha}{4}\,g(k(x-a_0)) + \\ &\qquad + \frac{\alpha}{8}\left[-\frac{\varphi}{\phi_0} + \mathrm{sgn}(x-a_0)\right]\left[1 - g\left(k\left(\frac{L}{2} - |x|\right)\right)\right]\Bigg\},\end{aligned} \tag{5.17}$$

with $a_k \equiv a_k(\varphi/\phi_0) = -(\varphi/\phi_0)(1 + (\alpha/4)k^2 + \cdots)L/2$. When $x \to L/2$, $\phi_{*k}(\mathbf{x})/\phi_0 \to 1 - k^2\xi^2(\alpha/8)(1 + \varphi/\phi_0)$ and when $x \to -L/2$, $\phi_{*k}(\mathbf{x})/\phi_0 \to -1 - k^2\xi^2(\alpha/8)(-1 + \varphi/\phi_0)$, all of this in the limit where $k \to 0$ and $L \to \infty$. Note that contrary to calculations of kinks and other instantons in zero applied field, the location of the domain wall is fixed by the condition that the spatial average of the saddle-point solution is equal to the classical field φ and that translational invariance is then broken in the x direction.

3 Scale-dependent effective potential at the saddle-point level

From the saddle-point solution obtained in the preceding section we can now calculate the inner part of the scale-dependent effective potential through Eq. (5.8). One has to be cautious about the noncommutation of the two limits $k \to 0$ and $L \to \infty$. After a lengthy calculation given in Appendix G, we obtain that the contribution associated with the IR regulator is equal to

$$\frac{1}{2L^d}\int_{\mathbf{xy}} \phi_{*k}(\mathbf{x})R_k(\mathbf{x}-\mathbf{y})\phi_{*k}(\mathbf{y}) - (\varphi^2/2)R_k(q^2=0) = \alpha\frac{k^2}{2}\left(\phi_0^2 - \varphi^2\right) + \mathcal{O}\left(\frac{k}{L}\right) \tag{5.18}$$

and the contribution coming from the bare action to

$$\frac{S[\phi_{*k}]}{L^d} = -\frac{\phi_0^2}{2\xi^2} + \frac{4}{3}\frac{\phi_0^2}{\xi L}, \tag{5.19}$$

up to subdominant terms at least in $\mathcal{O}(k^4)$. When $k = 0$ one recovers the $1/L$ contribution due to the domain wall, as discussed above.

However, the FRG considers a different limit where $L \to \infty$ before $k \to 0$. In this limit, the saddle-point approximation leads to

$$U_k^{\mathrm{SP}}(\varphi) = -\frac{\phi_0^2}{2\xi^2} + \frac{1}{2}\alpha k^2\phi_0^2 - \frac{1}{2}\alpha k^2\varphi^2, \tag{5.20}$$

which is precisely the form of Eq. (5.1) with $b = \alpha$.

The above result suggests several comments:

- First, contrary to what one may naively assume, the effective potential of a large but finite system is not simply obtained from the scale-dependent effective potential in the finite system by replacing k by $1/L$. Eq. (5.20) would then lead to a term in $1/L^2$, which is not the correct dependence.
- Second, the signature of the domain wall which is very clear in the $1/L$ correction is more indirect in the scale-dependent effective potential in the thermodynamic limit. For instance, the term in $k^2\varphi^2$, which is purely due to the regulator and appears very mundane as it only involves α, is present because of the presence of the domain wall separating two bulk regions of opposite average magnetization (otherwise the left-hand side of Eq. (5.18) is simply zero). The same reasoning applies to the contribution of the bare action.
- Finally, despite the fact that the dimension d no longer appears in the expression, the result is only valid for $d > 1$. Indeed, it assumes that the thermodynamics of the ordered phase is dominated by a single domain wall. This is only true if $d > 1$ so that the extensive contribution of the domain wall diverges as L^{d-1} when $L \to \infty$. In $d = 1$, the kinks and anti-kinks have an energy of $\mathcal{O}(1)$ and therefore proliferate (and destroy the long-range order).

Provided that the Hessian associated with the domain-wall saddle-point configuration is definite positive, which we will address in the next section, the expression for the scale-dependent average potential in Eq. (5.20) is valid in the inner region, i.e., when $|\varphi| \ll \phi_0$. To be more specific, we compare the results obtained with the domain wall and with the uniform configuration. As argued before, the latter is valid for large values of the average field. The nonuniform (domain-wall) result is less than the uniform one when

$$-\frac{\phi_0^2}{2\xi^2} + \frac{1}{2}\alpha k^2\phi_0^2 - \frac{1}{2}\alpha k^2\varphi^2 < \frac{\varphi^2}{2\xi^2}[-2 + (\varphi^2/\phi_0^2)], \tag{5.21}$$

which implies when $k \to 0$,

$$\frac{\varphi 2}{\phi_0^2} < 1 - \alpha k^2\xi^2. \tag{5.22}$$

We illustrate the scale-dependent effective potential obtained by simply patching the domain-wall and the uniform solutions for decreasing values of k in Fig. 5.1.

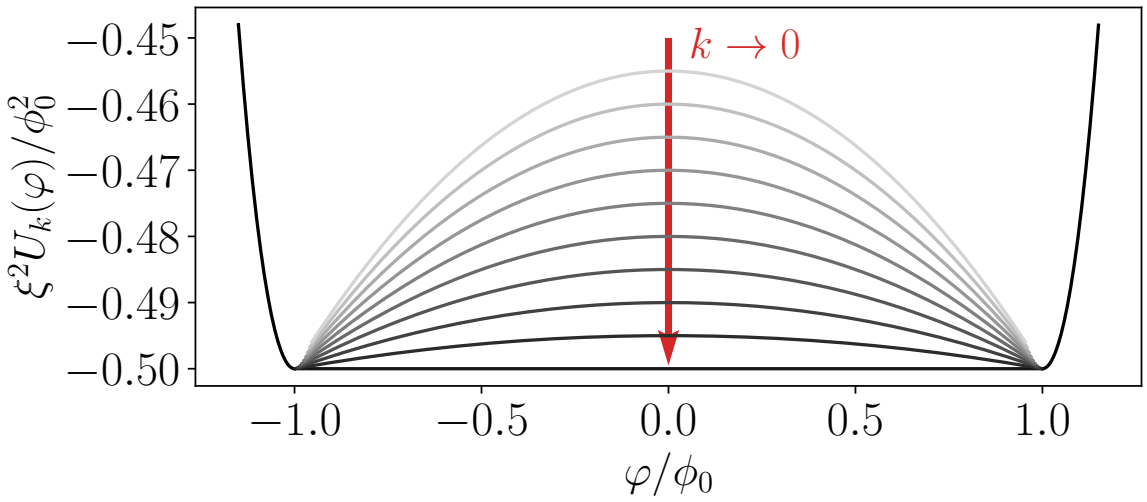

Figure 5.1 – Scale-dependent effective potential $U_k(\varphi)$ as a function of φ/ϕ_0 for decreasing values of the IR cutoff k in the ordered phase of the ϕ^4 theory in $d > 1$ dimensions. The potential is obtained at the saddle-point approximation level by simply patching together the contribution coming from the domain wall in the inner region and that coming from the uniform solution in the outer region.

4 Gaussian fluctuations around the domain-wall solution and 1-loop calculation

In the previous section we have derived the nonuniform saddle-solution in the form of a domain wall in dimension $d > 1$. We now need to consider the Gaussian fluctuations around the saddle-point, fluctuations that control the stability of the latter and, when integrated over, give a 1-loop contribution to the effective potential.

The Hessian operator around the domain-wall saddle point is given by

$$\Gamma^{(2)}_{k,\mathbf{xy}}(\varphi) = \left[-\partial_x^2 - \nabla^2_{\mathbf{x}_\perp} - \frac{2}{\xi^2}\left(1 - 3\frac{\phi_{*k}(x)^2}{\phi_0^2}\right)\right]\delta^{(d)}(\mathbf{x}-\mathbf{y}) + R_k(\mathbf{x}-\mathbf{y}) \tag{5.23}$$

and is no longer diagonalizable in Fourier space due to the nonuniform spatial dependence of $\phi_{*k}(x)$. It is nonetheless convenient to perform the Fourier transform on the transverse coordinates $\mathbf{x}_\perp$, which after inserting the first terms of the expansion of the saddle-point solution when $L \to \infty$ and $k \to 0$, leads to

$$\begin{aligned}\Gamma^{(2)}_{k,\mathbf{q}_\perp x,\mathbf{p}_\perp y}(\varphi) =& \delta(\mathbf{q}_\perp + \mathbf{p}_\perp)\Bigg(\Big[-\partial_x^2 + \mathbf{q}_\perp^2 - \frac{2}{\xi^2} + \frac{6}{\xi^2}\tanh^2\Big(\frac{x-a_k}{\xi}\Big)\Big]\delta(x-y) \\ &+ k^2\left[12\tanh\left(\frac{x-a_k}{\xi}\right)f_1\left(\frac{x}{\xi}\right)\delta(x-y) + kr\left(\frac{\mathbf{q}_\perp^2}{k^2}, k(x-y)\right)\right] + \cdots\Bigg),\end{aligned} \tag{5.24}$$

where $a_k(\varphi/\phi_0)$ and $f_1(x/\xi)$ are defined in Section 2. For the Gaussian regulator already introduced, $r(\mathbf{q}_\perp^2/k^2, k(x-y)) = \alpha \exp(-\mathbf{q}_\perp^2/(2k^2)) \exp(-k^2(x-y)^2/2)/\sqrt{2\pi}$. We rewrite

the above expression as

$$\Gamma^{(2)}_{k,\mathbf{q}_\perp x,\mathbf{p}_\perp y}(\varphi) = \delta(\mathbf{q}_\perp + \mathbf{p}_\perp)(M^{[0]}_{k;xy}(\mathbf{q}_\perp^2) + k^2 M^{[1]}_{k;xy}(\mathbf{q}_\perp^2) + \cdots), \tag{5.25}$$

where the operators $M^{[0]}_k(\mathbf{q}_\perp^2)$ and $M^{[1]}_k(\mathbf{q}_\perp^2)$ are defined by

$$\begin{aligned} M^{[0]}_{k;xy}(\mathbf{q}_\perp^2) &= \left[-\partial_x^2 + \mathbf{q}_\perp^2 + \alpha k^2 \exp\left(-\frac{\mathbf{q}_\perp^2}{2k^2}\right) - \frac{2}{\xi^2} + \frac{6}{\xi^2}\tanh^2\left(\frac{x-a_k}{\xi}\right)\right]\delta(x-y), \\ M^{[1]}_{k;xy}(\mathbf{q}_\perp^2) &= 12\tanh\left(\frac{x-a_k}{\xi}\right) f_1\left(\frac{x}{\xi}\right)\delta(x-y) + \\ &\quad + k\alpha \exp\left(-\frac{\mathbf{q}_\perp^2}{2k^2}\right)\left[\frac{\exp(-k^2(x-y)^2/2)}{\sqrt{2\pi}} - \delta(k(x-y))\right]. \end{aligned} \tag{5.26}$$

The stability of the saddle point is governed by the sign of the determinant of the Hessian operator and the 1-loop correction to the effective average potential is given by the logarithm of the determinant, or equivalently by the trace of the log of the Hessian, more precisely by

$$U_k^{1-\text{loop}}(\varphi) = \frac{1}{2L^d}\ln\det\Gamma^{(2)}_k(\varphi) = \frac{1}{2L}\int\frac{d^{d-1}q_\perp}{(2\pi)^{d-1}}\,\mathrm{Tr}\ln\left(M^{[0]}_k(\mathbf{q}_\perp^2;\varphi) + k^2 M^{[1]}_k(\mathbf{q}_\perp^2;\varphi) + \cdots\right). \tag{5.27}$$

If $M^{[0]}$ is invertible and $k \to 0$, one can rewrite the above expression as

$$\frac{1}{2L}\int\frac{d^{d-1}q_\perp}{(2\pi)^{d-1}}\Big(\mathrm{Tr}\ln M^{[0]}_k(\mathbf{q}_\perp^2;\varphi) + k^2\,\mathrm{Tr}\Big[M^{[0]}_k(\mathbf{q}_\perp^2;\varphi)^{-1}M^{[1]}_k(\mathbf{q}_\perp^2;\varphi)\Big] + \mathcal{O}(k^4)\Big) \tag{5.28}$$

where there is still some k dependence in the operators.

We are still working on the full calculation of the above expression when $L \to \infty$ and $k \to 0$, but we already have some preliminary results concerning the first contribution that only involves $M^{[0]}_k$. This operator indeed appears in the instanton literature, and the eigenfunctions and eigenvalues of the associated Schrödinger equation are exactly known [84, 138]: there are two discrete eigenvalues, $\mathbf{q}_\perp^2 + \alpha k^2\exp\left(-\mathbf{q}_\perp^2/(2k^2)\right)$ and $\mathbf{q}_\perp^2 + \alpha k^2\exp\left(-\mathbf{q}_\perp^2/(2k^2)\right) + 3/\xi^2$ and a continuum of eigenvalues indexed by a momentum q. The first discrete eigenvalue corresponds to a translation mode associated with the freedom to move the location of the kink. In the present problem where the location of the kink is fixed by Eq. (5.11) this mode cannot contribute to the spectrum of $M^{[0]}_k$. The second mode does contribute and gives a term in $(J_0 + J_1 k^{d+1})/L$. Finally, the contribution due to the continuum of eigenvalues is more conveniently calculated by considering the ratio of two operators, $M^{[0]}_k$ and the related φ-independent operator $[-\partial_x^2 + \mathbf{q}_\perp^2 + \alpha k^2\exp(-\mathbf{q}_\perp^2/(2k^2)) + 4/\xi^2]\delta(x-y)$ which is simply obtained by replacing the hyperbolic tangent by 1 (the associated contribution to the effective potential goes into the term $V(k)$ in Eq. (5.1) and is thus inessential). We are therefore interested in

$$\int\frac{d^{d-1}q_\perp}{(2\pi)^{d-1}}\ln\det\left[\frac{-\partial_x^2 + \mathbf{q}_\perp^2 + \alpha k^2\exp\left(-\frac{\mathbf{q}_\perp^2}{2k^2}\right) - \frac{2}{\xi^2} + \frac{6}{\xi^2}\tanh^2\left(\frac{x-a_k}{\xi}\right)}{-\partial_x^2 + \mathbf{q}_\perp^2 + \alpha k^2\exp\left(-\frac{\mathbf{q}_\perp^2}{2k^2}\right) + 4/\xi^2}\right] = \frac{J_0 + J_1 k^{d+1}}{L} + I_k, \tag{5.29}$$

where I_k only involves the continuum of eigenvalues in $M_k^{[0]}$ and the first term is due to the discrete mode. We consider the inner region of the effective potential where $|\varphi|$ is sufficient less than ϕ_0 so that $(L/2) \pm a_k(\varphi) \sim (1 \pm (\varphi/\phi_0))L/2 \sim L/2$. From [139], one knows the determinant of the ratio that appears in I_k in a closed form, which leads to

$$I_k = \int \frac{d^{d-1}q_\perp}{(2\pi)^{d-1}} \ln\left[\frac{(\sqrt{\cdots}-2)(\sqrt{\cdots}-1)}{(\sqrt{\cdots}+2)(\sqrt{\cdots}+1)}\right], \quad \sqrt{\cdots} = \sqrt{\xi^2\mathbf{q}_\perp^2 + \alpha\xi^2k^2\exp\left(-\frac{\mathbf{q}_\perp^2}{2k^2}\right)+4}. \tag{5.30}$$

An advantage of the above expression is that thanks to the ratio of operators one can take the UV cutoff to ∞ when $d < 2$ in the integral over $\mathbf{q}_\perp$, which can then be rewritten as

$$I_k = 2v_{d-1}\int_0^\infty dy\, y^{\frac{d-3}{2}} \ln\left[\frac{(\sqrt{\cdots}-2)(\sqrt{\cdots}-1)}{(\sqrt{\cdots}+2)(\sqrt{\cdots}+1)}\right], \quad \sqrt{\cdots} = \sqrt{\xi^2 y + \alpha\xi^2k^2\exp\left(-\frac{y}{2k^2}\right)+4}, \tag{5.31}$$

where $v_{d-1}^{-1} = 2^d\pi^{(d-1)/2}\Gamma((d-1)/2)$. Even when $k = 0$ the integrand in Eq. (5.31) is integrable when $y \to \infty$ (for $d < 2$) and $y \to 0$ (for $d > 1$), and one finds that

$$I_k = I_0 + I_1 k^{d-1} \tag{5.32}$$

where subdominant terms when $k \to 0$ are neglected. The term I_0 combines with J_0 to give the 1-loop correction to the surface tension in the ordered phase when $k = 0$. It is the counterpart of the calculation performed by Brezin and Feng near the critical point [139].

In the limit considered in the FRG where $L \to \infty$ before $k \to 0$, one can see that the first contribution to the 1-loop scale-dependent effective potential, involving the trace of the logarithm of $M_k^{[0]}$, is zero in the thermodynamic limit because it is multiplied by $1/L$. A nonvanishing contribution to the k^2 term is expected from the second contribution involving the trace of $(M_k^{[0]})^{-1}M_k^{[1]}$. It is however more difficult to handle and its calculation is still in progress.

5 Conclusion

We have obtained preliminary results concerning the scale-dependent effective action, the central quantity of the FRG, in the ordered phase of the ϕ^4 theory when $d > 1$. In this case the field configurations that control the thermodynamics and the associated phase coexistence are nonuniform domain-wall configurations. What is specific here compared to the critical point of the same model in $d = 1+\epsilon$ and the behavior at the lower critical dimension in $d = 1$ is that the excitations are still extended (although only in $\epsilon = d-1$ dimensions) so that their cost prevents them from proliferating, contrary to droplets near the critical point [12–14] in $d = 1+\epsilon$ or instantons in $d = 1$ [84, 109]. We have found that the excess free-energy of the domain wall associated with the surface tension does not appear in the expression of the scale-dependent effective potential, Eq. (5.1) or Eq. (5.20), because the latter is considered in the thermodynamic limit. The presence of the domain wall is nonetheless necessary to produce the specific form in $k^2\varphi^2$ that describes the return to convexity when $k \to 0$.

There are several aspects that have yet to be completed. First, we have to finish the 1-loop calculation to check if the nonvanishing contribution in the thermodynamic limit is proportional to k^2 as it naively appears or if the dependence on k is modified to a smaller power law, especially when $d < 2$. Second, we want to address if and how the lower truncations of the derivative expansion (LPA, LPA', second-order ∂_2) are able to reproduce the predicted behavior of the scale-dependent effective action. As already mentioned, this has been shown for a large class of IR regulators for $d > 2$. Yet, we are mostly interested here by $d < 2$ and more specifically by the vicinity of the lower critical dimension.

Chapter 6

Conclusions and perspectives

In this thesis we have presented a functional renormalization group (FRG) description of the approach to the lower critical dimension d_{lc} in the scalar ϕ^4 theory at criticality. We have explored this in the two lowest truncations of the (nonpertubative) derivative expansion approximation scheme of FRG. These are the minimally modified Local Potential Approximation (LPA', Chapter 2) and the second order of the derivative expansion (∂_2, Chapter 3). The motivation for the work was to test how this generic approximation scheme, which has proven to be accurate in dimensions $d \geqslant 2$ [16], is able to describe dimensions close to the lower critical dimension in a system with discrete symmetry. This is interesting because it is known that the long-distance physics is in this case controlled by the proliferation of localized, strongly nonuniform fluctuations. On the other hand, the derivative expansion by construction describes well the smooth, long-wavelength fluctuations around uniform configurations of the coarse-grained order-parameter field [15, 16]. It is not clear when and how the effects of strongly nonuniform fluctuations are captured by this approximation scheme. This is why we benchmark it on the case of the scalar ϕ^4 theory, where the mechanism of the transition and of its disappearance as one approaches the lower critical dimension is known. The strongly nonuniform configurations of relevance are droplets (enclosed domain walls) that become point-like kinks and anti-kinks at the lower critical dimension $d_{lc} = 1$ [12–14], where they proliferate. We stress that our goal is not to provide yet another theoretical description of the approach to the lower critical dimension for systems in the universality class of the Ising model, a question which has been quite well understood for several decades. It is to benchmark a generic nonperturbative but approximate FRG approach to later tackle problems that are still open and where strongly nonuniform configurations presumably play an important role such as the low-temperature phase of the Ising spin glasses [140] or the lower critical dimension of the athermally driven random-field Ising model (RFIM). The lower critical dimension of the RFIM in equilibrium has been rigorously shown to be $d_{lc} = 2$ [94, 95], but that for the far-from-equilibrium driven RFIM is still debated [100, 141, 142].

At the level of the LPA', we find that the limit of the fixed-point effective action is nonuniform in the (average) field when approaching the lower critical dimension, with the emergence of a boundary layer around the minimum of the dimensionless potential. The effective potential becomes singular. We use Singular perturbation Theory (SPT) [125–128] to investigate the leading-order fixed-point solution. From matching conditions between

different SPT regions, we analytically recover that the propagator develops a singularity at $\varphi = 0$, as one would expect from the merging of the critical and zero-temperature fixed points. This pushes the location of the minimum of the effective potential φ_{min} to diverge. We have found it to scale as $\sqrt{\ln(1/\tilde{\epsilon})}$, where $\tilde{\epsilon} = (d-2+\eta)/[2(2-\eta)]$ is proportional to the scaling dimension D_φ of the average field and vanishes in the $d \to d_{lc}$ limit ($\tilde{\epsilon} \to 0^+$). This scaling of φ_{min} is at odds with the outcome of an earlier FRG study [122]. We find the width of the boundary layer to vanish like $\delta(\tilde{\epsilon}) \propto \tilde{\epsilon}\sqrt{\ln(1/\tilde{\epsilon})} \to 0^+$. From the matching conditions we have also analytically found the dependence of the d_{lc} value on the regulator function (and its prefactor α). At the level of the LPA', the $d_{lc}(\alpha)$ curves do not have an extremum, preventing the use of PMS optimization to better pinpoint the value of d_{lc}.

We have studied whether the description of the approach to the lower critical dimension d_{lc} improves as one considers higher orders of the derivative expansion. The next step is the ∂_2, where one considers coupled flow equations for two functions, the effective potential and the field renormalization function. Work is now in progress to analytically solve the fixed-point equation via SPT along the lines of the LPA' calculation. However, the existence of two coupled differential equations make the problem much more difficult. As a result we have not been able so far to satisfy matching conditions between all the regions. We believe this matching would give us the scaling of $z(\varphi)$ in the boundary layer and the (regulator-dependent) value of d_{lc}. We have included preliminary results at the ∂_2 level, mostly relying on numerical calculations for $d > d_{lc}$. From the divergence of $u''(\varphi_{min})$ found there to be congruent with LPA' results, one expects the same mechanism of a nonuniform convergence to the lower critical dimension limit with the emergence of a boundary layer around the minimum of the dimensionless potential. The numerical results for $d > d_{lc}$ are compatible with φ_{min} scaling similarly as in LPA'. Based on a boundary layer solution, with an ansatz that $z(\varphi)$ diverges in the boundary layer (but subdominantly to $u''(\varphi)$), we have given a tentative argument supporting this result and showing that the propagator again develops a singularity. Using extrapolations of $\tilde{\epsilon}(d)$ curves to the $\tilde{\epsilon} \to 0^+$ limit, we have seen the possible appearance of an extremum in $d_{lc}(\alpha)$, opening the prospect for PMS optimization. We have also found that not all regulators produce numerical $\tilde{\epsilon}(d)$ curves that seem to have a propper $\tilde{\epsilon} \to 0^+$ limit.

Concerning other expectations that come from the merging of the critical fixed point and the zero-temperature fixed point associated with the ordered phase, at both LPA' and ∂_2 levels, we have found that the critical temperature T_c appropriately vanishes in the $d \to d_{lc}$ limit (Chapter 4). The way T_c behaves in $\tilde{\epsilon}$ or equivalently in the field dimension D_φ is found to be in agreement with the $d = 1 + \epsilon$ result of the droplet theory [12–14], and was missed by an earlier FRG study [122]. Regarding the expected marginality of the $-1/\nu$ eigenvalue, no analytical results have been found at either LPA' or ∂_2 level, but the numerical results for $d > d_{lc}$ given in Chapter 4 are compatible (yet not conclusive) with $-1/\nu \to 0$ at both levels. The ∂_2 results (compared to LPA') appear more in line with the form of divergence of the correlation length exponent ν predicted by the droplet theory [12–14]. Confirming or refuting that the truncated derivative expansion of the FRG appropriately captures the marginality of $-1/\nu$ is an important future goal, as it also relates to the essential scaling (exponential instead of power-law) of the correlation length ξ that is expected at the lower critical dimension (from, e.g., exact $1d$ Ising results, [60, 61]). The critical exponent ν diverging is a necessary but not sufficient condition for the exponential scaling of ξ with

the temperature distance from the transition. As marginal eigenvalues are accompanied by logarithmic corrections to scaling [17, 44] which might translate to this exponential behavior of ξ, it is possible marginality of $-1/\nu$ might nonetheless be a sufficient condition, which is something we aim to explore in the future.

The conclusion that can be drawn at this point is that low orders of the derivative expansion within the FRG appear to at least partially capture the effect of strongly nonuniform configurations in the form of droplets that control the critical behavior of pure Ising-like models when approaching the lower critical dimension ($d_{lc} = 1$ in the exact treatment). This takes place through the mathematical mechanism of a boundary layer in the fixed-point functions and is described within SPT. It remains to be seen in more detail if the proliferation of localized excitations (point-like droplets) that destroy the transition in d_{lc} and lead to essential scaling can be indirectly described by the approximations based upon expanding around uniform coarse-grained configurations.

In Chapter 5 we consider another problem where strongly nonuniform configurations of the field are important, the ordered phase of the scalar ϕ^4 theory. The return to convexity under the influence of spatial fluctuations requires taking into account the domain-wall configurations. We are interested in the way one can keep track of such configurations within the FRG. A calculation in the presence of an IR regulator was done by Ringwald and Wetterich in the case of the $\mathcal{O}(N \geq 3)$ model[67], but the study of the $N = 1$ case had never been undertaken. Another motivation is to investigate how the ordered fixed point behaves in the limit $d = 1 + \epsilon$ with $\epsilon \to 0$ because one knows that it should then merge with the critical fixed point that we have studied earlier. We find that the presence of the domain wall is necessary to produce a specific dependence in $k^2\varphi^2$ for the scale-dependent effective potential that describes the return to convexity when the IR cutoff $k \to 0$. We aim to finish the 1-loop calculation to check how its contribution scales with k in $d < 2$. This calculation is the necessary step to then assess if and how the lower truncations of the derivative expansion (LPA, LPA', second-order ∂^2) are able to reproduce the predicted behavior of the scale-dependent effective action, especially in the vicinity of the lower critical dimension.

Some points we have learned through this research about the d_{lc} limit and which we want to stress are as follows. The $d \to d_{lc}$ limit is marked by the dimensionful field not rescaling with the IR cutoff scale k, so that its scaling dimension $\propto \tilde{\epsilon}$ must vanish. The limit for the fixed-point functions is nonuniform in the field, i.e., the solutions to the $\tilde{\epsilon} = 0$ equations are not physical leading-order solutions and SPT must be used to construct proper ones. We stress that the value of the lower critical dimension should be calculated in a numerical FRG scheme from the $\tilde{\epsilon} \to 0^+$ condition (using some regulator optimization procedure). Inversely, if one works at a fixed spatial dimension that one anticipates to be the lower critical dimension (e.g., $d = 1$), care must be taken so that the $\tilde{\epsilon} \to 0^+$ condition is respected. As we have seen in the present work, depending on the choice of IR regulator, $d = 1$ may actually be above or below the lower critical dimension of the approximate FRG theory. This might thus involve regulator optimization. The idea to optimize a regulator so that the phase transition is not present in d_{lc} was proposed in [110]. The authors, though, needed to know a priori not only the value of d_{lc} but also some measure of distance in parameter space between fixed points that were to merge and disappear along with the transition (in [110] this was exemplified on the $1d$ sine-Gordon model). This severely limits the applicability of the methods to systems about which a lot is already known, and we wish to investigate systems whose theoretical

description is far from complete. Also, the method did not find an optimization for which the transition actually disappears, and the improvements were minimal. We are interested in whether the simpler $\tilde{\epsilon} \to 0^+$ condition can be implemented instead. This is a point we intend to investigate in subsequent research, as we have not yet found such regulator optimization in existing relevant systems, e.g., $1d$ barrier-penetrating problems [109, 135, 143–145].

Appendix A

Threshold functions - definitions and limits

Threshold functions contain the momentum integrals in the nontrivial parts of FRG flow equations in the derivative expansion scheme.

In this section expressions and properties of the threshold functions $\ell_{n,0}^{(d)}(\varphi;\eta)$ and $m_{n,0}^{(d)}(\varphi;\eta)$ will be given. Some of these can be found in the main text, but we restate them here for completeness.

We drop the index k from renormalization group functions, the anomalous dimension and the $\tilde{\epsilon}$-parameter to make the expressions clearer.

1 Definitions

$$\ell_{n\geqslant 0}^{(d)}(u(\varphi),z\left(\varphi\right);\eta)=-\frac{1}{2}\int_{0}^{+\infty}dyy^{d/2-1}\tilde{\partial}_{y}\begin{Bmatrix}g^{n}(y,\varphi), & n>0\\ \ln\left(g(y,\varphi)\right), & n=0\end{Bmatrix}, \tag{A.1}$$

$$m_{n,0}^{(d)}(u(\varphi),z\left(\varphi\right);\eta)=-\frac{1}{2}\int_{0}^{+\infty}dyy^{d/2}\tilde{\partial}_{y}\Big\{\left(\partial_{y}g(y,\varphi)\right)^{2}\left(g(y,\varphi)\right)^{n-4}\Big\}. \tag{A.2}$$

Here $g(y,\varphi)$ is the dimensionless propagator (not to be mistaken for the boundary layer function $g(x)=\delta\left(\tilde{\epsilon}\right)u''\left(\varphi\right)$) and the derivation operator $\tilde{\partial}_{y}$ marked by a tilde only acts on the dimensionless regulator $r(y)$, such that:

$$\tilde{\partial}_{y}r\left(y\right)=-\big(\eta_{k}r\left(y\right)+2yr'\left(y\right)\big). \tag{A.3}$$

This is because $\tilde{\partial}_{y}$ comes from the flow of the dimensionful regulator, $\partial_{t}R_{k}(\mathbf{q}^{2})$, and applies to dimensionless quantities. The threshold functions are defined with a minus sign, so that they would be overall positive.

2 Explicit expressions

We give the ∂_2 expressions as the LPA' ones are readily available from them by putting $z(\varphi) = 1$:

$$\ell^{(d)}_{n\geqslant 0}(u(\varphi), z(\varphi); \eta) = -\frac{1}{2}(n + \delta_{n,0}) \int_0^{+\infty} dy y^{d/2} (\eta r(y) + 2y r'(y)) (g(y, \varphi))^{n+1}, \tag{A.4}$$

$$\begin{aligned} m^{(d)}_{n,0}(u(\varphi), z(\varphi); \eta) = -\frac{1}{2} \int_0^{+\infty} dy y^{d/2} (z(\varphi) + r(y) + y r'(y)) (g(y, \varphi))^n \times \\ \times \Big\{ n y (z(\varphi) + r(y) + y r'(y)) (\eta r(y) + 2y r'(y)) g(y, \varphi) + \\ - 2\Big[\eta r(y) + y(\eta + 4) r(y) + 2y^2 r''(y)\Big]\Big\}, \end{aligned} \tag{A.5}$$

and the propagator (not to be mistaken for the boundary layer function $g(x) = \delta(\tilde{\epsilon})\, u''(\varphi)$) is given by:

$$g(y, \varphi) = \frac{1}{u''(\varphi) + y(z(\varphi) + r(y))}. \tag{A.6}$$

3 Limits in the boundary layer

Although explicitly derived for the boundary layer, the expression for $\ell^{(d)}_{n,0}(\varphi; \eta)$ derived in this section can be used any time $u''(\varphi)$ diverges, remembering to return $g(x) = \delta(\tilde{\epsilon})\, u''(\varphi)$ outside of the boundary layer.

3.1 At LPA'

The second derivative $u''(\varphi) = g(x)/\delta(\tilde{\epsilon})$ diverges as $1/\delta(\tilde{\epsilon})$, so the threshold functions in this limit must vanish as powers of $\delta(\tilde{\epsilon})$:

$$\begin{aligned} &\ell^{(d)}_{n\geqslant 0}(u(\varphi), 1; \eta) = -\frac{1}{2}(n + \delta_{n,0}) \int_0^{+\infty} dy y^{d/2} \frac{(\eta r(y) + 2y r'(y))}{(u''(\varphi) + y(1 + r(y)))^{n+1}} = \\ &= -\frac{1}{2}(n + \delta_{n,0}) \left(\frac{\delta(\tilde{\epsilon})}{g(x)}\right)^{n+1} \int_0^{+\infty} dy y^{d/2} (\eta r(y) + 2y r'(y)) + \mathcal{O}\Big((\delta(\tilde{\epsilon}))^{n+2}\Big) = \\ &= (\delta(\tilde{\epsilon}))^{n+1}\, L^{(d)}_n(g(x)) + \mathcal{O}\Big((\delta(\tilde{\epsilon}))^{n+2}\Big), \qquad L^{(d)}_n(g(x)) = \mathcal{O}(1). \end{aligned} \tag{A.7}$$

We integrate the $r'(y)$ by part and introduce the shorthand $A^{(d)}(\eta)$:

$$\begin{aligned} A^{(d)}(\eta) &= -\frac{1}{2} \int_0^{+\infty} dy y^{d/2} \left(\eta \left[\frac{r(y)}{\alpha}\right] + 2y \left[\frac{r'(y)}{\alpha}\right]\right) = \\ &= \left(\frac{d + 2 - \eta}{2}\right) \int_0^{+\infty} dy y^{d/2} \left[\frac{r(y)}{\alpha}\right]. \end{aligned} \tag{A.8}$$

Using this in the expression Eq. (A.7) for $\ell^{(d)}_{n\geqslant 0}(\varphi; \eta)$, we get:

$$L^{(d)}_n(g(x)) = (n + \delta_{n,0}) \frac{\alpha A^{(d)}(\eta)}{(g(x))^{n+1}}. \tag{A.9}$$

The threshold function $m_{n,0}^{(d)}(\varphi;\eta)$ is given by

$$\begin{aligned}
m_{n,0}^{(d)}(u(\varphi),1;\eta) &= -\frac{1}{2}\int_0^{+\infty} dy y^{d/2}\frac{1+r\left(y\right)+yr'\left(y\right)}{\left(u''\left(\varphi\right)+y(1+r\left(y\right))\right)^n}\times \\
&\quad\times\left\{ny(1+r\left(y\right)+yr'\left(y\right))\frac{(\eta r(y)+2yr'(y))}{u''\left(\varphi\right)+y(1+r\left(y\right))}+\right. \\
&\quad\left.-2\Big[\eta r\left(y\right)+y(\eta+4)r\left(y\right)+2y^2r''\left(y\right)\Big]\right\}= \\
&=\frac{1}{2}\left(\frac{\delta\left(\tilde{\epsilon}\right)}{g\left(x\right)}\right)^n\int_0^{+\infty} dy y^{d/2}\Big\{\alpha(d+2-\eta)\left[\frac{yr(y)}{\alpha}\right]'+ \\
&\quad-\alpha^2(d+2-2\eta)\left[\left(\frac{yr(y)}{\alpha}\right)'\right]^2\Big\}+\mathcal{O}\Big(\left(\delta\left(\tilde{\epsilon}\right)\right)^{n+1}\Big)= \\
&=\left(\delta\left(\tilde{\epsilon}\right)\right)^n\ M_n^{(d)}(g\left(x\right))+\mathcal{O}\Big(\left(\delta\left(\tilde{\epsilon}\right)\right)^{n+2}\Big),\qquad M_n^{(d)}(g\left(x\right))=\mathcal{O}(1).
\end{aligned} \tag{A.10}$$

We integrate the $r'\left(y\right)$ by part to use $A^{(d)}(\eta)$ (same as Eq. (A.8)), and introduce the shorthand $B^{(d)}(\eta)$:

$$B^{(d)}(\eta)=\left(\frac{d+2-2\eta}{2}\right)\int_0^{+\infty} dy y^{d/2}\left[\left(\frac{yr(y)}{\alpha}\right)'\right]^2. \tag{A.11}$$

Using this in the expression Eq. (A.10) for $m_{n\geqslant 0}^{(d)}$, we get:

$$M_n^{(d)}(g\left(x\right))=\frac{\alpha d A^{(d)}(\eta)-\alpha^2 B^{(d)}(\eta)}{\left(g\left(x\right)\right)^n}. \tag{A.12}$$

3.2 At ∂_2

We offer here general shapes of the threshold functions for all five conceivable regimes in the $x=\mathcal{O}(1)$ region for the behavior of $\kappa\left(\tilde{\epsilon}\right)$, which is defined as:

$$z\left(\varphi\right)=\frac{\kappa\left(\tilde{\epsilon}\right)}{\delta\left(\tilde{\epsilon}\right)}\zeta(x),\quad \text{where for}\quad x=\mathcal{O}(1)\quad \text{we have}\quad \zeta(x)=\mathcal{O}(1). \tag{A.13}$$

The scaling of the threshold functions is:

1. $z\left(\varphi\right)\to 0\quad\Longleftrightarrow\quad\kappa\left(\tilde{\epsilon}\right)\ll\delta\left(\tilde{\epsilon}\right)\to 0$:

$$\begin{aligned}
\ell_n^{(d)}(u''\left(\varphi\right),z\left(\varphi\right);\eta)&=\left(\delta\left(\tilde{\epsilon}\right)\right)^{n+1}L_1(g\left(x\right);n,d),\\
m_{n,0}^{(d)}(u''\left(\varphi\right),z\left(\varphi\right);\eta)&=\left(\delta\left(\tilde{\epsilon}\right)\right)^{n}M_1(g\left(x\right);n,d).
\end{aligned} \tag{A.14}$$

2. $z\left(\varphi\right)=\mathcal{O}(1)\quad\Longleftrightarrow\quad\kappa\left(\tilde{\epsilon}\right)=\delta\left(\tilde{\epsilon}\right)\to 0$:

$$\begin{aligned}
\ell_n^{(d)}(u''\left(\varphi\right),z\left(\varphi\right);\eta)&=\left(\delta\left(\tilde{\epsilon}\right)\right)^{n+1}L_2(g\left(x\right);n,d),\\
m_{n,0}^{(d)}(u''\left(\varphi\right),z\left(\varphi\right);\eta)&=\left(\delta\left(\tilde{\epsilon}\right)\right)^{n}M_2(g\left(x\right),\zeta\left(x\right);n,d).
\end{aligned} \tag{A.15}$$

3. $u''(\varphi) \gg z(\varphi) \to +\infty \quad \Longleftrightarrow \quad \delta(\tilde{\epsilon}) \ll \kappa(\tilde{\epsilon}) \to 0$:

$$\begin{aligned} \ell_n^{(d)}(u''(\varphi), z(\varphi); \eta) &= (\delta(\tilde{\epsilon}))^{n+1} L_3(g(x); n, d), \\ m_{n,0}^{(d)}(u''(\varphi), z(\varphi); \eta) &= \kappa(\tilde{\epsilon}) (\delta(\tilde{\epsilon}))^{n-1} M_3(g(x), \zeta(x); n, d). \end{aligned} \tag{A.16}$$

4. $z(\varphi) = \mathcal{O}(u''(\varphi)) \to +\infty \quad \Longleftrightarrow \quad \kappa(\tilde{\epsilon}) = 1$:

$$\begin{aligned} \ell_n^{(d)}(u''(\varphi), z(\varphi); \eta) &= (\delta(\tilde{\epsilon}))^{n+1} L_4(g(x), \zeta(x); n, d), \\ m_{n,0}^{(d)}(u''(\varphi), z(\varphi); \eta) &= (\delta(\tilde{\epsilon}))^{n-1} M_4(g(x), \zeta(x); n, d). \end{aligned} \tag{A.17}$$

5. $u''(\varphi) \ll z(\varphi) \to +\infty \quad \Longleftrightarrow \quad \kappa(\tilde{\epsilon}) = 1$:

$$\begin{aligned} \ell_n^{(d)}(u''(\varphi), z(\varphi); \eta) &= \left(\frac{\delta(\tilde{\epsilon})}{\kappa(\tilde{\epsilon})}\right)^{n+1} L_5(\zeta(x); n, d), \\ m_{n,0}^{(d)}(u''(\varphi), z(\varphi); \eta) &= \left(\frac{\delta(\tilde{\epsilon})}{\kappa(\tilde{\epsilon})}\right)^{n-1} M_5(\zeta(x); n, d). \end{aligned} \tag{A.18}$$

We call to attention that not all of the L_i and M_i functions depend on $\zeta(x)$, and some are in turn not dependent on $g(x)$.

3.2.1 Expressions for the threshold functions

In the relevant regime of $\delta(\tilde{\epsilon}) \ll \kappa(\tilde{\epsilon}) \to 0$, the threshold function $\ell_{n,0}^{(d)}(\varphi; \eta)$ is given by the same expression as for the LPA' case (see Eq. (A.7)), as the propagator again simplifies in the same way.

The expression for $m_{n,0}^{(d)}(\varphi; \eta)$ which has terms linear in $z(\varphi)$ is, however, different:

$$\begin{aligned} &m_{n,0}^{(d)}(u(\varphi), 1; \eta) = Eq.\ (A.5) = \\ &= \kappa(\tilde{\epsilon}) (\delta(\tilde{\epsilon}))^{n-1} M_n^{(d)}(g(x), \zeta(x)) + \mathcal{O}\Big(\max\Big\{(\delta(\tilde{\epsilon}))^n, (\kappa(\tilde{\epsilon}))^2 (\delta(\tilde{\epsilon}))^{n-1}\Big\}\Big), \\ &M_n^{(d)}(g(x)) = \mathcal{O}(1), \end{aligned} \tag{A.19}$$

with the function $M_n^{(d)}(g(x))$ given by

$$M_n^{(d)}(g(x), \zeta(x)) = \zeta(x) \frac{\alpha d A^{(d)}(\eta)}{(g(x))^n}, \quad \text{with} \quad A^{(d)}(\eta) \quad \text{defined in Eq. (A.8), as in LPA'.} \tag{A.20}$$

Appendix B

Canonical field

1 Boundary layer symmetry

If we are were to redefine the $\delta(\tilde{\epsilon})$ scale to $a\delta(\tilde{\epsilon})$, where a is of $\mathcal{O}(1)$, the new boundary layer function $g_{\text{new}}(x_{\text{new}})$ would now simply be $g(x/a)/a$ in terms of the old quantities, and the boundary layer equation for $g_{\text{new}}(x_{\text{new}})$ would be the same as Eq. (2.39). This happens because in the boundary layer we have only kept the lowest order in $\delta(\tilde{\epsilon})$, so all of the terms of course scale with the same multiple of $\delta(\tilde{\epsilon})$. In ∂_2 this is supplemented by the following symmetry in $\zeta(x)$:

$$\zeta(x) \to b\zeta\left(\frac{x}{a}\right), \tag{B.1}$$

where b is an $\mathcal{O}(1)$ scale. This scale is otherwise arbitrary, as the boundary-layer fixed-point Eq. (3.13) for the field renormalization function is linear in $\zeta(x)$. This is also true only for the regime where $z(\varphi)$ diverges subdominantly to $u''(\varphi)$ in the boundary layer. This is obviously not the case for the full equations, i.e. rescaling φ and $u''(\varphi)$ in the analogous manner would leave residual a's in the flow equation. It sounds trivial, but it also hangs on our choice to identify $\delta_u(\tilde{\epsilon})$ and $\delta_x(\tilde{\epsilon})$ in Section 3.1. While SPT tells us that these two scales must be of the same order, to put the proportionality constant between them to 1 was a choice, allowed by the fact that any other $\mathcal{O}(1)$ constant can be absorbed in the definition of the boundary layer field x (or the function $g(x)$). One of the takeaways from this is that we have not yet used the freedom in rescaling of x to simplify the boundary layer equations as much as we can, and we do this by introducing a canonical field. We call it so because equations are often termed *canonical* when they are cast in their simplest form.

2 Canonical equations

If we define a *canonical field* as

$$\varphi_c = \frac{\varphi}{\sqrt{\frac{2\alpha v_d A^{(d)}(\eta)}{(2-\eta)}}}, \tag{B.2}$$

this then reflects in the boundary layer field x:

$$x = \frac{\varphi - \varphi_{min}}{\delta\left(\tilde{\epsilon}\right)} \quad \Longrightarrow \quad x_c = \frac{\varphi_c - \varphi_{c,min}}{\delta\left(\tilde{\epsilon}\right)} = \frac{x}{\sqrt{\frac{2\alpha v_d A^{(d)}(\eta)}{(2-\eta)}}}. \tag{B.3}$$

We then call this the *canonical boundary layer field*. Correspondingly, we term any functions of the canonical field *canonical functions*.

The use of canonical variables and functions consequently simplifies the boundary-layer fixed-point equations:

$$0 = g\left(x\right) - \frac{g'(0)g'\left(x\right)}{\left(g(0)\right)^3} - 2\frac{\left(g'\left(x\right)\right)^2}{\left(g\left(x\right)\right)^3} + \frac{g''\left(x\right)}{\left(g\left(x\right)\right)^2}, \tag{B.4}$$

$$0 = \eta\zeta\left(x\right) - (2-\eta)\left[2\frac{\left(g'\left(x\right)\right)^2}{\left(g\left(x\right)\right)^4}\zeta\left(x\right) - \left(\frac{g'(0)}{\left(g(0)\right)^3} + \frac{4g'\left(x\right)}{\left(g\left(x\right)\right)^3}\right)\zeta'\left(x\right) + \frac{1}{\left(g\left(x\right)\right)^2}\zeta''\left(x\right)\right], \tag{B.5}$$

where we omit the index c of the canonical boundary layer field x_c and we reuse the existing pool of shorthands with $g_c(x_c) \to g\left(x\right)$, $\zeta_c(x_c) \to \zeta\left(x\right)$ for the canonical functions $g_c(x_c) := g(x_c)$ and $\zeta_c(x_c) := \zeta(x_c)$, to avoid cluttering the notation.

Appendix C

Concerning the location of the minimum of the effective potential

In this appendix we list some results and calculation steps that are needed to show the behavior of the location of the minimum of the effective potential φ_{min}.

1 Fixed-point expression for φ_{min}

This expression is obtained from the fixed point equation for the first derivative of the effective potential:

$$\begin{aligned} 0 &= \partial_t u'(\varphi) = \\ &= -\frac{1}{2}(d+2-\eta)u'(\varphi) - (2-\eta)\,\tilde{\epsilon}\,\varphi u''(\varphi) - 2v_d \ell_1^{(d)}\left(u''(\varphi), z(\varphi); \eta\right)\left(z'(\varphi) + u'''(\varphi)\right), \end{aligned} \tag{C.1}$$

by evaluating it in $\varphi = \varphi_{min}$ and using $u'(\varphi_{min}) = 0$.

As in $\varphi = \varphi_{min}$ the boundary layer scaling applies, we can use the expressions for the threshold functions found in that regime in Appendix A, to directly find the expression in the LPA' and ∂_2 case (corresponding to Chapter 2, Eq. (2.38) and Chapter 3, Eq. (3.8) in the main text):

$$\frac{\tilde{\epsilon}\,\varphi_{min}}{\delta(\tilde{\epsilon})} = \frac{2\alpha v_d A^{(d)}(\eta)}{(2-\eta)} \frac{g'(0)}{(g(0))^3} = \mathcal{O}(1). \tag{C.2}$$

The expression is the same at both approximation levels, as the subdominant divergence of $z(\varphi)$ in the used ansatz gives the same boundary layer limit for the threshold functions $\ell_n^{(d)}(\varphi;\eta)$ in the ∂_2, as it does with $z(\varphi) = 1$ in the LPA'.

2 From the inflection point to the location of the minimum at LPA'

From results of Chapter 2, Section 3.2.1 we can write the distance between the inflection point φ_i and the minimum/half-period φ_* of the $\tilde{\epsilon} = 0$ periodic solution for $u''(\varphi)$ as:

$$\varphi_* - \varphi_i = \int_{\Phi_*}^{\Phi_i} \frac{d\tilde{\Phi}}{\sqrt{\int_{\Phi_*}^{\tilde{\Phi}} d\hat{\Phi} F\left(\hat{\Phi}\right)}}, \qquad \Phi_* = \Phi(\varphi_*), \quad \Phi_i = \Phi(\varphi_i). \tag{C.3}$$

We examine the integral in the denominator, the function

$$H(\Phi) = \int_{\Phi_*}^{\Phi} d\hat{\Phi} F\left(\hat{\Phi}\right). \tag{C.4}$$

As $F\left(\hat{\Phi}\right) = u''(\varphi)$, $H(\Phi)$ is a monotonically increasing function of Φ for $\Phi \leqslant \Phi_i$. We can show that it is concave, by taking its second derivative:

$$H''(\Phi) = F'(\Phi) = \frac{d}{2v_d\left[\partial_{u''(\varphi)}\ell_0^{(d)}(u''(\varphi), 1; \eta)\right]} = -\frac{d}{2v_d\ell_1^{(d)}(u''(\varphi), 1; \eta)} < 0, \tag{C.5}$$

Any secant of a concave function lies beneath it [132]. We choose the intersection points to be Φ_i and Φ_*, using it to make an estimate for the Φ between the intersections:

$$H(\Phi) \geqslant H(\Phi_i)\left(\frac{\Phi - \Phi_*}{\Phi_i - \Phi_*}\right) \quad \Longrightarrow \quad \int_{\Phi_*}^{\Phi} d\hat{\Phi} F\left(\hat{\Phi}\right) \geqslant \int_{\Phi_*}^{\Phi_i} d\hat{\Phi} F\left(\hat{\Phi}\right)\left(\frac{\Phi - \Phi_*}{\Phi_i - \Phi_*}\right) \tag{C.6}$$

Inserting this into Eq. (C.3) results in the following upper bound:

$$\varphi_* - \varphi_i \leqslant \sqrt{\frac{\Phi_i - \Phi_*}{\int_{\Phi_*}^{\Phi_i} d\hat{\Phi} F\left(\hat{\Phi}\right)}} \int_{\Phi_*}^{\Phi_i} \frac{d\hat{\Phi}}{\sqrt{\hat{\Phi} - \Phi_*}} = 2\frac{\Phi_i - \Phi_*}{\sqrt{\int_{\Phi_*}^{\Phi_i} d\hat{\Phi} F\left(\hat{\Phi}\right)}}. \tag{C.7}$$

Going forward, we recall that $\Phi_i \propto \ell_0^{(d)}(u''(\varphi_i) = 0, 1; \eta) = \mathcal{O}(1)$. This allows us to neglect Φ_*, as $\Phi_* \propto \ell_0^{(d)}(u''(\varphi_*) \gg 1, 1; \eta) = \alpha A^{(d)}(\eta)/u''(\varphi_*) \to 0$ (because $u''(\varphi_*)$ must diverge to allow for a boundary layer), where results of Appendix A have been used. What remains is the following integral:

$$\int_{\Phi_*}^{\Phi_i} d\Phi F(\Phi) = -\int_0^{u''(\varphi_*)} dw w \partial_w \ell_0^{(d)}(w, 1; \eta) \sim \alpha A^{(d)}(\eta) \ln\left(u''(\varphi_*)\right). \tag{C.8}$$

where in the last step we used partial integration (and results of Appendix A for the behavior of the threshold function when $u''(\varphi) \gg 1$ - the asymptotic behavior is the same as in the boundary layer, as long as $u''(\varphi)$ diverges), and an $\mathcal{O}(1)$ contribution has been neglected.

The expressions Eqs. (C.7) and (C.8) combined finally give

$$\varphi_* - \varphi_i \lesssim 2\sqrt{\frac{v_d}{\alpha d A^{(d)}(\eta)}} \frac{\ell_0^{(d)}(u''(\varphi) = 0, 1; \eta)}{\sqrt{\ln\left(u''(\varphi_*)\right)}} \to 0^+, \tag{C.9}$$

which shows that φ_* and φ_i have the same asymptotic behavior.

Appendix D

The expression for d_{lc} at ∂_2

We start from the implicit solution Eq. (3.21) in Chapter 3 for the auxiliary function $f(x)$:

$$f(x) = \frac{\zeta(x)}{g(x)^2} \quad \text{and} \quad F(Y) = F_0 \mathcal{H}\left(-n, \frac{Y}{\sqrt{2}}\right), \quad \text{with} \quad F(Y) = f(x). \tag{D.1}$$

The constant F_0 can be expressed in terms of physical quantities (remember that $n = n(\eta)$ as in Eq. (3.21)):

$$F_0 = \frac{\zeta(0)}{g(0)^2 \mathcal{H}(-n, 0)} = \frac{2^n \zeta(0) \Gamma\left(\frac{n+1}{2}\right)}{\sqrt{\pi} g(0)^2}, \quad \text{as} \quad Y(x=0) = 0. \tag{D.2}$$

If we look at the first derivative of $f(x)$

$$f'(x=0) = \frac{\zeta'(0)}{(g(0))^2} - 2\sqrt{\frac{2}{\pi}} \frac{\zeta(0)}{g(0)} \tag{D.3}$$

and use that $f(x) = F(Y)$:

$$\left.\frac{dF(Y)}{dx}\right|_{x=0} = -\sqrt{2} n Y'(0) F_0 \mathcal{H}(-(n+1), 0) = -\sqrt{2} \frac{\zeta(0) \Gamma\left(\frac{n+1}{2}\right)}{g(0) \Gamma\left(\frac{n}{2}\right)}, \tag{D.4}$$

$$\text{using} \quad Y'(x) = g(x) \quad \text{(from Eqs. (2.42) and (2.43) in Chapter 2)},$$

we can combine Eqs. (D.2) to (D.4) into

$$\frac{\zeta'(0)}{g(0)\zeta(0)} = 2\sqrt{\frac{2}{\pi}} - \sqrt{2} \frac{\Gamma\left(\frac{n+1}{2}\right)}{\Gamma\left(\frac{n}{2}\right)}, \tag{D.5}$$

which is the expression Eq. (3.22) from Chapter 3 of the main text, where we use $\zeta(0) = 1$.

Appendix E

Supplementary plots of numerical ∂_2 fixed-point solutions for $d > d_{lc}$

The role of this section is to display some more fixed-point solutions above d_{lc}. In Figs. E.2 and E.3 we show fixed-point solutions for $u''(\varphi)$ and $z(\varphi)$ for a range of dimensions. The results do not differ qualitatively for most regulator and prefactor choices. What is problematic is r_Θ with $\alpha \geqslant z(0) = 1$. When plotting $\tilde{\epsilon}(d)$ curves, like in Fig. E.1, the r_Θ with $\alpha \geqslant z(0) = 1$ curves show that these choices should not be used to investigate the $\tilde{\epsilon} \to 0$ limit, as is also seen from the extrapolations of the d_{lc} values from these $\tilde{\epsilon}(d)$ curves in Chapter 3, Section 3.4. They seem to not be able to properly capture the limit $\tilde{\epsilon}(d) \to 0^+$. The problem does not exist for the analytical exponential regulator, and we think that this is an atypical and singular situation with the Theta regulator. This is why results with such regulator prefactor values have not been plotted in Chapter 3. We can also discern the different behavior of the fixed-point solution for the field renormalization function for these cases in Fig. E.3, especially in Fig. E.3f compared to the rest of $z(\varphi)$ plots in Figs. E.2 and E.3. From these fixed-point solutions, we also see that the numerical procedure has failed on strangely low dimensions, an artifact of the aforementioned mishandling of the $\tilde{\epsilon}(d) \to 0^+$ limit for these regulator choices.

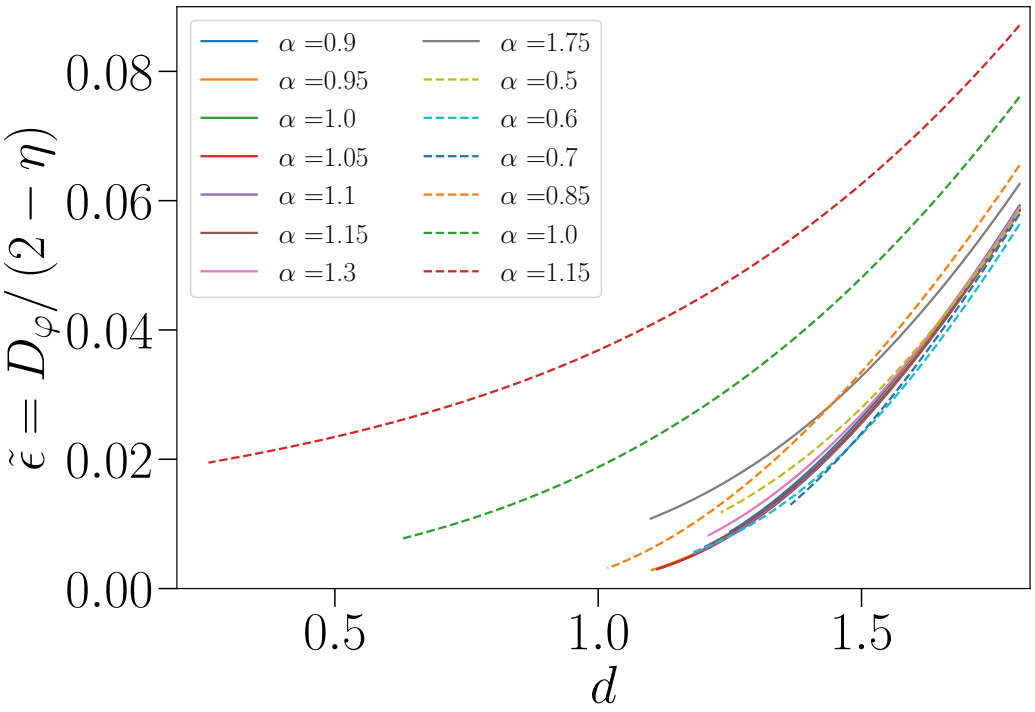

(a)

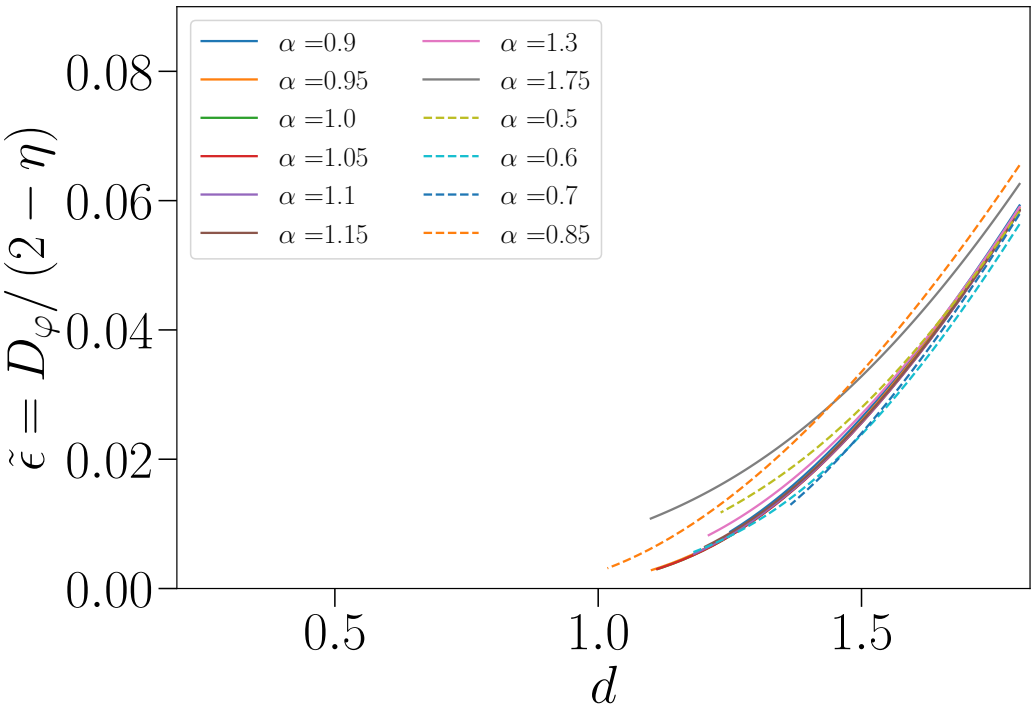

(b)

Figure E.1 – Numerical results for the dependence of the $\tilde{\epsilon}$ parameter on the spatial dimension, in the second order of the derivative expansion ∂_2. We remind that $\tilde{\epsilon}$ is proportional to the scaling dimension D_ϕ of the dimensionfull order-parameter field. We are showing results for multiple choices of regulator prefactors α, as listed on te legends. Full lines: r_{exp}, dashed lines: r_Θ. In Fig. E.1a, we show the problematic $\alpha \geqslant z(0) = 1$ values for the Theta regulator, while in Fig. E.1b they have been removed to illustrate otherwise good agreement between r_{exp} and r_Θ, and for different α.

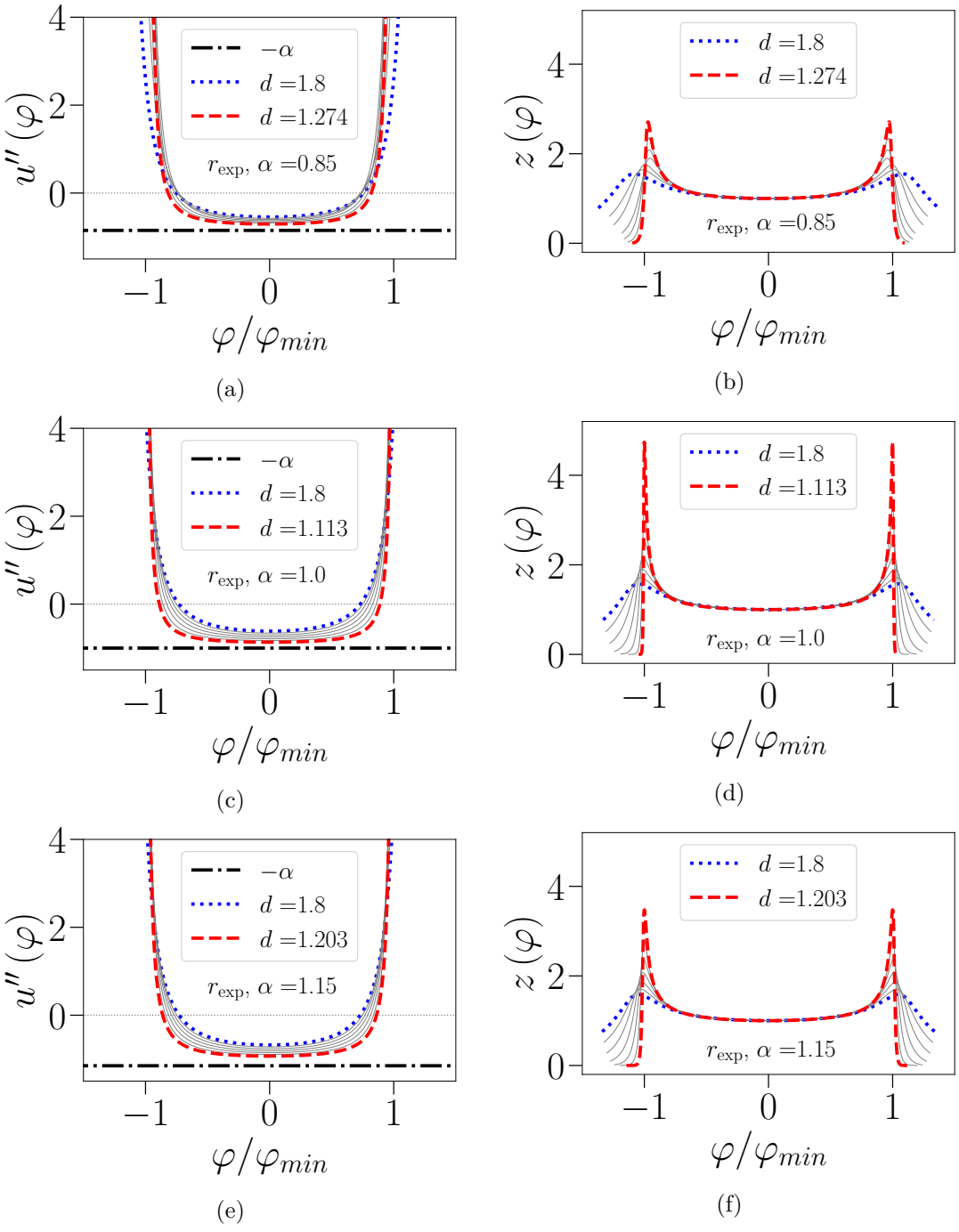

Figure E.2 – Numerical fixed-point solutions for the second derivative of the effective potential $u''(\varphi)$ and the field renormalization function $z(\varphi)$ calculated with $r_{\rm exp}$ for a range of dimensions and regulator prefactors.

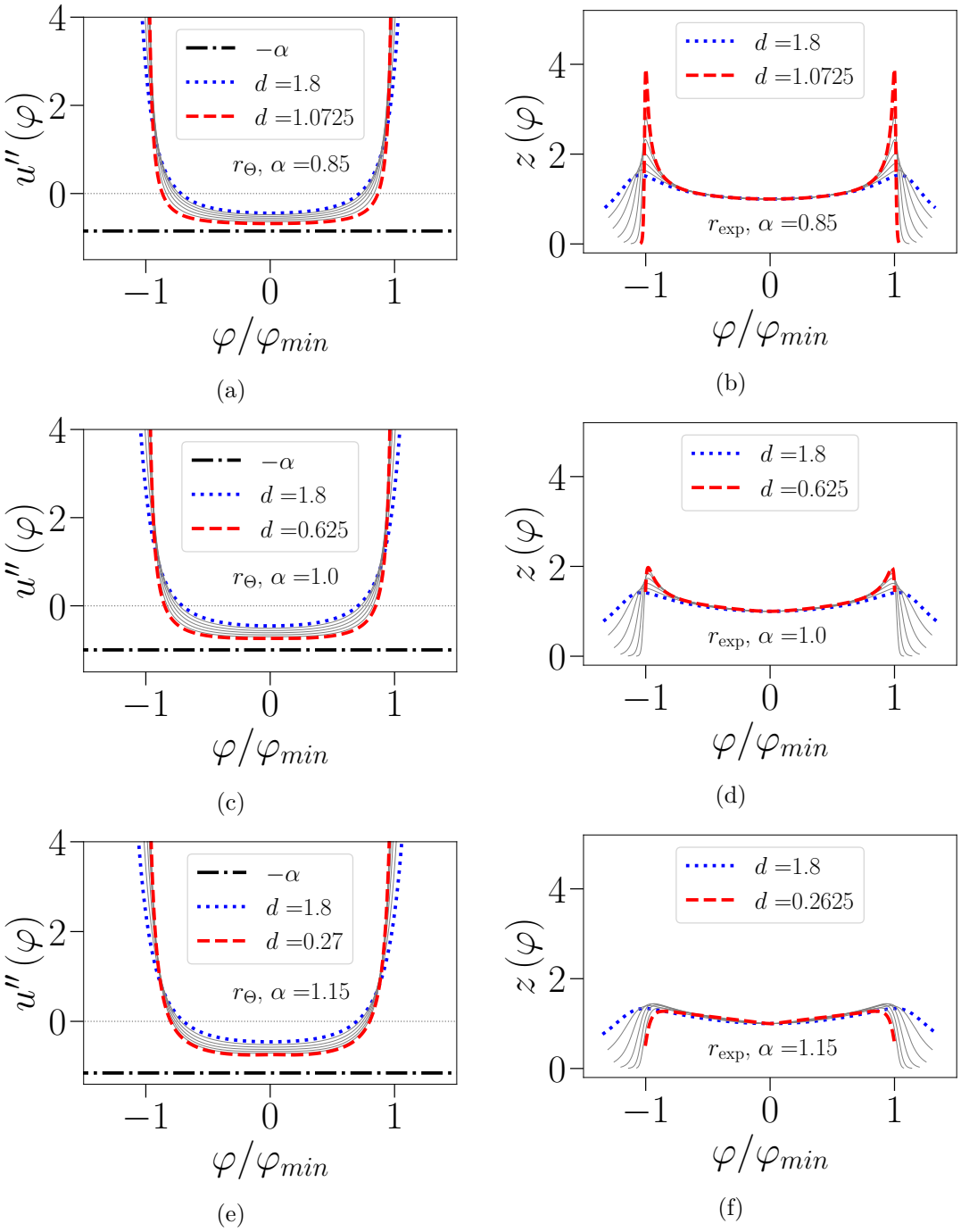

Figure E.3 – Numerical fixed-point solutions for the second derivative of the effective potential $u''(\varphi)$ and the field renormalization function $z(\varphi)$ calculated with r_Θ for a range of dimensions and regulator prefactors. We note the unreasonably low dimensions for $\alpha \geqslant z(0) = 1$.

Appendix F

Kink solution of the saddle-point equation when $k \to 0$

We seek the solution of the saddle-point Eq. (5.14) from Chapter 5 which we restate here:

$$f_1''(x) + 2f_1(x)[1 - 3f_0^2(x)] = k\int_{-L/2}^{L/2} dy\, r(k(x-y))f_0(y) - [b - \int_{-k(L/2+x)}^{k(L/2-x)} dy\, r(y)]\varphi. \quad \text{(F.1)}$$

For concreteness we consider the Gaussian IR regulator but similar results are obtained with other regulators. To start, we simplify the RHS of Eq. (F.1) by using $\tanh(x) \approx \mathrm{sgn}(x)$:

$$f_1''(x) + 2f_1(x)\left(1 - 3\tanh(x-a)^2\right) = \left\{b - \frac{1}{2}\left(\alpha\left[k(L/2-x)\right] + \alpha\left[k(L/2+x)\right]\right)\right\}\varphi + \\ + \alpha\left[k(x-a)\right] + \frac{1}{2}\left(\alpha\left[k(L/2-x)\right] - \alpha\left[k(L/2+x)\right]\right), \quad \text{(F.2)}$$

where $\alpha(x) = 2\int_0^x dy\, \mathrm{r}(y)$.

Using the Gaussian regulator, this turns into:

$$\mathrm{r}(x) = \frac{\alpha}{\sqrt{2\pi}}\exp\left(-x^2/2\right) \qquad \Longrightarrow \qquad \alpha(x) = \alpha\,\mathrm{erf}(x/\sqrt{2})$$

$$\overset{(F.2)}{\Longrightarrow} f_1''(x) + 2f_1(x)\left(1 - 3\tanh(x-a)^2\right) =$$

$$= \left\{b - \frac{\alpha}{2}\left(\mathrm{erf}\left[k(L/2-x)/\sqrt{2}\right] + \mathrm{erf}\left[k(L/2+x)/\sqrt{2}\right]\right)\right\}\varphi + \\ + \alpha\,\mathrm{erf}\left[k(x-a)/\sqrt{2}\right] + \frac{\alpha}{2}\left(\mathrm{erf}\left[k(L/2-x)/\sqrt{2}\right] - \mathrm{erf}\left[k(L/2+x)/\sqrt{2}\right]\right). \quad \text{(F.3)}$$

We introduce the spatial variable z with the origin in the location of the kink, and introduce the shorthand $\mu = a/L = O(1)$:

$$\begin{aligned} &z = x - a: \\ &f_1''(z) + 2f_1(z)\left(1 - 3\tanh(z)^2\right) = \\ &\qquad = \left\{b - \frac{\alpha}{2}\left(\operatorname{erf}\left[k(L/2(1+\mu) - z)/\sqrt{2}\right] + \operatorname{erf}\left[k(L/2(1-\mu) + z)/\sqrt{2}\right]\right)\right\}\varphi + \\ &\quad + \alpha \operatorname{erf}\left[kz/\sqrt{2}\right] + \frac{\alpha}{2}\left(\operatorname{erf}\left[k(L/2(1+\mu) - z)/\sqrt{2}\right] - \operatorname{erf}\left[k(L/2(1-\mu) + z)/\sqrt{2}\right]\right). \end{aligned} \tag{F.4}$$

We continue solving this equation depending on the scale of z:

1. $z \leq O(1/k)$:

$$f_1''(z) + 2f_1(z)\left(1 - 3\tanh(z)^2\right) \approx \{b - \alpha\}\varphi, \tag{F.5}$$

where we put $kL \to +\infty$, as $z \leq O(1/k)$ does not "see" the edges.
The solution to Eq. (F.5) is:

$$\begin{aligned} f_1(z \leq O(1/k)) = &\frac{\varphi}{4}(b - \alpha)\left(\cosh(z)^2 - \frac{3/2}{\cosh(z)^2}\right) + \\ &+ A\left(\tanh(z) + \frac{1}{3}\sinh(2z) + \frac{z}{\cosh(z)^2}\right) + \frac{B}{\cosh(z)^2}, \end{aligned} \tag{F.6}$$

where $A, B = \text{const.}$ are to be determined from joining the z domains.

2. $z = \zeta/k, \qquad \zeta = O(1)$:

$$\begin{aligned} &f_1(z = O(1/k)) = g(\zeta): \\ &k^2 g''(\zeta) + 2g(\zeta)\left(1 - 3\tanh(\zeta/k)^2\right) \approx -4g(\zeta) \approx \{b - \alpha\}\varphi + \alpha \operatorname{erf}\left(\zeta/\sqrt{2}\right) \implies \\ &\implies g(\zeta) = -\frac{b - \alpha}{4}\varphi - \frac{\alpha}{4}\operatorname{erf}\left(\zeta/\sqrt{2}\right), \end{aligned} \tag{F.7}$$

so the solution at this scale is

$$f_1(z = O(1/k)) = -\frac{b - \alpha}{4}\varphi - \frac{\alpha}{4}\operatorname{erf}\left(\frac{kz}{\sqrt{2}}\right). \tag{F.8}$$

3. $|x| = L/2 - u, \qquad u = O(1), \qquad u > 0$:
We use a boundary condition where we constrain $f_1''(x) \approx 0$ near the edges of the system, as we search for kink-like solutions.

(a) $x > 0$:

$$
\begin{aligned}
&f_1(z = L/2 + a - u) = h_+(u) : \\
&h''_+(u) + 2h_+(u)\left(1 - 3\tanh(L/2 + a - u)^2\right) \approx -4h_+(u) \approx \\
&\approx \left\{b - \frac{\alpha}{2}\left(\operatorname{erf}\left[\frac{ku}{\sqrt{2}}\right] + \operatorname{erf}\left[\frac{k(L-u)}{\sqrt{2}}\right]\right)\right\}\varphi + \\
&\qquad + \alpha \operatorname{erf}\left[\frac{k}{\sqrt{2}}\left(L/2(1+\mu) - u\right)\right] + \frac{\alpha}{2}\left(\operatorname{erf}\left[\frac{ku}{\sqrt{2}}\right] - \operatorname{erf}\left[\frac{k}{\sqrt{2}}(L-u)\right]\right) \implies \\
&\implies h_+(u) \approx -\frac{b-\alpha}{4}\varphi - \frac{\alpha}{4} + \frac{\alpha}{8}(1-\varphi)\operatorname{erfc}\left[\frac{ku}{\sqrt{2}}\right].
\end{aligned}
\tag{F.9}
$$

(b) $x < 0$:

$$
\begin{aligned}
&f_1(z = -L/2 + a + u) = h_-(u) : \\
&h''_-(u) + 2h_-(u)\left(1 - 3\tanh(L/2 + a - u)^2\right) \approx -4h_-(u) \approx \\
&\approx \left\{b - \frac{\alpha}{2}\left(\operatorname{erf}\left[\frac{k(L-u)}{\sqrt{2}}\right]\right) + \operatorname{erf}\left[\frac{ku}{\sqrt{2}}\right]\right\}\varphi + \\
&\qquad - \alpha \operatorname{erf}\left[\frac{k}{\sqrt{2}}\left(L/2(1-\mu) - u\right)\right] + \frac{\alpha}{2}\left(\operatorname{erf}\left[\frac{k}{\sqrt{2}}(L-u)\right] - \operatorname{erf}\left[\frac{ku}{\sqrt{2}}\right]\right) \implies \\
&\implies h_-(u) \approx -\frac{b-\alpha}{4}\varphi + \frac{\alpha}{4} - \frac{\alpha}{8}(1+\varphi)\operatorname{erfc}\left[\frac{ku}{\sqrt{2}}\right].
\end{aligned}
\tag{F.10}
$$

Combining the results of Eq. (F.9) and Eq. (F.10), we find the solution near the edges of the system to be:

$$
f_1(|x| = L/2 - O(1)) = -\frac{b-\alpha}{4}\varphi - \operatorname{sgn}(x)\frac{\alpha}{4} + \frac{\alpha}{8}(\operatorname{sgn}(x) - \varphi)\operatorname{erfc}\left(\frac{k}{\sqrt{2}}(L/2 - |x|)\right).
\tag{F.11}
$$

In table F.1, we track the limits of f_1 on the borders of the considered regions. We do this to join the solution across these domains. For this we need to make sure that the neighboring limits in the mentioned table correspond to each other. Here we took into account that $1/k \gg 1$, and that near the edges of the system $\operatorname{sgn}(x) = \operatorname{sgn}(z)$.

Table F.1 – The limits of f_1.

$z = 0$	$\lvert z\rvert \gg 1$	$\zeta = 0$
$f_1(0) = B - \varphi(b-\alpha)/8$	$(b-\alpha) \times (\gg 1) +$ $+ \operatorname{sgn}(z) A \times (\gg 1)$	$-(b-\alpha)\phi/4$
$\lvert\zeta\rvert \to +\infty$	$u \to +\infty$	$u = 0$
$-(b-\alpha)\varphi/4 - \operatorname{sgn}(z)\,\alpha/4$	$-(b-\alpha)\varphi/4 - \operatorname{sgn}(z)\,\alpha/4$	$-(b-\alpha)\varphi/4 - \alpha(\operatorname{sgn}(x) + \varphi)/8$

We see that to join the function together, we must have $b = \alpha$ and put $A = 0$. Now we have:

Table F.2 – The limits of f_1, connected.

$z = 0$	$\lvert z\rvert \gg 1$	$\zeta = 0$	$\lvert\zeta\rvert \to +\infty$	$u \to +\infty$	$u = 0$
$f_1(0) = B$	0	0	$-\operatorname{sgn}(z)\,\alpha/4$	$-\operatorname{sgn}(z)\,\alpha/4$	$-\alpha(\operatorname{sgn}(x)+\varphi)/8$

Now that we construct the full solution, we must be mindful not to include the same contributions twice. The table F.2 is a good check of that, and from the fourth and fifth column we conclude that keeping the erf in Eq. (F.8) means foregoing the $-\operatorname{sgn}(x)\alpha/4$ in Eq. (F.11). All in all, the solution for the k^2 correction over the whole domain is (where we put ϕ_0 and ξ back in):

$$\begin{aligned}\frac{f_1(x/\xi)}{\phi_0} =& \frac{f_1(0)}{\cosh\left((x-a)/\xi\right)^2} - \frac{\alpha}{4}\operatorname{erf}\left(\frac{k(x-a)}{\sqrt{2}}\right) + \\ &+ \frac{\alpha}{8}\left(\operatorname{sgn}\left(\frac{x}{\xi}\right) - \frac{\varphi}{\phi_0}\right)\operatorname{erfc}\left(\frac{k}{\sqrt{2}}(L/2-|x|)\right).\end{aligned} \tag{F.12}$$

Appendix G

Expression for the effective average potential for the domain-wall saddle point

1 Contribution associated with the IR regulator

For concreteness we consider the Gaussian IR regulator but similar results are obtained with other regulators. For the regulator[1] contribution we have the following simplification:

$$\begin{aligned}
&\frac{\alpha k^{2+d}}{2L^d\sqrt{2\pi}^d}\int_{L^d}d\mathbf{x}\int_{L^d}d\mathbf{y}\left(\phi_{*k}\left(\mathrm{x}_{\parallel}\right)-\varphi\right)\exp\left(-\frac{k^2\left(\mathbf{x}-\mathbf{y}\right)^2}{2}\right)\left(\phi_{*k}\left(y_{\parallel}\right)-\varphi\right)= \\
&=\frac{\alpha k^{2+d}}{2L^d\sqrt{2\pi}^d}\int_{L^{d-1}}d\mathbf{x}_{\perp}\int_{L^{d-1}}d\mathbf{y}_{\perp}\exp\left(-\frac{k^2\left(\mathbf{x}_{\perp}-\mathbf{y}_{\perp}\right)^2}{2}\right)\times \\
&\quad\times\int_{-L/2}^{L/2}dx_{\parallel}\int_{-L/2}^{L/2}dy_{\parallel}\left(\phi_{*k}\left(\mathrm{x}_{\parallel}\right)-\varphi\right)\exp\left(-\frac{k^2\left(x_{\parallel}-y_{\parallel}\right)^2}{2}\right)\left(\phi_{*k}\left(y_{\parallel}\right)-\varphi\right),
\end{aligned} \tag{G.1}$$

after which we calculate:

$$\begin{aligned}
\int_{L^{d-1}}d\mathbf{x}_{\perp}\int_{L^{d-1}}d\mathbf{y}_{\perp}\exp\left(-\frac{k^2\left(\mathbf{x}_{\perp}-\mathbf{y}_{\perp}\right)^2}{2}\right)&=L^{d-1}\int_{L^{d-1}}d\mathbf{x}_{\perp}\exp\left(-\frac{k^2\mathbf{x}_{\perp}^2}{2}\right)= \\
&=L^{d-1}k^{1-d}\sqrt{2\pi}^{d-1}
\end{aligned} \tag{G.2}$$

Putting Eq. (G.2) into Eq. (G.1), we continue:

[1] We use the regulator $R_k\left(\mathbf{q},\mathbf{p}\right)=\alpha k^2\delta\left(\mathbf{p}+\mathbf{q}\right)\exp\left(-\mathbf{q}/2k^2\right)$ and Fourier-transform it using the convention $\mathrm{FT}\left[f\right]\left(\mathbf{x}\right)=\int d\mathbf{q}/\sqrt{2\pi}^d\exp\left(-i\mathbf{q}\cdot\mathbf{x}\right)f\left(\mathbf{q}\right)$.

$$
\begin{aligned}
&\frac{\alpha k^{2+d}}{2L^d\sqrt{2\pi}^d}\int_{L^d}d\mathbf{x}\int_{L^d}d\mathbf{y}\left(\phi_{*k}\left(\mathrm{x}_\parallel\right)-\varphi\right)\exp\left(-\frac{k^2\left(\mathbf{x}-\mathbf{y}\right)^2}{2}\right)\left(\phi_{*k}\left(y_\parallel\right)-\varphi\right)=\\
&=\frac{\alpha k^3}{2L\sqrt{2\pi}}\left\{\int_{-L/2}^{L/2}dx_\parallel\int_{-L/2}^{L/2}dy_\parallel\left(\phi_{*k}\left(\mathrm{x}_\parallel\right)-\varphi\right)\exp\left(-\frac{k^2\left(x_\parallel-y_\parallel\right)^2}{2}\right)\left(\phi_{*k}\left(y_\parallel\right)-\varphi\right)\right\}=\\
&=\alpha\frac{k^2}{2}\left\{\varphi^2-2\varphi I_1+I_2\right\},\\
&I_1=\frac{k}{L\sqrt{2\pi}}\int_{-L/2}^{L/2}dx_\parallel\phi_{*k}\left(x_\parallel\right)\int_{-L/2}^{L/2}dy_\parallel\exp\left(-\frac{k^2\left(x_\parallel-y_\parallel\right)^2}{2}\right),\\
&I_2=\frac{k}{L\sqrt{2\pi}}\int_{-L/2}^{L/2}dx_\parallel\int_{-L/2}^{L/2}dy_\parallel\phi_{*k}\left(x_\parallel\right)\exp\left(-\frac{k^2\left(x_\parallel-y_\parallel\right)^2}{2}\right)\phi_{*k}\left(y_\parallel\right).
\end{aligned}
\tag{G.3}
$$

In the preceding expressions we used the index $\parallel$ to emphasize the direction parallel to the kink solution.
The next step is to calculate the integrals I_1 and I_2:

$$
\begin{aligned}
I_1=&\frac{1}{2L}\int_{-L/2}^{L/2}dx\phi_{*k}(x)\left(\mathrm{erf}\left(\frac{k(L/2+x)}{\sqrt{2}}\right)+\mathrm{erf}\left(\frac{k(L/2-x)}{\sqrt{2}}\right)\right)\approx\\
\approx&\frac{\phi_0}{2L}\int_{-L/2}^{L/2}dx\tanh\left(\frac{x-a}{\xi}\right)\left(\mathrm{erf}\left(\frac{k(L/2+x)}{\sqrt{2}}\right)+\mathrm{erf}\left(\frac{k(L/2-x)}{\sqrt{2}}\right)\right).
\end{aligned}
\tag{G.4}
$$

Here we neglected the part of ϕ_{*k} that is proportional to k^2, which will be shown to be appropriate later.
This is still incalculable, so we approximate tanh $\to$ sgn:

$$
\begin{aligned}
I_1\approx&\frac{\phi_0}{2L}\left\{-\int_{-L/2}^{a}dx\left(\mathrm{erf}\left(\frac{k(L/2+x)}{\sqrt{2}}\right)+\mathrm{erf}\left(\frac{k(L/2-x)}{\sqrt{2}}\right)\right)+\right.\\
&\left.+\int_{a}^{L/2}dx\left(\mathrm{erf}\left(\frac{k(L/2+x)}{\sqrt{2}}\right)+\mathrm{erf}\left(\frac{k(L/2-x)}{\sqrt{2}}\right)\right)\right\}=\\
=&\frac{\phi_0}{kL}\sqrt{\frac{2}{\pi}}e^{-\frac{1}{8}k^2(\mu+1)^2L^2}\left(e^{\frac{1}{2}k^2\mu L^2}-1\right)+\\
&-\frac{\phi_0}{2}\left((1+\mu)\,\mathrm{erf}\left(\frac{kL}{2\sqrt{2}}(1+\mu)\right)-(1-\mu)\,\mathrm{erf}\left(\frac{kL}{2\sqrt{2}}(1-\mu)\right)\right)\overset{kL\to+\infty}{\longrightarrow}-\mu\phi_0+\mathcal{O}\left(\frac{1}{kL}\right),\\
&\text{where}\quad\mu=\frac{2a}{L},\qquad 0<\mu<1
\end{aligned}
\tag{G.5}
$$

and combining with the expression for a from Eq. (5.16) in Chapter 5 we have $I_1\approx\alpha\varphi$.
We also check that it is justified to disregard the part of ϕ_{*k} that is proportional to k^2 in

expression Eq. (G.4),:

$$\frac{k^2}{L}\int_{-L/2}^{L/2} dx \left(\operatorname{erf}\left(\frac{k(L/2+x)}{\sqrt{2}}\right)+\operatorname{erf}\left(\frac{k(L/2-x)}{\sqrt{2}}\right)\right) f_1(x) \propto$$
$$\propto \frac{k^2}{L}\int_{-L/2}^{L/2} dx \left(\operatorname{erf}\left(\frac{k(L/2+x)}{\sqrt{2}}\right)+\operatorname{erf}\left(\frac{k(L/2-x)}{\sqrt{2}}\right)\right) \times$$
$$\times \left\{\frac{f_1(0)}{\cosh\left((x-a)/\xi\right)^2} - \frac{\alpha}{8}\left\{2\operatorname{erf}\left(\frac{k(x-a)}{\sqrt{2}}\right) - \left(\operatorname{sgn}(x/\xi) - \frac{\varphi}{\phi_0}\right)\operatorname{erfc}\left(\frac{k(L/2-|x|)}{\sqrt{2}}\right)\right\}\right\}. \tag{G.6}$$

Using the Jordan's estimation lemma [134] and seeing that all of the subintegral functions are at most of $\mathcal{O}(1)$, one promptly sees that Eq. (G.6) is at most of $\mathcal{O}(k^2)$, and I_1 is already multiplied by k^2 in the full expression for the regulator part of the action Eq. (G.3), so we can neglect the contribution in Eq. (G.6).
The approximation tanh $\to$ sgn is used to calculate I_2, too:

$$\begin{aligned} I_2 =& \frac{k}{L\sqrt{2\pi}}\int_{-L/2}^{L/2} dx_\parallel \int_{-L/2}^{L/2} dy_\parallel \phi_{*k}\left(x_\parallel\right)\exp\left(-\frac{k^2\left(x_\parallel - y_\parallel\right)^2}{2}\right)\phi_{*k}\left(y_\parallel\right) = \\ =& \frac{k\phi_0^2}{L\sqrt{2\pi}}\int_{-L/2}^{L/2} dx \int_{-L/2}^{L/2} dy \exp\left(-\frac{k^2(x-y)^2}{2}\right)\times \\ & \times\left\{\operatorname{sgn}\left((x-a)/\xi\right)\operatorname{sgn}\left((y-a)/\xi\right) + 2k^2\operatorname{sgn}\left((x-a)/\xi\right) f_1(y) + k^4 f_1(x) f_1(y)\right\}, \end{aligned} \tag{G.7}$$

We calculate I_2 part by part, but in all instances, it turns out to be beneficial to calculate the integral over x in Eq. (G.7) in the cases with $\operatorname{sgn}\left((x-a)/\xi\right)$ first:

$$\begin{aligned} &\int_{-L/2}^{L/2} dx \operatorname{sgn}\left((x-a)/\xi\right)\exp\left(-\frac{k^2(x-y)^2}{2}\right) = \\ &= \frac{1}{k}\sqrt{\frac{\pi}{2}}\left(2\operatorname{erf}\left(\frac{k(x-a)}{\sqrt{2}}\right)+\operatorname{erf}\left(\frac{k\left(L/2-x\right)}{\sqrt{2}}\right)-\operatorname{erf}\left(\frac{k\left(L/2+x\right)}{\sqrt{2}}\right)\right). \end{aligned} \tag{G.8}$$

We continue on with the integration:

1. $\operatorname{sgn}\left((x-a)/\xi\right)\operatorname{sgn}\left((y-a)/\xi\right)$:

$$\begin{aligned} &\frac{k\phi_0^2}{L\sqrt{2\pi}}\int_{-L/2}^{L/2} dx \int_{-L/2}^{L/2} dy \exp\left(-\frac{k^2(x-y)^2}{2}\right)\operatorname{sgn}\left((x-a)/\xi\right)\operatorname{sgn}\left((y-a)/\xi\right) = \\ &= \phi_0^2\left((1+\mu)\operatorname{erf}\left(\frac{kL}{2\sqrt{2}}(1+\mu)\right)+(1-\mu)\operatorname{erf}\left(\frac{kL}{2\sqrt{2}}(1-\mu)\right)-\operatorname{erf}\left(\frac{kL}{\sqrt{2}}\right)\right)+ \\ &-\frac{\phi_0^2}{kL}\sqrt{\frac{2}{\pi}}\left(3+e^{-\frac{1}{2}k^2L^2}-2e^{-\frac{1}{8}k^2L^2(1-\mu)^2}-2e^{-\frac{1}{8}k^2L^2(1+\mu)^2}\right)\overset{kL\to+\infty}{\longrightarrow}\phi_0^2+\mathcal{O}\left(\frac{1}{kL}\right) \end{aligned} \tag{G.9}$$

The rest of I_2 involves f_1:

2. $\operatorname{sgn}\left((x-a)/\xi\right)/\cosh\left(\dfrac{y-a}{\xi}\right)^2$:

$$\begin{aligned}
&\frac{k^3}{L}\int_{-L/2}^{L/2}dx\int_{-L/2}^{L/2}dy\operatorname{sgn}\left((x-a)/\xi\right)\exp\left(-\frac{k^2\left(x-y\right)^2}{2}\right)/\cosh\left(\frac{y-a}{\xi}\right)^2\propto\\
&\overset{(G.8)}{\propto}\frac{k^2}{L}\int_{-L/2}^{L/2}dx\frac{\left(2\operatorname{erf}\left(\dfrac{k(x-a)}{\sqrt{2}}\right)+\operatorname{erf}\left(\dfrac{k\left(L/2-x\right)}{\sqrt{2}}\right)-\operatorname{erf}\left(\dfrac{k\left(L/2+x\right)}{\sqrt{2}}\right)\right)}{\cosh\left((y-a)/\xi\right)^2}\leq\\
&\leq\frac{k^2}{L}\int_{-L/2}^{L/2}dx\frac{\left|\left(2\operatorname{erf}\left(\dfrac{k(x-a)}{\sqrt{2}}\right)+\operatorname{erf}\left(\dfrac{k\left(L/2-x\right)}{\sqrt{2}}\right)-\operatorname{erf}\left(\dfrac{k\left(L/2+x\right)}{\sqrt{2}}\right)\right)\right|}{\left|\cosh\left((y-a)/\xi\right)^2\right|}\leq\\
&\leq\frac{k^2}{L}\int_{-L/2}^{L/2}dx\left|\left(2\operatorname{erf}\left(\frac{k(x-a)}{\sqrt{2}}\right)+\operatorname{erf}\left(\frac{k\left(L/2-x\right)}{\sqrt{2}}\right)-\operatorname{erf}\left(\frac{k\left(L/2+x\right)}{\sqrt{2}}\right)\right)\right|\leq\\
&\leq k^2\max_{x\in[-L/2,L/2]}\left|\left(2\operatorname{erf}\left(\frac{k(x-a)}{\sqrt{2}}\right)+\operatorname{erf}\left(\frac{k\left(L/2-x\right)}{\sqrt{2}}\right)-\operatorname{erf}\left(\frac{k\left(L/2+x\right)}{\sqrt{2}}\right)\right)\right|\leq 4k^2.
\end{aligned}\tag{G.10}$$

Here we again used the Jordan's estimation lemma.
As I_2 is in Eq. (G.3) already multiplied by k^2, we neglect Eq. (G.10), which would be of order k^4.

3. $\operatorname{sgn}\left((x-a)/\xi\right)\left\{2\operatorname{erf}\left(\dfrac{k(x-a)}{\sqrt{2}}\right)-\left(\operatorname{sgn}(x/\xi)-\dfrac{\varphi}{\phi_0}\right)\operatorname{erfc}\left(\dfrac{k(L/2-|x|)}{\sqrt{2}}\right)\right\}$:

$$\begin{aligned}
&\frac{k^3}{L}\int_{-L/2}^{L/2}dx\int_{-L/2}^{L/2}dy\operatorname{sgn}\left((x-a)/\xi\right)\exp\left(-\frac{k^2\left(x-y\right)^2}{2}\right)\times\\
&\qquad\times\left\{2\operatorname{erf}\left(\frac{k(x-a)}{\sqrt{2}}\right)-\left(\operatorname{sgn}(x/\xi)-\frac{\varphi}{\phi_0}\right)\operatorname{erfc}\left(\frac{k(L/2-|x|)}{\sqrt{2}}\right)\right\}\propto\\
&\overset{(G.8)}{\propto}\frac{k^2}{L}\int_{-L/2}^{L/2}dx\left(2\operatorname{erf}\left(\frac{k(x-a)}{\sqrt{2}}\right)+\operatorname{erf}\left(\frac{k\left(L/2-x\right)}{\sqrt{2}}\right)-\operatorname{erf}\left(\frac{k\left(L/2+x\right)}{\sqrt{2}}\right)\right)\times\\
&\qquad\times\left\{2\operatorname{erf}\left(\frac{k(x-a)}{\sqrt{2}}\right)-\left(\operatorname{sgn}(x/\xi)-\frac{\varphi}{\phi_0}\right)\operatorname{erfc}\left(\frac{k(L/2-|x|)}{\sqrt{2}}\right)\right\}.
\end{aligned}\tag{G.11}$$

Due to erf, sgn and φ/ϕ_0 being of at most $\mathcal{O}(1)$, and the same logic used in Eq. (G.10), Eq. (G.11) can be disregarded too.

4. $f_1(x)f_1(y)$
This part of the integral is multiplied by k^7/L (k^3 from the regulator and k^2 from each f_1). The subintegral function is composed of $0<\exp\left(-k^2\left(x-y\right)^2/2\right)\leq 1$ and different powers of $0<1/\cosh\left((x-a)/\xi\right)^2\leq 1$ and erf, erfc and sgn functions, all of at most $\mathcal{O}(1)$. To make an estimate of the order of magnitude, we can put everything

but the regulator to be equal to 1. Then we have to assess the following:

$$\begin{aligned}&\frac{k^7}{L}\int_{-L/2}^{L/2}dy\int_{-L/2}^{L/2}dx\exp\left(-\frac{k^2\left(x-y\right)^2}{2}\right)=\\&=k^5\left(k\sqrt{2\pi}\,\mathrm{erf}\left(\frac{kL}{\sqrt{2}}\right)-\frac{2}{L}\left(1-\exp\left(-\frac{k^2L^2}{2}\right)\right)\right).\end{aligned}\tag{G.12}$$

This can be neglected.

All in all, we have

$$I_2\approx\phi_0^2+\mathcal{O}\left(\frac{1}{kL}\right)+\mathcal{O}\left(k^2\right)\tag{G.13}$$

The results of this subsection, combined, give the IR regulator contribution:

$$\frac{1}{2L^d}\left(\phi_{*k}-\varphi\right)\cdot R_k\cdot\left(\phi_{*k}-\varphi\right)\approx\alpha\frac{k^2}{2}\left(\phi_0^2-\varphi^2\right)+\mathcal{O}\left(\frac{k}{L}\right)+\mathcal{O}\left(k^4\right).\tag{G.14}$$

2 Contribution associated with the bare action

We calculate:

$$\frac{1}{L^d}S[\phi_{*k}]=\frac{1}{L}\int_{-L/2}^{L/2}dx\left\{\frac{1}{2}\left(\phi'_{*k}(x)\right)^2-\frac{1}{\xi^2}\phi_{*k}(x)^2+\frac{1}{2\xi^2\phi_0^2}\phi_{*k}(x)^4\right\}\tag{G.15}$$

1. The $k=0$ contribution from $\phi_0\tanh\left((x-a)/\xi\right)$:

$$\frac{1}{L^d}S[\phi_{*,k=0}]=-\frac{\phi_0^2}{2\xi^2}+\frac{4\phi_0^2}{3\xi L}\tag{G.16}$$

2. The $\mathcal{O}(k^2)$ terms in $\frac{1}{2L}\int_{-L/2}^{L/2}dx(\phi'_{*k}(x))^2$:
First we find the derivative:

$$\begin{aligned}\frac{d\phi_{*k}(x)}{dx}=\frac{\phi_0}{\xi}\Bigg\{&\frac{1}{\cosh\left((x-a)/\xi\right)^2}-2\xi^2k^2f_1(0)\frac{\sinh\left((x-a)/\xi\right)}{\cosh\left((x-a)/\xi\right)^3}+\\&-\alpha\frac{\xi^3k^3}{2\sqrt{2\pi}}\exp\left(-\frac{k^2}{2}(x-a)^2\right)+\alpha\frac{\xi^2k^2}{8}\,\mathrm{sgn}'\left(x\right)\mathrm{erfc}\left(\frac{k}{\sqrt{2}}\left(\frac{L}{2}-|x|\right)\right)+\\&+\alpha\frac{\xi^3k^3}{4\sqrt{2\pi}}|x|'\left(\mathrm{sgn}\left(\frac{x}{\xi}\right)-\frac{\varphi}{\phi_0}\right)\exp\left(-\frac{k^2}{2}\left(\frac{L}{2}-|x|\right)^2\right)\Bigg\}\end{aligned}\tag{G.17}$$

We can eliminate the $\mathrm{sgn}'(x/\xi)$ part from Eq. (G.17), because it is $\neq 0$ only at $x=0$, where the erfc decays as $\exp(-k^2L^2/8)/(kL)$ with the linear size of the system L. When we square the expression Eq. (G.17), no other factors can recuperate that, so we neglect the $\mathrm{sgn}'(x/\xi)$ term. Similarly, $|x|'=\mathrm{sgn}(x/\xi)$ everywhere except in $x=0$, but there it is multiplied by $\exp\left(-k^2L^2/8\right)$, so we can put $|x|'=\mathrm{sgn}(x/\xi)$:

$$\begin{aligned}\frac{d\phi_{*k}(x)}{dx}=\frac{\phi_0}{\xi}\Bigg\{&\frac{1}{\cosh\left((x-a)/\xi\right)^2}-2\xi^2k^2f_1(0)\frac{\sinh\left((x-a)/\xi\right)}{\cosh\left((x-a)/\xi\right)^3}+\\&-\alpha\frac{\xi^3k^3}{2\sqrt{2\pi}}\exp\left(-\frac{k^2}{2}(x-a)^2\right)+\alpha\frac{\xi^3k^3}{4\sqrt{2\pi}}\left(1-\mathrm{sgn}\left(\frac{x}{\xi}\right)\frac{\varphi}{\phi_0}\right)\exp\left(-\frac{k^2}{2}\left(\frac{L}{2}-|x|\right)^2\right)\Bigg\}.\end{aligned}\tag{G.18}$$

We continue on to the $\mathcal{O}(k^2)$ contribution of Eq. (G.18) part by part:

(a) $\sinh\left((x-a)/\xi\right)/\cosh\left((x-a)/\xi\right)^5$:

$$\begin{aligned}&\frac{k^2}{L}\int_{-L/2}^{L/2}dx\frac{\sinh\left((x-a)/\xi\right)}{\cosh\left((x-a)/\xi\right)^4}\propto\\&\propto\frac{k^2}{L}\left(\frac{1}{\cosh\left(L(1-\mu)/\xi\right)^4}-\frac{1}{\cosh\left(L(1+\mu)/\xi\right)^4}\right)\overset{L\to+\infty}{\longrightarrow}0.\end{aligned}\tag{G.19}$$

(b) $\exp\left(-k^2(x-a)^2/2\right)/\cosh\left((x-a)/\xi\right)^2$:

$$\begin{aligned}&\frac{k^3}{L}\int_{-L/2}^{L/2}dx\frac{\exp\left(-k^2(x-a)^2/2\right)}{\cosh\left((x-a)/\xi\right)^2}\leq\frac{k^3}{L}\int_{-L/2}^{L/2}dx\exp\left(-k^2(x-a)^2/2\right)=\\&=\frac{k^3}{kL}\sqrt{\frac{\pi}{2}}\left(\operatorname{erf}\left(\frac{(1+\mu)kL}{2\sqrt{2}}\right)+\operatorname{erf}\left(\frac{(1-\mu)kL}{2\sqrt{2}}\right)\right)\overset{kL\to+\infty}{\longrightarrow}0.\end{aligned}\tag{G.20}$$

(c) $\exp\left(-k^2(L/2-|x|)^2/2\right)/\cosh\left((x-a)/\xi\right)^2$:

$$\begin{aligned}0\leq&\frac{k^3}{L}\int_{-L/2}^{L/2}dx\frac{\exp\left(-k^2(L/2-|x|)^2/2\right)}{\cosh\left((x-a)/\xi\right)^2}\propto\\&\propto\frac{k^3}{L}\left(\int_{-L/2}^{0}dx\frac{\exp\left(-k^2(L/2+x)^2/2\right)}{\cosh\left((x-a)/\xi\right)^2}+\int_{0}^{L/2}dx\frac{\exp\left(-k^2(L/2-x)^2/2\right)}{\cosh\left((x-a)/\xi\right)^2}\right)\propto\\&\propto k^3\left(\int_{-1}^{0}dx\frac{\exp\left(-k^2L^2(1+x)^2/8\right)}{\cosh\left(L(x-\mu)/2\xi\right)^2}+\int_{0}^{1}dx\frac{\exp\left(-k^2L^2(1-x)^2/8\right)}{\cosh\left(L(x-\mu)/2\xi\right)^2}\right)\propto\\&\propto k^3\left(\int_{0}^{1}dx\frac{\exp\left(-k^2L^2(1-x)^2/8\right)}{\cosh\left(L(x+\mu)/2\xi\right)^2}+\int_{0}^{1}dx\frac{\exp\left(-k^2L^2(1-x)^2/8\right)}{\cosh\left(L(x-\mu)/2\xi\right)^2}\right)\leq\\&\leq 2k^3\int_{0}^{1}dx\exp\left(-\frac{k^2L^2}{8}(1-x)^2\right)\propto\frac{k^3}{kL}\operatorname{erf}\left(\frac{kL}{2\sqrt{2}}\right)\overset{kL\to+\infty}{\longrightarrow}0.\end{aligned}\tag{G.21}$$

(d) $\operatorname{sgn}(x/\xi)\exp\left(-k^2(L/2-|x|)^2/2\right)/\cosh\left((x-a)/\xi\right)^2$:
Can be neglected, with justification following Eq. (G.21) closely.

The rest of the terms are of $\mathcal{O}(k^4)$, as we integrate $\mathcal{O}(1)$ functions over the interval of size L, and there is a k^4/L prefactor. Concerning the functions of kx, they have an additional k prefactor with which the change in measure $dx\to d(kx)/k$ reduces.

3. The $\mathcal{O}(k^2)$ terms in $-\frac{1}{L\xi^2}\int_{-L/2}^{L/2}dx\phi_{*k}(x)^2$:

(a) $\tanh\left((x-a)/\xi\right)/\cosh\left((x-a)/\xi\right)^2$:

$$\begin{aligned}&\frac{k^2}{L}\int_{-L/2}^{L/2}dx\frac{\tanh\left((x-a)/\xi\right)}{\cosh\left((x-a)/\xi\right)^2}\propto\\&\propto\frac{k^2}{L}\left(\frac{1}{1+\cosh\left(L(1-\mu)/\xi\right)}-\frac{1}{1+\cosh\left(L(1+\mu)/\xi\right)}\right)\overset{L\to+\infty}{\longrightarrow}0.\end{aligned}\tag{G.22}$$

(b) $\tanh\left((x-a)/\xi\right)\operatorname{erf}\left(k(x-a)/\sqrt{2}\right)$:

$$\begin{aligned}
&k^2\frac{\alpha\phi_0^2}{2L}\int_{-L/2}^{L/2}dx\tanh\left(\frac{x-a}{\xi}\right)\operatorname{erf}\left(\frac{k}{\sqrt{2}}(x-a)\right)\approx\\
&\approx k^2\frac{\alpha\phi_0^2}{2L}\int_{-L/2}^{L/2}dx\operatorname{sgn}\left((x-a)/\xi\right)\operatorname{erf}\left(\frac{k}{\sqrt{2}}(x-a)\right)=\\
&=k^2\frac{\alpha\phi_0^2}{4}\left\{(1+\mu)\operatorname{erf}\left(\frac{kL}{2\sqrt{2}}(1+\mu)\right)+(1-\mu)\operatorname{erf}\left(\frac{kL}{2\sqrt{2}}(1-\mu)\right)\right\}+\\
&+\frac{k^2}{kL}\frac{\alpha\phi_0^2}{\sqrt{2\pi}}\left\{e^{-k^2L^2(1-\mu)^2/8}+e^{-k^2L^2(1+\mu)^2/8}-2\right\}\overset{kL\to+\infty}{\longrightarrow}\alpha k^2\frac{\phi_0^2}{2}
\end{aligned}\tag{G.23}$$

(c) $\tanh\left((x-a)/\xi\right)\operatorname{erfc}\left(k(L/2-|x|)/\sqrt{2}\right)$:

$$\begin{aligned}
&\frac{k^2}{L}\int_{-L/2}^{L/2}dx\tanh\left(\frac{x-a}{\xi}\right)\operatorname{erfc}\left(\frac{k}{\sqrt{2}}(L/2-|x|)\right)\approx\\
&\approx\frac{k^2}{L}\int_{-L/2}^{L/2}dx\operatorname{sgn}\left((x-a)/\xi\right)\operatorname{erfc}\left(\frac{k}{\sqrt{2}}(L/2-|x|)\right)=\\
&=-k^2\left\{\operatorname{erfc}\left(\frac{kL}{2\sqrt{2}}\right)-(1-\mu)\operatorname{erfc}\left(\frac{kL}{2\sqrt{2}}(1-\mu)\right)\right\}+\\
&\qquad+2\sqrt{\frac{2}{\pi}}\frac{k^2}{kL}\left\{e^{-k^2L^2/8}-e^{-k^2L^2(1-\mu)^2/8}\right\}\overset{kL\to+\infty}{\longrightarrow}0
\end{aligned}\tag{G.24}$$

(d) $\operatorname{sgn}(x/\xi)\tanh\left((x-a)/\xi\right)\operatorname{erfc}\left(k(L/2-|x|)/\sqrt{2}\right)$:

$$\begin{aligned}
&\frac{k^2}{L}\sqrt{\frac{\pi}{2}}\int_{-L/2}^{L/2}dx\operatorname{sgn}(x/\xi)\tanh\left(\frac{x-a}{\xi}\right)\operatorname{erfc}\left(\frac{k}{\sqrt{2}}(L/2-|x|)\right)\approx\\
&\approx\frac{k^2}{L}\int_{-L/2}^{L/2}dx\operatorname{sgn}(x/\xi)\operatorname{sgn}\left((x-a)/\xi\right)\operatorname{erfc}\left(\frac{k}{\sqrt{2}}(L/2-|x|)\right)\propto\\
&\propto\frac{k^2}{kL}\left\{e^{-k^2L^2(1-\mu)^2/8}-1\right\}-k^2\frac{\sqrt{\pi}}{2\sqrt{2}}(1-\mu)\operatorname{erfc}\left(\frac{kL}{2\sqrt{2}}(1-\mu)\right)\overset{kL\to+\infty}{\longrightarrow}0
\end{aligned}\tag{G.25}$$

(e) $f_1(x)^2$:

$$\frac{k^4}{L}\int_{-L/2}^{L/2}dx f_1(x)^2\quad\text{is at worst of order }\frac{k^4}{L}\times L=k^4,\tag{G.26}$$

and can thus be neglected ($f_1^2(x)$ is of order $\leq\mathcal{O}(1)$ on the whole domain, we use the Jordan's estimation lemma).

4. The $\mathcal{O}(k^2)$ terms in $\frac{1}{2L\xi^2\phi_0^2}\int_{-L/2}^{L/2}dx\phi_{*k}(x)^4$:

(a) $\tanh\left((x-a)/\xi\right)^3 / \cosh\left((x-a)/\xi\right)^2$:

$$\begin{aligned}&\frac{k^2}{L}\int_{-L/2}^{L/2} dx \frac{\tanh\left(\dfrac{x-a}{\xi}\right)^3}{\cosh\left(\dfrac{x-a}{\xi}\right)^2} \propto \\ &\propto \frac{k^2}{L}\left\{\tanh^4\left(\frac{L}{2\xi}(1-\mu)\right) - \tanh^4\left(\frac{L}{2\xi}(1+\mu)\right)\right\} \overset{L\to+\infty}{\longrightarrow} 0\end{aligned} \tag{G.27}$$

(b) $\tanh\left((x-a)/\xi\right)^3 \operatorname{erf}\left(k(x-a)/\sqrt{2}\right)$:

$$\begin{aligned}&-k^2\frac{\alpha\phi_0^2}{2L\xi^2}\int_{-L/2}^{L/2} dx \tanh\left(\frac{x-a}{\xi}\right)^3 \operatorname{erf}\left(\frac{k}{\sqrt{2}}(x-a)\right) \approx \\ &\approx -k^2\frac{\alpha\phi_0^2}{2L\xi^2}\int_{-L/2}^{L/2} dx \operatorname{sgn}\left((x-a)/\xi\right) \operatorname{erf}\left(\frac{k}{\sqrt{2}}(x-a)\right) = \\ &= -k^2\frac{\alpha\phi_0^2}{4\xi^2}\left\{(1+\mu)\operatorname{erf}\left(\frac{kL}{2\sqrt{2}}(1+\mu)\right) + (1-\mu)\operatorname{erf}\left(\frac{kL}{2\sqrt{2}}(1-\mu)\right)\right\} + \\ &+ k^2\frac{\alpha\phi_0^2}{\sqrt{2\pi}\xi^2}\left\{\frac{1}{kL}\left(2 - e^{-k^2L^2(1+\mu)^2/8} - e^{-k^2L^2(1-\mu)^2/8}\right)\right\} \overset{kL\to+\infty}{\longrightarrow} -k^2\frac{\alpha\phi_0^2}{2}\end{aligned} \tag{G.28}$$

(c) $\tanh\left((x-a)/\xi\right)^3 \operatorname{erfc}\left(k(L/2-|x|)/\sqrt{2}\right)$:

$$\begin{aligned}&\frac{k^2}{L}\int_{-L/2}^{L/2} dx \tanh\left(\frac{x-a}{\xi}\right)^3 \operatorname{erfc}\left(\frac{k}{\sqrt{2}}(L/2-|x|)\right) \approx \\ &\approx \frac{k^2}{L}\int_{-L/2}^{L/2} dx \operatorname{sgn}\left((x-a)/\xi\right) \operatorname{erfc}\left(\frac{k}{\sqrt{2}}(L/2-|x|)\right) \propto \\ &\propto \frac{k^2}{kL}\left\{e^{-k^2L^2(1-\mu)^2/8} - e^{-k^2L^2/8}\right\} + \\ &\qquad + \frac{k^2}{2}\sqrt{\frac{\pi}{2}}\left\{\operatorname{erfc}\left(\frac{kL}{2\sqrt{2}}\right) - (1-\mu)\operatorname{erfc}\left(\frac{kL}{2\sqrt{2}}(1-\mu)\right)\right\} \overset{kL\to+\infty}{\longrightarrow} 0\end{aligned} \tag{G.29}$$

(d) $\operatorname{sgn}(x/\xi)\tanh\left((x-a)/\xi\right)^3 \operatorname{erfc}\left(k(L/2-|x|)/\sqrt{2}\right)$:

$$\begin{aligned}&\frac{k^2}{L}\int_{-L/2}^{L/2} dx \operatorname{sgn}(x/\xi)\tanh\left(\frac{x-a}{\xi}\right)^3 \operatorname{erfc}\left(\frac{k}{\sqrt{2}}(L/2-|x|)\right) \approx \\ &\approx \frac{k^2}{L}\int_{-L/2}^{L/2} dx \operatorname{sgn}(x/\xi)\operatorname{sgn}\left((x-a)/\xi\right) \operatorname{erfc}\left(\frac{k}{\sqrt{2}}(L/2-|x|)\right) \propto \\ &\propto \frac{k^2}{kL}\left\{e^{-k^2L^2(1-\mu)^2/8} - 1\right\} - \frac{k^2}{2}(1-\mu)\operatorname{erfc}\left(\frac{kL}{2\sqrt{2}}(1-\mu)\right) \overset{kL\to+\infty}{\longrightarrow} 0\end{aligned} \tag{G.30}$$

(e) Involving $f_1^2(x)$, $f_1^3(x)$ and $f_1^4(x)$:

All of the functions involved in these integrations are at most of order $\mathcal{O}(1)$,

and we integrate on $(-L/2, L/2)$. Using the Jordan's estimation lemma again, the integrals can be maximally of order L, and are multiplied by k^{2n}/L, where $n = 2, 3, 4$. The "strongest" contribution is then maximally of order $\mathcal{O}(k^4)$, and can be neglected.

The $\mathcal{O}(k^2)$ contributions from $\phi_{*k}(x)^2$ and $\phi_{*k}(x)^4$ terms cancel out, as using tanh $\approx$ sgn we have:

$$\begin{aligned} &-\frac{1}{\xi^2}\phi_{*k}(x)^2 + \frac{1}{2\xi^2\phi_0^2}\phi_{*k}(x)^4 = \\ &= \mathcal{O}\Big(k^0\Big) - 2\frac{\phi_0^2}{\xi^2} f_1(x)\,\mathrm{sgn}\,(x-a)\Big(1 - \mathrm{sgn}\,(x-a)^2\Big) + \mathcal{O}\Big(k^4\Big), \end{aligned} \tag{G.31}$$

and $\mathrm{sgn}\,(x-a)^2 = 1$ (everywhere but $x = a$, but we are integrating this function).
Summing up all the contributions in this subsection, for the action contribution to the inner saddle point effective potential we get:

$$S\left[\phi_{*k}\right] = -\frac{\phi_0^2}{2\xi^2} + \frac{4\phi_0^2}{3\xi L} \tag{G.32}$$

Combining Eq. (G.14) and Eq. (G.32), we arrive at the full inner saddle point effective potential:

$$U_k^{\mathrm{SP}}(\varphi) = -\frac{\phi_0^2}{2\xi^2} + \frac{1}{2}\alpha k^2\phi_0^2 - \frac{1}{2}\alpha k^2\varphi^2. \tag{G.33}$$

Note that one can use the virial relation [84] that relates the contributions of the kinetic (derivative) term and of the potential term to the saddle-point action as a check of several formulas. Indeed, due to the fact that the field is a solution of the saddle-point differential equation,

$$\partial_x^2\phi_{*k}(\mathbf{x}) = V'(\phi_{*k}(\mathbf{x})), \tag{G.34}$$

where $V(\phi)$ is the bare potential. Multiplying both sides by $\partial_x\phi_{*k}(\mathbf{x})$ and integrating with respect to x gives

$$\frac{1}{2}[\partial_x\phi_{*k}(\mathbf{x})]^2 = V(\phi_{*k}(\mathbf{x})) + \text{const.}, \tag{G.35}$$

so that up to an additive constant (which is simply equal to $\phi_0^2/(2\xi^2)\left[1 + \mathcal{O}(k^4)\right]$ for the ϕ^4 theory) the kinetic and the potential contributions are equal at the saddle-point level.

We also note that we have replaced $a_k(\varphi)$ with the $k = 0$ value, which is justified as $a_k(\varphi)$ does not figure in the $\mathcal{O}(k^0)$ contribution to the action (and thus the effective potential). The next terms are of $\mathcal{O}(k^2)$, so their correction, if $a_{k\neq 0}(\varphi)$ was used, would be of $\mathcal{O}(k^4) \times a_{k=0}(\varphi)/L$, which we neglect.

Bibliography

[1] Kenneth G. Wilson. Renormalization group and critical phenomena. ii. phase-space cell analysis of critical behavior. *Phys. Rev. B*, 4:3184–3205, Nov 1971. doi: 10.1103/PhysRevB.4.3184. URL https://link.aps.org/doi/10.1103/PhysRevB.4.3184.

[2] Kenneth G. Wilson and Michael E. Fisher. Critical exponents in 3.99 dimensions. *Phys. Rev. Lett.*, 28:240–243, Jan 1972. doi: 10.1103/PhysRevLett.28.240. URL https://link.aps.org/doi/10.1103/PhysRevLett.28.240.

[3] Shang-keng Ma. Critical exponents for charged and neutral bose gases above λ points. *Phys. Rev. Lett.*, 29:1311–1314, Nov 1972. doi: 10.1103/PhysRevLett.29.1311. URL https://link.aps.org/doi/10.1103/PhysRevLett.29.1311.

[4] Alexander A. Migdal. Recursion Equations in Gauge Theories. *Sov. Phys. JETP*, 42: 413, 1975.

[5] Alexander A. Migdal. Gauge Transitions in Gauge and Spin Lattice Systems. *Sov. Phys. JETP*, 42:743, 1975.

[6] Leo P Kadanoff. Notes on migdal's recursion formulas. *Annals of Physics*, 100(1): 359–394, 1976. ISSN 0003-4916. doi: https://doi.org/10.1016/0003-4916(76)90066-X. URL https://www.sciencedirect.com/science/article/pii/000349167690066X.

[7] Joseph Polchinski. Renormalization and effective lagrangians. *Nuclear Physics B*, 231(2):269–295, 1984. ISSN 0550-3213. doi: https://doi.org/10.1016/0550-3213(84)90287-6. URL https://www.sciencedirect.com/science/article/pii/0550321384902876.

[8] Christof Wetterich. Exact evolution equation for the effective potential. *Physics Letters B*, 301(1):90–94, 1993. ISSN 0370-2693. doi: https://doi.org/10.1016/0370-2693(93)90726-X. URL https://www.sciencedirect.com/science/article/pii/037026939390726X.

[9] Franz J. Wegner and Anthony Houghton. Renormalization group equation for critical phenomena. *Physical Review A*, 401(8), 1973. doi: https://doi.org/10.1103/PhysRevA.8.401. URL https://journals.aps.org/pra/abstract/10.1103/PhysRevA.8.401.

[10] Tim R. Morris. On truncations of the exact renormalization group. *Physics Letters B*, 334(3):355–362, 1994. ISSN 0370-2693. doi: https://doi.org/10.1016/0370-2693(94)90700-5. URL https://www.sciencedirect.com/science/article/pii/0370269394907005.

[11] Tim R. Morris. Derivative expansion of the exact renormalization group. *Physics Letters B*, 329(2):241–248, 1994. ISSN 0370-2693. doi: https://doi.org/10.1016/0370-2693(94)90767-6. URL https://www.sciencedirect.com/science/article/pii/0370269394907676.

[12] A. D. Bruce and D. J. Wallace. Droplet theory of low-dimensional ising models. *Phys. Rev. Lett.*, 47:1743–1746, Dec 1981. doi: 10.1103/PhysRevLett.47.1743. URL https://link.aps.org/doi/10.1103/PhysRevLett.47.1743.

[13] A D Bruce and D J Wallace. Droplet theory in low dimensions: Ising systems in zero field. *Journal of Physics A: Mathematical and General*, 16(8):1721, jun 1983. doi: 10.1088/0305-4470/16/8/018. URL https://dx.doi.org/10.1088/0305-4470/16/8/018.

[14] D. J. Wallace. Perturbative approach to surface fluctuations. In *Les Houches Summer School in Theoretical Physics: Recent Advances in Field Theory and Statistical Mechanics*, 1982.

[15] Jürgen Berges, Nikolaos Tetradis, and Christof Wetterich. Non-perturbative renormalization flow in quantum field theory and statistical physics. *Physics Reports*, 363(4):223–386, 2002. ISSN 0370-1573. doi: https://doi.org/10.1016/S0370-1573(01)00098-9. URL https://www.sciencedirect.com/science/article/pii/S0370157301000989. Renormalization group theory in the new millennium. IV.

[16] N. Dupuis, L. Canet, A. Eichhorn, W. Metzner, J.M. Pawlowski, M. Tissier, and N. Wschebor. The nonperturbative functional renormalization group and its applications. *Physics Reports*, 910:1–114, 2021. ISSN 0370-1573. doi: https://doi.org/10.1016/j.physrep.2021.01.001. URL https://www.sciencedirect.com/science/article/pii/S0370157321000156. The nonperturbative functional renormalization group and its applications.

[17] John Cardy. *Scaling and Renormalization in Statistical Physics*. Cambridge Lecture Notes in Physics. Cambridge University Press, 1996. doi: 10.1017/CBO9781316036440.

[18] S. Ma. *Modern Theory Of Critical Phenomena*. Taylor & Francis, 2018. ISBN 9780429978517. URL https://books.google.fr/books?id=R0haDwAAQBAJ.

[19] H.E. Stanley. *Introduction to Phase Transitions and Critical Phenomena*. International series of monographs on physics. Oxford University Press, 1987. ISBN 9780195053166. URL https://books.google.fr/books?id=C3BzcUxoaNkC.

[20] Walter Metzner, Manfred Salmhofer, Carsten Honerkamp, Volker Meden, and Kurt Schönhammer. Functional renormalization group approach to correlated fermion systems. *Rev. Mod. Phys.*, 84:299–352, Mar 2012. doi: 10.1103/RevModPhys.84.299. URL https://link.aps.org/doi/10.1103/RevModPhys.84.299.

[21] N. Dupuis. Infrared behavior in systems with a broken continuous symmetry: Classical o(n) model versus interacting bosons. *Phys. Rev. E*, 83:031120, Mar 2011. doi: 10.1103/PhysRevE.83.031120. URL https://link.aps.org/doi/10.1103/PhysRevE.83.031120.

[22] Takeru Yokota and Tomoya Naito. Functional-renormalization-group aided density functional analysis for the correlation energy of the two-dimensional homogeneous electron gas. *Phys. Rev. B*, 99:115106, Mar 2019. doi: 10.1103/PhysRevB.99.115106. URL https://link.aps.org/doi/10.1103/PhysRevB.99.115106.

[23] Takeru Yokota, Kenichi Yoshida, and Teiji Kunihiro. Ab initio description of excited states of 1d uniform matter with the hohenberg–kohn-theorem-inspired functional-renormalization-group method. *Progress of Theoretical and Experimental Physics*, 2019 (1):011D01, 01 2019. ISSN 2050-3911. doi: 10.1093/ptep/pty139. URL https://doi.org/10.1093/ptep/pty139.

[24] Takeru Yokota, Kenichi Yoshida, and Teiji Kunihiro. Functional renormalization-group calculation of the equation of state of one-dimensional uniform matter inspired by the hohenberg-kohn theorem. *Phys. Rev. C*, 99:024302, Feb 2019. doi: 10.1103/PhysRevC.99.024302. URL https://link.aps.org/doi/10.1103/PhysRevC.99.024302.

[25] Sandra Kemler and Jens Braun. Towards a renormalization group approach to density functional theory—general formalism and case studies. *Journal of Physics G: Nuclear and Particle Physics*, 40(8):085105, jul 2013. doi: 10.1088/0954-3899/40/8/085105. URL https://dx.doi.org/10.1088/0954-3899/40/8/085105.

[26] J. Polonyi and K. Sailer. Effective action and density-functional theory. *Phys. Rev. B*, 66:155113, Oct 2002. doi: 10.1103/PhysRevB.66.155113. URL https://link.aps.org/doi/10.1103/PhysRevB.66.155113.

[27] Igor Boettcher, Jan M. Pawlowski, and Sebastian Diehl. Ultracold atoms and the functional renormalization group. *Nuclear Physics B - Proceedings Supplements*, 228:63–135, 2012. ISSN 0920-5632. doi: https://doi.org/10.1016/j.nuclphysbps.2012.06.004. URL https://www.sciencedirect.com/science/article/pii/S0920563212001612. "Physics at all scales: The Renormalization Group" Proceedings of the 49th Internationale Universitätswochen für Theoretische Physik.

[28] Ernst Carl Gerlach Stueckelberg de Breidenbach and Andreas Petermann. Normalization of constants in the quanta theory. *Helv. Phys. Acta*, 26:499–520, 1953. doi: 10.5169/seals-112426.

[29] M. Gell-Mann and F. E. Low. Quantum electrodynamics at small distances. *Phys. Rev.*, 95:1300–1312, Sep 1954. doi: 10.1103/PhysRev.95.1300. URL https://link.aps.org/doi/10.1103/PhysRev.95.1300.

[30] N.N. Bogoliubov and D.V. Shirkov. *Quantum Fields*. Advanced book program. Benjamin/Cummings Publishing Company, Advanced Book Program/World Science Division, 1982. ISBN 9780805309836. URL https://books.google.fr/books?id=wczvAAAAMAAJ.

[31] K. Symanzik. Small distance behaviour in field theory and power counting. *Communications in Mathematical Physics*, 18(3):227–246, 1970. ISSN 1432-0916. doi: 10.1007/BF01649434. URL https://doi.org/10.1007/BF01649434.

[32] Curtis G. Callan. Broken scale invariance in scalar field theory. *Phys. Rev. D*, 2:1541–1547, Oct 1970. doi: 10.1103/PhysRevD.2.1541. URL https://link.aps.org/doi/10.1103/PhysRevD.2.1541.

[33] M. Reuter. Nonperturbative evolution equation for quantum gravity. *Phys. Rev. D*, 57:971–985, Jan 1998. doi: 10.1103/PhysRevD.57.971. URL https://link.aps.org/doi/10.1103/PhysRevD.57.971.

[34] Djamel Dou and Roberto Percacci. The running gravitational couplings. *Classical and Quantum Gravity*, 15(11):3449, nov 1998. doi: 10.1088/0264-9381/15/11/011. URL https://dx.doi.org/10.1088/0264-9381/15/11/011.

[35] Leo P. Kadanoff. Scaling laws for ising models near T_c. *Physics Physique Fizika*, 2: 263–272, Jun 1966. doi: 10.1103/PhysicsPhysiqueFizika.2.263. URL https://link.aps.org/doi/10.1103/PhysicsPhysiqueFizika.2.263.

[36] Michel Le Bellac. Quantum and statistical field theory. 1991. URL https://api.semanticscholar.org/CorpusID:118078253.

[37] B. Widom. Equation of State in the Neighborhood of the Critical Point. *The Journal of Chemical Physics*, 43(11):3898–3905, 05 2004. ISSN 0021-9606. doi: 10.1063/1.1696618. URL https://doi.org/10.1063/1.1696618.

[38] Anson Cheung. Phase transitions and collective phenomena. Lecture notes, University of Cambridge, 2023.

[39] Kenneth G. Wilson. Renormalization group and critical phenomena. i. renormalization group and the kadanoff scaling picture. *Phys. Rev. B*, 4:3174–3183, Nov 1971. doi: 10.1103/PhysRevB.4.3174. URL https://link.aps.org/doi/10.1103/PhysRevB.4.3174.

[40] Kenneth G. Wilson. The renormalization group: Critical phenomena and the kondo problem. *Rev. Mod. Phys.*, 47:773–840, Oct 1975. doi: 10.1103/RevModPhys.47.773. URL https://link.aps.org/doi/10.1103/RevModPhys.47.773.

[41] M. Tabor. *Chaos and Integrability in Nonlinear Dynamics: An Introduction*. Wiley, 1989. ISBN 9780471827283. URL https://books.google.fr/books?id=5FfvAAAAMAAJ.

[42] S. H. Strogatz. *Nonlinear Dynamics and Chaos: With Applications to Physics, Biology, Chemistry, and Engineering*. CRC Press, 2nd edition, 2015. doi: 10.1201/9780429492563.

[43] N. Goldenfeld. *Lectures On Phase Transitions And The Renormalization Group*. CRC Press, 2018. ISBN 9780429973123. URL https://books.google.fr/books?id=HQpQDwAAQBAJ.

[44] Jean Zinn-Justin. *Quantum Field Theory and Critical Phenomena: Fifth Edition*. Oxford University Press, 04 2021. ISBN 9780198834625. doi: 10.1093/oso/9780198834625.001.0001. URL https://doi.org/10.1093/oso/9780198834625.001.0001.

[45] P. M. Chaikin and T. C. Lubensky. *Principles of Condensed Matter Physics*. Cambridge University Press, 1995. doi: 10.1017/CBO9780511813467.

[46] P. Kopietz, L. Bartosch, and F. Schütz. *Introduction to the Functional Renormalization Group*. Introduction to the Functional Renormalization Group. Springer, 2010. ISBN 9783642050930. URL https://books.google.fr/books?id=cGa5Q9BeMNUC.

[47] B. Delamote. *An Introduction to the Nonperturbative Renormalization Group*, pages 49–132. Springer, Berlin, Heidelberg, 2012.

[48] Daniel F. Litim. Derivative expansion and renormalisation group flows. *Journal of High Energy Physics*, 11(059), 2001. doi: 10.1088/1126-6708/2001/11/059.

[49] Daniel F. Litim. Optimisation of the exact renormalisation group. *Physics Letters B*, 486(1):92–99, 2000. ISSN 0370-2693. doi: https://doi.org/10.1016/S0370-2693(00)00748-6. URL https://www.sciencedirect.com/science/article/pii/S0370269300007486.

[50] Daniel F. Litim. Optimized renormalization group flows. *Phys. Rev. D*, 64:105007, Oct 2001. doi: 10.1103/PhysRevD.64.105007. URL https://link.aps.org/doi/10.1103/PhysRevD.64.105007.

[51] Jan M. Pawlowski. Aspects of the functional renormalisation group. *Annals of Physics*, 322(12):2831–2915, 2007. ISSN 0003-4916. doi: https://doi.org/10.1016/j.aop.2007.01.007. URL https://www.sciencedirect.com/science/article/pii/S0003491607000097.

[52] Léonie Canet, Bertrand Delamotte, Dominique Mouhanna, and Julien Vidal. Optimization of the derivative expansion in the nonperturbative renormalization group. *Phys. Rev. D*, 67:065004, Mar 2003. doi: 10.1103/PhysRevD.67.065004. URL https://link.aps.org/doi/10.1103/PhysRevD.67.065004.

[53] Ivan Balog, Hugues Chaté, Bertrand Delamotte, Maroje Marohnić, and Nicolás Wschebor. Convergence of nonperturbative approximations to the renormalization group. *Phys. Rev. Lett.*, 123:240604, Dec 2019. doi: 10.1103/PhysRevLett.123.240604. URL https://link.aps.org/doi/10.1103/PhysRevLett.123.240604.

[54] Ivan Balog, Gonzalo De Polsi, Matthieu Tissier, and Nicolás Wschebor. Conformal invariance in the nonperturbative renormalization group: A rationale for choosing the regulator. *Phys. Rev. E*, 101:062146, Jun 2020. doi: 10.1103/PhysRevE.101.062146.

[55] T. Papenbrock and C. Wetterich. Two-loop results from improved one loop computations. *Zeitschrift für Physik C Particles and Fields*, 65(3):519–535, 1995. ISSN 1431-5858. doi: 10.1007/BF01556140. URL https://doi.org/10.1007/BF01556140.

[56] Peter Kopietz. Two-loop β-function from the exact renormalization group. *Nuclear Physics B*, 595(1):493–518, 2001. ISSN 0550-3213. doi: https://doi.org/10.1016/S0550-3213(00)00680-5. URL https://www.sciencedirect.com/science/article/pii/S0550321300006805.

[57] E. Brézin. *Introduction to Statistical Field Theory*. Cambridge University Press, 2010. ISBN 9781139490146. URL https://books.google.fr/books?id=jLl6II1j8LgC.

[58] C. Kittel. *Introduction to Solid State Physics*. Wiley, 2004. ISBN 9780471415268. URL https://books.google.fr/books?id=kym4QgAACAAJ.

[59] Gonzalo De Polsi, Ivan Balog, Matthieu Tissier, and Nicolás Wschebor. Precision calculation of critical exponents in the o(n) universality classes with the nonperturbative renormalization group. *Phys. Rev. E*, 101:042113, Apr 2020. doi: 10.1103/PhysRevE.101.042113. URL https://link.aps.org/doi/10.1103/PhysRevE.101.042113.

[60] Ernst Ising. Beitrag zur theorie des ferromagnetismus. *Zeitschrift für Physik*, 31(1): 253–258, 1925. ISSN 0044-3328. doi: 10.1007/BF02980577. URL https://doi.org/10.1007/BF02980577.

[61] R.J. Baxter. *Exactly Solved Models in Statistical Mechanics*. Dover Books on Physics. Dover Publications, 2013. ISBN 9780486318172. URL https://books.google.fr/books?id=eQzCAgAAQBAJ.

[62] Ken-Ichi Aoki, Keiichi Morikawa, Wataru Souma, Jun-Ichi Sumi, and Haruhiko Terao. Rapidly Converging Truncation Scheme of the Exact Renormalization Group. *Progress of Theoretical Physics*, 99(3):451–466, 03 1998. ISSN 0033-068X. doi: 10.1143/PTP.99.451. URL https://doi.org/10.1143/PTP.99.451.

[63] N. Tetradis and C. Wetterich. Critical exponents from the effective average action. *Nuclear Physics B*, 422(3):541–592, 1994. ISSN 0550-3213. doi: https://doi.org/10.1016/0550-3213(94)90446-4. URL https://www.sciencedirect.com/science/article/pii/0550321394904464.

[64] N. Tetradis and D.F. Litim. Analytical solutions of exact renormalization group equations. *Nuclear Physics B*, 464(3):492–511, 1996. ISSN 0550-3213. doi: https://doi.org/10.1016/0550-3213(95)00642-7. URL https://www.sciencedirect.com/science/article/pii/0550321395006427.

[65] N. Tetradis and C. Wetterich. Scale dependence of the average potential around the maximum in φ^4 theories. *Nuclear Physics B*, 383(1):197–217, 1992. ISSN 0550-3213. doi: https://doi.org/10.1016/0550-3213(92)90676-3. URL https://www.sciencedirect.com/science/article/pii/0550321392906763.

[66] Marcela Peláez and Nicolás Wschebor. Ordered phase of the O(n) model within the nonperturbative renormalization group. *Phys. Rev. E*, 94:042136, Oct 2016. doi: 10.1103/PhysRevE.94.042136. URL https://link.aps.org/doi/10.1103/PhysRevE.94.042136.

[67] A. Ringwald and C. Wetterich. Average action for the n-component ϕ^4 theory. *Nuclear Physics B*, 334(2):506–526, 1990. ISSN 0550-3213. doi: https://doi.org/10.1016/0550-3213(90)90489-Z. URL https://www.sciencedirect.com/science/article/pii/055032139090489Z.

[68] P. Jakubczyk, N. Dupuis, and B. Delamotte. Reexamination of the nonperturbative renormalization-group approach to the kosterlitz-thouless transition. *Phys. Rev. E*, 90: 062105, Dec 2014. doi: 10.1103/PhysRevE.90.062105. URL https://link.aps.org/doi/10.1103/PhysRevE.90.062105.

[69] V. L. Berezinskiĭ. Destruction of long-range order in one-dimensional and two-dimensional systems having a continuous symmetry group i. classical systems. *JETP*, 32:493, 1971.

[70] V. L. Berezinskiĭ. Destruction of long-range order in one-dimensional and two-dimensional systems possessing a continuous symmetry group. ii. quantum systems. *JETP*, 34:610, 1972.

[71] J M Kosterlitz and D J Thouless. Ordering, metastability and phase transitions in two-dimensional systems. *Journal of Physics C: Solid State Physics*, 6(7):1181, apr 1973. doi: 10.1088/0022-3719/6/7/010. URL https://dx.doi.org/10.1088/0022-3719/6/7/010.

[72] J M Kosterlitz. The critical properties of the two-dimensional xy model. *Journal of Physics C: Solid State Physics*, 7(6):1046, mar 1974. doi: 10.1088/0022-3719/7/6/005. URL https://dx.doi.org/10.1088/0022-3719/7/6/005.

[73] Isadore Rudnick. Critical surface density of the superfluid component in ^{4}He films. *Phys. Rev. Lett.*, 40:1454–1455, May 1978. doi: 10.1103/PhysRevLett.40.1454. URL https://link.aps.org/doi/10.1103/PhysRevLett.40.1454.

[74] D. J. Bishop and J. D. Reppy. Study of the superfluid transition in two-dimensional ^{4}He films. *Phys. Rev. Lett.*, 40:1727–1730, Jun 1978. doi: 10.1103/PhysRevLett.40.1727. URL https://link.aps.org/doi/10.1103/PhysRevLett.40.1727.

[75] J. Maps and R. B. Hallock. Thermal transport on the superfluid side of the kosterlitz-thouless transition in ^{4}He films. *Phys. Rev. B*, 26:3979–3981, Oct 1982. doi: 10.1103/PhysRevB.26.3979. URL https://link.aps.org/doi/10.1103/PhysRevB.26.3979.

[76] J. Maps and R. B. Hallock. Onset of superfluid flow in ^{4}He films adsorbed on mylar. *Phys. Rev. Lett.*, 47:1533–1536, Nov 1981. doi: 10.1103/PhysRevLett.47.1533. URL https://link.aps.org/doi/10.1103/PhysRevLett.47.1533.

[77] Zoran Hadzibabic, Peter Krüger, Marc Cheneau, Baptiste Battelier, and Jean Dalibard. Berezinskii–kosterlitz–thouless crossover in a trapped atomic gas. *Nature*, 441(7097):1118–1121, 2006. ISSN 1476-4687. doi: 10.1038/nature04851. URL https://doi.org/10.1038/nature04851.

[78] P. Cladé, C. Ryu, A. Ramanathan, K. Helmerson, and W. D. Phillips. Observation of a 2d bose gas: From thermal to quasicondensate to superfluid. *Phys. Rev. Lett.*, 102: 170401, Apr 2009. doi: 10.1103/PhysRevLett.102.170401. URL https://link.aps.org/doi/10.1103/PhysRevLett.102.170401.

[79] S. Tung, G. Lamporesi, D. Lobser, L. Xia, and E. A. Cornell. Observation of the presuperfluid regime in a two-dimensional bose gas. *Phys. Rev. Lett.*, 105:230408, Dec

2010. doi: 10.1103/PhysRevLett.105.230408. URL https://link.aps.org/doi/10.1103/PhysRevLett.105.230408.

[80] Rémi Desbuquois, Lauriane Chomaz, Tarik Yefsah, Julian Léonard, Jérôme Beugnon, Christof Weitenberg, and Jean Dalibard. Superfluid behaviour of a two-dimensional bose gas. *Nature Physics*, 8(9):645–648, 2012. ISSN 1745-2481. doi: 10.1038/nphys2378. URL https://doi.org/10.1038/nphys2378.

[81] T Schneider and S Weyeneth. Quantum superconductor–insulator transition: implications of bkt critical behavior. *Journal of Physics: Condensed Matter*, 25(30):305701, jul 2013. doi: 10.1088/0953-8984/25/30/305701. URL https://dx.doi.org/10.1088/0953-8984/25/30/305701.

[82] N. D. Mermin and H. Wagner. Absence of ferromagnetism or antiferromagnetism in one- or two-dimensional isotropic heisenberg models. *Phys. Rev. Lett.*, 17:1133–1136, Nov 1966. doi: 10.1103/PhysRevLett.17.1133. URL https://link.aps.org/doi/10.1103/PhysRevLett.17.1133.

[83] Subir Sachdev. *Quantum Phase Transitions*. Cambridge University Press, 2 edition, 2011. ISBN 978-0-521-51468-2. LC Call No.: QC175.16.P5S23 2011.

[84] R. Rajaraman. *Solitons and Instantons: An Introduction to Solitons and Instantons in Quantum Field Theory*. North-Holland personal library. North-Holland Publishing Company, 1982. ISBN 9780444862297. URL https://books.google.fr/books?id=1XucQgAACAAJ.

[85] G. v. Gersdorff and C. Wetterich. Nonperturbative renormalization flow and essential scaling for the kosterlitz-thouless transition. *Phys. Rev. B*, 64:054513, Jul 2001. doi: 10.1103/PhysRevB.64.054513. URL https://link.aps.org/doi/10.1103/PhysRevB.64.054513.

[86] Alfio Bonanno, Alessandro Codello, and Dario Zappalà. Structural aspects of frg in quantum tunneling computations. *Annals of Physics*, 445:169090, 2022. ISSN 0003-4916. doi: https://doi.org/10.1016/j.aop.2022.169090. URL https://www.sciencedirect.com/science/article/pii/S000349162200197X.

[87] Gilles Tarjus and Matthieu Tissier. Nonperturbative functional renormalization group for random field models and related disordered systems. i. effective average action formalism. *Phys. Rev. B*, 78:024203, Jul 2008. doi: 10.1103/PhysRevB.78.024203. URL https://link.aps.org/doi/10.1103/PhysRevB.78.024203.

[88] Matthieu Tissier and Gilles Tarjus. Unified picture of ferromagnetism, quasi-long-range order, and criticality in random-field models. *Phys. Rev. Lett.*, 96:087202, Mar 2006. doi: 10.1103/PhysRevLett.96.087202. URL https://link.aps.org/doi/10.1103/PhysRevLett.96.087202.

[89] Matthieu Tissier and Gilles Tarjus. Supersymmetry and its spontaneous breaking in the random field ising model. *Phys. Rev. Lett.*, 107:041601, Jul 2011. doi: 10.1103/PhysRevLett.107.041601. URL https://link.aps.org/doi/10.1103/PhysRevLett.107.041601.

[90] Matthieu Tissier and Gilles Tarjus. Nonperturbative functional renormalization group for random field models and related disordered systems. iii. superfield formalism and ground-state dominance. *Phys. Rev. B*, 85:104202, Mar 2012. doi: 10.1103/PhysRevB.85.104202. URL https://link.aps.org/doi/10.1103/PhysRevB.85.104202.

[91] Matthieu Tissier and Gilles Tarjus. Nonperturbative functional renormalization group for random field models and related disordered systems. iv. supersymmetry and its spontaneous breaking. *Phys. Rev. B*, 85:104203, Mar 2012. doi: 10.1103/PhysRevB.85.104203. URL https://link.aps.org/doi/10.1103/PhysRevB.85.104203.

[92] Ivan Balog, Gilles Tarjus, and Matthieu Tissier. Criticality of the random field ising model in and out of equilibrium: A nonperturbative functional renormalization group description. *Phys. Rev. B*, 97:094204, Mar 2018. doi: 10.1103/PhysRevB.97.094204. URL https://link.aps.org/doi/10.1103/PhysRevB.97.094204.

[93] Gilles Tarjus and Matthieu Tissier. Random-field ising and o(n) models: theoretical description through the functional renormalization group. *The European Physical Journal B*, 93(3):50, 2020. ISSN 1434-6036. doi: 10.1140/epjb/e2020-100489-1. URL https://doi.org/10.1140/epjb/e2020-100489-1.

[94] Michael Aizenman and Jan Wehr. Rounding of first-order phase transitions in systems with quenched disorder. *Phys. Rev. Lett.*, 62:2503–2506, May 1989. doi: 10.1103/PhysRevLett.62.2503. URL https://link.aps.org/doi/10.1103/PhysRevLett.62.2503.

[95] M. Aizenman and J. Wehr. Rounding effects of quenched randomness on first-order phase transitions. *Communications in Mathematical Physics*, 130:489, 1990.

[96] Ivan Balog, Gilles Tarjus, and Matthieu Tissier. Benchmarking the nonperturbative functional renormalization group approach on the random elastic manifold model in and out of equilibrium. *Journal of Statistical Mechanics: Theory and Experiment*, 2019 (10):103301, oct 2019. doi: 10.1088/1742-5468/ab3da5. URL https://dx.doi.org/10.1088/1742-5468/ab3da5.

[97] Francisco J. Pérez-Reche and Eduard Vives. Spanning avalanches in the three-dimensional gaussian random-field ising model with metastable dynamics: Field dependence and geometrical properties. *Phys. Rev. B*, 70:214422, Dec 2004. doi: 10.1103/PhysRevB.70.214422. URL https://link.aps.org/doi/10.1103/PhysRevB.70.214422.

[98] Yang Liu and Karin A. Dahmen. Unexpected universality in static and dynamic avalanches. *Phys. Rev. E*, 79:061124, Jun 2009. doi: 10.1103/PhysRevE.79.061124. URL https://link.aps.org/doi/10.1103/PhysRevE.79.061124.

[99] Y. Liu and K. A. Dahmen. Random-field ising model in and out of equilibrium. *Europhysics Letters*, 86(5):56003, jun 2009. doi: 10.1209/0295-5075/86/56003. URL https://dx.doi.org/10.1209/0295-5075/86/56003.

[100] L. X. Hayden, Archishman Raju, and James P. Sethna. Unusual scaling for two-dimensional avalanches: Curing the faceting and scaling in the lower critical dimension.

Phys. Rev. Res., 1:033060, Oct 2019. doi: 10.1103/PhysRevResearch.1.033060. URL https://link.aps.org/doi/10.1103/PhysRevResearch.1.033060.

[101] Djordje Spasojević, Sanja Janićević, and Milan Knežević. Numerical evidence for critical behavior of the two-dimensional nonequilibrium zero-temperature random field ising model. *Phys. Rev. Lett.*, 106:175701, Apr 2011. doi: 10.1103/PhysRevLett.106.175701. URL https://link.aps.org/doi/10.1103/PhysRevLett.106.175701.

[102] Yoseph Imry and Shang-keng Ma. Random-field instability of the ordered state of continuous symmetry. *Phys. Rev. Lett.*, 35:1399–1401, Nov 1975. doi: 10.1103/PhysRevLett.35.1399. URL https://link.aps.org/doi/10.1103/PhysRevLett.35.1399.

[103] J. Bricmont and A. Kupiainen. Lower critical dimension for the random-field ising model. *Phys. Rev. Lett.*, 59:1829–1832, Oct 1987. doi: 10.1103/PhysRevLett.59.1829. URL https://link.aps.org/doi/10.1103/PhysRevLett.59.1829.

[104] T. Natterman. *Theory of the Random Field ising model*, pages 277–298. doi: 10.1142/9789812819437_0009. URL https://www.worldscientific.com/doi/abs/10.1142/9789812819437_0009.

[105] James P. Sethna, Karin Dahmen, Sivan Kartha, James A. Krumhansl, Bruce W. Roberts, and Joel D. Shore. Hysteresis and hierarchies: Dynamics of disorder-driven first-order phase transformations. *Phys. Rev. Lett.*, 70:3347–3350, May 1993. doi: 10.1103/PhysRevLett.70.3347. URL https://link.aps.org/doi/10.1103/PhysRevLett.70.3347.

[106] Karin Dahmen and James P. Sethna. Hysteresis, avalanches, and disorder-induced critical scaling: A renormalization-group approach. *Phys. Rev. B*, 53:14872–14905, Jun 1996. doi: 10.1103/PhysRevB.53.14872. URL https://link.aps.org/doi/10.1103/PhysRevB.53.14872.

[107] Olga Perković, Karin A. Dahmen, and James P. Sethna. Disorder-induced critical phenomena in hysteresis: Numerical scaling in three and higher dimensions. *Phys. Rev. B*, 59:6106–6119, Mar 1999. doi: 10.1103/PhysRevB.59.6106. URL https://link.aps.org/doi/10.1103/PhysRevB.59.6106.

[108] J. P. Sethna, K. A. Dahmen, and O. Perkovic. *The Science of Hysteresis*, page 107. Elsevier, Amsterdam, 2005.

[109] C Rulquin, P Urbani, G Biroli, G Tarjus, and M Tarzia. Nonperturbative fluctuations and metastability in a simple model: from observables to microscopic theory and back. *Journal of Statistical Mechanics: Theory and Experiment*, 2016(2):023209, feb 2016. doi: 10.1088/1742-5468/2016/02/023209. URL https://dx.doi.org/10.1088/1742-5468/2016/02/023209.

[110] I. Nándori, I. G. Márián, and V. Bacsó. Spontaneous symmetry breaking and optimization of functional renormalization group. *Phys. Rev. D*, 89:047701, Feb 2014. doi: 10.1103/PhysRevD.89.047701. URL https://link.aps.org/doi/10.1103/PhysRevD.89.047701.

[111] Romain Daviet and Nicolas Dupuis. On the nature of the schmid transition in a resistively shunted josephson junction, 2023.

[112] J. Hubbard. Calculation of partition functions. *Phys. Rev. Lett.*, 3:77–78, Jul 1959. doi: 10.1103/PhysRevLett.3.77. URL https://link.aps.org/doi/10.1103/PhysRevLett.3.77.

[113] Hagen Kleinert and Verena Schulte-Frohlinde. *Critical Properties of Phi4-Theories*. WORLD SCIENTIFIC, 2001. doi: 10.1142/4733. URL https://www.worldscientific.com/doi/abs/10.1142/4733.

[114] Michael Aizenman. Proof of the triviality of $\phi_d{}^4$ field theory and some mean-field features of ising models for d>4. *Phys. Rev. Lett.*, 47:1–4, Jul 1981. doi: 10.1103/PhysRevLett.47.1. URL https://link.aps.org/doi/10.1103/PhysRevLett.47.1.

[115] Jean-Philippe Bouchaud and Giulio Biroli. On the Adam-Gibbs-Kirkpatrick-Thirumalai-Wolynes scenario for the viscosity increase in glasses. *The Journal of Chemical Physics*, 121(15):7347–7354, 10 2004. ISSN 0021-9606. doi: 10.1063/1.1796231. URL https://doi.org/10.1063/1.1796231.

[116] Silvio Franz. First steps of a nucleation theory in disordered systems. *Journal of Statistical Mechanics: Theory and Experiment*, 2005(04):P04001, apr 2005. doi: 10.1088/1742-5468/2005/04/P04001. URL https://dx.doi.org/10.1088/1742-5468/2005/04/P04001.

[117] Maxim Dzero, Jörg Schmalian, and Peter G. Wolynes. Replica theory for fluctuations of the activation barriers in glassy systems. *Phys. Rev. B*, 80:024204, Jul 2009. doi: 10.1103/PhysRevB.80.024204. URL https://link.aps.org/doi/10.1103/PhysRevB.80.024204.

[118] J.J. Binney, N.J. Dowrick, A.J. Fisher, and M.E.J. Newman. *The Theory of Critical Phenomena: An Introduction to the Renormalization Group*. Clarendon Press, 1992. ISBN 9780191660566. URL https://books.google.fr/books?id=BCOQDwAAQBAJ.

[119] Kenneth G. Wilson and J. Kogut. The renormalization group and the ϵ expansion. *Physics Reports*, 12(2):75–199, 1974. ISSN 0370-1573. doi: https://doi.org/10.1016/0370-1573(74)90023-4. URL https://www.sciencedirect.com/science/article/pii/0370157374900234.

[120] Lars Onsager. Crystal statistics. i. a two-dimensional model with an order-disorder transition. *Phys. Rev.*, 65:117–149, Feb 1944. doi: 10.1103/PhysRev.65.117. URL https://link.aps.org/doi/10.1103/PhysRev.65.117.

[121] R. Peierls. On ising's model of ferromagnetism. *Mathematical Proceedings of the Cambridge Philosophical Society*, 32(3):477–481, 1936. doi: 10.1017/S0305004100019174.

[122] H. Ballhausen, J. Berges, and C. Wetterich. Critical phenomena in continuous dimension. *Physics Letters B*, 582(1):144–150, 2004. ISSN 0370-2693. doi: https://doi.org/10.1016/j.physletb.2003.12.033. URL https://www.sciencedirect.com/science/article/pii/S037026930400022X.

[123] M. Reuter, N. Tetradis, and C. Wetterich. The large-n limit and the high-temperature phase transition for the φ^4 theory. *Nuclear Physics B*, 401(3):567–590, 1993. ISSN 0550-3213. doi: https://doi.org/10.1016/0550-3213(93)90314-F. URL https://www.sciencedirect.com/science/article/pii/055032139390314F.

[124] Fortran 90 for the fortran 77 programmer, 2023. URL https://www.fortran90.org/. Accessed: 2023-09-20.

[125] J. Kevorkian and J. Cole. *Multiple Scale and Singular Perturbation Methods*, volume 114 of *AMS*. Applied Mathematical Sciences, 5 1996. Published 15 May 1996.

[126] John K. Hunter. *Asymptotic Analysis and Singular Perturbation Theory (Lecture notes)*. University of California at Davis, Davis, 2004.

[127] R.S. Johnson. *Singular Perturbation Theory: Mathematical and Analytical Techniques with Applications to Engineering*. Mathematical and Analytical Techniques with Applications to Engineering. Springer US, 2005. ISBN 9780387232171. URL https://books.google.fr/books?id=ud0zTKnXThUC.

[128] R.E. Meyer, S.V. Parter, and University of Wisconsin-Madison. Mathematics Research Center. *Singular Perturbations and Asymptotics: Proceedings of an Advanced Seminar*. Mathematics Research Center Symposia and Advanced Seminar Series. Academic Press, 1980. ISBN 9780124932609. URL https://books.google.fr/books?id=425JAQAAIAAJ.

[129] J. Kevorkian and J.D. Cole. *Perturbation Methods in Applied Mathematics*. Applied Mathematical Sciences. Springer New York, 2013. ISBN 9781475742138. URL https://books.google.hr/books?id=1YTSBwAAQBAJ.

[130] H. Goldstein, C.P. Poole, and J.L. Safko. *Classical Mechanics*. Addison Wesley, 2002. ISBN 9780201657029. URL https://books.google.fr/books?id=tJCuQgAACAAJ.

[131] Wolfram Research, Inc. Mathematica, Version 12.1. Champaign, IL, 2020.

[132] C.C. Pugh. *Real Mathematical Analysis*. Undergraduate Texts in Mathematics. Springer New York, 2003. ISBN 9780387952970. URL https://books.google.fr/books?id=R_ZetzxFHVwC.

[133] M. Abramowitz and I.A. Stegun. *Handbook of Mathematical Functions: with Formulas, Graphs, and Mathematical Tables*. Dover Books on Mathematics. Dover Publications, 2012. ISBN 9780486158242. URL https://books.google.fr/books?id=KiPCAgAAQBAJ.

[134] E.M. Stein and R. Shakarchi. *Complex Analysis*. Princeton lectures in analysis. Princeton University Press, 2010. ISBN 9781400831159. URL https://books.google.fr/books?id=jvB6ygAACAAJ.

[135] Ken-Ichi Aoki, Atsushi Horikoshi, Masaki Taniguchi, and Haruhiko Terao. Non-Perturbative Renormalization Group Analysis in Quantum Mechanics. *Progress of Theoretical Physics*, 108(3):571–590, 09 2002. ISSN 0033-068X. doi: 10.1143/PTP.108.571. URL https://doi.org/10.1143/PTP.108.571.

[136] N. Tetradis and C. Wetterich. Critical exponents from the effective average action. *Nuclear Physics B*, 422(3):541–592, 1994. ISSN 0550-3213. doi: https://doi.org/10.1016/0550-3213(94)90446-4. URL https://www.sciencedirect.com/science/article/pii/0550321394904464.

[137] Lapack – linear algebra package, 2023. URL https://netlib.org/lapack/. Accessed: 2023-09-20.

[138] E. Brézin, J. C. Le Guillou, and J. Zinn-Justin. Perturbation theory at large order. i. the φ^{2N} interaction. *Phys. Rev. D*, 15:1544–1557, Mar 1977. doi: 10.1103/PhysRevD.15.1544. URL https://link.aps.org/doi/10.1103/PhysRevD.15.1544.

[139] Edouard Brézin and Shechao Feng. Amplitude of the surface tension near the critical point. *Phys. Rev. B*, 29:472–475, Jan 1984. doi: 10.1103/PhysRevB.29.472. URL https://link.aps.org/doi/10.1103/PhysRevB.29.472.

[140] Daniel S. Fisher and David A. Huse. Equilibrium behavior of the spin-glass ordered phase. *Phys. Rev. B*, 38:386–411, Jul 1988. doi: 10.1103/PhysRevB.38.386. URL https://link.aps.org/doi/10.1103/PhysRevB.38.386.

[141] Djordje Spasojević, Sanja Janićević, and Milan Knežević. Analysis of spanning avalanches in the two-dimensional nonequilibrium zero-temperature random-field ising model. *Phys. Rev. E*, 89:012118, Jan 2014. doi: 10.1103/PhysRevE.89.012118. URL https://link.aps.org/doi/10.1103/PhysRevE.89.012118.

[142] Prabodh Shukla and Diana Thongjaomayum. Criteria for infinite avalanches in the zero-temperature nonequilibrium random-field ising model on a bethe lattice. *Phys. Rev. E*, 95:042109, Apr 2017. doi: 10.1103/PhysRevE.95.042109. URL https://link.aps.org/doi/10.1103/PhysRevE.95.042109.

[143] A.S. Kapoyannis and N. Tetradis. Quantum-mechanical tunnelling and the renormalization group. *Physics Letters A*, 276(5):225–232, 2000. ISSN 0375-9601. doi: https://doi.org/10.1016/S0375-9601(00)00671-X. URL https://www.sciencedirect.com/science/article/pii/S037596010000671X.

[144] D. Zappalà. Improving the renormalization group approach to the quantum-mechanical double well potential. *Physics Letters A*, 290(1):35–40, 2001. ISSN 0375-9601. doi: https://doi.org/10.1016/S0375-9601(01)00642-9. URL https://www.sciencedirect.com/science/article/pii/S0375960101006429.

[145] Michael Weyrauch. Functional renormalization group: Truncation schemes and quantum tunneling. *Journal of Molecular Liquids*, 127(1):21–27, 2006. ISSN 0167-7322. doi: https://doi.org/10.1016/j.molliq.2006.03.005. URL https://www.sciencedirect.com/science/article/pii/S0167732206000699. International Conference on Physics of Liquid Matter: Modern Problems.